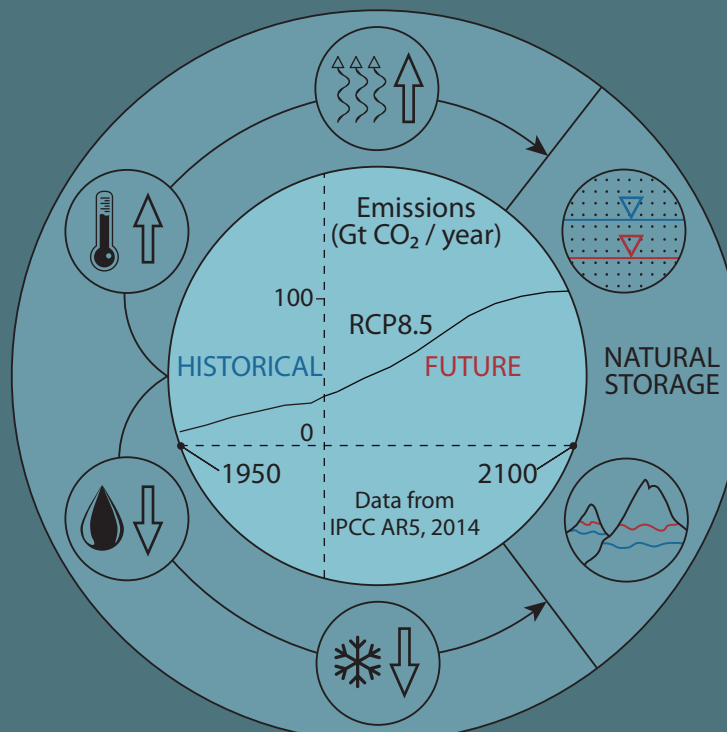


PhD Thesis

ASSESSING IMPACTS OF POTENTIAL CLIMATE CHANGE SCENARIOS IN WATER RESOURCES SYSTEMS DEPENDING ON NATURAL STORAGE FROM SNOWPACKS AND/OR GROUNDWATER

ANTONIO JUAN COLLADOS LARA



Supervisors

David Pulido Velázquez Eulogio Pardo Igúzquiza

Doctoral Programme in Civil Engineering
University of Granada

Granada, March 2019

PhD Thesis / Tesis Doctoral

**Assessing impacts of potential climate change scenarios in
water resources systems depending on natural storage from
snowpacks and/or groundwater**

/

**Evaluación de los impactos potenciales del cambio climático
en los recursos hídricos dependientes del almacenamiento
natural en forma de nieve y/o en acuíferos**

Antonio Juan Collados Lara

Doctoral programme in Civil Engineering / Programa de doctorado en Ingeniería Civil

Technical School of Civil Engineering / E.T.S.I. Caminos, Canales y Puertos

University of Granada / Universidad de Granada

Supervisors: / Directores:

Dr. David Pulido Velázquez

Dr. Eulogio Pardo Igúzquiza



UNIVERSIDAD
DE GRANADA



Instituto Geológico
y Minero de España

Granada, March 2019 / Marzo 2019

Editor: Universidad de Granada. Tesis Doctorales
Autor: Antonio Juan Collados Lara
ISBN: 978-84-1306-258-7
URI: <http://hdl.handle.net/10481/56521>

I raised the bucket to his lips. He drank, his eyes closed. It was as sweet as some special festival treat. This water was indeed a different thing from ordinary nourishment. Its sweetness was born of the walk under the stars, the song of the pulley, the effort of my arms. It was good for the heart, like a present.

The Little Prince, Antoine de Saint-Exupéry

Levanté el balde hasta sus labios y el principito bebió con los ojos cerrados. Todo era bello como una fiesta. Aquella agua era algo más que un alimento. Había nacido del caminar bajo las estrellas, del canto de la roldana, del esfuerzo de mis brazos. Era como un regalo para el corazón.

El Principito, Antoine de Saint-Exupéry

Quality indicators of the compendium of publications / Indicios de calidad del compendio de publicaciones

The scientific papers that constitute the compendium of publications, as well as the quality indicators for each are presented below. The quality indicators were obtained from the Journal Citation Reports (JCR) for the year of publication corresponding to each publication. For articles published after 2017 (last year with JCR data) the statistics for that year are presented.

/

A continuación se muestran los artículos que constituyen el compendio de publicaciones así como los indicios de calidad de cada uno de ellos. Se han usado los estadísticos del Journal Citation Reports (JCR) para el año correspondiente a cada publicación. Para los artículos publicados después de 2017 (último año con datos JCR) se muestran los estadísticos de este año.

Collados-Lara AJ, Pardo-Igúzquiza E, Pulido-Velazquez D. 2017. Spatiotemporal estimation of snow depth using point data from snow stakes, digital terrain models and satellite data. *Hydrological Processes*, 31(10): 1966–1982. doi: 10.1002/hyp.11165.

Impact factor JCR: 3.181 out of 7.051, Position: 13 out of 90 (Q1) in the Water Resources area. / Factor de impacto JCR: 3.181 de 7.051, Posición: 13 de 90 (Q1) en el área de Recursos Hídricos.

Pardo-Igúzquiza E, Collados-Lara AJ, Pulido-Velazquez D. 2017. Estimation of the spatiotemporal dynamics of snow covered area by using cellular automata models. *Journal of Hydrology*, 550: 230–238. doi: 10.1016/j.jhydrol.2017.04.058.

Impact factor JCR: 3.727 out of 5.475, Position: 7 out of 128 (Q1) in the Civil Engineering area. / Factor de impacto JCR: 3.727 de 5.475, Posición: 7 de 128 (Q1) en el área de Ingeniería Civil.

Pulido-Velazquez D, Collados-Lara AJ, Alcalá FJ. 2018. Assessing impacts of future potential climate change scenarios on aquifer recharge in continental Spain. *Journal of hydrology*, 567: 803–819. doi: 10.1016/j.jhydrol.2017.10.077.

Impact factor JCR: 3.727 out of 5.475, Position: 7 out of 128 (Q1) in the Civil Engineering area. / Factor de impacto JCR: 3.727 de 5.475, Posición: 7 de 128 (Q1) en el área de Ingeniería Civil.

Collados-Lara AJ, Pardo-Igúzquiza E, Pulido-Velazquez D, Jiménez-Sánchez J. 2018. Precipitation fields in an alpine Mediterranean catchment. Inversion of precipitation gradient with elevation or undercatch of snowfall? *International Journal of Climatology*, 38(9): 3565–3578. doi:10.1002/joc.5517.

Impact factor JCR: 3.1 out of 19.181, Position: 23 out of 86 (Q2) in the Meteorology and Atmospheric Sciences area. / Factor de impacto JCR: 3.1 de 19.181, Posición: 23 de 86 (Q2) en el área de Meteorología y Ciencias Atmosféricas.

Collados-Lara AJ, Pulido-Velazquez D, Pardo-Igúzquiza E. 2018. An Integrated Statistical Method to Generate Potential Future Climate Scenarios to Analyse Droughts. *Water*, 10(9), 1224. doi:10.3390/w10091224.

Impact factor JCR: 2.069 out of 7.051, Position: 34 out of 90 (Q2) in the Water resources area. / Factor de impacto JCR: 2.069 de 7.051, Posición: 34 de 90 (Q2) en el área de Recursos Hídricos.

Collados-Lara AJ, Pardo-Igúzquiza E, Pulido-Velazquez D. 2019. A distributed cellular automata model to simulate potential future impacts of climate change on snow cover area. *Advances in Water Resources*, 124, 106–119. doi: 10.1016/j.advwatres.2018.12.010.

Impact factor JCR: 3.512 out of 7.051, Position: 9 out of 90 (Q1) in the Water resources area. / Factor de impacto JCR: 3.512 de 7.051, Posición: 9 de 90 (Q1) en el área de Recursos Hídricos.

Collados-Lara AJ, Pardo-Igúzquiza E, Pulido-Velazquez D. Optimal design of snow stake networks to estimate snow depth in an alpine mountain range. *Hydrological Processes*, under review.

Impact factor JCR: 3.181 out of 7.051, Position: 13 out of 90 (Q1) in the Water Resources area. / Factor de impacto JCR: 3.181 de 7.051, Posición: 13 de 90 (Q1) en el área de Recursos Hídricos.

Funding / Financiación

This PhD dissertation has been possible thanks to the granting of a pre-doctoral contract for Training Research Staff (FPI, BES-2014-067699) funded by the Spanish Ministry of Economy and Competitiveness, together with funds from the European Investment Bank and the European Social Fund. The contract, undertaken by the Geological Survey of Spain, forms part of the project “Generation, simulation and integration of future hydrological scenarios in the analysis of impacts and adaptation strategies to global change in water resources systems” (CGL2013-48424-C2-2-R) granted by the Spanish Ministry of Economy and Competitiveness. Further funding for a stay at Colorado State University (USA) (EEBB-I-18-12762) was obtained from the Spanish Ministry of Economy, Industry and Competitiveness as part of its pre-doctoral mobility programme. In addition, partial funding of this research came from COST Action ES1404 within the European Union's Research and Innovation Financing Programme “Horizon 2020”, which also financed two training visits for the doctoral student in Italy (Bormio) and the Netherlands (Delft). The research was also partially funded from other projects, namely: CGL2015-71510-R from the Spanish Ministry of Economy and Competitiveness, GeoE.171.008-TACTIC from the European Union's Research and Innovation Financing Programme “Horizon 2020” and PMAFI/06/14 from the Catholic University of Murcia.

/

Esta tesis doctoral ha sido posible gracias a la concesión de un contrato predoctoral de Formación de Personal Investigador (FPI, BES-2014-067699) financiado por el Ministerio de Economía y Competitividad de España junto con fondos del Banco Europeo de Inversiones y el Fondo Social Europeo. El contrato, que se ha desarrollado en el Instituto Geológico y Minero de España, está adscrito al proyecto “Generación simulación e integración de escenarios hidrológicos futuros en el análisis de impactos y estrategias de adaptación al cambio global en sistemas de recursos hídricos” (CGL2013-48424-C2-2-R) del Ministerio de Economía y Competitividad de España. En el marco del contrato predoctoral se ha obtenido también financiación del Ministerio de Economía, Industria y Competitividad a través del programa de ayudas a la movilidad predoctoral para la realización de una estancia en Colorado State University (USA) (EEBB-I-18-12762). Por otro lado la acción COST ES1404 del Programa de Financiación de Investigación e Innovación de la Unión Europea “Horizonte 2020” ha contribuido parcialmente a la financiación de este trabajo y ha financiado dos estancias formativas del doctorando en Italia (Bormio) y en los Países Bajos (Delft). Además, otros proyectos han contribuido parcialmente a la financiación de este trabajo: CGL2015-71510-R del Ministerio de Economía y Competitividad de España, GeoE.171.008-TACTIC del Programa de Financiación de Investigación e Innovación de la Unión Europea “Horizonte 2020” y PMAFI/06/14 de la Universidad Católica de Murcia.



Instituto Geológico
y Minero de España



GOBIERNO
DE ESPAÑA

MINISTERIO
DE ECONOMÍA
Y COMPETITIVIDAD



Banco
Europeo de
Inversiones



UNIÓN EUROPEA
Fondo Social Europeo

El FSE invierte en tu futuro



European
Commission

Horizon 2020
European Union funding
for Research & Innovation

Agradecimientos / Acknowledgements

Esta tesis doctoral no hubiese sido posible sin mis directores de tesis, David Pulido Velázquez y Eulogio Pardo Igúzquiza, y su enorme calidad científica y personal. Gracias a los dos por haberme dado la oportunidad de trabajar y aprender con vosotros, ha sido una experiencia muy enriquecedora que nunca olvidaré. Ambos sois y seréis referentes para mí en la labor investigadora. Estaré siempre agradecido a David por la oportunidad que me dio para formarme como investigador durante estos cuatro años y por todos los conocimientos que me ha transmitido, siempre con paciencia, respeto, mano izquierda, asertividad, empatía y rigor en el trabajo. Su calidad científico-técnica y capacidad de liderazgo han hecho posible el desarrollo de esta tesis. Igualmente Eulogio siempre ha mostrado interés en el avance de los trabajos, aportando magníficas ideas, conocimientos y tiempo, desde su enorme experiencia científica y respeto a los demás. Cuando me disponía a empezar esta etapa no podría haber imaginado unos directores de tesis mejores.

Me gustaría agradecer también al Instituto Geológico y Minero de España y a las personas que lo componen la buena acogida desde el principio y la oportunidad de formar parte de este organismo durante estos cuatro años. Gracias a los compañeros de la oficina de Granada por la ayuda ofrecida cuando la he necesitado y por compartir conmigo su día a día. Gracias también a todos los compañeros que han participado en los diferentes trabajos realizados durante esta etapa.

Quisiera agradecer también a todos los organismos y proyectos (recogidos en el apartado “Financiación”) que han contribuido con fondos a mi formación durante mi etapa predoctoral.

I would also like to thank Dr. Ali Nadir Arslan (MC Chair of the COST ES1404 action) for the training opportunities in Bormio (Italy) and Delft (Netherlands) and Rodolfo Alvarado for hosting me in Deltares.

On the other hand, I would like to thank Dr. Steven Fassnacht and the people who work in the Snow Hydrology lab for hosting me at Colorado State University (USA). Thank you Steven for sharing your great scientific and personal quality with me.

Por supuesto gracias a mis padres, Antonio y Loli, por el apoyo recibido en todo momento y los valores que me han transmitido a lo largo de mi vida. A mi hermana Loli le agradezco su apoyo y confianza en mí en todo momento. A Tania, mi novia, le agradezco que siempre haya estado a mi lado apoyándome y haciéndome ver la vida desde otros puntos de vista. A los cuatro gracias por sentiros orgullosos de mí, yo también lo estoy de vosotros.

Por último quisiera agradecer el apoyo e interés mostrado durante esta etapa a mi familia, a la familia de Tania y a mis amigos.

Contents

Resumen extendido	xxv
Referencias del resumen extendido	xxxii
Summary.....	xxxv
Chapter 1: Introduction.....	1
1. Motive for undertaking this research study	1
2. General objectives	3
3. Case studies	4
4. Thesis outline.....	4
References	6
Chapter 2: Precipitation fields in an alpine Mediterranean catchment: Inversion of precipitation gradient with elevation or undercatch of snowfall?	9
Abstract.....	9
1. Introduction	10
2. Methodology.....	12
2.1 Analysis of historical data (measurements and corrected values) vs elevation	12
2.2 Assessment of precipitation fields	13
3. Case study and data	14
4. Results	15
4.1 Elevation relationship hypothesis	15
4.2 Spatio-temporal assessment of precipitation estimates.....	16
5. Discussion.....	17
6. Conclusions	18
Acknowledgements	19
References	19
Appendix 2A. Estimation techniques	23
A.1. Kriging with external drift	23
A.2. Regression kriging	24
Appendix 2B. Cross validation methodology.....	26
Chapter 3: Spatiotemporal estimation of snow depth using point data from snow stakes, digital terrain models, and satellite data.....	35
Abstract.....	35
1. Introduction	36

2. Methods	38
3. Study area: Description of the case study and the available data.....	41
4. Results	42
4.1 Analysis of the explanatory variables	42
4.2 Definition and selection of the best models and explanatory variables.....	43
4.3 Snowpack extension and thickness estimates	45
4.4 Cross validation of results.....	46
4.5 Estimates of SWE	46
5. Discussion.....	46
5.1 Limitations and future works	48
6. Conclusions	48
Acknowledgments and Data	49
References	49
Appendix 3A: Equations complementary to the text.....	54
Chapter 4: Optimal design of snow stake networks to estimate snow depth in an alpine mountain range.....	67
Abstract.....	67
1. Introduction	68
2. Method.....	69
2.1. Snow depth estimation from snow stakes by Regression Kriging.....	70
2.2. Optimization approach.....	70
2.3. Simplifications	72
3. Case study and data employed.....	72
4. Results and discussion	73
4.1. Augmentation and reduction cases	74
4.2. Pairwise reduction case.....	74
4.3. Augmentation case considering the zeros of the boundary	75
4.4. Combination of the one-by-one reduction and augmentation cases	75
4.5. Limitations and future work.....	75
5. Conclusions	76
Acknowledgments	76
References	76
Chapter 5: Estimation of the spatiotemporal dynamics of snow covered area by using cellular automata models.....	91

Abstract.....	91
1. Introduction	92
2. Methodology.....	93
3. Case study.....	95
4. Conclusions	99
Acknowledgements	99
References	99
Chapter 6: An Integrated Statistical Method to Generate Potential Future Climate Scenarios to Analyse Droughts.....	115
Abstract.....	115
1. Introduction	116
2. Method.....	117
2.1. Generation of Future Individual Projections.....	117
2.2. Multi-Objective Analysis of the Main Statistics (Basic and Drought Statistics)....	119
2.3. Ensembles of Predictions to Define More Representative Future Climate Scenarios	120
3. Study Area: Description and Available Data	121
3.1. Location and Description of the Alto Genil Basin.....	121
3.2. Historical Climate Data.....	121
3.3. Climate Model Simulation Data. Control and Future Scenarios	122
4. Results and Discussion	122
4.1. Application of Different Correction Techniques	122
4.2. Multi-Objective Analysis of Basic and Drought Statistics	124
4.3. Ensembles of Predictions to Define More Representative Future Climate Scenarios	125
4.4. Sensitivity of Results to Spatial Scale	126
5. Limitations and Future Research Works	127
6. Conclusions	128
Acknowledgments	129
References	129
Chapter 7: A distributed cellular automata model to simulate potential future impacts of climate change on snow cover area.....	147
Abstract.....	147
1. Introduction	148

2. Methodology.....	150
3. Application to the case study and data employed.....	153
3.1. Case study	153
3.2. Application to the case study	154
4. Limitations and future research	157
5. Conclusions	158
Acknowledgements	159
References	159
Chapter 8: Assessing impacts of future potential climate change scenarios on aquifer recharge in continental Spain.....	173
Abstract.....	173
1. Introduction	174
2. Materials: Description of the case study and available data.....	176
2.1 Case study: continental Spain	176
2.2 Historical climatic data	177
2.3 Historical recharge data	177
2.4 Climatic model simulation data. Control and future scenarios	178
3. Methods	178
3.1 Precipitation-recharge model	179
3.2 Generation of future potential climatic scenarios	180
3.2.1 Application of downscaling techniques: bias correction and delta change approaches.....	181
3.2.2 Multi-criteria analysis of the main statistic.....	181
3.2.3 Prediction ensembles to define more representative future climatic scenarios	182
3.3 Assessment of future climate impacts on aquifer recharge	183
4. Results and discussion	183
4.1. Future aquifer recharge scenarios	183
4.2 Limitations: assumptions, uncertainties, and usefulness of the results.....	185
5. Conclusions	187
Acknowledgments	187
References	187
Chapter 9: General conclusions, limitations and future research	207
1. Contributions	207
2. Limitations and future lines of research	209

List of tables

Table 1.1. List of articles (chapters) that form part of the doctoral thesis, objectives they address, and journals in which they have been published.	5
Tables of the Chapter 2.....	27
Table 2.1. Parameters of the regression function ($P = a_1 + a_2 \cdot h + a_3 \cdot h^2$) for mean precipitation vs. elevation.....	27
Table 2.2. Mean error and mean squared error of the cross validation experiment for the different techniques, data and variogram model.	27
Tables of the Chapter 3.....	58
Table 3.1. Explanatory variables for the optimal models. LATI (latitude), LONG (longitude), ELEV (elevation), EAST (eastness), NORT (northness), SLOP (slope), Sx (maximum upwind slope), RADI (radiation), CURV (curvature).	58
Tables of the Chapter 4.....	80
Table 4.1. Available SWE products for Europe.	80
Table 4.2. Previous works on snow observation network optimization.	80
Tables of the Chapter 6.....	135
Table 6.1. Summary of advantages and disadvantages of each correction technique (P stands for precipitation).	135
Table 6.2. Regional climatic models (RCMs) and global climate models (GCMs) considered.	135
Table 6.3. Eliminated and uneliminated models in the multi-objective analysis of the delta change approaches for the lumped and distributed cases.	135
Table 6.4. Eliminated and uneliminated combinations of model and bias correction technique for the lumped and distributed cases.	136
Table 6.5. Changes of overall mean values for precipitation and temperature scenarios compared to historical data.	137
Tables of the Chapter 7.....	164
Table 7.1. Summary of the CA numerical experiments carried out in this study.	164
Table 7.2. Optimal values of parameters and standard deviations for the lumped CA model.	165
Table 7.3. Regional Climatic Models (RCMs) and General Circulation Models (GCMs) considered for simulations.....	165
Table 7.4. Potential relative changes in SCA for the two scenarios considered	165
Tables of the Chapter 8.....	195
Table 8.1. Regional Climatic Models (RCMs) and General Circulation Models (GCMs) considered for simulations.....	195

Table 8.2. Inferior and non-inferior models in the multicriteria analysis.....	195
Table 8.3. Inferior and non-inferior combination of models and bias-correction techniques.	
.....	195
Table 8.4. Basic statistics of governing variables P, T, and R for the historical period, the four considered scenarios, and the two recharge models utilized.	196

List of figures

Figures of the Chapter 2	28
Figure 2.1. Flow chart of the proposed methodology.....	28
Figure 2.2. Location of the study area and available gauges.....	28
Figure 2.3. A: Mean daily precipitation data for different elevations. B: mean daily temperature data for different elevations. Dots represent the data (black) and modified data corrected for undercatch (orange); their trends are marked by lines.	29
Figure 2.4. Percentile distribution of the snowline for each month of the snow season and for the whole snow season.....	29
Figure 2.5. A, B, C: Spatial distribution of estimated mean precipitation using QKED, LKED, RK and original data for the period 1980-2014. D, E, F: Spatial distribution of standard deviation of estimated precipitation using QKED, LKED, RK and original data for the period 1980-2014.....	30
Figure 2.6. Estimated mean daily precipitation data in each cell using the various geostatistical techniques considered vs elevation of the cell. A: using a yearly variogram model. B: using a monthly variogram model.	30
Figure 2.7. Estimated mean daily precipitation (using modified data corrected for undercatch) in each cell using the various geostatistical techniques considered vs elevation of the cell. A: using a yearly variogram model. B: using a monthly variogram model.	31
Figure 2.8. Comparison between precipitation original and modified data vs. elevation using different estimation techniques and the monthly variogram model.....	31
Figure 2.9. A, C, E: Estimated daily precipitation (QKED, LKED, RK) within the basin using the yearly model vs. the monthly model and the original data. B, D, F: Standard deviation of precipitation (QKED, LKED, RK) using the yearly model vs. the monthly model and the original data.	32
Figure 2.10. Mean error (A, C, E) and mean squared error (B, D, F) of the cross validation experiment using quadratic KED, linear KED and RK using the original data.	33
Figure 2.11. Scheme of the precipitation flow dynamics and proposed hypothesis for the case study.....	33
Figures of the Chapter 3	59
Figure 3.1. Flow chart of the proposed systematic method.....	59
Figure 3.2. Location of the Sierra Nevada mountain range and the stakes where the snow depth is measured.	59
Figure 3.3. Variability of the snow depth data. A: For individual dates. B: For the snow season and the months. The top and bottom of boxes represent the interquartile range.	60
Figure 3.4. Maps of explanatory variables for the Sierra Nevada mountain range. A: Elevation; B: Slope; C: Eastness; D: Northness; E: Radiation; F: Maximum upwind slope; G: Curvature.	61

Figure 3.5. R ² values for the linear regression of snow depth and maximum upwind slope with dmax=300 m.....	61
Figure 3.6. Ranges the value of each predictor for the observations in stakes and the study area. The top and bottom of boxes represent the interquartile range.	62
Figure 3.7. Best models for the coefficient of determination for the survey of 21/04/2003.	63
Figure 3.8. Frequency of the explanatory variables in the non-eliminated models for different model complexities. LATI (latitude), LONG (longitude), ELEV (altitudeelevation), EAST (eastness), NORT (northness), SLOP (slope), Sx (maximum upwind slope), RADI (radiation), CURV (curvature).	63
Figure 3.9. Frequency of the explanatory variables involved within interaction of variables (products of variables) in the not-eliminated models for different model complexities. LATI (latitude), LONG (longitude), ELEV (elevation), EAST (eastness), NORT (northness), SLOP (slope), Sx (maximum upwind slope), RADI (radiation), CURV (curvature).	64
Figure 3.10. Coefficients of determination of the models considered for the different surveys. The top and bottom of boxes represent the interquartile range.....	64
Figure 3.11. Estimated snow depth in centimeters for the 24/03/2005 survey: A) using model 2, B) using model 4, C) using model 7 and D) using the optimal model. Standard deviation of estimated snow depth in centimeters for the 13/01/2004 survey: E) using model 2, F) using model 4, G) using model 7 and H) using the optimal model.	65
Figure 3.12. Mean error of the cross-validation experiment for the optimal model and mean standardized squared error of the cross-validation experiment for the optimal model.	65
Figure 3.13. A: Estimated snow water equivalent for the Sierra Nevada mountains. B: Estimated snow water equivalent for the Canales basin. C: Estimated snow water equivalent for the Guadaleo basin.....	66
Figures of the Chapter 4	81
Figure 4.1. Flow chart of the proposed methodology.....	81
Figure 4.2. A) Location of the case study area. B) Digital elevation map of the case study.	82
Figure 4.3. Standard deviation of estimates from the initial situation using regression (a), kriging (b) and the total standard deviation (c).	83
Figure 4.5. Spatial evolution of the total standard deviation in the reduction steps.....	84
Figure 4.6. Mean variance and standard deviation (a and b, respectively) for the augmentation and reduction cases.	85
Figure 4.7. Location of the added stakes (a) and eliminated stakes (b) in the augmentation and reduction cases.	86
Figure 4.8. Mean variance and standard deviation (a and b, respectively) for the one-by-one and pairwise reductions.	87
Figure 4.9. Location of the eliminated stakes for the pairwise reduction case.....	87

Figure 4.10. Total standard deviation of estimation considering SCA zeros.....	88
Figure 4.11. Mean variance and standard deviation (a and b, respectively) without considering SCA zeros and considering SCA zeros.....	88
Figure 4.12. Location of the added stakes considering SCA zeros	89
Figure 4.13. Mean variance and standard deviation (a and b, respectively) for the combination of augmentation and reduction cases.....	89
Figure 4.14. Location of the eliminated stakes in the reduction phase (a) and added stakes in the augmentation phase (b).....	90
Figures of the Chapter 5	103
Figure 5.1. A: Location of the Sierra Nevada mountain range in Southern Spain. B: the digital elevation model of the study area. C: Landsat image, provided by the USGS, that shows the snow covered area in Sierra Nevada for the date 20/01/2000.	103
Figure 5.2. Daily dynamics of the snow covered area for three consecutive years, from the 1st of July of 2000 to the 30th of June 2003.	104
Figure 5.3. Daily temperature indexes calculated as A: the mean of the minimum temperatures of the stations of SPAIN02 that are above 1000 and 3000 m and B: the mean of the maximum temperatures of the stations of SPAIN02 that are above 1000 and 3000 m.	105
Figure 5.4. A: Daily precipitation index (calculated as the mean precipitation from stations of SPAIN02 above 1000 m) and the SCA time series, and B: Daily precipitation index (calculated as the mean maximum temperature from stations from SPAIN02 above 1000 m and SCA) and the SCA time series.....	106
Figure 5.5. Mean square error (solid line) and mean error (dashed line) when the only varying parameter is the temperature threshold Tc while the rest of the parameters are hold at their optimal values. It may be seen how the lowest MSE is given by the value of 0 °C which gives also an acceptable ME.....	107
Figure 5.6. Mean square error (solid line) and mean error (dashed line) when the only varying parameter is the precipitation threshold while the rest of the parameters are hold at their optimal values. The precipitation threshold with minimum mean square error statistic is 6.8 mm (vertical gray bar) which gives an acceptable mean error of -20 cells.....	107
Figure 5.7. Mean square error (solid line) and mean error (dashed line) when the only varying parameter is the number Nm of neighbours with snow which controls if a pixel with snow will change to the state of no snow when temperature increases and there is no precipitation. The Nm with minimum mean square error statistic is 14 (vertical gray bar) which gives an acceptable mean error.....	108
Figure 5.8. Mean square error (proportional to the width of the circles) when the only varying parameters are a (interception with the origin) and the parameter b (slope) of the straight line between temperature and altitude of the snow line. The values of 1170 and 80, for a and b respectively, provides the minimum mean square error (solid black circle)....	108

Figure 5.9. Experimental SCA and estimated SCA by the calibrated cellular automata model	109
Figure 5.10. Experimental lineal relation between temperature and altitude of the snow line for the three years calibration period (dots and solid line) and the independent lineal relation obtained from model calibration (dashed line).....	109
Figure 5.11. Experimental SCA and estimated SCA by the calibrated cellular automaton model	110
Figura 5.12. Spatial daily evolution of the experimental (left) and the estimated by the cellular automaton (right) from the 19th of December 2005 (top) to the 26th of December 2005 (bottom).	111
Figure 5.13. Mean square error (solid line) and mean error (dashed line) when the only varying parameter is the global temperature threshold Tcc while the rest of the parameters are hold at their optimal values. It may be seen how the lowest MSE is given by the value of 13 °C which gives also an acceptable ME.....	112
Figure 5.14. Experimental SCA and estimated SCA by the calibrated cellular automata model with the global criterion given in Equation (9).....	112
Figure 5.15. Experimental SCA and estimated SCA by the calibrated cellular automaton model with the global criterion given in Equation (9).....	113
Figures of the Chapter 6	138
Figure 6.1. Flow chart of the proposed methodology.....	138
Figure 6.2. Location of the case study.....	138
Figure 6.3. Historical precipitation and temperature in Alto Genil basin. Above: Monthly precipitation and temperature time series. Below: Spatial distribution of mean precipitation and temperature.	139
Figure 6.4. Monthly mean and standard deviation for the historical and control series (precipitation and temperature) for the mean year in the period 1971–2000—lumped approaches.	139
Figure 6.5. Drought statistics for the historical and control series in the period 1971–2000—lumped approaches.	140
Figure 6.6. Dimensionless relative monthly change in mean and standard deviation of the future P and T series (2071–2100) with respect to the control series (1971–2000)—lumped approaches. Relative changes calculated as $(F - C)/C$ where F stands for future model projections and C control model simulations.	140
Figure 6.7. Mean, standard deviation, and asymmetry coefficients of the corrected control scenario (1971–2000) for precipitation (left column) and temperature (right column). Average year for HIRHAM5 RCM model nested inside EC-EARTH GCM—lumped approaches.	141
Figure 6.8. Drought statistics of the corrected precipitation control scenario (1971–2000) for the HIRHAM5 RCM model nested inside EC-EARTHGCM—lumped approaches... .	141

Figure 6.9. Mean, standard deviation and asymmetry coefficients of future precipitation (left column) and temperature series (right column). Average year for HIRHAM5 RCM model nested inside EC-EARTH GCM—lumped approaches.....	142
Figure 6.10. Drought statistics of future precipitation series for the HIRHAM5 RCM model nested inside EC-EARTH GCM—lumped approaches.....	142
Figure 6.11. (A) Times that the techniques are not eliminated in the multi-objective analysis (bias correction approach); (B) Times that the RCMs are not eliminated in the multi-objective analysis (bias correction change approach).	143
Figure 6.12. Mean and standard deviation of future precipitation and temperature series obtained by the four ensemble options (E1, E2, E3, and E4)—lumped approaches.....	143
Figure 6.13. Drought statistics of future precipitation series obtained by the four ensemble options (E1, E2, E3, and E4)—lumped approaches.	144
Figure 6.14. Spatial distribution of the mean relative change (expressed in %) in precipitation and temperature obtained by the four ensemble options (E1, E2, E3, and E4)—distributed approaches.	145
Figure 6.15. Monthly differences in mean and standard deviation in an average year between distributed (D) and lumped (L) approaches $((L - D)/D) \times 100$ for the four ensembles scenarios (E1, E2, E3 and E4).	146
Figures of the Chapter 7	166
Figure 7.1. A) Location of the study area. B) Land cover of the area of interest (Day image from 01/11/1999 from the Landsat 7 satellite).	166
Figure 7.2. Mean squared error estimated from the number of errors in cells in the area in the calibration period for numerical experiment A1.	166
Figure 7.3. Value of the calibrated parameters in the various climatic zones compared to the mean elevation of each climatic zone.....	167
Figure 7.4. Experimental SCA and SCA estimated by the calibrated CA model over the calibration period.....	167
Figure 7.5. Cells where snow cover exceeds 5, 15, 25 and 35% of days for experimental and estimated SCA using the calibrated cellular automata model over the calibration period.	168
Figure 7.6. Experimental SCA and SCA estimated by the calibrated CA model for the validation period.....	168
Figure 7.7. Cells where snow cover exceeds 5, 15, 25 and 35% of days for the experimental and estimated SCA using the calibrated CA model for the validation period.....	169
Figure 7.8. Failure probability of the CA model in the calibration and validation periods.	169
Figure 7.9. Experimental and estimates \pm standard deviation of SCA using lumped CA model for the validation period.	170

Figure 7.10. Historical and ensemble of future precipitation and maximum temperature series for the bias correction and delta change approaches for a given climatic zone	170
Figure 7.11. Relative changes in precipitation and temperature with respect to the elevation of each climatic zone	171
Figure 7.12. Historical and future monthly estimated SCA using the calibrated cellular automata model.....	171
Figure 7.13. Historical and future daily estimated SCA using the calibrated cellular automata model.....	172
Figure 7.14. Cells with snow cover for more than 5, 15, 25 and 35% of days for the historical and future scenarios	172
Figures of the Chapter 8	197
Figure 8.1. Map of continental Spain, showing the main mountain ranges and hydrographic basins, and the hydrogeological behaviour of geological materials according to permeability type (IGME, 1993), modified from Alcalá and Custodio (2014): (a) low to moderate permeability pre-Triassic metamorphic rocks, granitic outcrops, and Triassic to Miocene marly sedimentary formations; (b) moderate to high permeability Palaeozoic to Tertiary carbonates; (c) moderate to high permeability Plio-Quaternary detritic materials; and (d) Triassic to Miocene evaporitic outcrops.....	197
Figure 8.2. Spatio-temporal distribution of historical mean (a) precipitation (mm year ⁻¹) and (b) temperature (°C) in continental Spain during the reference period (1976-2005)...	198
Figure 8.3. Historical net aquifer recharge (NAR) from precipitation over continental Spain from the CMB method application for the period 1996-2005, after Alcalá and Custodio (2014, 2015): (a) annual mean NAR (mm year ⁻¹) and (b) standard deviation of annual mean NAR (mm year ⁻¹).	198
Figure 8.4. Dimensionless spatial monthly mean relative differences between the control simulation and the historical precipitation time series for an average year in the reference period (1976-2005). The ±0.5 range is indicated.	199
Figure 8.5. Dimensionless spatial monthly mean relative differences between future (2016-2045) and control (1976-2005) precipitation time series. The ±0.1 range is indicated.....	200
Figure 8.6. Historical mean net aquifer recharge (mm year ⁻¹) for the period 1976-2005 obtained when simulating with two different hypotheses regarding the length of the PE recharge time series used to calibrate the precipitation-recharge model: mod_1976-2005 and mod_1996-2005.	201
Figure 8.7. Potential future mean temperature (°C) scenarios obtained with the four ensemble options (E1, E2, E3, and E4).	201
Figure 8.8. Potential future mean precipitation (mm year ⁻¹) scenarios obtained with the four ensemble options (E1, E2, E3, and E4).	202

Figure 8.9. Future potential mean net aquifer recharge (mm year-1) scenarios for the period (2011-2045) by combining future potential scenarios defined by the four ensemble options (E1, E2, E3, and E4) and two recharge models (mod_1976-2005 and mod_1996-2005)..	203
Figure 8.10. Absolute differences in mean net aquifer recharge (mm year-1) for the historical series under four different scenarios (E1, E2, E3, and E4) and recharge models (mod_1976-2005 and mod_1996-2005).....	204
Figure 8.11. Future potential scenarios of standard deviation of mean net aquifer recharge (mm year-1) for the period (2011-2045) from combining future potential scenarios defined by the four ensemble options (E1, E2, E3, and E4) and two recharge models (mod_1976-2005 and mod_1996-2005).....	204
Figure 8.12. Potential future mean net aquifer recharge (NAR) (mm year-1), standard deviation of future mean NAR (mm year-1), and dimensionless relative differences between historical and future scenarios (equi-feasible ensemble of the eight scenarios). .	205
Figure 8.13. Elevation and latitude vs. dimensionless relative differences between future and historical net aquifer recharge (mean and standard deviation). ..	205

Resumen extendido

El cambio climático asociado a las emisiones de gases de efecto invernadero como el dióxido de carbono representa uno de los mayores retos a los que se enfrentará la sociedad en las próximas décadas. El calentamiento global es inequívoco. Desde la década de 1950 se vienen observando cambios que no tienen precedentes, como aumentos de temperatura de la atmósfera y los océanos, disminución de las cantidades de nieve, hielo y reservas de agua subterránea y aumentos del nivel del mar (IPCC, 2014). En el Quinto Informe de Evaluación del Panel Intergubernamental sobre Cambio Climático (IPCC, por sus siglas en inglés) se incluyen cuatro trayectorias o proyecciones futuras de emisiones de dióxido de carbono de origen antrópico para el siglo XXI denominadas trayectorias de concentración representativas (RCP, por sus siglas en inglés). Dichas trayectorias incluyen un escenario de mitigación (RCP2.6), dos escenarios intermedios (RCP4.5 y RCP6.0), y un escenario con un nivel alto de emisiones (RCP8.5). Los escenarios sin esfuerzos adicionales por parte de la sociedad para limitar las emisiones dan lugar a trayectorias que se sitúan entre RCP6.0 y RCP8.5.

Desde el punto de vista de los recursos hídricos, el cambio climático modificará la variabilidad espaciotemporal de las variables climáticas e hidrológicas que condicionan la disponibilidad de agua en estos sistemas. Los últimos estudios sobre cambio climático proyectan importantes disminuciones de los recursos en las cuencas mediterráneas, con importantes impactos ambientales, económicos y sociales (Iglesias et al., 2007). El cambio climático se asocia además a un incremento en la aparición de eventos extremos como pueden ser las sequías o inundaciones. A nivel europeo, mientras que las zonas Norte y Noreste son más propensas al incremento de la frecuencia de inundaciones, el Sur y Sureste muestran un aumento significativo en la frecuencia de las sequías (Voss et al., 2002). La evaluación de los impactos potenciales del cambio climático conlleva una importante propagación de incertidumbres a través de todas sus fases. Sin embargo, estas incertidumbres no deben constituir una excusa para retrasos o inacción en la evaluación, dado que los sistemas de recursos hídricos pueden ser muy vulnerables (UN, 2009). Las aguas subterráneas y el almacenamiento en forma de nieve pueden jugar un papel fundamental en la definición de estrategias de adaptación al cambio climático que permitan un suministro sostenible de las demandas (Barnett et al., 2005; Dragoni and Sukhiga, 2008). De estos dos sistemas de almacenamiento natural, las aguas subterráneas son las que ofrecen más flexibilidad para la gestión de los recursos, ya que la disponibilidad de agua a través de extracciones puede ser más o menos inmediata en cualquier época del año. El impacto del cambio climático en las aguas subterráneas es un tema abordado por la comunidad científica desde la década de los 90, y en el que se ha incrementado el interés en los últimos años (McIntyre, 2017). Con respecto a la nieve, la fusión se produce de forma natural en períodos concretos de acuerdo con las condiciones climáticas. En cuencas alpinas la nieve juega un papel fundamental, no sólo desde el punto de vista del turismo, sino también desde el punto de vista de la gestión de los recursos hídricos. En estos sistemas, en los que la mayoría de precipitación es sólida, se dispone de recursos procedentes de la fusión de nieve, cuya distribución espaciotemporal tiene una elevada sensibilidad al cambio climático (Steger et al., 2013).

El almacenamiento de agua en estos sistemas se encuentra estrechamente relacionado con las variables climáticas de la región. Los cambios de temperatura y precipitación pueden producir alteraciones significativas en los sistemas naturales de almacenamiento hídrico (Piani et al., 2010). Estas variaciones influyen directamente sobre las variables hidrológicas que condicionan la disponibilidad de agua en los sistemas hídricos. La evaluación de la recarga de acuíferos procedente de la precipitación es crucial a la hora de cuantificar los recursos hídricos subterráneos renovables. Este aspecto resulta de gran interés a la hora de diseñar políticas de agua adecuadas en un país. En los sistemas alpinos, el equivalente de agua en la nieve está estrechamente relacionado con la precipitación y la temperatura. Dicha variable depende del espesor, la cubierta y la densidad de la nieve.

El estudio de los impactos del cambio climático en sistemas de recursos hídricos requiere conocer y caracterizar previamente la distribución histórica de las variables climáticas principales, precipitación y temperatura. Generalmente las variables relacionadas con la orografía tienen una influencia importante en la distribución espacial de la temperatura y precipitación. Cuando se analizan variables climatológicas, la altitud se constituye como un condicionante fundamental y puede ser empleada como información secundaria cuando no existe información suficiente para caracterizar el sistema. Normalmente se acepta que la temperatura disminuye y la precipitación aumenta con la altitud pero esto no siempre es así (Immerzeel et al., 2014). Se hace necesario un adecuado estudio de los gradientes altitudinales de las variables climáticas. La información que estos gradientes aportan a veces es fundamental para el completado de datos en problemas hidrológicos mediante técnicas de estimación geoestadística (Haberlandt, 2007).

Para la propagación de los impactos del cambio climático se precisa calibrar modelos matemáticos que relacionan las variables climáticas con las variables hidrológicas. El espesor de nieve (López-Moreno and Nogués-Bravo, 2006), la cubierta de nieve (Mir et al., 2015), la densidad (Bormann et al., 2013) o, directamente, el equivalente de agua en la nieve (Harshburger et al., 2010) han sido estimados mediante modelos de interpolación y simulación geoestadística. Algunos modelos hidrológicos conceptuales (p.ej. HBV (Lindström et al., 1997); “Snowmelt Runoff Model” (SRM) (Martinec et al., 2008)) permiten aproximar los procesos que condicionan la evolución de la dinámica del equivalente de agua en la nieve. La mayor parte de trabajos científicos relacionados con los recursos nivales se han desarrollado a escala de ladera o de cuenca. Por su parte, la recarga, variable que condiciona la distribución de los recursos renovables en los acuíferos puede ser estimada a través de diferentes técnicas (trazadores, modelos físicos, numéricos y/o empíricos.) (Lerner et al., 1990; Scanlon et al., 2002, 2006; Coes et al., 2007; McMahon et al., 2011). Los modelos de recarga generalmente se aplican a escala de acuífero.

La propagación de impactos del cambio climático a través de estos modelos requiere generar previamente escenarios potenciales futuros de clima para evaluar los impactos sobre el almacenamiento en forma nieve o las aguas subterráneas. Los modelos regionales de clima proporcionan información de los cambios potenciales que se producirán en la precipitación y temperatura a partir de trayectorias probables de emisiones de gases de efecto invernadero (RCP). Los últimos escenarios de concentraciones publicados por el IPCC (IPCC, 2014), han

sido simulados mediante modelos climáticos físicos para producir proyecciones futuras en el marco de diferentes proyectos europeos, como CORDEX (2013), cuyos resultados están disponibles en abierto. Para poder utilizar esta información en el estudio de problemas hidrológicos, debemos generar escenarios climáticos regionales o locales a partir de la información que aportan los modelos regionales de clima. Dichos escenarios pueden generarse aplicando técnicas de corrección estadística considerando las series o campos históricos generados y las simulaciones proporcionadas por los modelos climáticos. Existen numerosas técnicas de corrección estadística que pueden ser empleadas bajo dos enfoques conceptuales, “bias correction” y “delta change” (Watanabe et al., 2012; Räisänen y Räty, 2013). Para obtener unas predicciones más robustas se pueden considerar ensamblados de proyecciones obtenidas con diferentes modelos climáticos y diferentes técnicas de corrección estadística (AEMET, 2009). Estos ensamblados pueden definirse dando más peso a los modelos que, al simular el periodo histórico (simulación de control) aproximen mejor los estadísticos de dicho periodo. Los estadísticos habitualmente analizados/considerados son los básicos, la media y la desviación estándar, siendo escasa la atención prestada a los estadísticos de sequía, a pesar de su importancia en zonas áridas y semiáridas.

Esta investigación se desarrolla en respuesta a la necesidad de avanzar en el desarrollo y aplicación de metodologías para la evaluación de impactos potenciales del cambio climático en los recursos almacenados en acuíferos y/o en forma de nieve en sistemas que abarcan grandes extensiones de terreno. Se estudia la dinámica nival en una cordillera, Sierra Nevada y se evalúan potenciales escenarios futuros de recarga en acuíferos a escala nacional. La mayor parte de trabajos científicos sobre impactos del cambio climático en los recursos subterráneos se desarrollan para sistemas a escala de acuífero. De igual forma, la dinámica nival suele estudiarse en laderas o cuencas concretas, no siendo habituales los análisis a nivel de macizo o cordillera. Los datos en estos sistemas alpinos normalmente son escasos, debido a la baja accesibilidad y los limitados recursos existentes. Se propone una metodología para estimar la ubicación óptima de los puntos de monitoreo. Para el estudio de impactos del cambio climático es necesario generar escenarios climáticos locales o regionales adaptados al sistema a analizar. Se propone una metodología para la definición de dichos escenarios considerando estadísticos de sequías. La revisión del estado del arte ha puesto de relieve que a pesar de la importancia de las sequías en la gestión de zonas áridas y semiáridas, en la generación de escenarios locales y regionales futuros no se consideran los estadísticos de sequías. Aunque existen numerosos trabajos de análisis de sequías en periodos históricos, el número de ellos dedicado a escenarios futuros es aún escaso. En las citadas lagunas o necesidades de estudio científico se encontró la motivación para desarrollar este trabajo.

De acuerdo con las motivaciones expuestas, el propósito principal de la tesis doctoral es desarrollar herramientas y metodologías para el estudio de impactos potenciales del cambio climático en los recursos almacenados en acuíferos y/o en forma de nieve en sistemas que abarcan grandes extensiones de terreno. Dichas metodologías se aplicaron en sistemas a escala de cuenca, cordillera y en la España peninsular. En este objetivo general se integran los siguientes objetivos específicos:

- (1) Estudio de los gradientes altitudinales de precipitación y temperatura y generación de campos de precipitación histórica mediante técnicas geoestadísticas empleando la altitud como información secundaria para la estimación.
- (2) Desarrollo de una metodología para estimar espesores de nieve mediante técnicas geoestadísticas aplicables a escala de cordillera.
- (3) Optimización de la red de monitoreo de nieve para reducir la incertidumbre en la estimación del espesor de nieve. Aplicación a escala de cordillera.
- (4) Desarrollo de un modelo para simular la dinámica de la cubierta de nieve mediante autómatas celulares. Aplicación a escala de cordillera.
- (5) Evaluación de la recarga neta histórica en acuíferos mediante un modelo empírico de recarga neta. Aplicación a escala de España continental.
- (6) Propuesta de una metodología para la generación de escenarios potenciales de cambio climático teniendo en cuenta los estadísticos de sequías.
- (7) Propagación de los impactos potenciales de cambio climático a la cubierta de nieve y a la recarga neta en acuíferos. Aplicación a escala de cordillera y de país respectivamente.

Aunque los objetivos de la tesis doctoral son principalmente metodológicos, es necesario el uso de casos de estudio para evaluar la aplicabilidad de las metodologías propuestas. Los casos de estudio seleccionados para llevar a cabo los trabajos de investigación en el marco de la tesis son la cuenca del Alto Genil, la cordillera de Sierra Nevada y la España continental. Todos los casos de estudio se encuentran en la España peninsular, muy vulnerable a los potenciales efectos futuros del cambio climático, especialmente el área mediterránea (Iglesias et al., 2007), donde se encuentran la cuenca del Alto Genil y Sierra Nevada. En los capítulos, en los que se aplican las metodologías propuestas, se recoge una descripción de los citados casos de estudio.

Los objetivos establecidos en la tesis doctoral han permitido realizar importantes contribuciones en el campo de estudio. A continuación se recopilan las principales contribuciones de esta tesis.

- Estudio de los gradientes altitudinales de precipitación y temperatura y generación de campos de precipitación histórica mediante técnicas geoestadísticas empleando la altitud como información secundaria para la estimación.

En la cuenca del Alto Genil se ha detectado una inversión del gradiente pluviométrico en torno a los 1600 m. Aunque se contempló la posibilidad de que este patrón de precipitación se deba a errores sistemáticos en las mediciones de precipitación sólida (fenómeno conocido como “undercatch”), el análisis climático de los datos en las estaciones del año no nivales permitió concluir que la inversión del gradiente es real, aunque su intensidad puede verse amplificada por este fenómeno. La temperatura muestra una relación descendente lineal con la altitud. Las técnicas geoestadísticas empleadas para generar los campos de precipitación,

krigeaje con deriva externa (lineal y cuadrática) y regresión con krigeaje de residuos, muestran amplias diferencias entre ellas mientras que la influencia de la escala temporal (anual o mensual) para definir el variograma climático es baja. A pesar de que la técnica de krigeaje con deriva externa lineal muestra los mejores resultados en la validación cruzada, la inversión de gradiente no es reproducida por ésta. Sin embargo la técnica de regresión con krigeaje de residuos si muestra esta inversión. Por tanto a la hora de generar campos de variables climáticas es necesario estudiar diferentes técnicas para elegir la que menos incertidumbres aporte al proceso.

- Desarrollo de una metodología para estimar espesores de nieve mediante técnicas geoestadísticas aplicables a escala de cordillera.

Se ha propuesto una metodología parsimoniosa para la estimación mediante regresión con krigeaje de residuos del espesor de nieve en sistemas alpinos basada en (1) variables explicativas (geográficas (latitud, longitud, curvatura del terreno y altitud), orográficas (“eastness”, “northness” y pendiente), y “pseudo-climáticas” (índice de radiación medio y “maximum upwind slope”)) que pueden ser obtenidas de un modelo digital de elevaciones y (2) datos de cubierta de nieve que pueden ser obtenidos de información de satélite. Los datos de espesor de nieve empleados proceden del programa ERHIN (Evaluación de recursos hídricos procedentes de la innovación) de la Dirección General del Agua de España. La metodología se ha aplicado a Sierra Nevada con resultados satisfactorios en la validación cruzada. En este caso de estudio el análisis multi-objetivo de los distintos modelos de regresión ha permitido detectar que las variables explicativas más importantes son altitud, “northness” y pendiente.

- Optimización de la red de monitoreo de nieve para reducir la incertidumbre en la estimación del espesor de nieve. Aplicación a escala de cordillera.

Se ha desarrollado una metodología que permite optimizar la red de monitoreo de espesor de nieve en una cordillera a partir de un modelo de regresión que cuenta con diferentes variables explicativas para estimar el espesor de nieve. La metodología de optimización propuesta minimiza el error en el proceso de estimación del espesor de nieve mediante regresión con krigeaje de residuos considerando dos fuentes de incertidumbre: la del modelo de regresión que tiene en cuenta el efecto de las variables explicativas y la de krigeaje que tiene en cuenta la localización de los puntos de monitoreo. Se han propuesto diferentes casos de optimización para el aumento, reducción y combinación de ambos. La metodología se ha aplicado al caso de estudio de Sierra Nevada. Combinando los casos de reducción y aumento óptimos se ha obtenido una nueva configuración de la red de monitoreo en Sierra Nevada que reduce la incertidumbre total de estimación.

- Desarrollo de un modelo para simular la dinámica de la cubierta de nieve mediante autómatas celulares. Aplicación a escala de cordillera.

Se ha desarrollado un modelo de autómatas celulares parsimonioso para la estimación de la cubierta de nieve a partir de información de índices climáticos de precipitación y temperatura, modelo digital de elevaciones y una serie de reglas de interacción entre las variables. En una

primera aproximación se ha desarrollado un modelo con índices climáticos y parámetros agregados para toda la cordillera para posteriormente desarrollar un modelo distribuido con diferentes zonas climáticas. Para cada una de las zonas climáticas, definidas por series de precipitación y temperatura, se han calibrado los parámetros del modelo. Ambas metodologías han sido aplicadas a la cordillera de Sierra Nevada con resultados satisfactorios tanto en el proceso de calibración como en el de validación. La versión distribuida permite obtener mejores aproximaciones de la dinámica de la cubierta de nieve, y permite estudiar el comportamiento heterogéneo de dicha evolución, reflejado en los parámetros y series históricas.

- Evaluación de la recarga neta histórica en acuíferos mediante un modelo empírico de recarga neta. Aplicación a escala de España continental.

Se ha elaborado un modelo empírico parsimonioso de recarga para estimar la recarga neta en acuíferos sobre una malla regular de 10 km x 10 km para el caso de estudio de España continental. Usando datos históricos de recarga media y su varianza, que fueron obtenidos mediante el método de balance de masa de cloruro en un estudio previo, se ha definido un modelo que estima recarga neta a partir de la precipitación, temperatura y evapotranspiración real. Las series de recarga obtenidas para cada una de las celdas de la malla considerada han permitido evaluar la distribución espaciotemporal de la recarga.

- Propuesta de una metodología para la generación de escenarios potenciales de cambio climático teniendo en cuenta los estadísticos de sequías.

Se ha desarrollado una metodología para generar escenarios potenciales locales o regionales de cambio climático. Se exploraron diferentes enfoques conceptuales y técnicas de corrección. Se propuso un análisis multi-criterio para la definición de ensamblados de escenarios no equiprobables teniendo en cuenta estadísticos de sequías. La metodología ha sido aplicada a la cuenca del Alto Genil, donde se obtuvieron variaciones cercanas al -27% en precipitación y +32% en temperatura en el horizonte 2071-2100 para el escenario de emisiones más pesimista, RCP8.5.

- Propagación de los impactos potenciales de cambio climático a la cubierta de nieve y a la recarga neta en acuíferos. Aplicación a escala de cordillera y de país respectivamente.

Para la propagación de impactos de escenarios potenciales futuros de cambio climático a la cubierta de nieve y en la recarga subterránea se han utilizado los modelos descritos anteriormente. La simulación con el modelo de autómata celular de las series climáticas futuras generadas para el horizonte 2071-2100 considerado el escenario de emisiones RCP8.5, muestra significativas reducciones en la cubierta de nieve en Sierra Nevada, alrededor de un 60% en media. Además las series futuras de precipitación y temperatura generadas muestran que los impactos potenciales del cambio climático aumentarán con la altitud en el caso de la temperatura y disminuirán con la altitud en el caso de la precipitación. La propagación con el modelo empírico de recarga neta proporciona reducciones en la recarga en el 99.8% de la España Peninsular, las cuales se distribuyen muy heterogéneamente. Más de 2/3 del área muestra reducciones superiores al 10%, siendo la media de las reducciones obtenida en el

territorio el 12%. En algunas zonas mediterráneas (la región que más sufrirá los efectos del CC) se han obtenido reducciones medias de hasta el 25%. Estos resultados reflejan la necesidad de que se establezcan las medidas necesarias para elaborar políticas de agua basadas en la adaptación y mitigación de los efectos del cambio climático en los sistemas de recursos hídricos.

Por otro lado, durante el desarrollo de los trabajos realizados en el marco de la tesis doctoral se han detectado una serie de limitaciones. A continuación se recogen las principales limitaciones que pueden constituir al mismo tiempo potenciales líneas de investigación futuras.

Los estudios preliminares realizados han detectado una inversión del gradiente pluviométrico en la cuenca del Alto Genil del que se ha concluido que es real y que posiblemente esté agravado por el fenómeno del “undercatch”. La evaluación de este fenómeno supone una línea de investigación futura de interés.

Los modelos de regresión analizados/propuestos para estimar la distribución de los espesores de nieve no incluyen ninguna variable explicativa dependiente del tiempo, por lo que no permiten aproximar la dinámica temporal en la estimación. Por otro lado, a partir de las estimaciones de espesores de nieve obtenidas con el modelo de regresión con krigaje de residuos se ha cuantificado preliminarmente el equivalente de agua en la nieve en la cordillera. El equivalente de agua en la nieve depende del espesor, la cubierta y la densidad de la nieve. Las dos primeras han sido estudiadas/modeladas en este trabajo, pero para la densidad se ha asumido un valor constante por falta de datos. Normalmente la densidad en un paquete puede tener importantes variaciones espaciotemporales e incluso en el propio espesor. Esto supone una limitación de la metodología que a la vez define una potencial línea de investigación futura.

La optimización de la red de monitoreo de espesor de nieve se ha realizado de forma que la incertidumbre de estimación sea la menor posible pero no se han considerado aspectos de coste de operación para la toma de datos relacionados con la accesibilidad al punto de monitoreo. Este criterio se podría incluir en la definición de la ubicación óptima de pértigas de monitoreo.

En la aplicación de la metodología para la generación de escenarios climáticos futuros, las series históricas disponibles no eran lo suficientemente largas para realizar, explícitamente, una calibración y una validación del modelo. Por ese motivo el análisis multi-criterio para el ensamblado de escenarios se basó en los resultados obtenidos en el periodo de calibración. Sería interesante evaluar otros casos de estudio donde la información sea lo suficientemente larga para realizar una validación explícita de los modelos.

En esta tesis se evalúan los impactos potenciales del cambio climático en la cubierta de nieve y en la recarga neta. Sin embargo, no se han analizado impactos en otras variables relacionadas con la evolución de los recursos almacenados de forma natural en la nieve o en sistemas acuíferos. Por ejemplo, sería interesante desarrollar un modelo que combine las

variables espesor, cubierta y densidad de nieve para propagar los impactos potenciales del cambio climático sobre el equivalente de agua en la nieve.

Palabras clave: cambio climático, modelos regionales de clima, paquetes de nieve, aguas subterráneas

Referencias del resumen extendido

- AEMET (Spanish Meteorological Agency). 2009. Generación de Escenarios Regionalizados de Cambio Climático Para España; Agencia Estatal de Meteorología (Ministerio de Medio Ambiente y Medio Rural y Marino): Madrid, Spain.
- Barnett, T.P., Adam, J.C., Lettenmaier, D.P. 2005. Potential impacts of a warming climate on water availability in snowdominated regions. *Nature*, 438, 7066, 303–309.
- Bormann, K.J., Westra, S., Evans, J.P., McCabe, M.F. 2013. Spatial and temporal variability in seasonal snow density. *Journal of Hydrology*, 484, 63-73.
- Coes, A.L., Spruill, T.B., Thomasson, M.J. 2007. Multiple-method estimation of recharge rates at diverse locations in the North Caroline Coastal Plains, USA. *Hydrogeology Journal*, 15, 773-788.
- CORDEX PROJECT. 2013. The Coordinated Regional Climate Downscaling Experiment CORDEX. Program sponsored by World Climate Research Program (WCRP). Available at: <http://wcrp-cordex.ipsl.jussieu.fr/>
- Dragoni, W., Sukhiga, B.S. 2008. Climate change and groundwater: a short review. *Geol. Soc. Lond. Spec. Publ.*, 288, 1–12.
- Haberlandt, U. 2007. Geostatistical interpolation of hourly precipitation from rain gauges and radar for a large-scale extreme rainfall event. *J. Hydrol.*, 332, 144–157.
- Harshburger, B.J., Humes, K.S., Walden, V., Blandford, T.R., Moore, B.C., Dezzani, R.J. 2010. Spatial interpolation of snow water equivalency using surface observations and remotely sensed images of snow-covered area. *Hydrological Processes*, 24, 10, 1285-1295.
- Iglesias, A., Garrote, L., Flores, F., Moneo, M. 2007. Challenges to Manage the Risk of Water Scarcity y Climate Change in the Mediterranean. *Water Resour. Manag.*, 21, 775–788.
- Immerzeel, W., Petersen, L., Ragettli, S., Pellicciotti, F. 2014. The importance of observed gradients of air temperature and precipitation for modeling runoff from a glacierized watershed in the Nepalese Himalayas. *Water Resour. Res.*, 50, 3, 2212–2226.
- IPCC, 2014: Climate Change 2014: Synthesis Report. Contribution of Working Groups I, II and III to the Fifth Assessment Report of the Intergovernmental Panel on Climate Change [Core Writing Team, R.K. Pachauri and L.A. Meyer (eds.)]. IPCC, Geneva, Switzerland, 151 pp.

- Lerner, D.N., Issar, A.S., Simmers, I. 1990. Groundwater recharge. A guide to understanding and estimating natural recharge. IAH International Contributions to Hydrogeology. 8. Heise, Hannover. 345 pp.
- Lindström, G., Johansson, B., Persson, M., Gardelin, M., Bergström, S. 1997. Development and test of the distributed HBV-96 hydrological model. *Journal of Hydrology*, 201, 272–288.
- López-Moreno, J.I., Nogués-Bravo, D. 2006. Interpolating local snow depth data: an evaluation of methods. *Hydrol. Process.*, 20, 2217–2232.
- Martinec, J., Rango, A., Roberts, R. 2008. Snowmelt Runoff Model SRM User's Manual. New Mexico State University 178 pp.
- McIntyre, O. 2017. EU legal protection for ecologically significant groundwater in the context of climate change vulnerability. *Water International*, 42, 6. doi:10.1080/02508060.2017.1351060
- McMahon, P.B., Plummer, L.N., Bohlke, J.K., Shapiro, S.D., Hinkle, S.R. 2011. A comparison of recharge rates in aquifers of the United States based on groundwater-based data. *Hydrogeology Journal*, 19, 779–800.
- Mir, R.A., Jain, S.K., Saraf, A.K., Goswami A. 2015. Accuracy assessment and trend analysis of MODIS-derived data on snow-covered areas in the Sutlej basin, Western Himalayas. *International Journal of Remote Sensing*, 36, 15, 3837-3858.
- Piani, C., Weedon, G.P., Best, M., Gomes, S.M., Viterbo, P., Hagemann, S., Haerter, J.O. 2010. Statistical bias correction of global simulated daily precipitation and temperature for the application of hydrological models. *J. Hydrol.*, 395, 199–215.
- Räisänen, J., Räty, O. 2013. Projections of daily mean temperature variability in the future: cross-validation tests with ENSEMBLES regional climate simulations. *Climate Dynamics*. doi:10.1007/s00382-012-1515-9.
- Scanlon, B.R., Healy, R.W., Cook, P.G. 2002. Choosing appropriate techniques for quantifying groundwater recharge. *Hydrogeology Journal*, 10, 18-39.
- Scanlon, B.R., Keese, K.E., Flint, A.L., Flint, L.E., Gaye, C.B., Edmunds, W.M., Simmers, I. 2006. Global synthesis of groundwater recharge in semiarid and arid regions. *Hydrological Processes*, 20, 3335–3370.
- Steger, C., Kotlarski, S., Jonas, T., Schär, C. 2013. Alpine snow cover in a changing climate: a regional climate model perspective, *Clim. Dynam.*, 41, 735–754.
- UN (United Nations). 2009. Guidance on Water and Adaptation to Climate Change, ECE/MR/WAT/30, United Nations, Geneva.

Voss, R., May, W., Roeckner, E. 2002. Enhanced resolution modeling study on anthropogenic climate change: changes in extremes of the hydrological cycle. *Int. J. Climatol.*, 22, 755-777.

Watanabe, S., Kanae, S., Seto, S., Yeh, P.J.F., Hirabayashi, Y., Oki, T. 2012. Intercomparison of bias-correction methods for monthly temperature and precipitation simulated by multiple climate models. *Journal of Geophysical Research*, 117, D23114. doi:10.1029/2012JD018192.

Summary

Climate change represents one of the greatest challenges that society will face in the coming decades. From a hydrological perspective, climate change will greatly modify the spatiotemporal distribution of water resources. The assessment of potential impacts of climate change on a water system inevitably involves the propagation of uncertainties, but this should not be used as an excuse for delay or inaction to address these impacts. A country's water resources policy must consider the future impacts of climate change, since water resources systems can be very vulnerable. Resources stored as groundwater or as snow can play a fundamental role in defining adaptation strategies to climate change that can allow sustainable supply of water demands.

The objective of the pre-doctoral research undertaken and presented in this thesis was to advance the development and application of methodologies for evaluating potential impacts of climate change on water resources stored naturally in aquifers and/or in snowpack in systems covering large tracts of land. The snow dynamics of the Spanish Sierra Nevada mountain range were studied, as well as potential future recharge scenarios in aquifers on a national scale. The majority of scientific studies of the impacts of climate change on groundwater resources have been developed for aquifer scale systems. In contrast, snow dynamics are usually studied for specific mountain slopes or basins, while analyses on the scale of an entire mountain range are unusual. Data in alpine systems are usually scarce, due to poor accessibility and limited funds. A methodology is proposed to estimate the optimal siting of monitoring points. Assessing the impacts of climate change requires local or regional climate scenarios adapted to the system to be generated. A methodology is proposed that uses drought statistics to define these scenarios. A review of the state of the art highlights that, despite the importance of droughts in the management of arid and semi-arid zones, drought statistics are not considered in the generation of future local and regional scenarios. Although there are numerous analyses of droughts for historical periods, few are dedicated to future scenarios. It is precisely these requirements and data gaps that provided the motive to develop this research work.

The methodological framework proposed in the doctoral thesis requires (1) a spatiotemporal analysis of the historical distribution of meteorological variables and their relationship with elevation, and the generation of fields of these variables using geostatistical techniques; (2) development of models to estimate and simulate the variables that influence the availability of water in snowpack and/or in aquifers (snow depth, snow cover and recharge); (3) generation of potential climate change scenarios for the meteorological variables of interest; (4) propagation of the potential impacts of climate change on hydrological variables using the models developed.

The proposed methodologies were applied to three case studies at the scale of basin, mountain range and nation.

The relationship of the main climatic variables (precipitation and temperature) with elevation in the Alto Genil basin (Granada province, southern Spain) was investigated. An inversion of

the precipitation gradient with elevation was detected at an elevation of around 1600 m. The possible causes, including systematic errors in snow measurement (undercatch of solid precipitation) were discussed and noted. The analysis of these gradients with elevation was used as secondary information to generate precipitation fields using various geostatistical techniques and time scales. A sensitivity analysis revealed wide differences between estimates produced using the different techniques and a poor sensitivity to the time scale (monthly or annual) used to define the climate variogram.

A parsimonious methodology using regression kriging is proposed for estimating snow depth in alpine systems. This method was developed using snow depth data from the Programme to Evaluate Water Resources from Snowmelt (dubbed ERHIN in Spanish) undertaken by the General Directorate for Water in Spain. In the case of Sierra Nevada, existing information is scarce. Monitoring is done at 23 points (snow stakes) and the frequency of measurement is once or twice a year. The snowpack has been estimated using explanatory variables that can be estimated from a digital elevation model and snow cover data from satellite information. The proposed methodology gave satisfactory results when applied to the Sierra Nevada mountain range, as demonstrated from the cross validation experiment performed. A multi-objective analysis of the regression models led to the conclusion that the key variables for estimating snow depth in the Spanish Sierra Nevada are elevation, northness and slope.

Based on these regression models obtained, a methodology was developed to optimise the sampling network for monitoring snow depth at the mountain-range scale. This methodology minimises the error in calculating snow depth by considering two sources of uncertainty: regression model and kriging. Various optimisation hypotheses were proposed regarding the increase, decrease and number of stakes added or eliminated in each step. These hypotheses were applied to the case of the Sierra Nevada mountain range, with the result that a new configuration of the monitoring network is obtained that reduces the overall uncertainty of the estimates.

Cellular automata techniques were applied to estimate snow cover area by using parsimonious lumped and distributed models. The inputs of these models were defined by using series and/or fields of precipitation and temperature, and a digital elevation model. A number of rules of interaction between input variables were calibrated to estimate the dynamics of the snow cover area, minimising the difference between estimates and observations (satellite products) of the snow cover area variable. Both models, lumped and distributed, were applied to the Sierra Nevada mountain range with satisfactory results, as demonstrated by the results obtained in the validation phase.

An empirical model was proposed to estimate the net recharge to aquifers on a regular 10 km x 10 km grid at the scale of continental Spain. It is a parsimonious model that simulates net recharge from precipitation, temperature and actual evapotranspiration. The model was calibrated using historical data of average recharge and its variance obtained by chloride mass balance method in a previous investigation.

A methodology was developed to generate potential local or regional climate change scenarios. Different conceptual approaches and correction techniques were explored. A multi-

criteria analysis was proposed to define ensembles of non-equi-feasible scenarios that take drought statistics into account. The methodology was applied to the Alto Genil basin, where variations close to -27% in precipitation and + 32% in temperature for the horizon 2071-2100 were obtained for the most pessimistic emissions scenario, RCP8.5.

The methods described above were applied to propagate the impacts of potential future scenarios of climate change to snow cover area and groundwater recharge. The simulation using the cellular automata model and the future climate series generated for the 2071-2100 horizon considering the RCP8.5 emission scenario, shows significant reductions in snow cover area in the Sierra Nevada – around 60% on average. Moreover, the future temperature and precipitation series generated indicate that the potential climate change in this alpine system at the highest elevations will be greater in the case of temperature and smaller in the case of precipitation. Propagation of net recharge using the empirical model predicts a reduction in recharge over 99.8% of peninsular Spain, distributed in a very heterogeneous way. A greater than 10% reduction in recharge was indicated over more than two thirds of the territory, while the average reduction predicted is 12%.

These results reflect the need to establish proper measures to devise water policies based on the adaptation and mitigation of the effects of climate change on water resources systems.

Keywords: climatic change, regional climate models, snowpacks, groundwater

Chapter 1: Introduction

In this chapter the fundamental motives for undertaking this research study are given. Some introductory reflections are made on the problem of climate change (CC) associated with greenhouse gas emissions, and the assessment of its effects on water resources systems of natural storage. Then the general and specific objectives of the doctoral thesis are specified and the structure of the remainder of the thesis is outlined. The chapter concludes with a list of references used.

1. Motive for undertaking this research study

CC linked to greenhouse gas emissions such as carbon dioxide represents one of the greatest challenges that society will face in coming decades. Global warming is unequivocal. Since the 1950s, we have observed unprecedented changes, such as the rise in temperature of the atmosphere and oceans, the decline in snow, ice and groundwater reserves and rises in sea level (IPCC, 2014). The Fifth Assessment Report of the Intergovernmental Panel on Climate Change (IPCC) includes four future trajectories or projections of anthropogenic carbon dioxide emissions for the twenty-first century, called representative concentration pathways (RCPs). These trajectories include a mitigation scenario (RCP2.6), two intermediate scenarios (RCP4.5 and RCP6.0), and a scenario with a high level of emissions (RCP8.5). Scenarios lacking additional efforts by society to limit emissions give rise to trajectories between RCP6.0 and RCP8.5.

From the point of view of water resources, CC will modify the spatiotemporal variability of climatic and hydrological variables that affect the availability of water in these systems. The most recent studies on CC project significant declines in water resources in the Mediterranean basin, leading to significant environmental, economic and social impacts (Iglesias et al., 2007). CC is also linked to an increase in the intensity and frequency of extreme events such as droughts or floods. While the northern and north-eastern Europe will be more prone to flooding, southern and south-eastern Europe will suffer a significantly more frequent droughts (Voss et al., 2002). The evaluation of the potential impacts of CC includes significant propagation of uncertainty through all its phases. However, these uncertainties should not be used as an excuse to delay the assessment of CC impacts because water resources systems can be very vulnerable (UN, 2009). Groundwater and snowpack can play a fundamental role in defining the CC adaptation strategies that will allow the sustainable supply of water demand (Barnett et al., 2005; Dragoni and Sukhiga, 2008). Of the two (groundwater and snowpack), groundwater offers greater flexibility for management of resources, since water abstractions can be made more or less immediately and at any time of the year. The impact of CC on groundwater is a topic that has been addressed by the scientific community since the 1990s, and its interest has increased in recent years (McIntyre, 2017). Concerning the other topic, snowmelt occurs naturally in specific periods according to weather conditions. In alpine basins, snow is essential, not only from the economic point of view of the tourism industry, but also in the management of water resources. In alpine systems where the majority of

precipitation is solid, water resources are available from the snowmelt, but the spatiotemporal distribution of snowmelt is highly sensitivity to CC (Steger et al., 2013).

Water storage in these systems is closely linked to the regional climate. Changes in temperature and precipitation can significantly impact natural water storage systems (Piani et al., 2010). These variations directly influence the hydrological variables that condition the availability of water. The evaluation of aquifer recharge from precipitation is crucial when renewable groundwater resources are quantified. This aspect is of great interest to design adequate water policies in any country. Similarly, in alpine systems, snow water equivalent depends on the depth, cover and density of the snow and it is also closely related to precipitation and temperature.

The study of CC impacts on water resources systems requires prior knowledge and characterisation of the historical distribution of the main climatic variables, precipitation and temperature. In general, orographic variables have an important influence on the spatial distribution of temperature and precipitation. When climatological variables are analysed, elevation is a fundamental conditioning variable that can be used as secondary information when there is insufficient information to characterise the system. It is usually accepted that the temperature falls and precipitation rises with elevation but this is not always the case (Immerzeel et al., 2014). Therefore, adequate study of the elevation gradients of the climatic variables is required. The information that these gradients provide is sometimes essential for the completion of data on hydrological problems using geostatistical estimation techniques (Haberlandt, 2007).

The propagation of CC impacts requires that mathematical models be calibrated in order to relate climatic variables to hydrological variables, whether for groundwater or snowpack resources. In terms of snowpack resources, interpolation and geostatistical simulation models have been used to calculate snow depth (López-Moreno and Nogués-Bravo, 2006), snow cover area (Mir et al., 2015) and density (Bormann et al., 2013), or snow water equivalent directly (Harshburger et al. al., 2010). Conceptual hydrological models (*e.g.* HBV (Lindström et al., 1997), Snowmelt Runoff Model (SRM) (Martinec et al., 2008)) allowed the processes that affect the evolution of the snow water equivalent dynamics to be approximated. The majority of scientific studies of snow resources have been carried out at mountain slope or basin scale. Meanwhile, when considering groundwater resources, recharge is the variable that conditions the distribution of renewable resources in aquifers, and this can be calculated using various techniques (tracer tests, physical, numerical and/or empirical models) (Lerner et al., 1990; Scanlon et al., 2002, 2006; Coes et al., 2007; McMahon et al., 2011). Recharge models are generally applied at aquifer scale.

The propagation of CC impacts using these models also requires the prior generation of potential future climate scenarios in order to evaluate impacts on snowpack or groundwater storage. Regional climate models provide information about the potential changes that will occur in precipitation and temperature from probable trajectories of greenhouse gas emissions (representative concentration pathways, RCP). The most recent emission scenarios published by the IPCC (IPCC, 2014) were simulated using physical climate models to produce future

projections within the framework of different European projects, such as CORDEX (2013); the results are available as open source information. In order that such information can be applied to hydrological problems, regional or local climate scenarios need to be generated based on the information provided by regional climate models. These scenarios are generated by applying statistical correction techniques to the series or historical fields and the simulations made by the climate models. There are numerous statistical correction techniques that can be used; they fall into two conceptual approaches, namely bias correction and delta change (Watanabe et al., 2012; Räisänen and Räty, 2013). Ensembles of projections obtained using different climate models and different statistical correction techniques can be considered in order to obtain more robust predictions (AEMET, 2009). These ensembles can be defined by giving more weight to the models which, when simulating the historical period (simulation of control), better approximate the statistics for that period. The most basic statistics are usually considered, including mean and standard deviation, with little attention given to drought statistics, despite their importance in arid and semi-arid zones.

This research has been undertaken in response to the need to advance the development and application of methodologies for assessing the potential CC impacts on water resources stored in aquifers and/or snowpacks in systems that cover large territories. This dissertation presents the assessment of snow dynamics in the Spanish mountain range of Sierra Nevada, and the potential future recharge scenarios in aquifers at a national scale.

Most scientific work to date on CC impacts on groundwater resources have been undertaken on aquifer scale systems. In contrast, snow dynamics are usually studied for specific mountain slopes or basins, while analysis at mountain range scale is unusual. In these alpine systems, data are usually scarce, due to poor accessibility and limited funds. Here, a methodology was proposed to estimate the optimal location of the monitoring points. Assessing the impacts of climate change requires local or regional climate scenarios adapted to the system to be generated. A methodology is proposed that uses drought statistics to define these scenarios. A review of the state of the art highlighted that, despite the importance of droughts in the management of arid and semi-arid zones, drought statistics are not considered in the generation of future local and regional scenarios. Although there are numerous analyses of droughts for historical periods, few are dedicated to future scenarios. It is precisely these requirements and data gaps that provided the motive to undertake this research work.

2. General objectives

In accordance with the motives outlined in the previous section, the main purpose of the doctoral thesis is to develop tools and methodologies for the study of potential impacts of CC on resources stored in aquifers and/or snowpacks systems that cover large areas of land. These methodologies were applied at basin, mountain range and peninsular Spain scale systems. That general objective incorporates the following specific objectives:

- (1) Study of gradients of precipitation and temperature with elevation, generation of historical precipitation fields using geostatistical techniques and elevation as secondary information for estimation.

- (2) Development of a methodology applicable at the mountain range scale to estimate snow depth using geostatistical techniques.
- (3) Optimisation of the snow monitoring network to reduce uncertainty in snow depth estimates. Application at mountain range scale.
- (4) Development of a model to simulate the dynamics of snow cover area using a cellular automata model. Application at mountain range scale.
- (5) Evaluation of historical net recharge in aquifers through an empirical model of net recharge. Application at continental Spain scale.
- (6) Proposal of a methodology to generate potential scenarios of CC that takes drought statistics into account.
- (7) Propagation of the potential impacts of CC on snow cover area and net recharge in aquifers. Application at mountain range and country scale, respectively.

3. Case studies

Though the objectives of the doctoral thesis are mainly methodological, case studies are required to assess the applicability of the proposed methodologies. All the case studies selected to apply the research developed in this thesis are located in peninsular Spain, which is very vulnerable to the potential future effects of CC. They are the Alto Genil basin, the Sierra Nevada mountain range and continental Spain. The Alto Genil basin and Sierra Nevada are located in the Mediterranean area, which is especially vulnerable to CC (Iglesias et al., 2007). The case studies are included in the chapters where the methodologies are presented and applied.

4. Thesis outline

The thesis is organised into nine chapters whose content is summarised below.

In the first introductory chapter we have outlined the reasons why the doctoral thesis is developed and its objectives. It is a doctoral thesis by compendium of seven articles. Six of them have been published (the remaining one is under review) in journals indexed in the Journal Citation Report (JCR). Each of the published articles is included in the appropriate chapter of the thesis (from 2 to 8), which includes the research carried out to achieve the partial objectives, described above. Each article or chapter constitutes a research study in its own right, with different organisation but maintaining the customary structure of a scientific paper. Tables and figures are included at the end of each chapter. Table 1.1 shows the objectives addressed in each chapter and the journals in which the corresponding studies were published.

Chapter	Contributing to objective	Published in:
2	(1)	International Journal of Climatology
3	(2)	Hydrological Processes
4	(3)	Hydrological Processes (under review)
5	(4)	Journal of Hydrology
6	(6)	Water
7	(4) y (7)	Advances in Water Resources
8	(5) y (7)	Journal of Hydrology

Table 1.1. List of articles (chapters) that form part of the doctoral thesis, objectives they address, and journals in which they have been published.

In Chapter 2 the precipitation and temperature gradients with elevation in the Alto Genil basin (southeastern Spain) are analysed. The possible causes of the inverse precipitation gradient observed at high elevations are discussed, including systematic errors in the measurement of snow (undercatch of solid precipitation). Precipitation fields are generated by geostatistical estimation. Different techniques and time scales are evaluated to define variograms by means of a cross validation experiment. Elevation was incorporated as secondary information for the estimation.

In Chapter 3 a methodology that uses regression kriging to calculate snow depth in the Spanish Sierra Nevada mountain range is presented. The information used for the estimates are specific measurements (from the 23 snow stakes of the ERHIN programme), a digital elevation model and snow cover area from satellite information. Several model structures of varying complexity were assessed by means of a multi-objective analysis that takes into account different indexes of goodness of fit. The proposed methodology allows identification of which explanatory variables (geographic, orographic and climatic) are the most important to analyse the spatial distribution of snow depth.

In Chapter 4 a methodology is developed to optimise the snow depth monitoring network in the Sierra Nevada. The method is based on the regression model that best fits the historical period. Various hypotheses were studied to define the optimal expansion or contraction of the current observation network (23 stakes). The most applicable alternative will depend on the funds available for monitoring. In addition, a methodology combining these two hypotheses (expansion or contraction of the network) was developed, which designs a new optimal siting of the existing 23 stakes.

In Chapter 5 a methodology is designed to approximate the dynamics of snow cover area in mountain systems based on evolutionary algorithms of cellular automata. It is a parsimonious methodology that uses climatic indices of precipitation and temperature and a digital model of elevations to simulate the evolution of the snow cover area. The model determines if a cell will be covered by snow or not by applying a series of rules that involve the climatic variables and the elevation of the cell in question and its neighbours. This methodology was applied to the Sierra Nevada, obtaining satisfactory results in the calibration and validation of the model.

Chapter 6 presents a methodology for the generation of potential CC scenarios that uses several regional climate models and various approaches and correction techniques. More robust ensembles of future scenarios are obtained by using those that best fit the historical information for the control period. The various models and correction techniques are selected through a multi-objective analysis that considers basic and drought statistics. This methodology was applied to the case study of the Alto Genil basin, indicating that precipitation would be reduced and temperatures would rise significantly under the hypotheses considered.

In Chapter 7 an extension of the lumped model of cellular automata developed in Chapter 5 is presented. This extension generates a distributed model by using different climatic zones. For each zone (each defined by the climatic indices of precipitation and temperature) the parameters of the model are calibrated. In addition, the methodology for generating potential CC scenarios is applied. By this means, a future series to propagate potential CC impacts to snow cover area in the Sierra Nevada is defined. The case study reveals alarming results with respect to the reduction of the area covered by snow in the future long term and under the most pessimistic emissions scenario.

In Chapter 8, an empirical recharge model is developed at the scale of continental Spain. It allows assessment of the spatiotemporal distribution of net recharge to aquifers as a function of climatic conditions. Potential future climate scenarios were generated by applying the methodology proposed in Chapter 6; their impacts on net recharge were simulated by propagating them using the recharge model. The results indicate significant reductions in recharge, especially in the Mediterranean regions.

The final chapter (Chapter 9) draws general conclusions from the research. It also summarises possible future lines of research that were identified during the development of the research undertaken in preparation of this doctoral thesis.

References

- AEMET (Spanish Meteorological Agency). 2009. Generación de Escenarios Regionalizados de Cambio Climático Para España; Agencia Estatal de Meteorología (Ministerio de Medio Ambiente y Medio Rural y Marino): Madrid, Spain.
- Barnett, T.P., Adam, J.C., Lettenmaier, D.P. 2005. Potential impacts of a warming climate on water availability in snowdominated regions. *Nature*, 438, 7066, 303–309.
- Bormann, K.J., Westra, S., Evans, J.P., McCabe, M.F. 2013. Spatial and temporal variability in seasonal snow density. *Journal of Hydrology*, 484, 63-73.
- Coes, A.L., Spruill, T.B., Thomasson, M.J. 2007. Multiple-method estimation of recharge rates at diverse locations in the North Caroline Coastal Plains, USA. *Hydrogeology Journal*, 15, 773-788.

CORDEX PROJECT. 2013. The Coordinated Regional Climate Downscaling Experiment CORDEX. Program sponsored by World Climate Research Program (WCRP). Available at: <http://wcrp-cordex.ipsl.jussieu.fr/>

Dragoni, W., Sukhiga, B.S. 2008. Climate change and groundwater: a short review. *Geol. Soc. Lond. Spec. Publ.*, 288, 1–12.

Haberlandt, U. 2007. Geostatistical interpolation of hourly precipitation from rain gauges and radar for a large-scale extreme rainfall event. *J. Hydrol.*, 332, 144–157.

Harshburger, B.J., Humes, K.S., Walden, V., Blandford, T.R., Moore, B.C., Dezzani, R.J. 2010. Spatial interpolation of snow water equivalency using surface observations and remotely sensed images of snow-covered area. *Hydrological Processes*, 24, 10, 1285–1295.

Iglesias, A., Garrote, L., Flores, F., Moneo, M. 2007. Challenges to Manage the Risk of Water Scarcity y Climate Change in the Mediterranean. *Water Resour. Manag.*, 21, 775–788.

Immerzeel, W., Petersen, L., Ragettli, S., Pellicciotti, F. 2014. The importance of observed gradients of air temperature and precipitation for modeling runoff from a glacierized watershed in the Nepalese Himalayas. *Water Resour. Res.*, 50, 3, 2212–2226.

IPCC, 2014: Climate Change 2014: Synthesis Report. Contribution of Working Groups I, II and III to the Fifth Assessment Report of the Intergovernmental Panel on Climate Change [Core Writing Team, R.K. Pachauri and L.A. Meyer (eds.)]. IPCC, Geneva, Switzerland, 151 pp.

Lerner, D.N., Issar, A.S., Simmers, I. 1990. Groundwater recharge. A guide to understanding and estimating natural recharge. IAH International Contributions to Hydrogeology. 8. Heise, Hannover. 345 pp.

Lindström, G., Johansson, B., Persson, M., Gardelin, M., Bergström, S. 1997. Development and test of the distributed HBV-96 hydrological model. *Journal of Hydrology*, 201, 272–288.

López-Moreno, J.I., Nogués-Bravo, D. 2006. Interpolating local snow depth data: an evaluation of methods. *Hydrol. Process.*, 20, 2217–2232.

Martinec, J., Rango, A., Roberts, R. 2008. Snowmelt Runoff Model SRM User's Manual. New Mexico State University 178 pp.

McIntyre, O. 2017. EU legal protection for ecologically significant groundwater in the context of climate change vulnerability. *Water International*, 42, 6. doi:10.1080/02508060.2017.1351060

McMahon, P.B., Plummer, L.N., Bohlke, J.K., Shapiro, S.D., Hinkle, S.R. 2011. A comparison of recharge rates in aquifers of the United States based on groundwater-based data. *Hydrogeology Journal*, 19, 779–800.

- Mir, R.A., Jain, S.K., Saraf, A.K., Goswami A. 2015. Accuracy assessment and trend analysis of MODIS-derived data on snow-covered areas in the Sutlej basin, Western Himalayas. *International Journal of Remote Sensing*, 36, 15, 3837-3858.
- Piani, C., Weedon, G.P., Best, M., Gomes, S.M., Viterbo, P., Hagemann, S., Haerter, J.O. 2010. Statistical bias correction of global simulated daily precipitation and temperature for the application of hydrological models. *J. Hydrol.*, 395, 199–215.
- Räisänen, J., Räty, O. 2013. Projections of daily mean temperature variability in the future: cross-validation tests with ENSEMBLES regional climate simulations. *Climate Dynamics*. doi:10.1007/s00382-012-1515-9.
- Scanlon, B.R., Healy, R.W., Cook, P.G. 2002. Choosing appropriate techniques for quantifying groundwater recharge. *Hydrogeology Journal*, 10, 18-39.
- Scanlon, B.R., Keese, K.E., Flint, A.L., Flint, L.E., Gaye, C.B., Edmunds, W.M., Simmers, I. 2006. Global synthesis of groundwater recharge in semiarid and arid regions. *Hydrological Processes*, 20, 3335–3370.
- Steger, C., Kotlarski, S., Jonas, T., Schär, C. 2013. Alpine snow cover in a changing climate: a regional climate model perspective, *Clim. Dynam.*, 41, 735–754.
- UN (United Nations). 2009. Guidance on Water and Adaptation to Climate Change, ECE/MR/WAT/30, United Nations, Geneva.
- Voss, R., May, W., Roeckner, E. 2002. Enhanced resolution modeling study on anthropogenic climate change: changes in extremes of the hydrological cycle. *Int. J. Climatol.*, 22, 755-777.
- Watanabe, S., Kanae, S., Seto, S., Yeh, P.J.F., Hirabayashi, Y., Oki, T. 2012. Intercomparison of bias-correction methods for monthly temperature and precipitation simulated by multiple climate models. *Journal of Geophysical Research*, 117, D23114. doi:10.1029/2012JD018192.

Chapter 2: Precipitation fields in an alpine Mediterranean catchment: Inversion of precipitation gradient with elevation or undercatch of snowfall?

Received: 26 September 2017 | Revised: 26 January 2018 | Accepted: 28 February 2018 | Published on: 25 March 2018
DOI: 10.1002/joc.5517

International Journal
of Climatology 

RESEARCH ARTICLE

Precipitation fields in an alpine Mediterranean catchment: Inversion of precipitation gradient with elevation or undercatch of snowfall?

Antonio-Juan Collados-Lara¹  | Eulogio Pardo-Igúzquiza² | David Pulido-Velazquez¹ |
Jorge Jiménez-Sánchez¹

Antonio-Juan Collados-Lara^(1,*), Eulogio Pardo-Igúzquiza⁽²⁾, David Pulido-Velazquez⁽¹⁾,
Jorge Jiménez-Sánchez⁽¹⁾

(1) Instituto Geológico y Minero de España, Urb. Alcázar del Genil, 4. Edificio Zulema Bajo, 18006, Granada (Spain). E-mails: aj.collados@igme.es, d.pulido@igme.es, j.jimenez@igme.es

(2) Instituto Geológico y Minero de España, Ríos Rosas, 23, 28003 Madrid (Spain). E-mail: e.pardo@igme.es

* Corresponding author

Abstract

The mean precipitation measurements in a Mediterranean alpine catchment in Sierra Nevada show an inversion of the gradient with the altitude beyond a certain threshold. Is it due to a real pattern or it can be explained by systematic error of solid precipitation measurement in gauges? Can we assess climatic fields in an alpine catchment from gauge measurement? This paper describes a research developed to answer both questions in the Alto Genil Basin. As commonly happens in most of the basins, the spatio-temporal information from climate gauges is limited; therefore to reduce uncertainty in estimates of climatic fields, some secondary information should be introduced. Since orographic conditions clearly influence precipitation, the relationship between this climatic variable and elevation is usually included as secondary information into the estimates. However, while there is a clear relationship between temperature and elevation, the relationship between precipitation and elevation is not so simple. In this paper the analysis of the data performed allow us to demonstrate that there is a real inversion of the gradient within this Mediterranean Alpine area as other authors previously pointed in some tropical and sub-tropical zones. The intensity of this phenomenon

and the altitude threshold from which it appears can be altered as a consequence of the undercatch of the solid precipitation. To estimate precipitation fields, we have used different hypotheses about the intensity of the undercatch taking into account empirical corrections obtained for nearby mountain ranges. An analysis of the sensitivity of the results to the assumed undercatch hypothesis shows that it is not possible to estimate properly precipitation fields (the sensitivity of the results to the adopted hypothesis is high) in these alpine areas if we only have information about the precipitation measurements at the stations.

Keywords: climatic estimation, inverse precipitation gradient with elevation, snow undercatch, alpine basin, Alto Genil Basin.

1. Introduction

Generally, orographical conditions have a clear influence on the distributions of precipitation. The term “orographic precipitation” is used to define the modification or reorganisation of precipitation (liquid or solid) distribution when certain topographical characteristics are present (Smith 1979; Houze, 2012). This modification of precipitation is due to alterations in the topography-induced flow patterns close to the surface, which provokes a spatial variation of the precipitation deposition. This preferential deposition of precipitation has been investigated in some studies (e.g., Lehning et al., 2008; Gerber et al., 2017). Many studies show linear increases in precipitation with elevation (Daly et al., 1994; Lloyd, 2005; Yao et al., 2016). Nevertheless, in certain alpine areas in tropical and subtropical zones, such as the Andes Mountains, some African mountain ranges and the Himalaya Mountains, precipitation measurements do not increase with elevation above a certain point (Anders et al., 2006; Yang et al., 2011; Hirpa et al., 2010; Anders and Nesbitt, 2014). Others studies have focussed on understanding orographic precipitation on scales smaller than entire mountain ranges (e.g., Cosma et al., 2002; Minder et al., 2008). Small-scale orography (tens of km or less) can play an important role in preferential precipitation by forcing it into bands.

In several alpine systems, the majority of precipitation is solid, and orographic effects can govern the snowfall patterns (Dore and Choularton, 1992; Mott et al., 2014), or snow accumulation (Scipión et al., 2013; Kirchner et al., 2014). Some authors have investigated elevation gradients in snow accumulation, discovering inverse gradients above certain elevations (Grünwald and Lehning, 2011; Lehning et al., 2011). The processes that govern snow accumulation patterns are preferential deposition of precipitation, redistribution of snow by wind, sloughing and avalanching (Elder et al., 1991; Grünwald et al., 2014).

Such variations in the relationship between the precipitation measured and elevation may reflect a real change in the precipitation pattern with elevation; however, systematic errors in gauge measurement can modify this pattern. The aim of gauge systems measurement is to obtain representative samples of precipitation (liquid or solid). The catch of the gauge should represent the precipitation in the surrounding area; however, wind effects can reduce the catch of the gauge. These effects can be related to the geometry of the gauge or with obstacles on the wind trajectories, which are frequently more important. Although wind effects are the main sources of uncertainty, others errors of measurement can be induced by losses caused by wetting of the inner walls of the gauge, evaporation of water accumulated in the gauge, and

splashing of rain drops or blowing of snowflakes out of or into the container (Legates and Willmott, 1990; Prein and Gobiet, 2017). Solid precipitation is much more affected by wind effects than liquid precipitation. Thus in areas with significant snowfall, the phenomenon known as undercatch of solid precipitation should be considered.

Undercatch is a systematic error of precipitation measurement in gauges, which produces significant bias in measurements with respect to the real values. This phenomenon is especially significant in measurements of solid precipitation under windy conditions (Sevruk, 1991; Rasmussen et al., 2012), when gauges modify the wind fields producing significant errors in the measurement of solid precipitation (Goodison et al., 1988).

The undercatch issue has been studied for years. For example, Brown and Peck (1962) described some of the challenges of measuring precipitation. Sevruk (1982) proposed a method for correcting systematic errors in precipitation measurements for operational use. The World Meteorological Organization (WMO) has performed various tests within the framework of different projects. They started to develop the Solid Precipitation Intercomparison Experiment between 1987 and 1993 (Goodison et al., 1988), assessing and deriving adjustment functions for solid precipitation measurements. More recently, as part of the Solid Precipitation Intercomparison Experiment project of the World Meteorological Organization (WMO-SPICE) (2012-2015), similar issues were analysed in more depth, focussing mainly on the amount, intensity and type of precipitation (liquid, solid, mixed), over various time periods.

Proper identification and approximation of the true relationship between precipitation and elevation is important in assessing the available resources in a system, which is essential for a proper analysis of its management (Pedro-Mozonis et al., 2016). Available resources can be estimated using hydrological balance models, whose inputs are precipitation and temperature data (Escriba-Bou et al., 2017). These models can be based on elevation gradients, such as the Parameter-elevation Regressions on Independent Slopes Model (PRISM) that uses point data to generate gridded estimates of climatic variables (Daly et al., 1994). In alpine catchments, these balance models need to identify the processes related to snowpack. Appropriate analysis of snow processes requires an accurate assessment of the spatio-temporal distribution of precipitation. However, the number of precipitation gauges is usually restricted and, moreover, they provide limited information about the spatial distribution and overall precipitation in a system. Therefore, the estimated precipitation fields can change substantially depending on the hypothesis assumed or the approach adopted to approximate the relationship between precipitation and elevation.

Estimation of fields requires that their spatial correlation is captured. Geostatistical methods take spatial correlation of experimental data into account using the variogram function. Kriging is the most widely used geostatistical technique for estimating climatic variables. Several studies have used ordinary kriging (OK) to generate fields of climatic variables (Hunter and Meentemeyer, 2005; Chen et al., 2010). Sometimes, it can be useful to consider extra information by means of a secondary variable correlated with the target variable. Techniques such as kriging with external drift (KED) and regression kriging (RK) allow other

information to be incorporated into the estimate. KED has been extensively studied to assess whether precipitation is correlated to elevation (either positive or negative gradient) (Pardo-Iguzquiza, 1998; Goovaerts, 2000). The RK technique allows consideration of several secondary variables to calculate the target variable (Pardo-Iguzquiza et al., 2015; Hengl et al., 2007). Normally, elevation is the most commonly used secondary information for estimating climatic variables.

The objective of this paper is to assess climatological gradients of precipitation at catchment scale. We have analysed and approached the relationship between measurements of precipitation and elevation in an alpine basin (the Alto Genil Basin, southern Spain), where an inversion of the gradient between measured precipitation and elevation is observed and has not been previously analysed. We have compared this inverse precipitation gradient from a certain elevation with other cases studied previously. In addition, we intend to answer two questions: is the inverse precipitation gradient due to a real pattern or can it be explained by systematic error of the measurement of solid precipitation gauges? Can we assess climatic fields in an alpine catchment from gauge measurements?

The paper has been organised as follow. Section 2 describes the proposed methodology, based on the analyses of historical data and results of several estimation techniques under a set of hypotheses. Section 3 includes the description of the case study and the available data. Section 4 shows the results which are discussed in section 5. Finally, section 6 presents the main conclusions.

2. Methodology

We have assessed climatological gradients for precipitation and temperature. These gradients have been calculated from meteorological gauges using the mean for each variable over the period considered, and the elevation of the gauges. In the case of precipitation, different hypotheses have been considered in order to explain the observed inversion of the gradient with elevation. In addition, we estimated precipitation fields with different techniques in order to assess their sensitivity to the considered hypotheses. A flowchart of the methodology used is given in Figure 2.1.

2.1 Analysis of historical data (measurements and corrected values) vs elevation

We first analysed how the experimental data of precipitation varied with elevation. We studied how different regression models (linear and quadratic) calculate the relationship between this climatic variable with elevation, and how these variables are correlated at yearly and monthly scale.

Different hypotheses were considered to assess the changes in the pattern of precipitation with elevation beyond a certain threshold. We assume these changes are either real or are due to systematic errors in precipitation measurements, produced by undercatch of solid precipitation. Various empirical corrections of precipitation measurements have been developed in the framework of the WMO-SPICE. In this study, we applied one of the correction functions proposed by Buisan et al. (2017) for some Spanish Mountain Ranges.

These functions were not obtained for the mountain range in our case study (a catchment in the Spanish Sierra Nevada where no previous work on this issue has been done). Nevertheless, we apply one of these correction functions to perform a sensitivity analysis to the undercatch hypothesis assuming that these functions are also valid for our case. We used the 3-hour accumulation transfer function with higher R^2 , where the catch ratio (CR) is expressed as:

$$CR = 0.892 \text{EXP}(0.067T - 0.212W + 0.049Acc) \quad (1)$$

where T is temperature ($^{\circ}\text{C}$), W is wind speed (m/s) and Acc is accumulation (mm). The true accumulation ($TAcc$) in the gauge can be calculated using Equation 2.

$$TAcc = \frac{Acc}{CR} \quad (2)$$

The aim in this study was to correct the experimental data from the gauges located at elevation, where solid precipitation is commonplace. The threshold elevation from which we apply it was estimated as the median (percentile 50) of the snowline elevation for each month of the snow season (October to May) in the historical period with available information. In our case, the monthly snowline was calculated from the daily data provided by the MODIS/Terra Snow Cover Daily Global 500 m Grid (Data Set ID: MOD10A1) for the period 01/04/2000 to 30/09/2015. Note, that the cloudy days have been estimated applying linear interpolation of the closest previous and subsequent days without clouds (Collados-Lara et al., 2017).

The relationship between the corrected data and elevation was analysed in the same way as for the original experimental data at yearly and monthly scale. Comparing the difference between them (corrected and original data) at monthly scale during the snow season and outside this period we intend to identify if there is a real inversion of gradient (first of the objective of this paper).

2.2 Assessment of precipitation fields

Geostatistical methods of spatial estimation are known generically as kriging techniques and are optimal for assessing precipitation fields because they take into account the spatial correlation between experimental data (Matheron, 1963; Chiles and Delfiner, 1999). The usual way to include the spatial correlation in geostatistical estimations is using the variogram function (see Appendix 2A). Moreover, geostatistical techniques allow us to include the relationship of the target variable with a secondary variable in the estimation procedure in order to reduce the uncertainties of estimates.

The relationship between precipitation and elevation is included in the calculation of precipitation fields from the experimental and corrected data in order to fill the gaps in the limited information available about spatial distribution of the studied variables. In this paper we explore different hypotheses about the mathematical expressions (linear or quadratic functions) that give the best estimate of the relationship between climatic variables and

elevation, in accordance with the analysis of data previously performed (section 2.1). We have tested linear and quadratic estimates.

Another important issue is how the relationship between the climatic variable and elevation is integrated in the calculation of the fields. Two types of geostatistical techniques were considered, RK and KED. RK integrates the elevation information into a previously-defined regression model in a first procedure. The second procedure uses the residues of the regression to spatially interpolate using the OK technique. In KED the relationship between the climatic variables and elevation is integrated in the kriging process as external drift that influences the kriging parameters. The geostatistical techniques used are described in Appendix 2A.

We also tested the sensitivity of results to the temporal scale used. Two different spatial correlation models (yearly and monthly) were considered for the precipitation calculations. The first uses a single variogram and regression model for the year, while the second uses twelve variogram models and regression models for each month of the year. Sensitivity analysis was used to identify which model (yearly or monthly) provides more accurate estimates.

In order to analyse the estimation of precipitation fields we have performed the following tasks:

- We compared the relationship between the means of the estimated precipitation in each estimation cell and elevation for both the original measurements and the corrected values. A sensitivity analyses is performed in order to assess the significance of the differences obtained depending on the hypothesis.
- The influence of temporal scale adopted to define the variogram was also analysed, comparing the estimates at basin scale obtained under both hypotheses.
- The performance of each hypothesis and geostatistical approach was assessed using a cross validation experiment (described in Appendix 2B).

3. Case study and data

The study catchment is situated in southern Spain (Figure 2.2) and covers 2596 km². Its river ‘Genil’ is one of the most important in Andalusia and the largest in Granada province. Most of its flow comes from the Sierra Nevada mountain range, with its biggest inflow coming from snowmelt. Elevation varies between approximately 528 m and 3471 m (h data was from a digital elevation model with a spatial resolution of 5 metres, from the National Geographic Institute of Spain). Figure 2.2 shows the location of the available gauges that provide data in the period (1980-2014). Data were provided by AEMET, IFAPA, PNS and REDIAM Spanish agencies, comprising 119 precipitation gauges. This number includes all the stations located within the catchment plus those no further than 6 km outside its boundary. The temperature and wind data to apply the undercatch correction of precipitation were obtained from AEMET, IFAPA, PNS and REDIAM Spanish agencies, as per the precipitation data.

4. Results

4.1 Elevation relationship hypothesis

The assessment of climatological gradients with elevation over and near mountains is essential to understand patterns in the climatic variables. Normally, climatic variables vary linearly with elevation, having a positive precipitation gradient. However, in some cases topography can induce alterations in flow patterns or reorganisation of precipitation (liquid or solid) (Smith 1979; Houze, 2012). In our case study, we observe an inversion of the precipitation gradient (it become negative above a certain elevation) and a linear variation of temperature. The precipitation distribution is better approximated using a quadratic function, while the temperature distribution fits a linear function (see Figure 2.3). This pattern of an inversion of precipitation gradient has also been described for alpine basins in tropical and subtropical zones (Yang et al., 2011; Anders and Nesbitt, 2014). Nevertheless, in order to analyse other hypotheses to explain this issue, we performed a sensitivity analysis of the data to systematics errors in precipitation measurements due to undercatch of solid precipitation. Undercatch produces significant bias in measurements with respect to real values especially in measurements taken under windy conditions (Sevruk, 1991). We applied the transfer function proposed by Buisan et al. (2017) to experimental data located above a certain elevation during the snow season (October-May). This elevation has been calculated as the median of the snowline for each month (see Figure 2.4).

Figure 2.3 shows an inversion of the precipitation gradient at elevations above a threshold of 1600 m (original data) and 2200 m (modified data with the undercatch correction) for annual daily means. For a mean year, these points of gradient inversion change each month (See Table 2.1), indicating a seasonal behaviour. The point of inversion in the gradient using the original data is similar to the results obtained by others authors. In many places on the Tibetan Plateau and Himalaya mountains above 1500 metres, the precipitation-elevation gradient becomes negative (Anders et al., 2006; Yang et al., 2011). In high mountain ranges in the tropics, precipitation increases with elevation up to between 1000 and 2000 metres and then decreases with elevation (Hirpa et al., 2010; Anders and Nesbitt, 2014). When the undercatch correction is applied, the gradient inversion is moved to a higher elevation (above 2200 m). Others authors found similar results for snow deposition gradients in the Swiss Alps (e.g., Grünwald et al., 2014; Mott et al., 2014) and Sierra Nevada Mountains (California) (e.g., Kirchner et al., 2014).

A priori, one might consider that this inversion would be eliminated by applying a different correction function more appropriate for this area (as noted above, the function used was derived for other Spanish mountain ranges). However, if we analyse the months when there is no solid precipitation (June-September), an inversion of gradient is also seen, except for July, which is the month with the lowest mean precipitation (a mean of 0.0848 mm/day). Therefore, this gradient inversion cannot be explained exclusively by an undercatch of solid precipitation. There is a real inversion of the gradient within this Mediterranean alpine area, just as other authors (e.g. Anders et al., 2006; Hirpa et al., 2010) previously pointed in some tropical and sub-tropical zones. The intensity of this phenomenon would be reduced and the

altitude threshold from which it appears would be moved to higher altitudes as a consequence of the undercatch of the solid precipitation.

4.2 Spatio-temporal assessment of precipitation estimates

Daily precipitation was calculated using yearly and monthly models for a 1x1 km grid with 5082 cells using KED with linear and quadratic drift, and RK, within the domain defined in Figure 2.1. Thus precipitation estimates were made using three techniques (linear KED, quadratic KED and RK) and two variogram models (yearly and monthly). Figure 2.5 summarises the spatial distribution of the mean and standard deviation obtained for the daily precipitation variable. For KED techniques precipitation increases with elevation, in contrast to the RK technique where precipitation may decrease at higher elevations. In the remaining areas the spatial distribution of precipitation is very similar for the three techniques, although the values can change. Regarding the standard deviation of precipitation, the spatial distribution is similar for KED techniques (although the values are different) and RK shows a different spatial distribution of standard deviation.

The estimated precipitation shows a different kind of relationship, depending on the assumption and techniques applied, using both the original data (Figure 2.6) and the corrected data (Figure 2.7) and applying the undercatch hypothesis. The quadratic KED technique gives high precipitation at high elevations, despite the fact that the experimental data shows low precipitation at high elevations. The linear KED technique has a linear behaviour and does not reproduce the shape of the experimental data. The RK technique gives a shape closer to the experimental data but this does not imply that RK is the best approximation to the available data. A cross validation experiment is needed to determine the technique with lowest mean and mean squared error.

On the other hand using a monthly or a yearly variogram model does not lead to larger differences in the precipitation-elevation relationship. To determine the best approximation, a cross validation experiment is again useful. Figures 2.6 and 2.7 demonstrate that there are significant differences in the results obtained using one or other technique.

We also compared the relationship between estimated precipitation fields using original and modified data vs elevation in our estimates, using their trends (Figure 2.8). Although we show that there is a gradient inversion above a certain elevation for the original data (Figure 2.3), the two KED estimates show greater precipitation over the whole range of elevations. As commented above, only RK reproduces an inversion of the precipitation gradient, with the inversion point located at 1666 m for the original data or 2250 m for the modified data.

Note that despite having modified data above 2000 metres, the estimates change below this elevation to a variable degree, depending on the technique used, and this is due to the fact that kriging techniques assume spatial correlation of the target variable. Figure 2.8 also shows that the sensitivity of the precipitation fields to the adopted corrected field is significant (maximum mean differences of 0.84 mm/day, 0.75 mm/day and 1.38 mm/day, respectively for RK, LKED and QKED). This implies that further research about the corrections that should be applied in this area would be needed to make a proper assessment of rainfall fields.

Nevertheless, in our case study, the sensitivity of the results to the estimation method (maximum mean differences of 0.68 mm/day and 0.63 mm/day for the original and corrected data, respectively) is even comparable to the adopted data correction.

For the sensitivity analysis of results to the temporal scale adopted to define the variogram, we plotted the estimates of the original precipitation series in the basin for both yearly and monthly models in the same graphic. For the mean precipitation series obtained with KED (linear and quadratic) using the monthly variogram, we observe slightly larger standard deviation and slightly lower estimates (Figure 2.9). For the RK estimate, the yearly model standard deviation is slightly higher and the estimate is slightly lower. In all cases, the difference in estimates between the yearly and monthly models is small, and a cross-validation is needed to identify the best model with the original data and the corrected data hypothesis.

Figure 2.10 shows the results of the cross-validation experiment for the precipitation estimate using original and modified data. The monthly model gives better results in the cross validation experiment for all precipitation estimates when the mean error is considered. The mean-squared-error monthly model gives the best results for all cases, with the exception of RK for modified data, though the difference is small. The mean reduction of absolute mean error is 10.6% using the monthly model; the maximum and minimum reduction are 30.0% and 0% for LKED using modified data and RK using original data, respectively. In the case of mean squared error, the mean reduction using the monthly model is 3.2%, and the maximum and minimum reduction are 9.1% for QKED using original data and -2.7% for RK using modified data (the only method that does not lead to a reduction using the monthly model).

On the other hand, the cross-validation experiments allows us to determine which technique provides better estimates in terms of mean and mean squared error. Table 2.2 shows the mean and mean squared error for the three techniques. Despite RK being the technique that best reproduces the shape of the data, LKED is the technique that gives the best results in all the cases (modified data, original data, annual variogram and monthly variogram).

5. Discussion

Results suggest a real pattern of inverse precipitation gradient in the case study. This study is the first that points to this effect for the case study area, though throughout the world there are several cases where an inverse gradient is observed either for deposition (e.g., Hirpa et al., 2010; Anders and Nesbitt, 2014) or accumulation (e.g., Grünewald and Lehning, 2011; Lehning et al., 2011).

The studied mountain range is a natural barrier to air dynamics. The main flows of rain in the study area come from the Atlantic (West and South-West). The combination of these flows, with the Sierra Nevada Mountain and other mountain systems acting as barriers, induces the dry conditions in the “Tabernas Desert” (see Figure 2.11). However, the study catchment is situated on the north face of the mountain range, located inside the Intrabetic zone (see Figure 2.11). The flows arrive in the Intrabetic zone with more difficulty than the Atlantics flows through the Guadalquivir and its tributary valleys (García de Pedraza and García Vega, 1993).

In the case study, the rain flows arrive through the river Genil valley. According to the results obtained, we suggest one of the mechanisms by which mountains and hills affect precipitating clouds, as proposed by Houze (2012). These flows could suffer a “partial blocking, with a lee-side supercritical flow accelerating down the mountain, and the return to equilibrium in the form of a hydraulic jump producing a precipitating cloud downstream of the barrier”. This mechanism would explain the inverse gradient of precipitation with elevation. Figure 2.11 shows a scheme of the flow dynamics in the Sierra Nevada and the proposed hypothesis for the flow that arrives through the Genil valley.

The consideration of the inversion gradient mechanism proposed could improve predictions of snow hydrological models and climate studies in this area. On the other hand, correction functions of undercatch that take into account climatic variables to correct precipitation in high elevations have been used in this study. These functions could be improved in future work that considers orographic conditions. Despite the focus of the present study being on the assessment of precipitation gradients, we have proposed a mechanism that can explain the observed inverse gradients. This is an interesting, preliminary hypothesis that can be investigated in depth in the future.

6. Conclusions

In this paper we have analysed the relationship between the measurements of one of the main climatic variables (P) and elevation in an alpine basin, the Alto Genil basin in Sierra Nevada, in which the snow measurements show an inversion of the gradient with the altitude beyond a certain threshold. We discuss two hypotheses (a real change of pattern and a systematic errors due to undercatch of solid P) to explain the observed relationship between precipitation and elevation, taking into account previous alpine studies that share certain similarities.

The analyses of the climatic data during the non-snow allowed us to conclude that there is a real inversion pattern, but that the undercatch phenomenon may intensify the real value. We investigate the influence that these hypotheses and other adopted approaches have on calculation of the relationship between precipitation and elevation when estimating precipitation fields, and therefore on overall precipitation. We study the sensitivity of the solutions to different methods and assumptions, namely: the function used to calculate precipitation depending on elevation (linear and quadratic functions are explored), the calculation technique used (KED or RK), and the temporal scale to calculate the variogram. The results shows an important sensitivity of the estimated precipitation fields to the adopted corrected field (maximum differences of mean precipitation of 0.84 mm/day, 0.75 mm/day and 1.38 mm/day respectively for the RK, LKED and QKED), and therefore more research about the corrections that should be applied in this mountain area would be needed for an appropriate assessment of rainfall fields. Anyway, in our case study, the sensitivity of the results to the estimation method (function used to calculate precipitation depending on elevation (linear and quadratic functions are explored), the calculation technique used) is even greater than to the adopted data correction and should be also analysed carefully. Nevertheless, the influence of the temporal scale (annual and monthly) adopted to define the variorum is low. A cross-validation of the results was performed with the aim of to

identifying the solutions that provide the best approximation to the available data. It is obtained by using the monthly variogram model and LKED show the best results in the cross validation experiment, despite it does not reproduce the inversion of gradient, which is approximated by the RK. QKED provides the worst approximation of P-h relationship.

In order to explain the observed inversion gradient we have proposed a mechanism that could explain the inversion of precipitation gradient based on orographic effects on precipitation. These flows of precipitation could be partially blocked, which would induce precipitation downstream of the barrier defined by the mountain range. Thus snow hydrological models and climate studies in this area should consider this pattern in order to obtain more reliable results. Moreover, orographic conditions should be included in undercatch correction functions to improve their corrections.

Acknowledgements

This research has been partially supported by the GESINHIMPADAPT project (CGL2013-48424-C2-2-R) with Spanish MINECO funds. We would also like to thank AEMET, IFAPA, PNS and REDIAM Spanish agencies for providing the precipitation data and the NASA DAAC for the SCA data. We appreciate the valuable suggestions provided by two anonymous referees.

References

- Anders AM, Nesbitt SW. 2014. Altitudinal Precipitation Gradients in the Tropics from Tropical Precipitation Measuring Mission (TRMM) Precipitation Radar. *Journal of Hydrometeorology*. doi:10.1175/JHM-D-14-0178.1.
- Anders AM, Roe GH, Hallet B, Montgomery DR, Finnegan NJ, Putkonen J. 2006. Spatial patterns of precipitation and topography in the Himalaya. In: Willett, S.D., Hovius, N., Brandon, M.T. and Fisher, D. (Eds.) *Tectonics, Climate, and Landscape Evolution: Geological Society of America Special Paper 398*. Boulder, CO: Geological Society of America, pp. 39–53. doi:10.1130/2006.2398(03).
- Brown M, Peck E. 1962. Reliability of Precipitation Measurements as Related to Exposure. *J. Appl. Meteor.* 1: 203-207. doi:10.1175/15200450(1962)001<0203:ROPMAR>2.0.CO;2.
- Buisán ST, Earle ME, Collado JL, Kochendorfer J, Alastrué J, Wolff M, Smith CD, López-Moreno JI. 2017. Assessment of snowfall accumulation underestimation by tipping bucket gauges in the Spanish operational network. *Atmos. Meas. Tech.* 10: 1079-1091. doi:10.5194/amt-10-1079-2017.
- Chen D, Ou T, Gong L, Xu CY, Li W, Ho CH, Qian WH. 2010. Spatial interpolation of daily precipitation in China: 1951–2005. *Adv. Atmos. Sci.* 27: 1221-1232. doi:10.1007/s00376-010-9151-y.
- Chiles JP, Delfiner P. 1999. *Geostatistics: Modelling Spatial Uncertainty*. Wiley, New York.

- Collados-Lara AJ, Pardo-Iguzquiza E, Pulido-Velazquez D. 2017. Spatiotemporal estimation of snowpack thickness using point data from snow stakes, digital terrain models and satellite data. *Hydrol. Process.* 31(10): 1966-1982. doi:10.1002/hyp.11165
- Cosma S, Richard E, Miniscloux F. 2002. The role of small-scale orographic features in the spatial distribution of precipitation. *Q. J. R. Meteorol. Soc.* 128: 75-92.
- Daly C, Neilson RP, Phillips DL. 1994. A statistical topographic model for mapping climatological precipitation over mountainous terrain. *J. Appl. Meteor.* 33: 140-158.
- Dore AJ, Choularton TW. 1992. Orographic enhancement of snowfall. *Environ. Pollut.* 75: 175-179.
- Elder K, Dozier J, Michaelsen J. 1991. Snow Accumulation and Distribution in an Alpine Watershed. *Water Resour. Res.* 27: 1541–1552. doi:10.1029/91wr00506, 1991.
- Escriva-Bou A, Pulido-Velazquez M, Pulido-Velazquez D. 2017. The Economic Value of Adaptive Strategies to Global Change for Water Management in Spain's Jucar Basin. *Journal of Water Resources Planning and Management.* doi:10.1061/(ASCE)WR.1943-5452.0000735.
- García de Pedraza L, García Vega C. 1993. La cordillera Bética: aspectos meteorológicos. In: Calendario Meteorológico. Ponta Porã: Instituto Nacional de Meteorología, pp. 204–215.
- Gerber F, Lehning M, Hoch SW, Mott R. 2017. A close-ridge small-scale atmospheric flow field and its influence on snow accumulation. *J. Geophys. Res. Atmos.* 122: 7737-7754. doi:10.1002/2016JD026258.
- Goodison BE, Louie PYT, Yang D. 1988. WMO solid precipitation measurement intercomparison, Final report, WMO/TD-No. 872, WMO, Geneva, 212pp.
- Goovaerts P. 2000. Geostatistical approaches for incorporating elevation into the spatial interpolation of rainfall. *Journal of Hydrology* 228(1-2): 113-129. doi:10.1016/S0022-1694(00)00144-X.
- Grünewald T, Lehning M. 2011. Altitudinal dependency of snow amounts in two small alpine catchments: Can catchment-wide snow amounts be estimated via single snow or precipitation stations?. *Ann. Glaciol.* 52: 153-158.
- Grünewald T, Bühler Y, Lehning M. 2014. Elevation dependency of mountain snow depth. *The Cryosphere* 8: 2381-2394. doi:10.5194/tc-8-2381-2014.
- Hengl T, Heuvelink GBM, Rossiter DG. 2007. About regression-kriging: From equations to case studies. *Computers & Geosciences* 33: 1301-1315.
- Hirpa FA, Gebremichael M, Hopson T. 2010. Evaluation of high-resolution satellite precipitation products over very complex terrain in Ethiopia. *J. Appl. Meteor. Climatol.* 49: 1044-1051. doi:10.1175/2009JAMC2298.1.

- Houze RA, Jr. 2012. Orographic effects on precipitating clouds. *Reviews of Geophysics*, 50, RG1001. doi:10.1029/2011RG000365.
- Hunter R, Meentemeyer R. 2005. Climatologically aided mapping of daily precipitation and temperature. *Journal of Applied Meteorology* 44:1501-1510.
- Kirchner PB, Bales RC, Molotch NP, Flanagan J, Guo Q. 2014. LiDAR measurement of seasonal snow accumulation along an elevation gradient in the southern Sierra Nevada, California. *Hydrol. Earth Syst. Sci.* 18: 4261-4275. doi:10.5194/hess-18- 4261-2014.
- Legates, DR, Willmott CJ. 1990. Mean seasonal and spatial variability in gauge-corrected, global precipitation. *International Journal of Climatology* 10: 111–127. doi: 10.1002/joc.3370100202
- Lehning M, Grünwald T, Schirmer M. 2011. Mountain snow distribution governed by elevation and terrain roughness. *Geophys. Res. Lett.* 38, L19504. doi:10.1029/2011GL048927.
- Lehning M, Löwe H, Ryser M, Raderschall N. 2008. Inhomogeneous precipitation distribution and snow transport in steep terrain. *Water Resour. Res.* 44, W07404. doi:10.1029/2007WR006544.
- Lloyd CD. 2005. Assessing the effect of integrating elevation data into the estimation of monthly precipitation in Great Britain. *J. Hydrol.* 308:128-150. doi:10.1016/j.jhydrol.2004.10.026.
- Matheron G. 1963. ‘Principles of Geostatistics’, *Econ. Geol.* 58: 1246–1266.
- Minder JR, Durran DR, Roe GH, Anders AM. 2008. The climatology of small-scale orographic precipitation over the Olympic mountains: Patterns and processes. *Q. J. R. Meteorol. Soc.* 134: 817-839.
- Mott R, Scipión D, Schneebeli M, Dawes N, Berne A, Lehning M. 2014. Orographic effects on snow deposition patterns in mountainous terrain. *J. Geophys. Res. Atmos.* 119: 1363-1385. doi:10.1002/2013JD019880.
- Pardo-Igúzquiza E. 1998. Comparison of geostatistical methods for estimating the areal average climatological precipitation mean using information of precipitation and topography. *Int. J. Climatol.* 18: 1031-1047.
- Pardo-Iguzquiza E, Heredia J, Rodriguez-Arevalo J. 2015. Is it possible to select a unique best model in regression when the number of experimental data is small and the number of explicative variables large? *IAMG2015-Proceedings*, G0904.
- Pedro-Monzonis MP, Solera A, Ferrer J, Estrela T. 2016. Water accounting for stressed river basins based on water resources management models. *Science of The Total Environment* 565:181-190. doi:10.1016/j.scitotenv.2016.04.161.

- Prein AF, Gobiet A. 2017. Impacts of uncertainties in European gridded precipitation observations on regional climate analysis, International Journal of Climatology 37, 1, 305.
- Rasmussen R, Baker B, Kochendorfer J, Meyers T, Landolt S, Fischer AP, Black J, Thériault JM, Kucera P, Gochis D, Smith C, Nitu R, Hall M, Ikeda K, Gutmann E. 2012. How well are we measuring snow: The noaa/faa/ncar winter precipitation test bed. Bulletin of the American Meteorological Society 93:811-829.
- Scipión DE, Mott R, Lehning M, Schneebeli M, Berne A. 2013. Seasonal small-scale spatial variability in alpine snowfall and snow accumulation. Water Resour. Res. 49: 1446-1457. doi:10.1002/wrcr.20135.
- Sevruk B. 1982. Methods of correction for systematic error in point precipitation measurement for operational use. World Meteorol. Org., Operational Hydrol. Rep. 21, WMO-NO. 589, 91 p.
- Sevruk B. 1991. International workshop on precipitation measurement I: Preface. Hydrological Processes 5(3): 229-232. doi:10.1002/hyp.3360050302.
- Smith RB. 1979. The influence of mountains on the atmosphere. Adv. Geophys., 21, 87–230. doi:10.1016/S0065-2687(08)60262-9.
- Yang Q, Ma ZG, Chen L. 2011. A Preliminary Analysis of the Relationship between Precipitation Variation Trends and Altitude in China. Atmospheric and oceanic science letters 4(1): 41-46.
- Yao J, Yang Q, Mao W, Zhao Y, Xu X. 2016. Precipitation trend-Elevation relationship in arid regions of the China. Global and Planetary Change 143(8): 1-9. doi:10.1016/j.gloplacha.2016.05.007

Appendix 2A. Estimation techniques

P is a variable with spatial continuity (low values are close to other low values and high values are close to the other high values). The variable changes gradually. Considering this assumption, the variogram is the habitual way to quantify the spatial correlation. The variogram for a given variable can be expressed as:

$$\gamma(h) = \frac{1}{2n(h)} \sum_{i=1}^{n(h)} [z(s_i) - z(s_i + h)]^2 \quad (2A1)$$

where $\gamma(h)$ is the experimental variogram, elevation is the step or distance, $n(h)$ is the number of steps and $z(s_i)$ is the variable value at the location s_i . Normally, the experimental variogram is adjusted using one of the next models: spherical (equation (2A2)), exponential (equation (2A3)) and Gaussian (equation (2A4)).

$$\gamma(h) = C \left[\frac{3h}{2a} - \frac{1}{2} \left(\frac{h}{a} \right)^3 \right] \quad (2A2)$$

$$\gamma(h) = C \left[1 - e^{-\left(\frac{h}{a}\right)} \right] \quad (2A3)$$

$$\gamma(h) = C \left[1 - e^{-\left(\frac{h}{a}\right)^2} \right] \quad (2A4)$$

where a and C are adjusted parameters, the range and variance respectively. In this study we used the exponential model to fit the variogram models.

Considering a catchment with area A divided in N grids of equal area B , the mean value of the target variable variable $z_B(x_i)$ can be expressed as:

$$z_B(x_i) = \frac{1}{B} \int_{B(x_i)} z(x) dx \quad (2A5)$$

where $z(x)$ is the mean of the target variable in the location x . The value of the target variable is known in the meteorological station being considered and we want to know it in the points of the grid.

Kriging methods provide estimates for equation (2A5) using the experimental data:

$$z'_B(x_i) = \sum_{j=1}^n \lambda_j \cdot z(x_j) \quad (2A6)$$

A.1. Kriging with external drift

In KED, a secondary variable is used to interpolate the target variable. Normally, in calculating climatic variables the explicative variable with greatest influence is elevation. Analysis of the relationship between precipitation and elevation was done using regression functions with yearly and monthly means. This analysis revealed the relationship of the target variable with elevation. The climatic variogram models used to carry out the KED were obtained from the residues of the regression function at the data station.

In KED the mathematical expected value of the target variable mean random function $Z(x)$ is expressed as a function of the drift variable $Y(x)$. In this study, elevation is the drift variable. Normally the function is linear for precipitation but in some cases the relationship between precipitation and elevation can be quadratic (inverse precipitation gradient). The function for the linear and quadratic cases can be expressed, respectively, as:

$$E[Z(x)] = a_1 + a_2 Y(x) \quad (2A7)$$

$$E[Z(x)] = a_1 + a_2 Y(x) + a_3 Y^2(x) \quad (2A8)$$

The target variable $z'_B(x_i)$ for the linear case, with weights λ_j obtained as solutions of the KED system, is calculated as:

$$\begin{cases} \sum_{j=1}^n \lambda_j \cdot \gamma_P(x_i, x_j) + \mu_1 + \mu_2 y(x_i) = \bar{y}(x_i, B(x_o)) & i = 1, \dots, n \\ \sum_{j=1}^n \lambda_j \cdot y(x_j) = y(x_o) \\ \sum_{j=1}^n \lambda_j = 1 \end{cases} \quad (2A9)$$

with estimated variance $\hat{\sigma}^2$ expressed as:

$$\hat{\sigma}^2 = \sum_{j=1}^n \lambda_j \cdot \bar{y}(x_i, B(x_o)) + \mu_1 + \mu_2 y(x_o) \quad (2A10)$$

The calculation of the target variable $z'_B(x_i)$ for the quadratic case can be obtained by solving the following KED system:

$$\begin{cases} \sum_{j=1}^n \lambda_j \cdot \gamma_P(x_i, x_j) + \mu_1 + \mu_2 y(x_i) + \mu_3 y^2(x_i) = \bar{y}(x_i, B(x_o)) & i = 1, \dots, n \\ \sum_{j=1}^n \lambda_j \cdot y(x_j) = y(x_o) \\ \sum_{j=1}^n \lambda_j \cdot y^2(x_j) = y^2(x_o) \\ \sum_{j=1}^n \lambda_j = 1 \end{cases} \quad (2A11)$$

with estimated variance $\hat{\sigma}^2$ expressed as:

$$\hat{\sigma}^2 = \sum_{j=1}^n \lambda_j \cdot \bar{y}(x_i, B(x_o)) + \mu_1 + \mu_2 y(x_o) + \mu_3 y^2(x_o) \quad (2A12)$$

where μ_1 , μ_2 and μ_3 are the Lagrange multiplier, $\gamma_P(x_i, x_j)$ is the variogram function for the points x_i and x_j and $\bar{y}(x_i, B(x_o))$ is the mean variogram function between point x_i and support B with centroid x_o .

The values of the coefficients a_1 , a_2 and a_3 are not needed for solving equation systems (2A9) and (2A11). To apply KED it is not necessary to know them. However the mean elevation must be known at the experimental location and the estimated grids.

A.2. Regression kriging

RK is a hybrid spatial interpolation technique which is normally used when the number of explicative variables is high. The technique requires using two separate procedures. The first procedure is a regression with a certain number of explicative variables. The second

procedure uses the residues of the regression to spatially interpolate using the kriging technique. The predicted value of the target variable $\hat{z}(s_0)$ at location s_0 can be calculated as:

$$\hat{z}(s_0) = \hat{Y}(s_0) + \hat{e}(s_0) \quad (2A13)$$

$\hat{Y}(s_0)$ is the estimated value with the selected multiple regression model. The multiple linear regression models are defined by the equation:

$$Y_n(s_0) = \beta_0 + \beta_1 X_{1i} + \cdots + \beta_m X_{mi} \quad (2A14)$$

where Y_n is the variable to be estimated, $\{X_{1i}, \dots, X_{mi}\}$ are the explanatory variables and $\{\beta_1, \dots, \beta_m\}$ are unknown parameters estimated from experimental data. In this study we used the simplest regression model with a single explanatory variable (Equation A15).

$$Y = \beta_0 + \beta_1 x_i \quad (2A15)$$

where Y represents precipitation, x_i is elevation and β_0 and β_1 are coefficients.

The interpolated residual $\hat{e}(s_0)$ can be expressed as:

$$\hat{e}(s_0) = \sum_{i=1}^t \lambda_i e(s_i) \quad (2A16)$$

where λ_i are the kriging weights determined by the spatial correlation of the residual and $e(s_i)$ is the residual at location s_i

In OK the kriging weights are obtained by solving (2A7):

$$\begin{cases} \sum_{j=1}^n \lambda_j \cdot \gamma_P(x_i, x_j) + \mu = \bar{\gamma}(x_i, B(x_o)) & i = 1, \dots, n \\ \sum_{j=1}^n \lambda_j = 1 \end{cases} \quad (2A17)$$

with estimated variance $\hat{\sigma}^2$ expressed as:

$$\hat{\sigma}^2 = \sum_{j=1}^n \lambda_j \cdot \bar{\gamma}(x_i, B(x_o)) + \mu \quad (2A18)$$

where μ is the Lagrange multiplier, $\gamma_P(x_i, x_j)$ is the variogram function for the points x_i and x_j and $\bar{\gamma}(x_i, B(x_o))$ is the mean variogram function between point x_i and support B with centroid x_o .

Appendix 2B. Cross validation methodology

The cross-validation methodology is used in geostatistics for assessing the performance of the spatial interpolation by kriging. It can be used for checking the effect of different kriging neighbourhoods, different types of kriging, different kind of variogram models or different sets of variogram parameters for the same type of model. In cross-validation, each experimental datum is dropped from the experimental data set in turn and is calculated from the remaining experimental data. Thus it is possible to determine the true error of the interpolation by kriging:

$$e(u_i) = \hat{z}(u_i) - z(u_i) \quad (2B1)$$

where $e(u_i)$ is the true error in the estimate of the i^{th} experimental datum, $\hat{z}(u_i)$ is the estimate of the variable of interest at the location of the i^{th} experimental datum, and $z(u_i)$ is the true value of the experimental datum of the variable of interest at the i^{th} experimental location.

Thus if there are N experimental data, cross-validation will give a set of N true errors $\{e(u_i), i = 1, \dots, N\}$. From these errors, the following cross-validation statistics can be obtained: mean error (ME), mean squared error (MSE) and mean standardized squared error ($MSSE$).

ME is defined as the mean of the true errors:

$$ME = \frac{1}{N} \sum_{i=1}^N e(u_i) \quad (2B2)$$

The ME is the bias of the estimation, whose value should be around zero. This criterion should always be met because kriging is an unbiased estimator.

MSE is defined as the mean of the squared true errors:

$$MSE = \frac{1}{N} \sum_{i=1}^N e^2(u_i) \quad (2B3)$$

The MSE is the accuracy of the estimate and the value should be as small as possible.

$MSSE$ is defined as the mean of the standardized squared true errors:

$$MSSE = \frac{1}{N} \sum_{i=1}^N \frac{e^2(u_i)}{\sigma_K^2(u_i)} \quad (2B4)$$

where $\sigma_K^2(u_i)$ is the kriging variance in the estimate of the i^{th} datum.

The $MSSE$ is the evaluation of how well (statistically) the kriging variance is a realistic measure of uncertainty. The value should be around 1 if the kriging variance is a good measure of uncertainty.

Tables of the Chapter 2

Period	Original data				Modified data			
	a ₁	a ₂	a ₃	Inflection point (km)	a ₁	a ₂	a ₃	Inflection point (km)
Yearly	0.4260	1.3328	-0.4133	1.6124	0.5036	1.0910	-0.2466	2.2121
January	0.4230	1.9618	-0.6330	1.5496	0.2605	2.0674	-0.5255	1.9671
February	0.2176	2.4924	-0.7369	1.6911	-0.0167	2.5616	-0.4851	2.6403
March	0	2.4112	-0.7004	1.7213	0.2257	1.8416	-0.3679	2.5029
April	0.4600	1.8729	-0.5895	1.5885	0.7280	1.3242	-0.3388	1.9543
May	-0.1863	2.2723	-0.6793	1.6725	0.0516	1.8354	-0.5115	1.7941
June	0.1082	0.5386	-0.1340	2.0097	0.1082	0.5386	-0.1340	2.0097
July	0.0376	0.4070	-	-	0.0376	0.0407	-	-
August	-0.0991	0.4431	-0.1360	1.6290	-0.0991	0.4431	-0.1360	1.6290
September	0.1773	1.0212	-0.2940	1.7367	0.1773	1.0212	-0.2940	1.7367
October	0.7587	1.2084	-0.3470	1.7412	1.0567	0.6571	-0.1335	2.4610
November	0.7987	2.0795	-0.6829	1.5226	0.8416	1.8213	-0.4513	2.0178
December	0.9420	1.9762	-0.6824	1.4480	1.0831	1.5339	-0.3784	2.0268

Table 2.1. Parameters of the regression function ($P = a_1 + a_2 \cdot h + a_3 \cdot h^2$) for mean precipitation vs. elevation.

Technique	Original data				Modified data			
	Yearly Model		Monthly Model		Yearly Model		Monthly Model	
	ME (mm)	MSE (mm ²)						
QKED	0.11	23.52	0.10	21.39	0.09	26.52	0.08	24.36
LKED	0.02	10.44	0.02	10.19	0.01	13.47	0.01	13.18
RK	1.70	12.39	1.54	12.35	1.73	15.45	1.62	15.88

Table 2.2. Mean error and mean squared error of the cross validation experiment for the different techniques, data and variogram model.

Figures of the Chapter 2

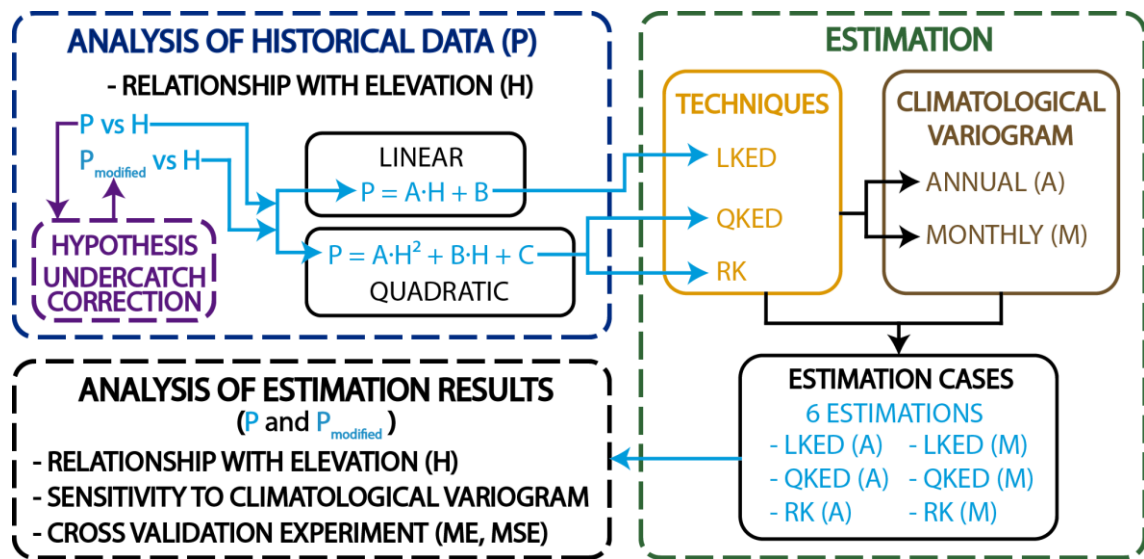


Figure 2.1. Flow chart of the proposed methodology.

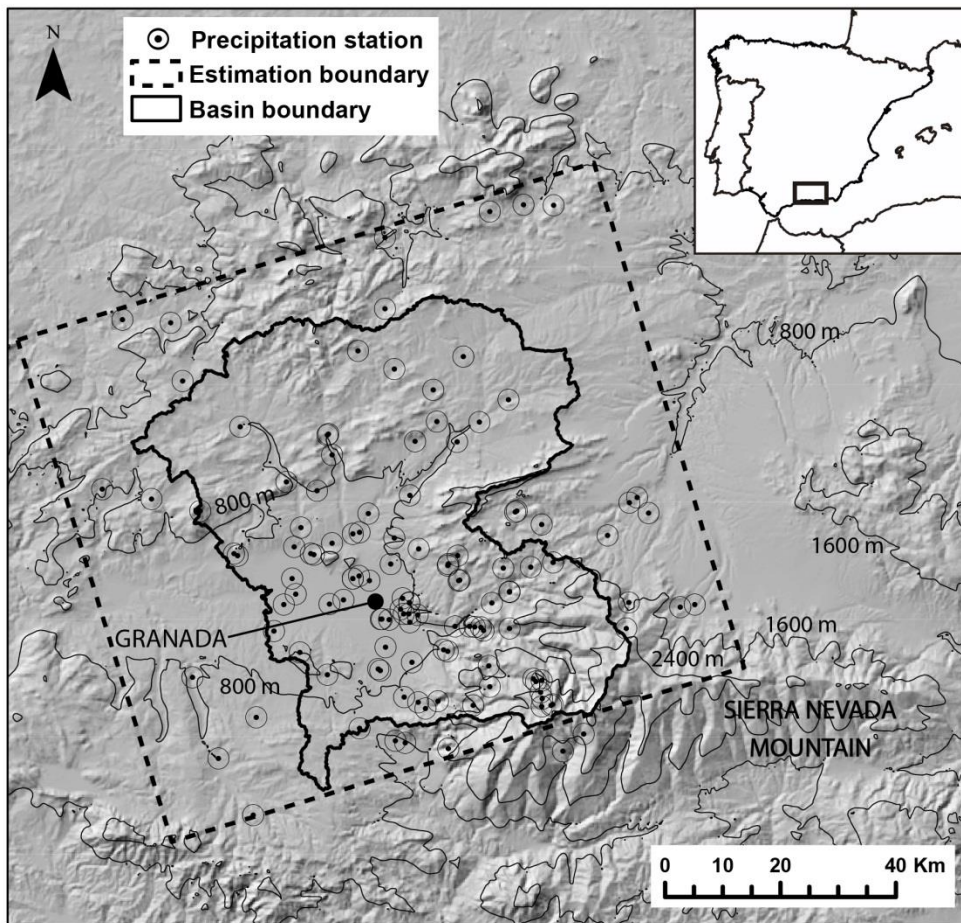


Figure 2.2. Location of the study area and available gauges.

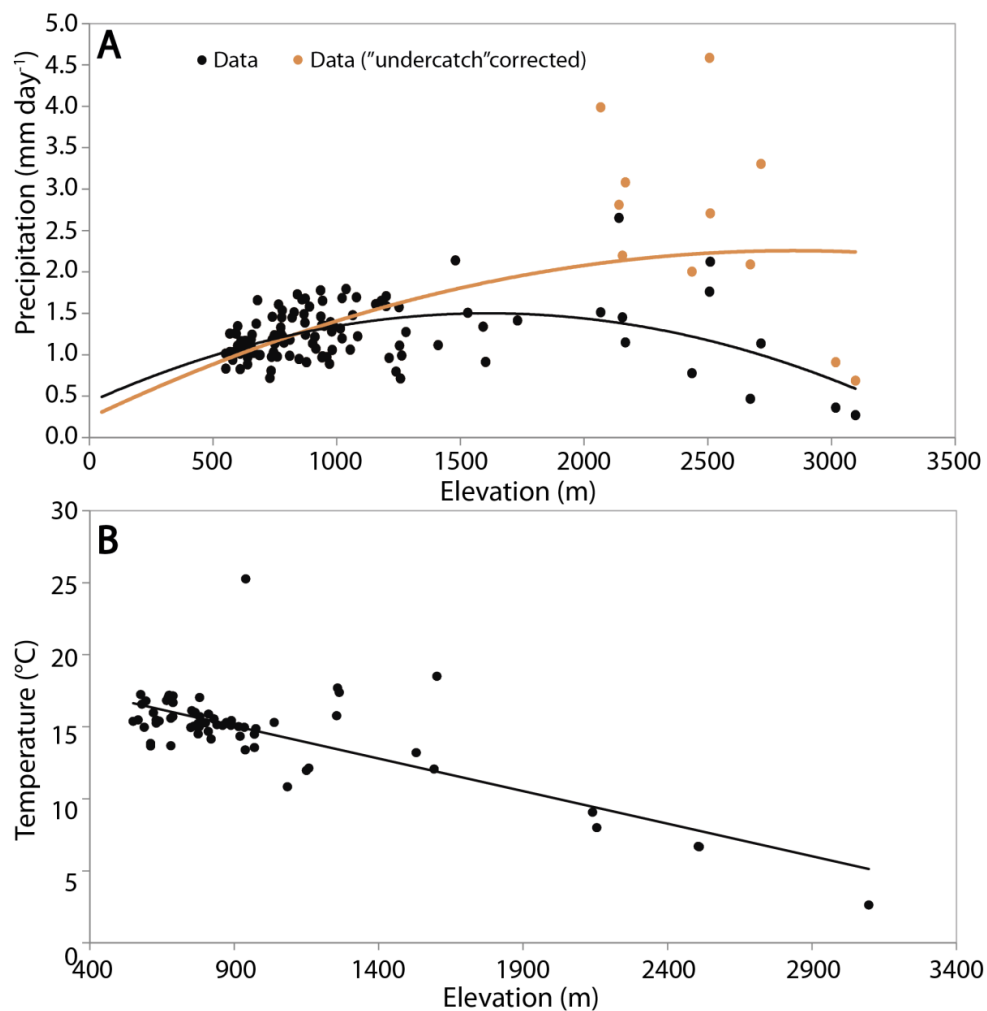


Figure 2.3. A: Mean daily precipitation data for different elevations. B: mean daily temperature data for different elevations. Dots represent the data (black) and modified data corrected for undercatch (orange); their trends are marked by lines.

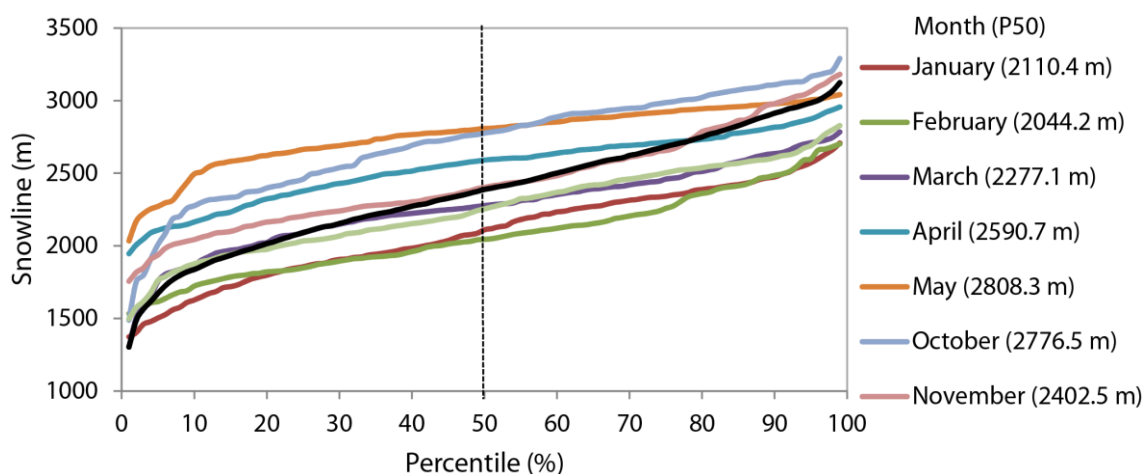


Figure 2.4. Percentile distribution of the snowline for each month of the snow season and for the whole snow season.

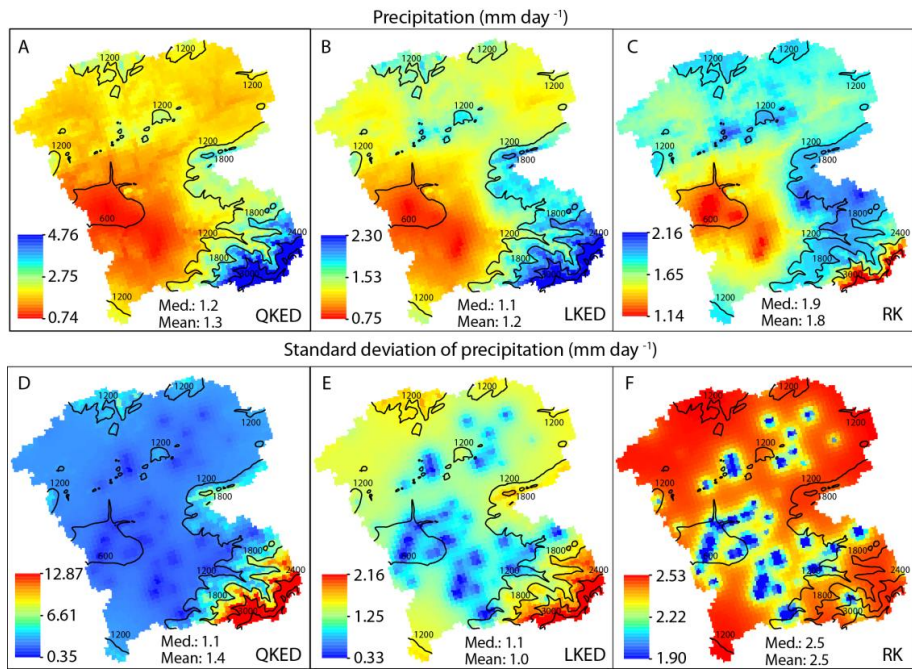


Figure 2.5. A, B, C: Spatial distribution of estimated mean precipitation using QKED, LKED, RK and original data for the period 1980-2014. D, E, F: Spatial distribution of standard deviation of estimated precipitation using QKED, LKED, RK and original data for the period 1980-2014.

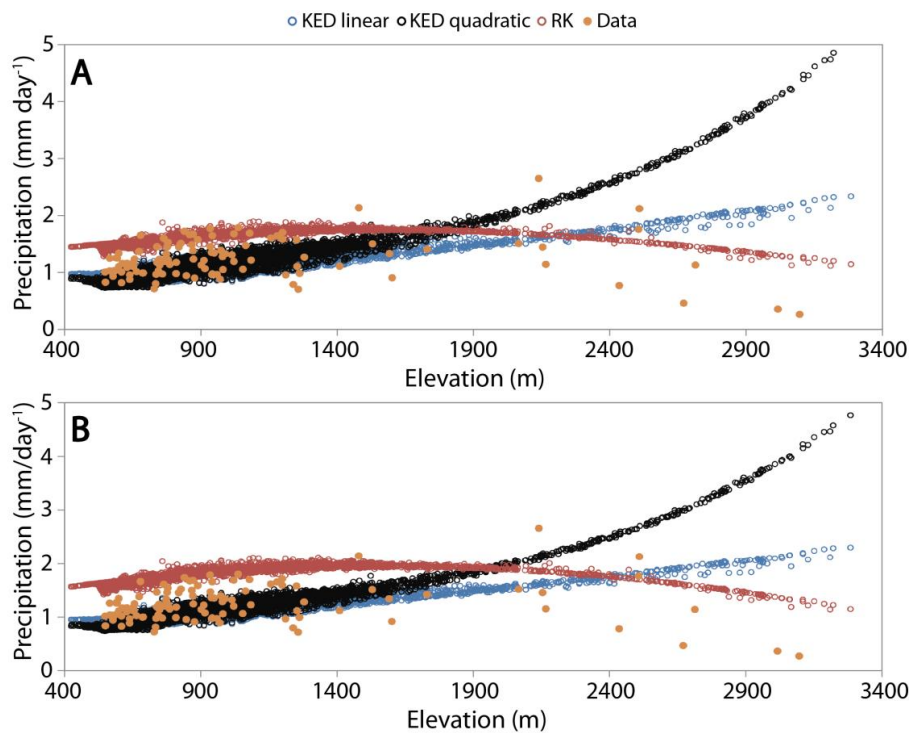


Figure 2.6. Estimated mean daily precipitation data in each cell using the various geostatistical techniques considered vs elevation of the cell. A: using a yearly variogram model. B: using a monthly variogram model.

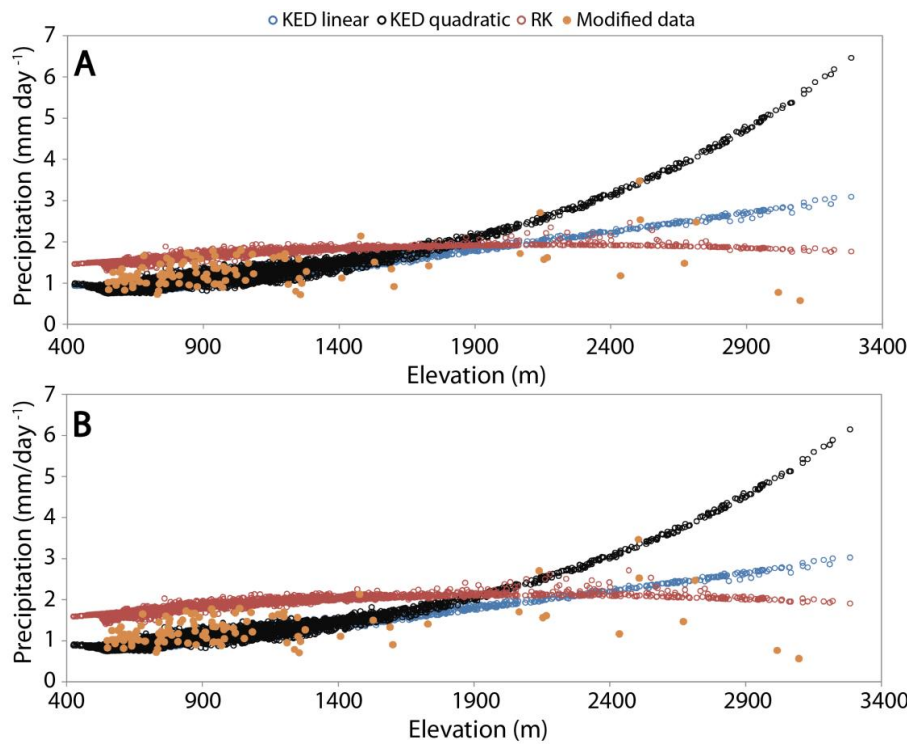


Figure 2.7. Estimated mean daily precipitation (using modified data corrected for undercatch) in each cell using the various geostatistical techniques considered vs elevation of the cell. A: using a yearly variogram model. B: using a monthly variogram model.

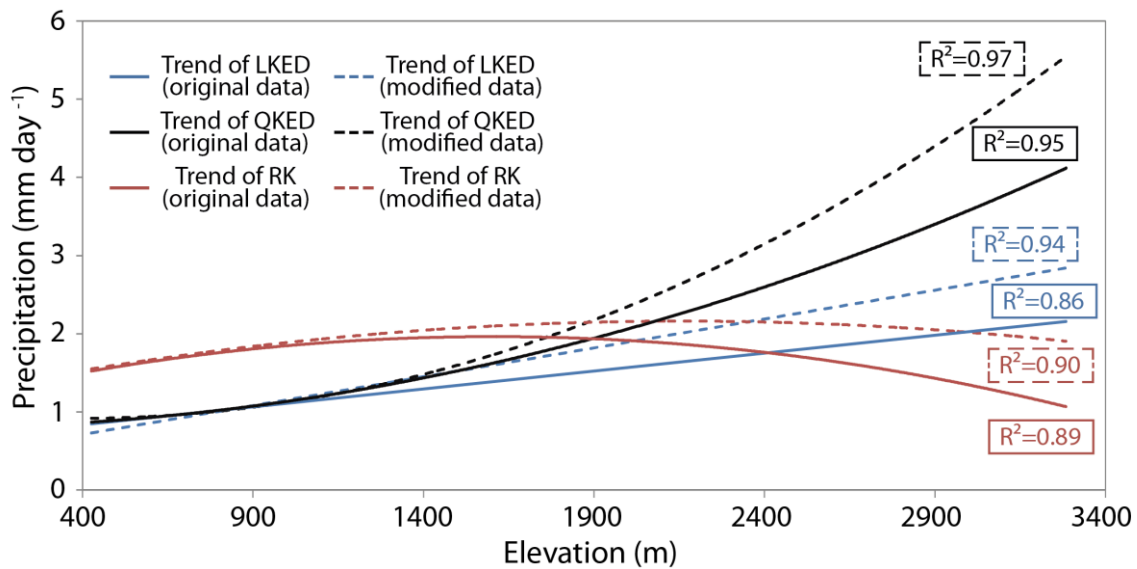


Figure 2.8. Comparison between precipitation original and modified data vs. elevation using different estimation techniques and the monthly variogram model.

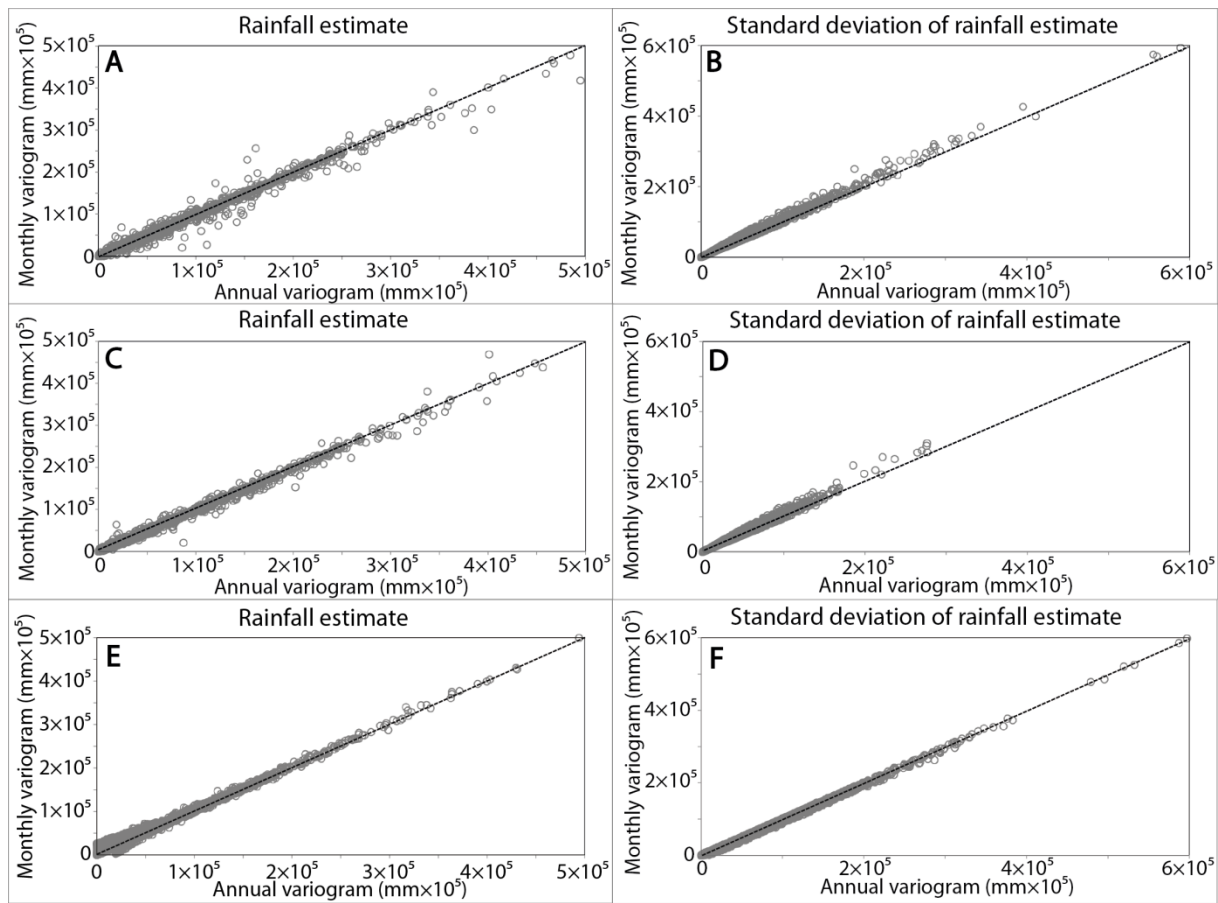


Figure 2.9. A, C, E: Estimated daily precipitation (QKED, LKED, RK) within the basin using the yearly model vs. the monthly model and the original data. B, D, F: Standard deviation of precipitation (QKED, LKED, RK) using the yearly model vs. the monthly model and the original data.

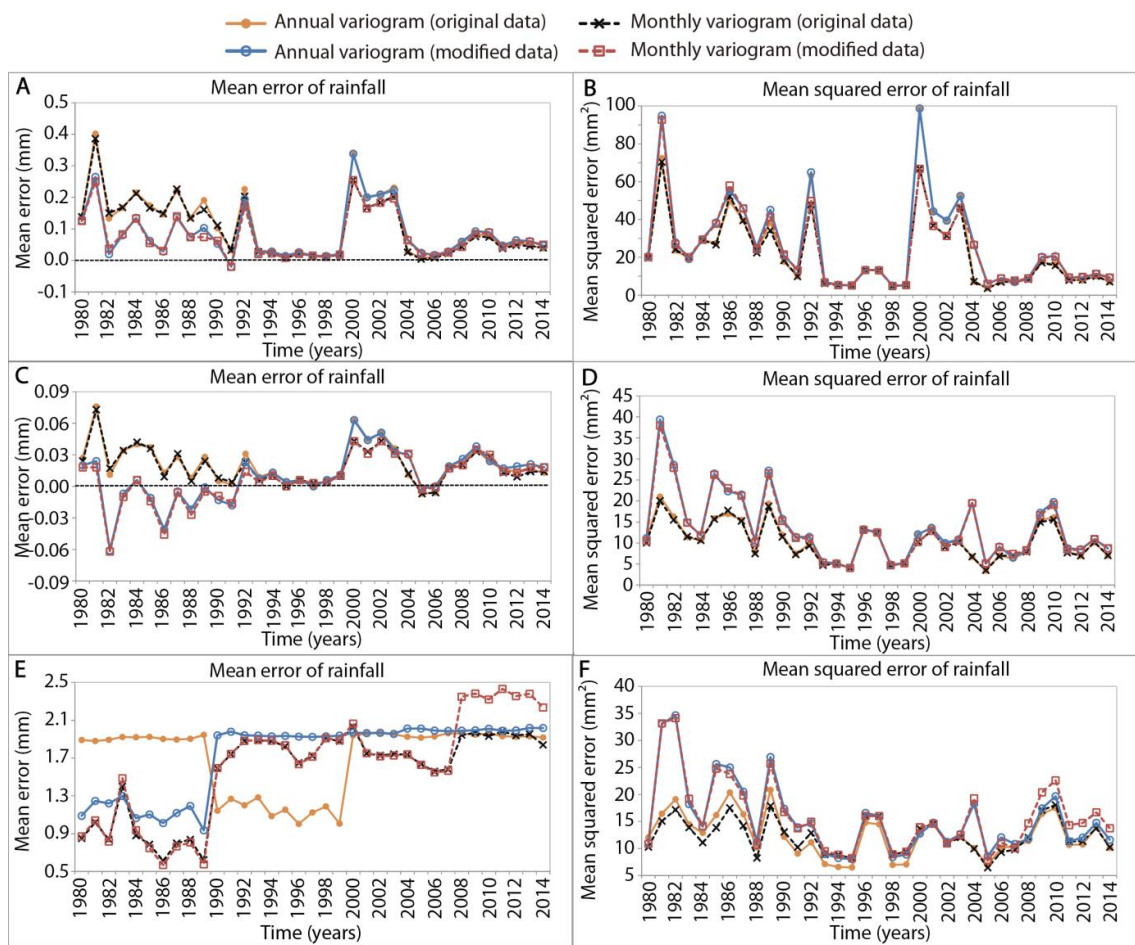


Figure 2.10. Mean error (A, C, E) and mean squared error (B, D, F) of the cross validation experiment using quadratic KED, linear KED and RK using the original data.

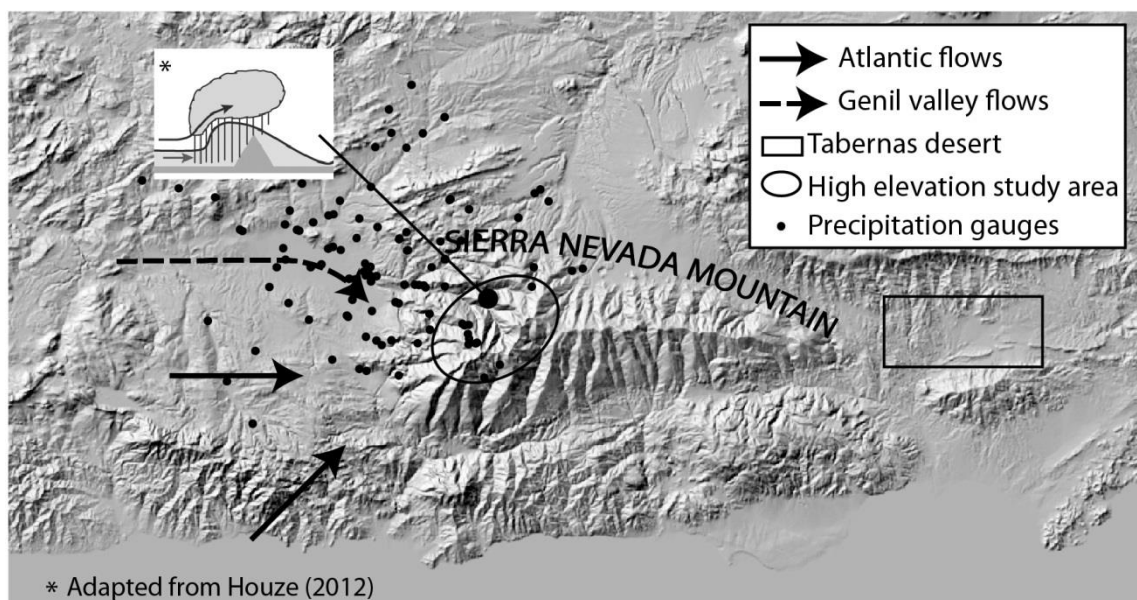


Figure 2.11. Scheme of the precipitation flow dynamics and proposed hypothesis for the case study.

Chapter 3: Spatiotemporal estimation of snow depth using point data from snow stakes, digital terrain models, and satellite data

Received: 7 April 2016 | Accepted: 1 March 2017
DOI: 10.1002/hyp.11165

WILEY

RESEARCH ARTICLE

Spatiotemporal estimation of snow depth using point data from snow stakes, digital terrain models, and satellite data

Antonio-Juan Collados-Lara¹  | Eulogio Pardo-Igúzquiza² | David Pulido-Velazquez¹

Antonio-Juan Collados-Lara^(1,*), Eulogio Pardo-Igúzquiza⁽²⁾ and David Pulido-Velazquez⁽¹⁾

Corresponding author: Antonio-Juan Collados-Lara (ajcollados@gmail.com)

(1) Instituto Geológico y Minero de España (IGME), Urb. Alcázar del Genil, 4, bajo. Edificio Zulema. 18006, Granada (Spain). E-mail address: ajcollados@gmail.com, d.pulido@igme.es.

(2) Instituto Geológico y Minero de España (IGME), Ríos Rosas, 23. 28003 Madrid (Spain). E-mail address: e.pardo@igme.es.

* Corresponding author

Abstract

Snow availability in Alpine catchments plays an important role in water resources management. In this paper we propose a method for an optimal estimation of snow depth (areal extension and thickness) in Alpine systems from point data and satellite observations by using significant explanatory variables deduced from a digital terrain model. It is intended to be a parsimonious approach that may complement physical-based methodologies. Different techniques (multiple regression, multi-criteria analysis and kriging) are integrated to address the following issues: We identify the explanatory variables that could be helpful based on a critical review of the scientific literature. We study the relationship between ground observations and explanatory variables using a systematic procedure for a complete multiple regression analysis. Multiple regression models are calibrated combining all suggested model structures and explanatory variables. We also propose an evaluation of the models (using indices to analyze the goodness of fit) and select the best approaches (models and variables) based on multi-criteria analysis. Estimation of the snow depth is performed with the selected regression models. The residual estimation is improved by applying kriging in cases with spatial correlation. The final estimate is obtained by combining regression and kriging results, and constraining the snow domain in accordance with satellite data. The method is

illustrated using the case study of the Sierra Nevada mountain range (Southern Spain). A cross validation experiment has confirmed the efficiency of the proposed procedure. Finally, although it is not the scope of this work, the snow depth is used to asses a first estimation of snow water equivalent (SWE) resources.

Keywords: Snow depth, Parsimonious estimation method, Regression models, Explanatory variables, Multi-criteria analysis, Sierra Nevada (Spain)

1. Introduction

Snow availability in Alpine catchments is an essential feature in the economy of these areas. Snow plays an important role not only for the development of tourism but also in the management of water resources (Liu et al., 2012). Thus, estimation of snow depth is an important applied problem but one that has not yet been completely resolved. The hydrologic regime in these areas is dominated by the storage of water in the snowpack, which is discharged to rivers throughout the melt season (Viviroli et al., 2007). Accurate estimates of these resources are necessary for making pertinent analyses of system operation alternatives using basin scale management models (Pulido-Velazquez et al., 2011).

In order to obtain an appropriate estimate of the snow depth, we need to know the spatial distribution of snow depth within the Snow Cover Area (SCA). Data for these snow variables can be extracted from in-situ point measurements and air-borne/space-borne remote sensing observations. From field surveys we can obtain point measurements of snow depth and snow density. Snow is one of the most investigated hydrologic variables by remote sensing (Liu et al., 2012). Several SCA products based on visible sensors with different spatial and temporal resolutions have been defined over various historical periods. Using information from the National Oceanic and Atmospheric Administration (NOAA), the Rutgers University Global Snow Lab (or GSL, part of the RUCL, the Climate Lab of Rutgers University, New Jersey, USA) has been collecting measurements of SCA at weekly intervals and with a spatial resolution of 190.6 km (i.e. side length of a square pixel) at a latitude of 60°, since 1966. NASA has also been collecting SCA information at various temporal resolutions (1 day, 8 day and 1 month) and an approximate spatial resolution of 463 m since 2000, using the Moderate Resolution Imaging Spectroradiometer (MODIS) (Hall and Riggs, 2007). SWE products have been also developed from passive microwave radiometry data, such as the Advanced Microwave Scanning Radiometer (AMSR-E) sensor, which has been in operation since 2002 (Kelly, 2009). There are also blended snow products, such as the Air Force Weather Agency (AFWA)/NASA snow algorithm (ANSA), which was developed by combining MODIS and AMSR-E retrievals (Foster et al., 2011).

A variety of interpolation and simulation techniques have been used for estimating the above-mentioned variables. For example, SCA has been analyzed using regression techniques (Richer et al., 2013; Mir et al., 2015) and artificial neural networks (Hou and Huang, 2014), which were used to develop predictive models (Thirel et al., 2013; Mishra et al., 2014). López-Moreno and Nogués-Bravo (2006) evaluated a number of interpolation methods for mapping snow depth from point data, including regression-tree models, linear regression and generalized additive models (GAMs). Tabari et al. (2010) compared snow depth estimated by

artificial neural network (ANN) and neural network-genetic algorithm (NNGA) models with other combined models (multivariate linear regression (MLR), discriminant function analysis, ordinary kriging, ordinary kriging-multivariate linear regression, ordinary kriging-discriminant function analysis). Other studies report on mapping snow depth from point data (Kucerova and Jenicek, 2014) and from the combined use of point data and remote sensing data (Stähli et al., 2002).

Other studies focused on the analysis of snow density distribution from point data (Bormann et al., 2013; Lopez-Moreno et al., 2013). Snow density mapping, which can be obtained by applying regression techniques combined with snow depth mapping, allows the spatial distribution of SWE to be determined (Sexstone and Fassnacht, 2014; Elder et al., 1998). Many studies have been developed to map SWE for dates with available ground-truth data, matching them with satellite-based observations (Harshburger et al. (2010)) applying multiple regression techniques). Dariane et al. (2014) applied an artificial neural network coupled with wavelet transform to estimate the SWE using passive microwave data.

From a hydrological point of view, the snow variable of greatest interest is SWE, due to its influence on snowmelt fluxes. Other studies have simulated the evolution of SWE and snowmelt fluxes. López-Moreno and García-Ruiz (2004) presented an approximation of spring discharge by using regression models with spring rainfall and snow depth as predictor variables. Simulation of snowmelt fluxes has been also performed by applying stochastic models [ARMAX (Haltiner and Salas, 1998), Markov chains and Bayesian models (Krzysztofowicz and Watada, 1986; Kim and Palmer, 1997)), neural network models (Tedesco et al., 2004); Caiping and Yongjian, (2009)), conceptual models (e.g. HBV (Lindström et al., 1997); SRM (Martinec et al., 2008); (Sensoy and Uysal, 2012)), physical models (e.g. CROCUS (Bruland et al., 2001); ECHAM (Foster et al., 1996)] with various levels of complexity. These models allow simulation of both SWE and snow melt fluxes.

The current paper focuses on interpolation methods to give a systematic spatio-temporal estimate of the snow depth. Regression based methodologies are used to study snow depth distribution using different kinds of explanatory variables: geographic (see López-Moreno and Nogués-Bravo, 2006), topographic (Fassnacht et al., 2012, 2013), climatic (Sospedra-Alfonso et al., 2015b; Morán-Tejeda et al., 2013) and forest variables (Lopez-Moreno and Stähli, 2008; Garvelmann et al., 2015). There are only a few applications of the regression kriging technique to estimate snow depth in the literature (see Kucerova and Jenicek 2014; Carroll et al., 1995). Applications that estimate snow distribution and snow depth using combined point data and satellite observations are scarce (Stähli et al., 2002). In the current study, we propose a parsimonious approach for optimal estimation of snow depth (areal extension and thickness) in Alpine systems. We define a new systematic method that integrates a number of techniques (multiple regression, multi-criteria analysis and kriging of the residuals), data and prior knowledge (possible explanatory variables) about the snow depth distribution. Our aim is to provide an insight to address several issues, such as which regression structural model is best and which are the best explanatory variables for a fixed structural model. We have solved both questions simultaneously in order to find optimal solutions. We deal with the difficult but common case of having a small number of

experimental data (ground measurements of snow thickness) but a high number of explanatory variables. The Snow Cover of the MODIS Cryosphere Products (Hall et al., 2006) are used as a mask to determine the area covered by snow (see Bales et al., 2008). The values obtained with the regression model are further refined by estimating the regression residuals by kriging (Fassnacht et al., 2003). In the final step, the residual estimates are added to the regression estimates to give the final regression kriging estimates. The various steps of the method are detailed in the next section.

Our approach is illustrated through the analysis of a case study of the Sierra Nevada (Southern Spain), the most important mountain range in southern continental Europe. We propose a mountain range scale study covering rainfall over a whole mountain, while snow interpolation methods found in the scientific literature are applied at catchment scale to more local problems.

2. Methods

The steps for an optimal estimation of snow depth in accordance with the methodology proposed can be observed at Figure 3.1 and they are described below.

1) Identification of the variables involved

Our aim is to estimate the snow depth at any position $Y(s_0)$ using point data coming from snow stakes $Y'(s_i)$ for a certain location s_i , satellite data and a number of explanatory variables. In accordance with previous snow interpolation works cited in the introduction (Fassnacht et al. (2013)) we propose to use a number of explanatory variables deduced from digital terrain models.

These variables belong to three classes: geographic (latitude, longitude, terrain curvature and elevation), orographic (eastness, northness and slope), and “pseudo-climatic” (mean radiation index and maximum upwind slope). The pseudo-climatic variables are obtained by combining orographic and climatic characteristics such as solar radiation assuming absence of clouds or wind direction (for the maximum upwind slope).

Some of these explanatory variables such as the geographic characteristics (longitude, latitude, elevation, terrain curvature) and slope are well known and do not need any definition. Others require an explanation about how they are defined and obtained. The eastness and northness variables summarize the east–west and north–south orientations of the slopes, respectively. They are obtained as the sines and cosines of the aspect by a procedure that converts linear degree units (1 to 360) to circular units (1 to -1) (Fassnacht et al., 2013). The radiation index was obtained from the viewshed algorithm from the ArcGIS platform developed by Rich et al. (1994), as further developed by Fu and Rich (Fu and Rich, 2000; Fu and Rich, 2002). Global radiation is calculated as the sum of direct and diffuse radiation.

The maximum upwind slope parameter (S_x) quantifies the degree of wind exposure (Winstral et al., 2002) (see equation 3A1 in Appendix 3A). S_x quantifies the snow exposed areas to wind blowing (negative value) and snow accumulation (positive value).

2) Definition of multiple regression models

Snow depth (our dependent variable) can be related to different variables (see equation 3A2 of appendix 3A)

In this study we consider eight different regression model structures with different degrees of complexity (see equations 3A3 to 3A10 of appendix 3A). All these linear models have been named with numbers starting from the simplest one to the most complex, defined by a higher number of parameters, variables and interactions between them. We intend to test a wide range of combinations and transformations of explanatory variable in order to identify which of them provides a better approximation of our problem.

Multiple models are calibrated combining all possible model structures (eight structures defined combining 1, 2, 3 or 4 variables) and variables (the explanatory variables described in section 2.1 and logarithm, inverse, square and square root mathematical transformations of them).

The information available to calibrate the models is provided by the observations of snow-depth at a particular location, s_i and the value adopted by the various explanatory variables at the same location. Applying maximum likelihood normal regression, the parameters can be estimated by solving an optimization problem (see Equation 3A11 of appendix 3A). The maximum likelihood of the variance of residuals $\hat{\sigma}^2$ can be also easily estimated (see Equation 3A12 of appendix 3A).

3) Assessment of the models and selection of the best approaches

A multi-criteria analysis is proposed to identify the best models and predictive variables in accordance with those indices (NLLF, AIC, BIC, KIC, R² and R²-adj) (see explanations in Appendix 3A). The ‘inferior’ models (in terms of goodness of fit) were identified (dominated solutions, using the terminology of multi-objective analysis) and eliminated. In this way, a model is eliminated if any other model’s predictions are better, as judged by all the cited indices. Statistical analysis of these results allows conclusions to be drawn about the model structures and variables that provide the best approach to the problem.

4) Estimation of the snow-depth (value and uncertainty) by regression

The snow depth $\hat{Y}(s_0)$ at location s_0 can be obtained by using the selected regression models and explanatory variables. This estimate has an associated variance (see Equation 3A19 of Appendix 3A).

5) Improvement of the residual estimate (values and uncertainties) by applying kriging in cases with spatial correlation.

The residuals $e(s_i)$ at the location with point data s_i can be obtained as the difference between the estimated value and the data in that point (see Equation 3A20 in Appendix 3A). The correlation structure of these residuals is analyzed by estimating the variogram $\gamma(h)$ (see Equation 3A21 in Appendix 3A).

It is necessary to adjust a model for the experimental variogram. Normally the models used are spherical, exponential or Gaussian (Chiles and Delfiner, 1999). The residuals ($\hat{e}(s_0)$) and their uncertainty ($\sigma_k^2(s_0)$) can be estimated by kriging (See equations 3A22 and 3A23 in Appendix 3A).

The kriging of the residuals can only be done when there are experimental measurements of thickness. If there are measurements of snow, most of the variability will be explained by the regression. At the experimental data the value of the residuals is known and kriging provides an estimate of this residual (at non-sampled locations) that will provide a better final estimate. Note that the mean of the residual is zero and that the kriging estimate at a location far from the experimental data will be then close to zero. Thus kriging does not hinder the regression estimates.

6) Final estimates: combining regression, kriging results (regression kriging) and satellite data

A better estimate is obtained by combining the regression and satellite data using the regression kriging technique. The final results are defined as the sum of regression estimation and residual estimation (see Eq. 3A24 and 3A25 in Appendix 3A).

The satellite data are also used to constrain the domain for the snow depth estimates in accordance with the SCA. For cloudy days, when SCA cannot be deduced from satellite data, this information could be estimated using the closest previous and subsequent days without cloud and applying linear interpolation.

7) Cross validation of the estimated values by regression kriging

Cross-validation is a common method in geostatistics for assessing the performance of the spatial interpolation by kriging. In cross-validation, each experimental datum in turn is dropped from the experimental data set and it is estimated using the rest of experimental data (Chiles and Delfiner, 1999). Thus, it is possible to determine the true error of the interpolation by regression kriging (see Equation 3A26 in Appendix 3A):

From these errors, the following cross-validation statistics can be obtained: mean error (ME), mean squared error (MSE) and mean standardized squared error (MSSE), whose equations are included in Appendix 3A (Equations 3A27, 3A28 and 3A29).

ME is defined as the mean of the true errors.

The ME is the bias of the estimate. The value should be around zero. This criterion should always be met because kriging is an unbiased estimator.

MSE is defined as the mean of the squared true errors.

The MSE is the precision of the estimate. The value should be as small as possible.

MSSE is defined as the mean of the standardized squared true errors:

The MSSE evaluates how well (statistically) the variance of the estimate is a realistic measure of uncertainty. The value should be around one if the kriging variance is a good measure of uncertainty.

8) Estimation of snow SWE and its uncertainty

Although it is not the scope of this work, we also propose to perform a first estimation of the SWE, which is a variable defined to assess the volume of water in the snow. It can be calculated by using the estimated snow depth, the SCA, the snow density and the water density (see Equation 3A30 in Appendix 3A).

The uncertainty of the estimated SWE can be assessed by propagation of the uncertainty of each of the terms; for example, using a Monte Carlo approach where possible values of each term are generated many times to obtain a histogram of SWE. From this histogram, different uncertainty measures can be obtained.

3. Study area: Description of the case study and the available data

In order to illustrate our methodology, we applied it to a case study, the Sierra Nevada mountain range in Southern Spain.

The Sierra Nevada is a mountainous massif situated in the Betic mountain range system in the south of the Iberian Peninsula (see Figure 3.2). It is almost 80 Km long and between 15 and 30 Km wide, covering an area of more than 2000 Km². The Sierra Nevada is important to the region from an economic point of view, with many tourists traveling there in winter to ski. In addition, the snow is an important water resource for the city of Granada. In the melt season there are significant water inputs to the city reservoir. The Sierra Nevada has a high-mountain Mediterranean climate with a relatively dry summer and more precipitation in winter. In winter the majority of the precipitation falls as snow.

Our aim was to estimate the snow depth in the Sierra Nevada using the MODIS Sinusoidal Tile Grid which has 500 m of spatial resolution at nadir and approximately 460 m at the study area. Although it is not the scope of this paper we have also performed a first simplified approximation to quantify the SWE for the Canales and Guadaleo river basins (see Figure 3.2). The size of the basins is 176 and 1300 km² respectively. In this study we employed snow depth information from 23 snow stakes from 11 surveys provided by the Spanish Ministry of Agriculture Food and Environment (within the framework of the ERHIN program (Evaluación de los Recursos Hídricos Procedentes de la Innovación: Assessment of Water Resources from Snow Accumulation; <http://www.magrama.gob.es/es/agua/temas/evaluacion-de-los-recursos-hidricos/erhin/>) for the period 2000-2014. Most of times the snow depth was measured by visual inspection from helicopter in the available stakes (See Figure 3.2) with a measurement error around 10 cm. Snow depth data coming from the ERHIN program in the Pyrenees was employed in the development of previous research works (Lopez-Moreno and García-Ruiz, 2004; Lopez-Moreno and Nogués-Bravo, 2006), but this is the first application of them in the S. Nevada system. We also used daily MODIS SCA data for the same period. In this study we have used the data set MODIS/Terra Snow Cover Daily Global 500m Grid

(Data Set ID: MOD10A1). The spatial and temporal resolution of this data set is 500 m at nadir and 1 day respectively and the temporal coverage is 24 February 2000 to the present. Snow covered land has a very high reflectance in visible bands and very low reflectance in the shortwave infrared. The difference of both determines the SCA. Each observation represents the best sensor view of the product MODIS/Terra Snow Cover 5-Min Swath 500m (Data Set ID: MOD10_L2) in the cell.

The mean value of the snow depth measurements for the period 2000-2014 is 99 cm. They vary between 0 and 450 cm within the period with available data. The variability of the measured data can be observed in Figure 3.3. For example, it shows as the maximum mean thickness measured in stakes appears in April (147.6 cm) and the minimum value in March (52.9 cm). Note that the number of available measurements in each month is quite different. There is not any year in which we have measurements in each month of the snow season. Therefore we cannot draw conclusions about the monthly variability in a year. The number of available data varies in each campaign. The mean value is 21 and the maximum and minimum are 23 and 19 respectively.

The high uncertainty in the density, with even less number of data than the available for thickness, and the important doubts about how and where it was measurement, push us to focus the target of our paper in snow depth estimation. Nevertheless a first approximation of the SWE is obtained by using the mean snow density (0.4 g/cm³) reported by the ERHIN program in the stakes.

4. Results

4.1 Analysis of the explanatory variables

We estimated and represented the values of all the variables described in section 2 (longitude, latitude, elevation, terrain curvature, slope, eastness, northness, mean radiation index, maximum upwind slope) (Fig. 4). We could have considered vegetation cover as a binary variable but the satellite images show that vegetation cover is not important at the location of the stakes. The stakes are situated above 2100 meters where, in our case study, only low vegetation (shrubs, grasses, forbs, etc.) are present.

The Sx represented in Fig 4.F, which depends on the azimuth (A) of the search direction and the extent of the search (dmax). Due to we do not know the dominant wind direction for the whole Sierra Nevada system we propose to obtain it as follow. We prepared Sx maps for different dmax (100, 200, 300, 400 and 500 m) and azimuths (0°, 45°, 90°, 135°, 180°, 225°, 270° and 315°). Then we related the maps to mean snow depth in order to identify the pair of values (dmax, azimuth) with the highest coefficient of determination for the snow season. In our case study, this corresponded to 90° azimuth and 300 m dmax. We checked whether the pair of values obtained was also representative for different months. Figure 3.5 shows the prevailing wind direction is the same for each month of the snow season. The correlation between snow depth and Sx is not high because the snow distribution must be explained by more variables.

We prepared the Sx map using the pair of values obtained and used this map as the explanatory variable for the snow depth estimate. In Figure 3.4.F, the negative values are snow drag zones and the positive values are snow accumulation zones.

In order to apply the proposed regression method we require to know the value adopted by the explicative variables in each snow stake. We have also estimated and represented (see Figure 3.6) the ranges in which observations in snow stakes lies for each predictor and the range in which they change in our case study in order to check if they are representative of the geographic and topographic variability of the study area. In all the cases the range defined by the extreme of the whiskers cover the extreme of the box obtained for the case study (values between the 25% and 75% of those obtained for the whole case study). Therefore, the stakes allows to cover the range defined by the most frequent value in the case study. In most of the variables the box for the snow stakes cover an important range of the value cover by the box of the case study (the mean value is higher than 64%). The highest statistical differences between the values in the stakes and in the study area are obtained for the solar radiation variable.

4.2 Definition and selection of the best models and explanatory variables

In order to identify the best regression models, we assessed the goodness of fit for all possible combinations of model structures (the eight formulations defined in section 2) and the forty five variables tested, namely the nine explanatory variables described in the previous section and the transformed variables obtained by applying four mathematical transformations (logarithm, inverse, square and square root) to these nine.

Next, indices (described in section 2.3) were selected to assess the goodness of fit: coefficient of determination; adjusted coefficient of determination; negative log-likelihood function; Akaike information criterion; Bayesian information criterion; Kashyap information criterion.

Figure 3.7 shows (for the survey of 21/04/2003) the value of these indices for the eight optimal models (one for each model structure) attending to the coefficients of determination. In general, the coefficients of determination and adjusted coefficients of determination increase (indicating a closer fit) as the model complexity increases. For the other four indices, an inverse trend is observed, with lower values of the index as the complexity increases (which also shows a closer fit).

A multi-objective analysis was performed to identify the best models and predictive variables in accordance with those indexes. The inferior models (in terms of goodness of fit) were identified and eliminated. In this way, a model is eliminated if any other model's predictions are better for all the cited indices. Statistical analysis of these results allows conclusions to be drawn about the model structures and variables that provide the best approach to the problem.

Over all the surveys, only one model is not eliminated, namely the model of complexity 7. Therefore, this is the “optimal model structure” to estimate snow depth over the eleven surveys. This analysis also allowed us to identify the most significant explanatory variables in the case study. Figure 3.8 shows, for each explanatory variable, the frequency with which it

appears in the non-eliminated models. This frequency was obtained for each of the eight model complexities by counting the number of times that the variable appears in the non-eliminated models and expressing it as a percentage of the total number of variables (including the repeated ones) that define the selected models.

In general, the variables appearing with highest frequencies in the non-eliminated models are elevation and slope – which is physically reasonable. If we use a model with a unique explanatory variable, elevation is the selected variable in 67.5% of cases. In models with two variables (models 2 and 3), elevation appears as the most frequent variable (around 40% of the selected models). For the more complex models, slope appears with a high frequency, especially for models of complexity 3, 6 and 8. In the case of the model of complexity 7, previously described as the “optimal model structure” because it is not eliminated in any survey, the most frequent variables are elevation and terrain curvature. As the complexity increases, so does the participation of other variables.

We have also analyzed the interaction of variables that help to explain snow depth distribution based on the multicriteria analysis performed. The variables that appear more frequently as product of variables in the non-eliminated models have been represented in Fig. 9. The most important product of variables is curvature-eastness (24.7% of participation) but other products have a high participation as Sx-northness (16.8% of participation), curvature-slope (13.5% of participation) and northness-eastness (9.9% of participation). Note that from a statistical point of view the interaction between variables does not increase the complexity of the model, although certainly may complicate the physical interpretation. That is, fixing the number of terms, and hence the number of coefficients that must be estimated, the use of more variables does not imply the necessity of more experimental data to have robust estimations of the coefficients.

For each survey, the snow-pack was estimated using four regression models defined using the “optimal structure” (model complexity 7). Table 3.1 shows the explanatory variables of the models obtained for each survey with model complexity 7.

For each survey, we compared the results obtained using the “optimal survey model” (a model structure that might be different for each survey) and a single fixed model used to approximate all of the surveys together, the “optimum global model” (whose structure allows a better approximation of the totality of the surveys, taking into account the values obtained for the regression coefficient, the adjusted coefficient of determination, negative log-likelihood function; Akaike information criterion and Bayesian information criterion) using the various predictive variables.

Figure 3.10 shows the coefficients of determination obtained for each of these approximations, where the optimal model corresponds to the optimal model for each survey and 1, 2, 3, 4, 5, 6, 7, 8, 9 and 10 are the models noted in Table 3.1. It shows that the optimal model has a high mean coefficient of determination (exceeding 0.8).

4.3 Snowpack extension and thickness estimates

The areal extension and thickness of the snowpack was estimated by adding the multiple regression estimates to the estimates of the regression residuals (a procedure known in geostatistical literature as regression kriging, described in section 2). The domain for the snowpack estimation was constrained using MODIS SCA data.

On cloudy days when SCA could not be deduced from MODIS data, we approximated it by linear interpolation between the nearest previous and subsequent cloudless days. Note that in our case study we are estimating snow extent in periods with a reduced number of cloudy dates (in the pixel with the highest number of cloudy dates in the historical period we have a mean number of 7 cloudy days per snow season) in a high elevation area where the inertia of the snowpack is high enough to apply a simple linear interpolation. Nevertheless, more elaborated physically based methods to interpolate snow extent beneath cloud cover could be explored in future works (Molotch, et al., 2004).

The snow depth was obtained for each survey using the optimal regression models. In order to perform a sensitivity analysis, we also obtained the snow depth using the worst and best models (in terms of mean correlation), which are model 7 (for the 27/02/2006 survey) and model 4 (for the 13/01/2004 survey). We also used model 2 (05/04/2003 survey), which gave an intermediate coefficient of determination (see Figure 3.10). These sensitivity analyses allowed us to check whether a fixed model (with the same structure and explanatory variables) could be employed to make a good estimate for all surveys, providing snow depth or SWE estimates close to the values obtained with the optimal model for each survey.

Figure 3.11 shows that there can be significant differences in estimated snow depth in some cells when the model used has a low coefficient of determination. For the optimal models and the other three approaches (2, 4, 7), the mean estimated snow depth (in the snow covered cells of the grid) are 32.9 cm, 32.0 cm, 30.6 cm, and 27.0 cm, respectively. Figure 3.11 shows the standard deviation of the estimate for the 24/03/2005 survey. The largest difference compared to the optimal solution appears with model 7 (with high standard deviation of 217 cm). They are less significant in the other two cases.

Note that, in cases with a reduced number of experimental data (as this study case) visual inspection of the snow depth maps obtained with different models (for example model 4 and the optimum model) could show quite rather differences with quite similar goodness indicators. It is due to the change on the independent variables can be quite different depending on the variable (distance, slope, elevation, terrain curvature, etc.). However the model gives an average behavior of the snow depth as defined by the multiple regression that best fits the experimental data, although it can be quite different in areas far from the experimental data.

4.4 Cross validation of results

A cross validation analysis using the technique “leave one out” (using all the data except the one that you are estimating) was performed for the optimal to check the accuracy of the model estimates.

Figure 3.12 show the mean error and the mean standardized squared error of the cross-validation experiment. The mean errors are good for all surveys; the mean error for all surveys was -0.15 cm and the mean maximum errors were -9.9 and -11.5 cm in the 05/04/2001 and 05/04/2003 surveys, respectively. The mean standardized squared error is 0.81 (close to 1), which is a conservative value whereby the estimated uncertainty (standard error) is larger (on average) than the true error.

4.5 Estimates of SWE

Assuming a constant snow density (equal to the mean density obtained from measurements taken for the ERHIN program) a first approximation of SWE was performed for the whole of the Sierra Nevada Mountains and the two largest watersheds in the system (Canales and Guadaleo). SWE was obtained for each survey using the snow depth calculated from the regression kriging of the SCA deduced from MODIS data.

Figure 3.13 show the estimated SWE using the four selected models and the standard deviation for the optimal solutions. It shows a very extreme SWE for the 13/02/2009 survey, more than three times higher than the others.

In the Sierra Nevada system, the relative mean differences (with respect to the optimal solution) considering all surveys were 18.4%, 11.7% and 20.8% for models 2, 4 and 7, respectively. For the 21/04/2003 and 13/01/2004 surveys, models 2 and 7 showed significant differences (around 45%). For the other surveys, these models have reasonable differences (mean differences of 12.10% and 15.5% and maximum of 31.4% and 34.7%, respectively). For the 13/02/2009 and 08/05/2013 surveys, model 4 showed important differences (around 45%) but for the other surveys the model has a good behavior (mean differences of 4.4% and maximum of 12.4%).

The mean SWE over all surveys for the Guadaleo basin was around three times higher than in the Canales basin. In terms of mean SWE, the relative differences between the optimal model estimate and models 2, 4 and 7 are a little more significant in the Canales basin (21.3%, 24.3% and 24.7%, respectively) than in the Guadaleo basin (19.89%, 15.75% and 19.15%, respectively).

5. Discussion

This paper focuses on estimating snow depth in the Sierra Nevada Mountain from a reduced number of experimental data.

It is the first investigation that attempts to address the snow depth spatial distribution of the whole Sierra Nevada system, which is the most southerly Alpine system in Europe. A

previous snow modeling work was developed in this area by Herrero et al. (2009), but it was focus in a totally different problem, the definition of a snowmelt point model. They used data of snow evolution at a monitoring point in the Guadalefeo Basin for two seasons (2004-2005 for the calibration and 2005-2006 for the validation) in order to develop a mass and energy balance . Previous work has addressed the calculation of snow depth over large areas where the availability of experimental observations was restricted, such as in the Spanish Pyrenees (López-Moreno and Nogués-Bravo, 2006).

A new systematic method that integrates a number of techniques (multiple regression, multi-criteria analysis and kriging of the residuals), data (experimental observations and satellite information about SCA) and prior knowledge (possible explanatory variables) about snow depth distribution. The usefulness of regression techniques to approach this issue (of large Alpine areas with a reduced number of data) has been previously demonstrated in other case studies, such as in the Spanish Pyrenees (see López-Moreno and Nogués-Bravo, 2006). They showed that this global method (based on the response of the snow depth to the explanatory variables) provides better results than local or geostatistical methods. In the current study, we propose the analysis of other regression model structures (including products of explanatory variables and certain mathematical transformations of these) and their combined use with multi-criteria analysis (in order to identify the most valuable explanatory variables) and kriging of the residuals. This kriging improves the final estimate only in cases where the residuals showed some spatial correlation, which was demonstrated to happen in our case. It is intended to be a parsimonious approach to complement physical-based methodologies. It only uses easily accessible experimental data (experimental measurements of snow thickness, the DEM and MODIS data) and there are not assumptions on the physical or dynamical behavior of the snow depth, therefore it could help to identify a priori some important parameters that influence on the snow depth distribution. In some cases, it may help to identify which could be the origin of some problems in physical models if they could not provide good approximation to the observations.

The multi-criteria analysis shows that the best model structure is number 7, which includes the products of explanatory variables. The coefficients of determination produced by the optimal models were high (greater than 0.8). The explanatory variables to be considered in the study were deduced from the previous regression studies available (see section 2.1). The multi-criteria analysis indicates that elevation is the most important explanatory variable, which concurs with results obtained from other case studies (e.g., the Spanish Pyrenees study already cited). In the case of the model of complexity 7 (described as the “optimal model structure”), the most frequent variables are elevation and terrain curvature. Although in many of the available studies (eg. Lopez-Moreno and Nogués-Bravo, 2006; Lopez-Moreno and Stähli, 2008) the solar radiation is usually one of the most important predictor in this case it does not happen. It may be due to the range of this variable for the places where the stakes are located is quite different to the range for the whole case study area (see Figure 3.6). Therefore, it could be the reason why it does not allow to capture the effect of this variable in the snow distribution.

Another difference compared to previous studies is that we also propose the use of satellite information about SCA as a means to improve our estimates. There are only a few applications that employ regression techniques and which can also consider satellite information (Kucerova and Jenicek, 2014).

The cross validation analysis for the optimal model shows good results for all surveys. The mean error was 0.15 cm and the mean maximum error was -11.5 cm. The mean standardized squared error was 0.81 (which is a conservative value), whereby the estimated uncertainty (standard error) is larger (on average) than the true error.

5.1 Limitations and future works

Although we have developed a general method and algorithm (that could be applied to any case study) to analyze an exhaustive number of regression structures to estimate snow depth we wanted to highlight some limitations and hypotheses assumed in this application:

- 1) The data available are very limited (only 11 surveys with 23 ground observations). It would be also interesting to test the method in the future in cases with a higher number of available data. Note that the sample size for the regression modeling should not be incremented by adding zeros data from snow free areas due to it would modify the skewness of the dataset and would introduce higher errors in the estimation of the snow depth in the stakes. The information of the zeros is already taken when applying the mask with the MODIS image. It has already been proved with the estimation of rain (Barancourt et al., 1992) that it is better to separate the problem in two sub-problems 1) estimation of rainy and non-rainy areas and 2) estimation of rain inside the rainy areas using rainy data ($\text{rain} > \text{zero}$) only. The same happens with the snow. It is better to model the snow depth with snow data ($\text{snow} > \text{zero}$) to estimate snow inside the snowpack because the snow and non-snow areas is already given by the MODIS image.
- 2) Although it is not the target of this work, we also performed a first estimation of the SWE, which is the variable of greatest interest from a hydrological point of view. In this study, we assumed a constant snow density (the mean density obtained from measurements from the ERHIN program) to obtain a first approximation of SWE for our case study. A more detailed analysis and assessment of the variability (spatial and temporal) of snow density would be required for a more accurate approximation of SWE (Bormann et al., 2013; Lopez-Moreno et al., 2013). Nevertheless, the SWE results have been included only as a first approximation of this hydrological variable.
- 3) We have approximated the SCA in cloudy dates without MODIS information by linear interpolation between the nearest previous and subsequent cloudless days. More elaborated physically based methods to interpolate the snow extent beneath cloud cover could be explored in future works (Molotch, et al., 2004).

6. Conclusions

A parsimonious approach for an optimal estimation of snow depth (areal extension and thickness) in Alpine systems is proposed. It is based on the relationship between ground

experimental data and a number of explanatory variables (obtained from a digital terrain model) of the SCA, which can be deduced from satellite data. A systematic method is defined by integrating different techniques (multiple regression, multi-criteria analysis and residual kriging), data, and prior knowledge about snow depth distribution. It is easy to apply, operational and does not have demanding data requirements. The main steps to be followed for its systematic application, (described in detail and illustrated in the paper) are: (a) Identification of the explanatory variables to be explored, deduced from the digital terrain model. (b) An exhaustive multiple regression analysis using the ground observations and the proposed explanatory variables. Multiple models are calibrated combining all possible model structures (combining 1, 2, 3 or 4 variables) and explanatory variables. (c) Assessment of the models and selection of the best approaches (model structures and explanatory variables). A multi-criteria analysis is applied in accordance with the indices proposed to analyze the goodness of fit of the models. (d) Estimation of snow depth and uncertainties with the selected regression models. (e) Improvement of the residual estimates (values and uncertainties) by applying kriging in cases with spatial correlation. (f) The final estimates are obtained by combining the regression and kriging results (a regression kriging technique) and constraining the snow domain in accordance with the satellite data. The proposed method was applied to the Sierra Nevada (Southern Spain) with interesting results. The best regression model (model structure 7) was identified in accordance with the available data. The most important explanatory variables (elevation, northness and slope) were also identified. (g) Cross validation of the results was performed with good results. The mean errors were good for all surveys, with a mean error over all surveys of 2.4% and maximum errors of -13.5 and -15.3 cm. (h) Finally, the results were used to obtain a first approximation of the SWE for the Sierra Nevada system as a whole and for some specific sub-basins. Due to its generality, the methodology can be easily implemented in other areas of interest.

Acknowledgments and Data

This research was partially supported by the GESINHIMPADAPT project (CGL2013-48424-C2-2-R) with Spanish MINECO funds. We would also like to thank the ERHIN program and NASA DAAC for the data provided for this study. The authors thank Steven Fassnacht and two anonymous reviewers for their detailed and helpful comments on improving the paper.

References

- Bales RC, KA Dressler, B Imam, SR Fassnacht, DJ Lampkin . 2008. Fractional snow cover in the Colorado and Rio Grande basins. *Water Resour. Res.* 44: 1995–2002 W01425. doi:10.1029/2006WR005377.
- Barancourt C, Creutin JD, Rivoirard J. 1992. A method for delineating and estimating rainfall fields. *Water Resources Research* 28 (4): 1133–1144.
- Bormann KJ, Westra S, Evans JP, McCabe MF. 2013. Spatial and temporal variability in seasonal snow density. *Journal of Hydrology* 484: 63-73.

- Bruland O, Maréchal D, Sand K, Killingtveit Å. 2001. Energy and water balance studies of a snow cover during snowmelt period at a high arctic site. *Theoretical and Applied Climatology* 70: 53–63.
- Caiping C, Yongjian D. 2009. The application of artificial neural networks to simulate meltwater runoff of Keqikaer Glacier, south slope of Mt Tuomuer, Western China. *Environmental Geology* 575: 1839–1845.
- Carroll SS, Day GN, Cressie N, Carroll TR. 1995. Spatial modelling of snow water equivalent using airborne and ground-based snow data. *Environmetrics* 6: 127–139. doi: 10.1002/env.3170060204
- Chiles J, Delfiner P. 1999. *Geostatistics: Modeling Spatial Uncertainty*. Wiley, New York, 695 pp.
- Molotch NP, Fassnacht SR, Bales RC, Helfrich SR. 2004. Estimating the distribution of snow water equivalent and snow extent beneath cloud cover in the Salt–Verde River basin, Arizona. *Hydrological Processes* 18(9):1595-1611.
- Dariane AB, Azimi S, Zakerinejad A .2014. Artificial neural network coupled with wavelet transform for estimating snow water equivalent using passive microwave data. *Journal of Earth System Science* 123 7: 1591-1601.
- Elder K, Rosenthal W, Davis RE. 1998. Estimating the spatial distribution of snow water equivalence in a montane watershed. *Hydrological Processes* 12 10-11: 1793-1808.
- Fassnacht SR, Lopez-Moreno JI, Toro M, Hultstrand DM. 2013. Mapping snow cover and snow depth across the Lake Limnopolar watershed on Byers Peninsula, Livingston Island, Maritime Antarctica. *Antarctic Science* 252: 157–166.
- Fassnacht SR, KA Dressler, DM Hultstrand, RC Bales, G Patterson. 2012. Temporal Inconsistencies in Coarse-scale Snow Water Equivalent Patterns: Colorado River Basin Snow Telemetry-Topography Regressions. *Pirineos*, 167, 167-186. doi:10.3989/Pirineos.2011.166008.
- Fassnacht SR, KA Dressler, RC Bales. 2003. Snow water equivalent interpolation for the Colorado River Basin from snow telemetry (SNOWTELE) data. *Water Resour. Res.* 39(8): 1208. doi:10.1029/2002WR001512, 2003.
- Foster JL, Hall DK, Eylander JB, Riggs GA, Nghiem SV, Tedesco M, Kim E, Montesano PM, Kelly REJ, Case, KA, Choudhury B. 2011. A blended global snow product using visible, passive microwave and scatterometer satellite data. *Int. J. Remote Sens.* 32: 1371–1395.
- Foster J, Liston G, Koster R, Essery H, Behr H, Dümenil L, Verseghy D, Thompson S, Pollard D, Cohen J. 1996. Snow Cover and Mass Intercomparisons of General Circulation Models and Remotely Sensed Data. *J. Clim.* 9: 409–426.

- Fu P, Rich PM. 2000. The Solar Analyst user manual. USA: Helios Environmental Modeling Institute.
- Fu P, PM Rich. 2002. A Geometric Solar Radiation Model with Applications in Agriculture and Forestry. Computers and Electronics in Agriculture 37: 25–35.
- Garvelmann J, Pohl S, Weiler M. 2015. Spatio-temporal controls of snowmelt and runoff generation during rain-on-snow events in a mid-latitude mountain catchment. 29:3649–3664. doi:10.1002/hyp.10460.
- Hall DK, GA Riggs. 2007. Accuracy assessment of the MODIS products. Hydrological Processes 21:1534-1547.
- Hall DK, GA Riggs, VV Salomonson. 2006. MODIS/Terra Snow Cover 5-Min L2 Swath 500m. Version 5. Boulder, Colorado USA: NASA National Snow and Ice Data Center Distributed Active Archive Center. doi:10.5067/ACYTYZB9BEOS.
- Haltiner JP, Salas JD. 1998. Short-term forecasting of snowmelt runoff using armax models. Water Resources Bulletin 24 5: 1083–1089.
- Harshburger BJ, Humes KS, Walden V, Blandford TR, Moore BC, Dezzani, RJ. 2010. Spatial interpolation of snow water equivalency using surface observations and remotely sensed images of snow-covered area. Hydrological Processes 24 10: 1285-1295.
- Herrero J, Polo MJ, Moñino A, Losada MA. 2009. An energy balance snowmelt model in a Mediterranean site. Journal of Hydrology 371: 98-107. doi:10.1016/j.jhydrol.2009.03.021.
- Hou JL, Huang CL. 2014. Improving Mountainous Snow Cover Fraction Mapping via Artificial Neural Networks Combined With MODIS and Ancillary Topographic Data. IEEE Transactions on Geoscience and Remote Sensing 52 9: 5601-5611.
- Kelly, REJ. 2009. The AMSR-E snow depth algorithm: Description and initial results. Japanese Journal of Remote Sensing 29 1: 307–317. (GLI/AMSR Special Issue).
- Kim YO, Palmer RN. 1997. Value of Seasonal Flow Forecasts in Bayesian Stochastic Programming. Journal of Water Resources Planning and Management 123: 327–335.
- Krzysztofowicz, R and Watada, LM 1986, Stochastic Model of Seasonal Runoff Forecasts, Water Resources Research, 22, 296–302
- Kucerova D, Jenicek M. 2014. Comparison of selected methods used for the calculation of the snowpack spatial distribution, Bystrice river basin, Czechia. Geografie 119 3: 199-217.
- Lindström G, Johansson B, Persson M, Gardelin M, Bergström S. 1997. Development and test of the distributed HBV-96 hydrological model. Journal of Hydrology 201: 272–288.
- Liu Y, Weerts A, Clark M, Franssen H, Kumar S, Moradkhani H, Seo D, Schwanenberg D, Smith P, van Dijk A. 2012. Advancing data assimilation in operational hydrologic

forecasting: progresses, challenges, and emerging opportunities. *Hydrol Earth Syst Sc* 16 10: 3863-3887.

López-Moreno JI, García-Ruiz JM. 2004. Influence of snow accumulation and snowmelt on streamflow in the central Spanish Pyrenees. *Hydrological Sciences–Journal–des Sciences Hydrologiques* 495: 787-802.

López-Moreno JI, Nogués-Bravo D. 2006. Interpolating local snow depth data: an evaluation of methods. *Hydrol Process* 20: 2217–2232.

Lopez-Moreno JI, Stähli M. 2008. Statistical analysis of the snow cover variability in a subalpine watershed: Assessing the role of topography and forest interactions. *J. Hydrol.* 348: 379–394, doi:10.1016/j.jhydrol.2007.10.018.

Lopez-Moreno JI, Fassnacht SR, Heath, J.T., Jonas T., 2013. Small scale spatial variability of snow density and depth over complex alpine terrain: Implications for estimating snow water equivalent. *Advances in Water Resources* 55:40–52 · DOI: 10.1016/j.advwatres.2012.08.010

Martinec J, Rango A, Roberts R. 2008. Snowmelt runoff model SRM user's manual (pp. 178). Las Cruces, New Mexico, USA: New Mexico State University.

Mir RA, Jain SK, Saraf AK, Goswami A. 2015. Accuracy assessment and trend analysis of MODIS-derived data on snow-covered areas in the Sutlej basin, Western Himalayas. *International Journal of Remote Sensing* 36 15: 3837-3858.

Mishra B, Tripathi NK, Babel MS. 2014. An artificial neural network based snow cover predictive modeling in the higher Himalayas. *Journal of Mountain Science* 114: 825-837.

Morán-Tejeda E, López-Moreno JI, Beniston M. 2013. The changing roles of temperature and precipitation on snowpack variability in Switzerland as a function of elevation. *Geophysical Research Letters*, doi: 10.1002/grl.50463

Pulido-Velazquez D, Garrote L, Andreu J, Martin-Carrasco FJ, Iglesias A. 2011. A methodology to diagnose the effect of climate change and to identify adaptive strategies to reduce its impacts in conjunctive-use systems at basin scale. *Journal of Hydrology* 405: 110–122, doi:10.1016/j.jhydrol.2011.05.014.

Rich PM, Dubayah R, Hetrick WA, Saving SC. 1994. Using Viewshed models to calculate intercepted solar radiation: applications in ecology. *American Society for Photogrammetry and Remote Sensing Technical Papers* 524- 529.

Richer EE, Kampf SK, Fassnacht SR, Moore CC. 2013. Spatiotemporal index for analyzing controls on snow climatology: application in the Colorado Front Range. *Physical Geography* 342: 85-107.

- Sensoy A, Uysal G. 2012. The Value of Snow Depletion Forecasting Methods Towards Operational Snowmelt Runoff Estimation Using MODIS and Numerical Weather Prediction Data. *Water Resources Management* 26(12): 3415-3440
- Sexstone GA, Fassnacht SR. 2014. What drives basin scale spatial variability of snowpack properties in northern Colorado?. *Cryosphere* 8(2): 329-344.
- Sospedra-Alfonso R, JR Melton, WJ Merryfield. 2015b. Effects of temperature and precipitation on snowpack variability in the Central Rocky Mountains as a function of elevation. *Geophysical Research Letters* 42: 4429–4438.
- Stähli M, Schaper J, Papritz A. 2002. Towards a snow-depth distribution model in a heterogeneous subalpine forest using a Landsat TM image and an aerial photograph. *Annals of Glaciology* 34.
- Tabari H, Marofi S, Abyaneh HZ, Sharifi MR. 2010. Comparison of artificial neural network and combined models in estimating spatial distribution of snow depth and snow water equivalent in Samsami basin of Iran. *Neural Computing & Applications* 19(4): 625-635.
- Tedesco M, Pulliainen J, Takala M, Hallikainen M, Pampaloni P. 2004. Artificial neural network-based techniques for the retrieval of SWE and snow depth from SSM/I data. *Remote Sensing of Environment* 90: 76–85.
- Thirel G, Salamon P, Burek P, Kalas M. 2013. Assimilation of MODIS Snow Cover Area Data in a Distributed Hydrological Model Using the Particle Filter. *Remote Sens* 5: 5825-5850. doi:10.3390/rs5115825.
- Viviroli D, Dürr HH, Messerli B, Meybeck M, Weingartner R. 2007. Mountains of the world, water towers for humanity: Typology, mapping, and global significance. *Water Resour Res* 43: W07447. doi:10.1029/2006WR005653.
- Winstral A, Elder K, Davis RE. 2002. Spatial Snow Modeling of Wind-Redistributed Snow Using Terrain-Based Parameters. *J. Hydrometeorol* 3: 524–538.

Appendix 3A: Equations complementary to the text

The parameter S_x quantifies the degree of wind exposure and can be expressed as:

$$S_{x_{A,dmax}}(x_i, y_i) = \max \left[\tan^{-1} \left(\frac{\text{elev}(x_v, y_v) - \text{elev}(x_i, y_i)}{\sqrt{(x_v - x_i)^2 + (y_v - y_i)^2}} \right) \right] \quad (3A1)$$

where A is the azimuth of the search direction, d_{max} defines the lateral extent of the search, (x_i, y_i) are the coordinates of the grid of interest, and (x_v, y_v) are the set of all cell coordinates located along the line segment defined by (x_i, y_i) . The parameter d_{max} modifies the extent of analyzed area in the search and can have an important effect on the distribution of maximum upwind slope.

In a general way, the multiple linear regression models can be defined by the equation:

$$\hat{Y}_n(s_0) = \beta_0 + \beta_1 X_{1i} + \cdots + \beta_m X_{mi} \quad (3A2)$$

where \hat{Y}_n is the variable to be estimated, $\{X_{1i}, \dots, X_{mi}\}$ are the explanatory variables and $\{\beta_1, \dots, \beta_m\}$ are unknown parameters estimated from experimental data. The different regression model structures considered in this study are:

$$\hat{Y}_1 = \beta_0 + \beta_1 x_i \quad (3A3)$$

$$\hat{Y}_2 = \beta_0 + \beta_1 x_i x_j \quad (3A4)$$

$$\hat{Y}_3 = \beta_0 + \beta_1 x_i + \beta_2 x_j \quad (3A5)$$

$$\hat{Y}_4 = \beta_0 + \beta_1 x_i + \beta_2 x_j x_\ell \quad (3A6)$$

$$\hat{Y}_5 = \beta_0 + \beta_1 x_i x_k + \beta_2 x_j x_\ell \quad (3A7)$$

$$\hat{Y}_6 = \beta_0 + \beta_1 x_i + \beta_2 x_j + \beta_3 x_\ell \quad (3A8)$$

$$\hat{Y}_7 = \beta_0 + \beta_1 x_i + \beta_2 x_j + \beta_3 x_\ell x_k \quad (3A9)$$

$$\hat{Y}_8 = \beta_0 + \beta_1 x_i + \beta_2 x_j + \beta_3 x_\ell + \beta_4 x_k \quad (3A10)$$

The estimation of the regression parameters by maximum likelihood normal regression, can be approached by the values that maximize the equation:

$$L(\beta_0, \beta_1, \dots, \beta_m, \sigma^2) = \prod_{i=1}^n \frac{1}{(2\pi\sigma^2)^{1/2}} \exp \left(\frac{-1}{2\sigma^2} (\hat{Y}_i - \beta_0 - \beta_1 X_{1i} - \cdots - \beta_m X_{mi})^2 \right) \quad (3A11)$$

The maximum likelihood of the variance of residuals $\hat{\sigma}^2$ is:

$$\hat{\sigma}^2 = \frac{\sum_{i=1}^n (\hat{Y}_i - Y_i^{ML})^2}{n} \quad (3A12)$$

where n is the number of experimental data of the independent variable.

The following indices were used to assess the goodness of fit of the estimates provided by each of the calibrated models:

The negative of the logarithm of likelihood function (NLLF) can be expressed using the estimate of the variance of the residual equation as:

$$\text{NLLF} = -\ln L(\beta_0, \beta_1, \dots, \beta_m, \sigma^2) = \frac{n}{2} + \frac{n}{2} \ln(2\pi) - \frac{n}{2} \ln(n) + \frac{n}{2} \ln(\text{RSS}) \quad (3A13)$$

where RSS is the residual sum of squares:

$$\text{RSS} = \sum_{i=1}^n (Y_i - \hat{Y}_i)^2 \quad (3A14)$$

with $\hat{Y}_i = \hat{\beta}_0 + \hat{\beta}_1 X_{1i} + \dots + \hat{\beta}_m X_{mi}$ being the maximum likelihood (or least squares) estimate of Y_i . There are many criteria related to the NLLF, which include the number of parameters used in the regression (m), to consider the parsimony or simplicity of the models, in order to avoid the problem of overfitting. The Akaike information criterion (AIC) can be expressed as:

$$\text{AIC} = 2\text{NLLF} + 2m \quad (3A15)$$

The Bayesian information criterion (BIC) provides more weight to the parsimony using the following equation:

$$\text{BIC} = 2\text{NLLF} + \ln(n)m \quad (3A16)$$

Another criterion is the Kashyap information criterion (KIC), expressed as:

$$\text{KIC} = 2\text{NLLF} + \ln(n)m + \ln|B| \quad (3A17)$$

where $|B|$ is the determinant of the information matrix.

Another criterion used for selection of the model is the coefficient of determination. To take into account the parsimony principle, the adjusted- R^2 has been proposed:

$$R_{\text{adj}}^2 = 1 - \left(\frac{n-1}{n-m} \right) (1 - R^2) \quad (3A18)$$

Note that the use of the R^2 index is equivalent to perform a cross-validation analysis (in particular the mean square error) of the regression models if we assume that the models are not affected by reducing the number of data in only one value.

The variance of the estimation of snow depth by regression, $\sigma_r^2(s_0)$, can be calculated as:

$$\sigma_r^2(s_0) = \hat{\sigma}^2 (1 + X'(s_0)(X'X)^{-1}X(s_0)) \quad (3A19)$$

where $X(s_0)$ is the $m \times 1$ vector of independent variables at location s_0 .

The residual of the estimation $e(s_i)$ at the location with ground point data s_i can be expressed as:

$$e(s_i) = \hat{Y}(s_i) - Y'(s_i) \quad (3A20)$$

The correlation structure of these residuals is analyzed by estimating the variogram,

$$\gamma(h) = \frac{1}{2n(h)} \sum_{i=1}^{n(h)} (e(s_i) - e(s_i + h))^2 \quad (3A21)$$

where $\gamma(h)$ is the experimental variogram, h is the lag or distance, $n(h)$ is the number of data pairs and $e(s_i)$ is the variable value at the location s_i .

The residuals and their uncertainty can be estimated by kriging. The interpolate residual $\hat{e}(s_0)$ can be expressed as:

$$\hat{e}(s_0) = \sum_{i=1}^t \lambda_i e(s_i) \quad (3A22)$$

The estimation variance is given by:

$$\sigma_k^2(s_0) = \sum_{i=1}^t \lambda_i \gamma(s_i, s_0) - \mu \quad (3A23)$$

where λ_i are the kriging weights determined by the spatial correlation of the residual, $e(s_i)$ is the residual at location s_i , μ is the Lagrange multiplier and $\gamma(s_i, s_0)$ is the variogram function.

The final results are defined as the sum of regression estimation and residual estimation are:

$$Y(s_0) = \hat{Y}(s_0) + \hat{e}(s_0) \quad (3A24)$$

$$\sigma^2(s_0) = \sigma_r^2(s_0) + \sigma_k^2(s_0) \quad (3A25)$$

The true error of the interpolation can be determined by regression kriging:

$$e(s_i) = Y(s_i) - Y'(s_i) \quad (3A26)$$

where $e(s_i)$ is the true error in the estimate of the i^{th} experimental datum, $Y(s_i)$ is the estimate of the variable of interest at the location of the i^{th} experimental datum, and $Y'(s_i)$ is the true value of the experimental datum of the variable of interest at the i^{th} experimental location.

Thus, if there are N experimental data, cross-validation will give a set of N true errors $\{e(s_i), i = 1, \dots, N\}$.

ME is the mean of the true errors:

$$ME = \frac{1}{N} \sum_{i=1}^N e(s_i) \quad (3A27)$$

MSE is the mean of the squared true errors:

$$MSE = \frac{1}{N} \sum_{i=1}^N e^2(s_i) \quad (3A28)$$

MSSE is the mean of the standardized squared true errors:

$$MSSE = \frac{1}{N} \sum_{i=1}^N \frac{e^2(s_i)}{\sigma_k^2(s_i)} \quad (3A29)$$

where $\sigma_k^2(s_i)$ is the regression kriging variance in the estimation of the i^{th} datum.

The SWE can be calculated for a specific area SWE_A with the following equation:

$$SWE_A = \sum_{j=1}^n Y(s_j) \cdot SCA(s_j) \cdot GA(s_j) \cdot \frac{DS}{DW} \quad (3A30)$$

where $Y(s_j)$ is the estimated snow depth in the grid, $SCA(s_j)$ is the SCA in the grid in parts per unit, $GA(s_j)$ is the grid area at location s_j , DS and DW are the snow density and water density, respectively, and considered constant over area A .

Tables of the Chapter 3

Model	x_i	x_j	x_ℓ	x_k	Optimal for:
1	(ELEV)	(ELEV) ²	(MUWS) ²	(CURV) ²	16/03/2000
2	1/(LATI)	1/(ELEV)	(NORT) ²	(MUWS) ²	05/04/2001, 05/04/2003
3	LN(NORT)	1/(ELEV)	SQRT(LONG)	SQRT(NORT)	21/04/2003
4	(ELEV)	(SLOP) ²	(EAST) ²	(CURV) ²	13/01/2004
5	1/(SLOP)	(ELEV) ²	(SLOP) ²	SQRT(CURV)	26/04/2004
6	LN(CURV)	(ELEV) ²	(EAST) ²	(CURV) ²	24/03/2005
7	LN(CURV)	(LONG) ²	(MUWS) ²	(CURV) ²	27/02/2006
8	(LONG) ²	(SLOP) ²	(EAST) ²	(CURV) ²	13/02/2009
9	(ELEV)	(EAST)	LN(NORT)	1/(EAST)	08/05/2013
10	LN(ELEV)	1/(ELEV)	(SLOP) ²	(CURV) ²	21/03/2014

Table 3.1. Explanatory variables for the optimal models. LATI (latitude), LONG (longitude), ELEV (elevation), EAST (eastness), NORT (northness), SLOP (slope), Sx (maximum upwind slope), RADI (radiation), CURV (curvature).

Figures of the Chapter 3

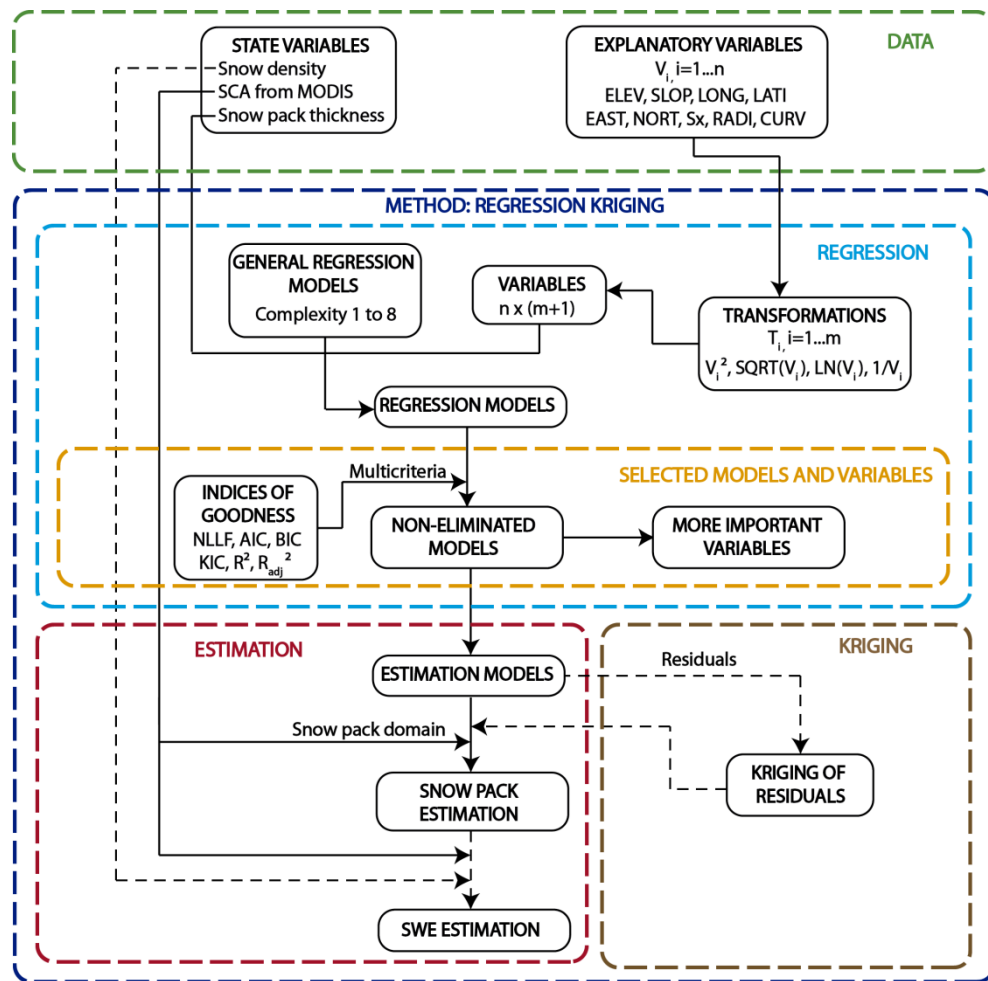


Figure 3.1. Flow chart of the proposed systematic method.

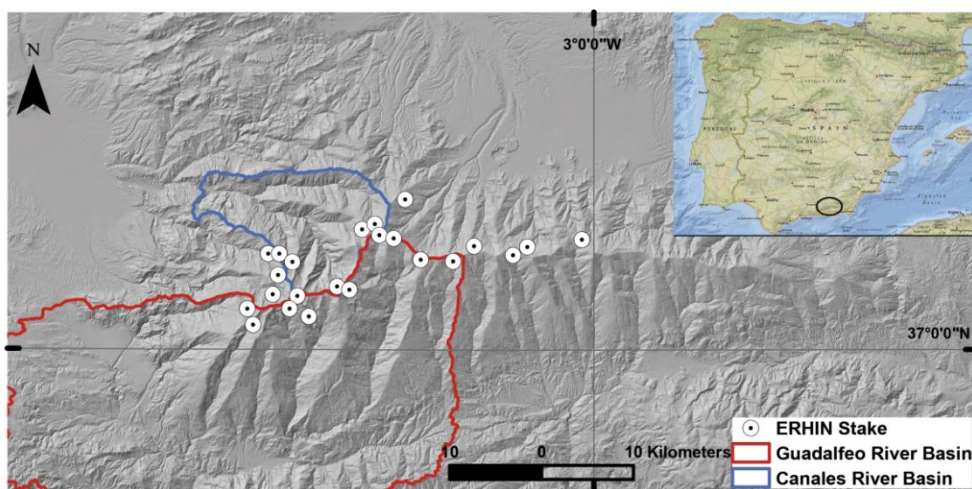


Figure 3.2. Location of the Sierra Nevada mountain range and the stakes where the snow depth is measured.

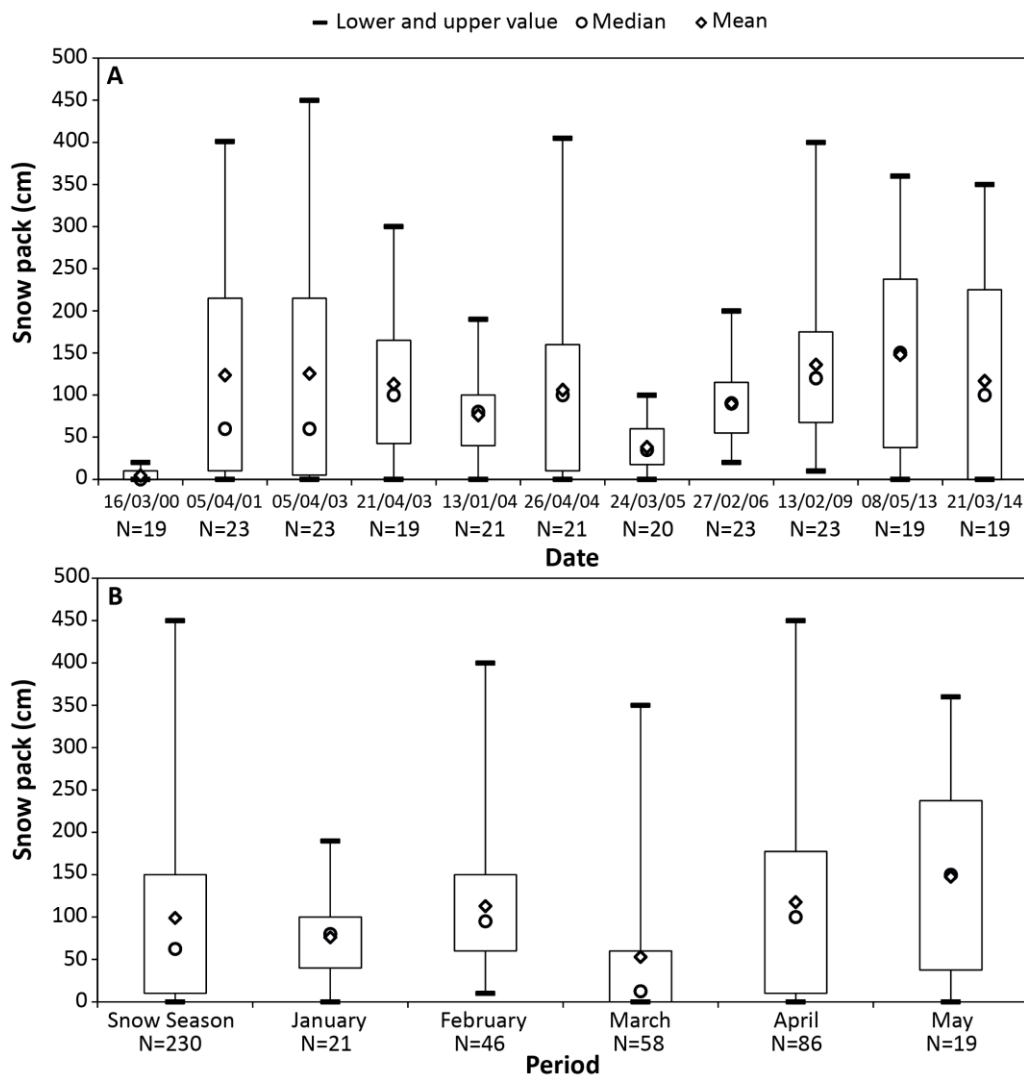


Figure 3.3. Variability of the snow depth data. A: For individual dates. B: For the snow season and the months. The top and bottom of boxes represent the interquartile range.

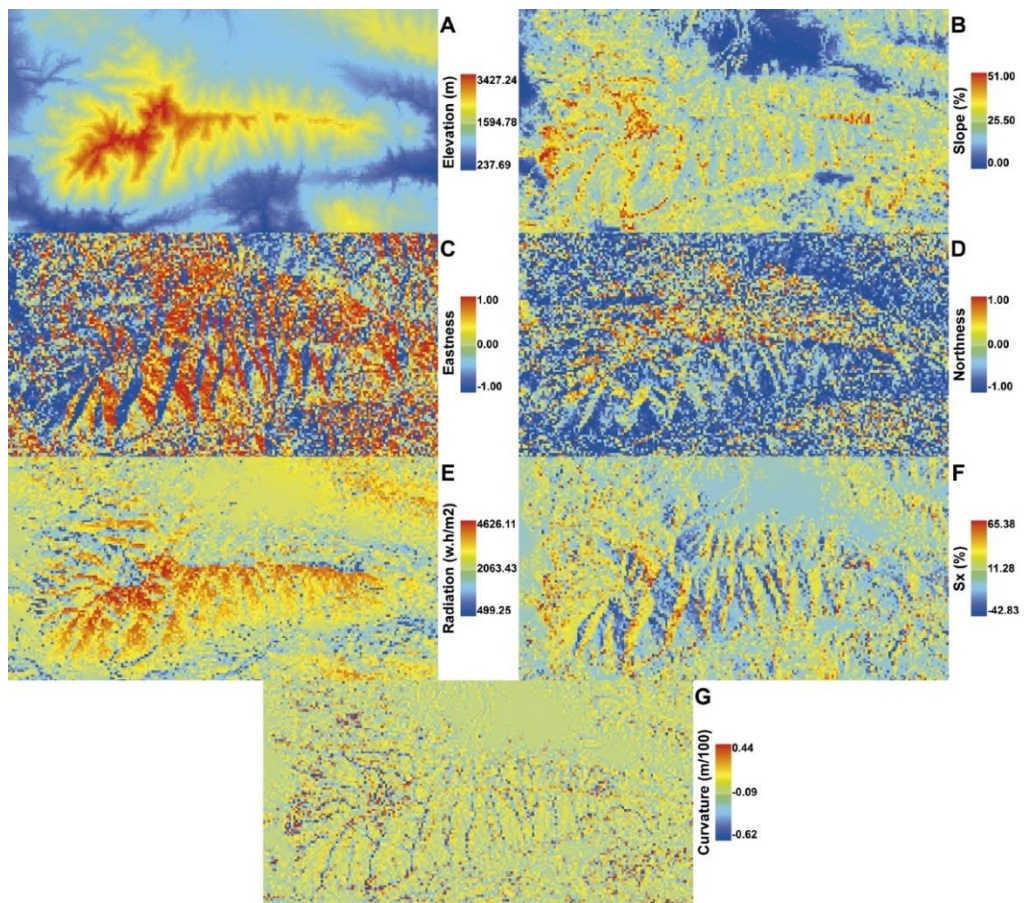


Figure 3.4. Maps of explanatory variables for the Sierra Nevada mountain range. A: Elevation; B: Slope; C: Eastness; D: Northness; E: Radiation; F: Maximum upwind slope; G: Curvature.

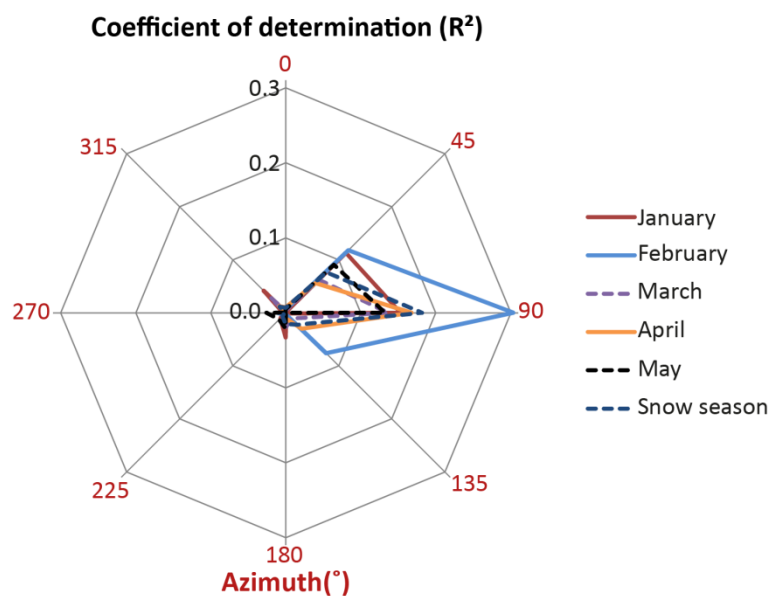


Figure 3.5. R^2 values for the linear regression of snow depth and maximum upwind slope with $d_{max}=300$ m.

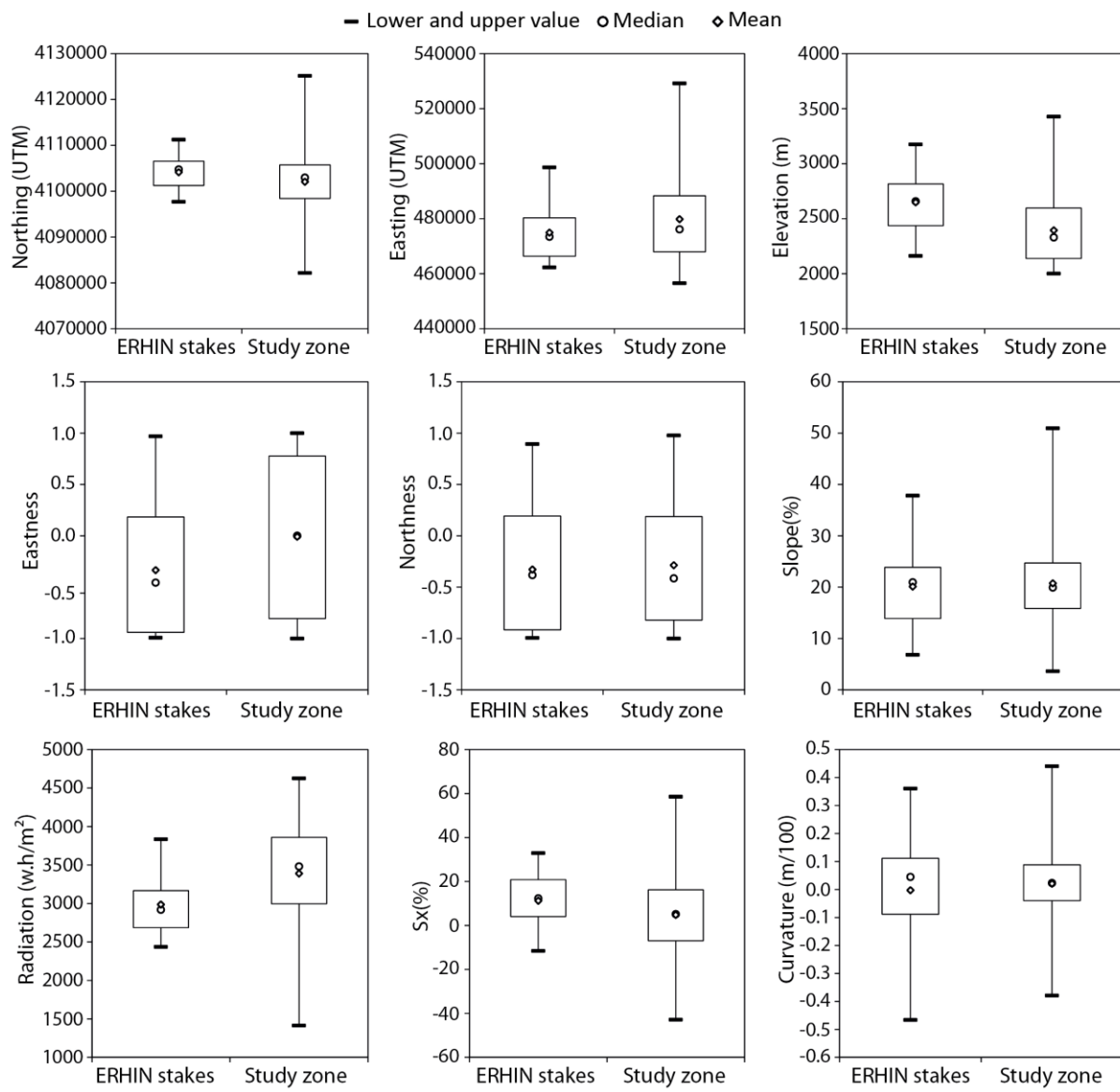


Figure 3.6. Ranges the value of each predictor for the observations in stakes and the study area. The top and bottom of boxes represent the interquartile range.

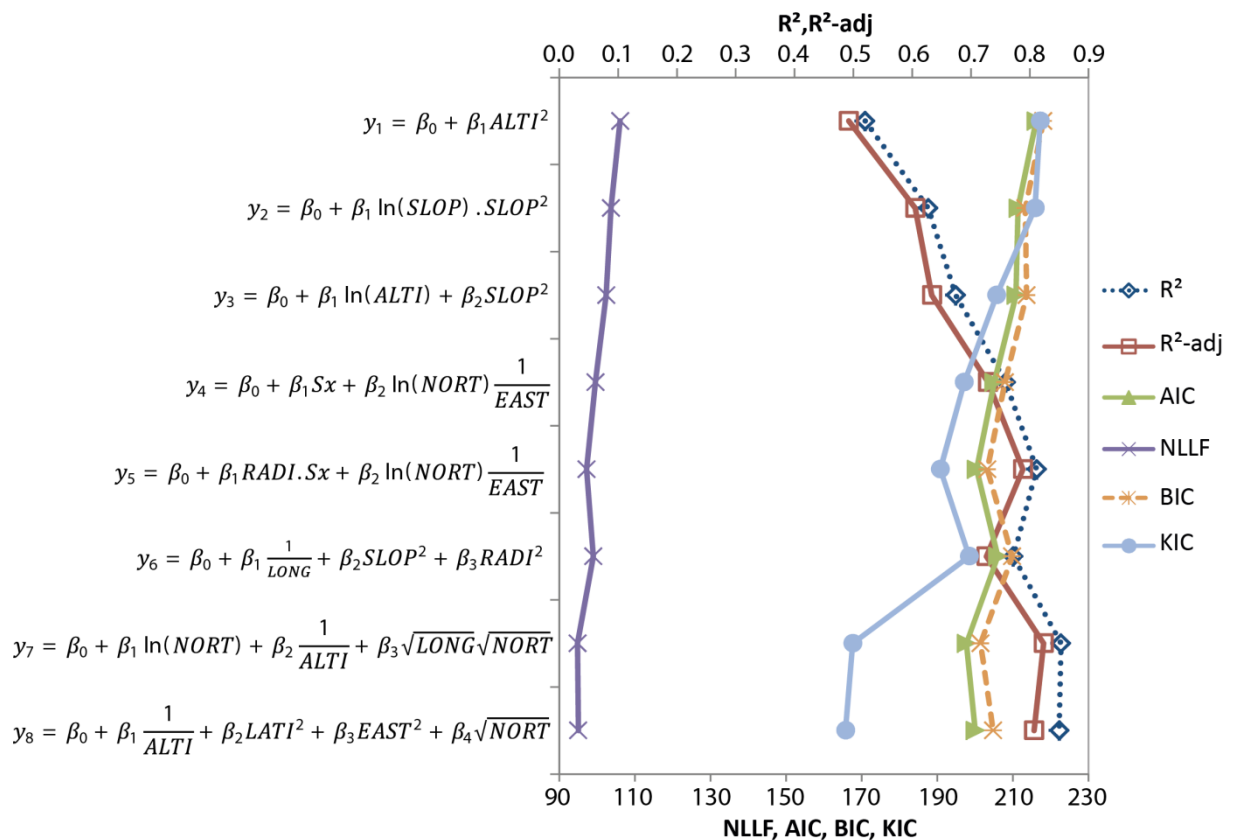


Figure 3.7. Best models for the coefficient of determination for the survey of 21/04/2003.

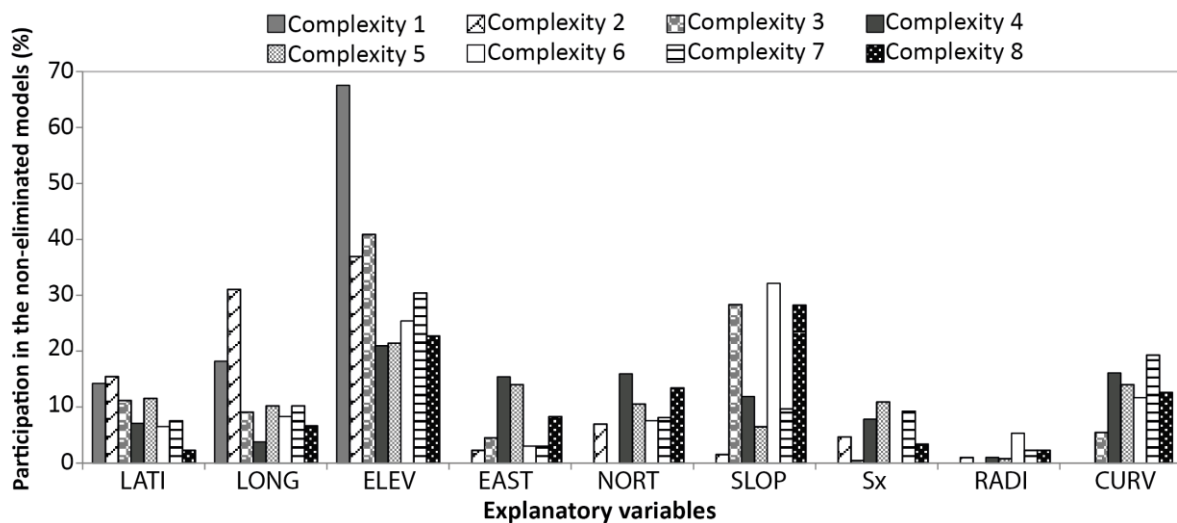


Figure 3.8. Frequency of the explanatory variables in the non-eliminated models for different model complexities. LATI (latitude), LONG (longitude), ELEV (altitude/elevation), EAST (eastness), NORT (northness), SLOP (slope), Sx (maximum upwind slope), RADI (radiation), CURV (curvature).

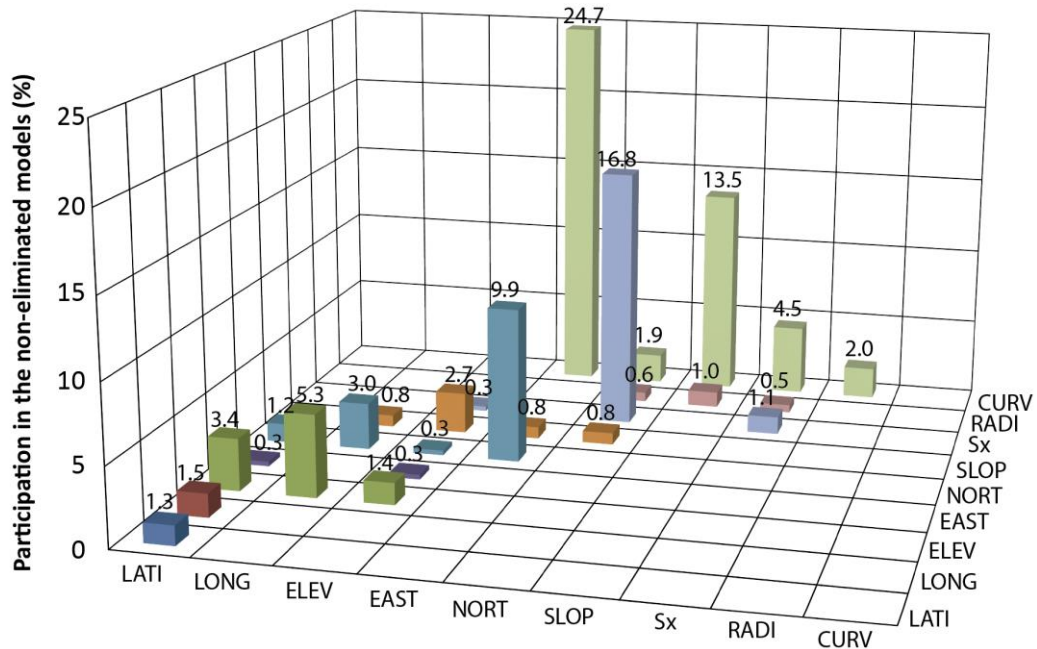


Figure 3.9. Frequency of the explanatory variables involved within interaction of variables (products of variables) in the not-eliminated models for different model complexities. LATI (latitude), LONG (longitude), ELEV (elevation), EAST (eastness), NORT (northness), SLOP (slope), Sx (maximum upwind slope), RADI (radiation), CURV (curvature).

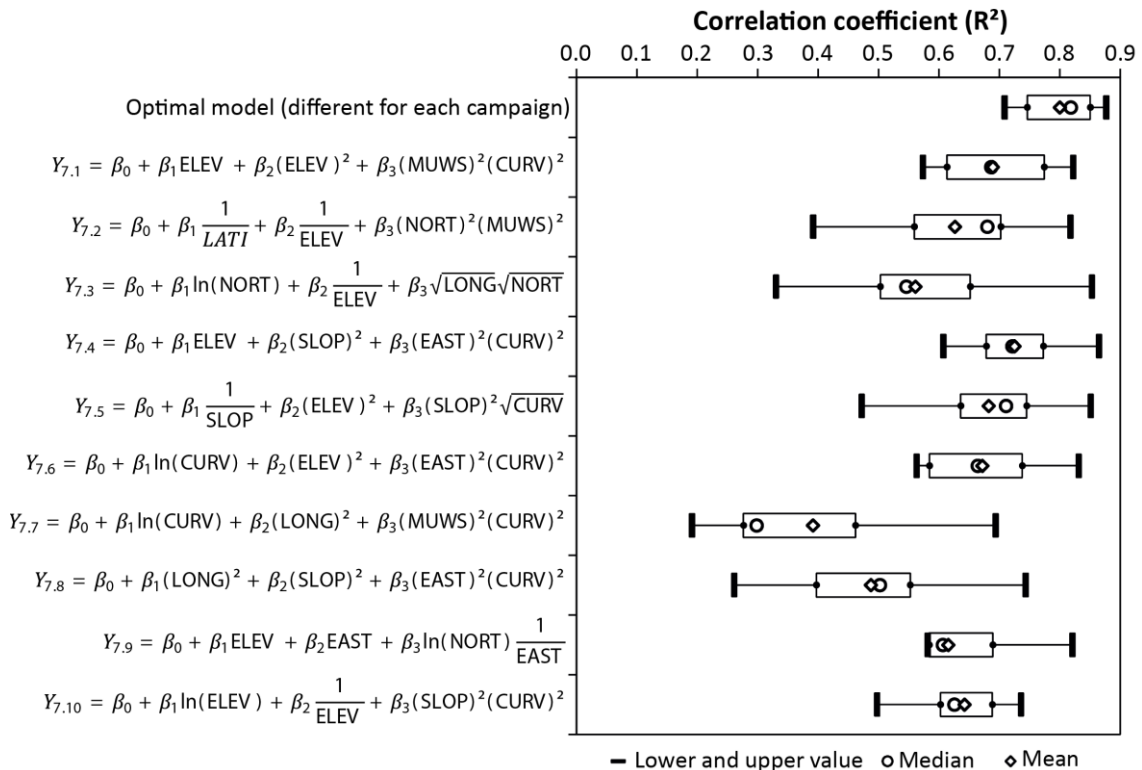


Figure 3.10. Coefficients of determination of the models considered for the different surveys. The top and bottom of boxes represent the interquartile range.

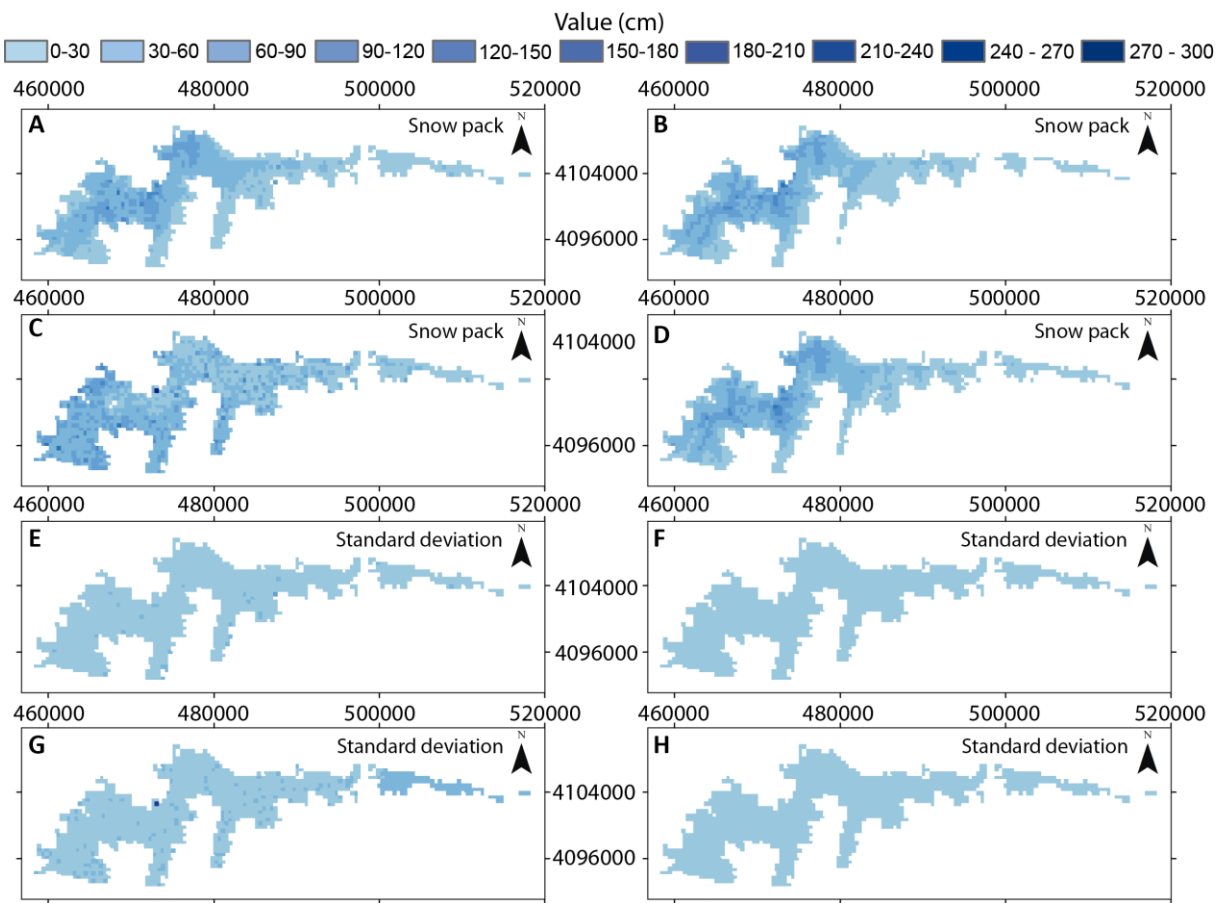


Figure 3.11. Estimated snow depth in centimeters for the 24/03/2005 survey: A) using model 2, B) using model 4, C) using model 7 and D) using the optimal model. Standard deviation of estimated snow depth in centimeters for the 13/01/2004 survey: E) using model 2, F) using model 4, G) using model 7 and H) using the optimal model.

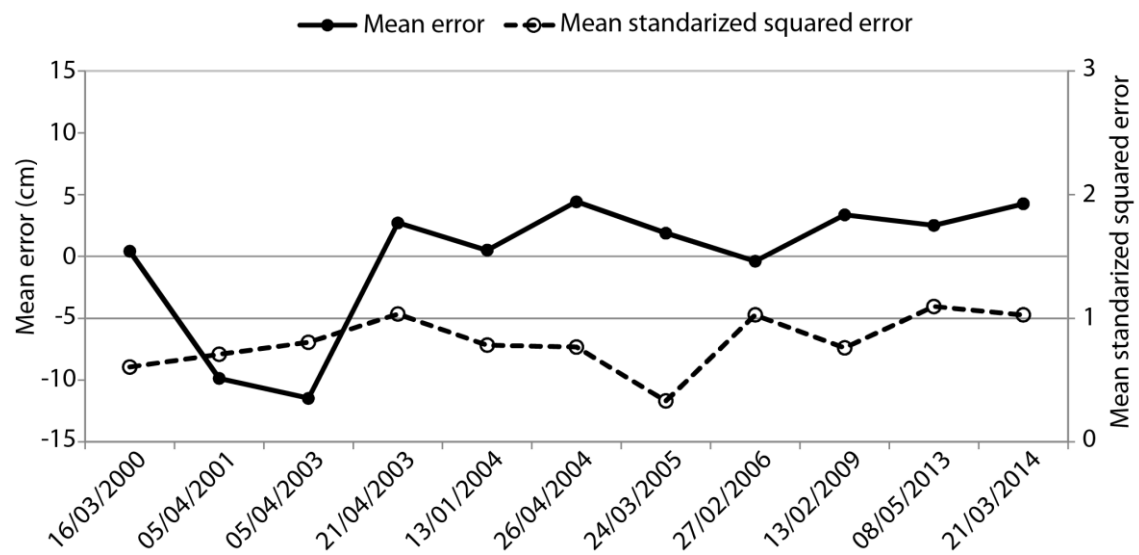


Figure 3.12. Mean error of the cross-validation experiment for the optimal model and mean standardized squared error of the cross-validation experiment for the optimal model.

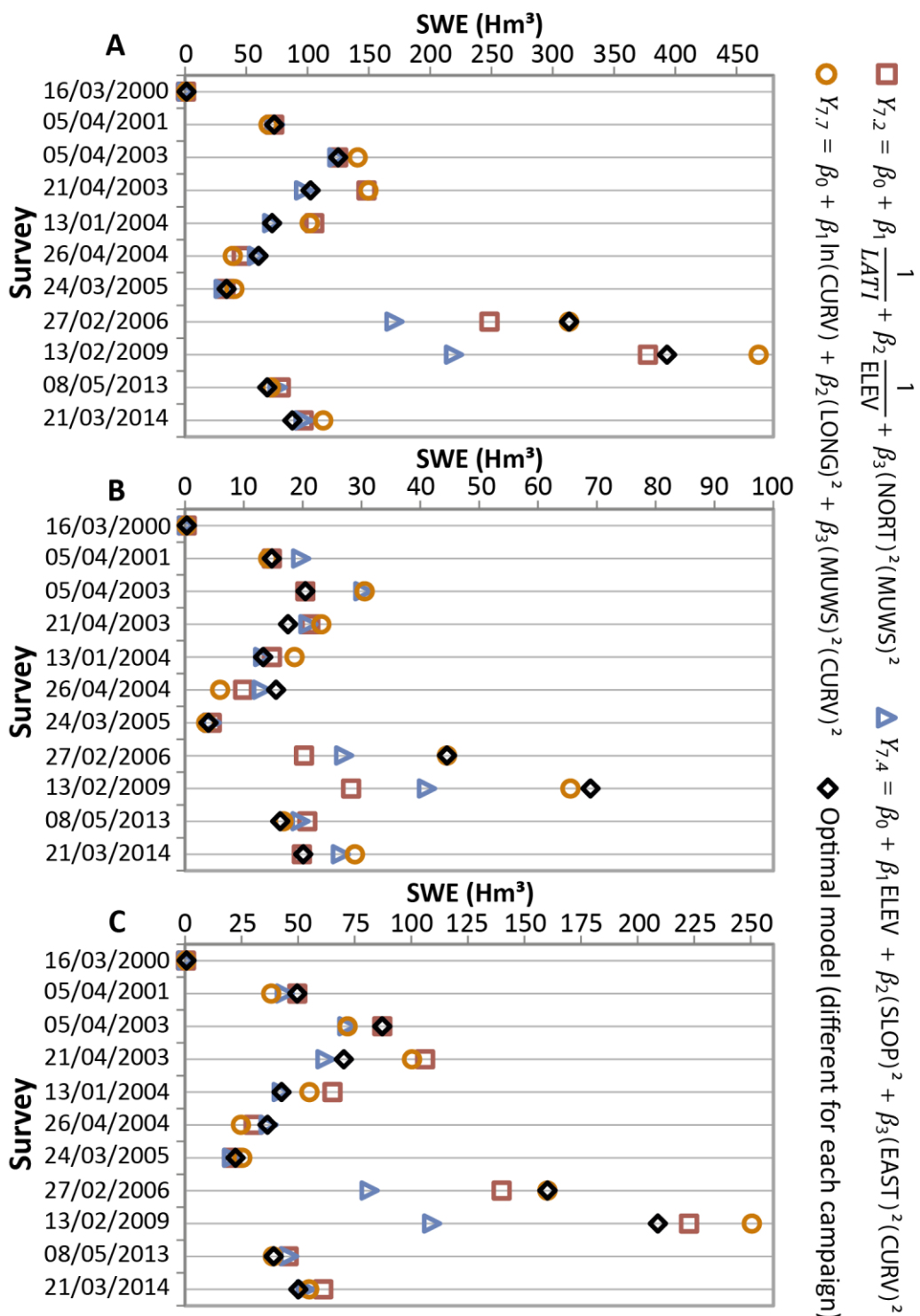


Figure 3.13. A: Estimated snow water equivalent for the Sierra Nevada mountains. B: Estimated snow water equivalent for the Canales basin. C: Estimated snow water equivalent for the Guadaleo basin.

Chapter 4: Optimal design of snow stake networks to estimate snow depth in an alpine mountain range

Antonio-Juan Collados-Lara^{(1,*),} Eulogio Pardo-Igúzquiza⁽²⁾, David Pulido-Velazquez⁽¹⁾

(1) Instituto Geológico y Minero de España, Urb. Alcázar del Genil, 4. Edificio Zulema Bajo, 18006, Granada (Spain). E-mails: ajcollados@gmail.com, d.pulido@igme.es

(2) Instituto Geológico y Minero de España, Ríos Rosas, 23, 28003 Madrid (Spain). E-mail: e.pardo@igme.es

* Corresponding author

Abstract

Monitoring and estimation of snow depth in alpine catchments is important for a proper assessment of management alternatives in these water resources systems. The distribution of snowpack thickness is usually approached by using field data which come from snow samples collected at a given number of locations that constitute the monitoring network. Optimal design of this network is required to obtain the best possible estimates. Assuming that there is an existing monitoring network, its optimization may imply the selection of an optimal network as a subset of the existing one (if there are not funds to maintain them) or enlarging the existing network by one or more stations (optimal augmentation problem). In this paper, we propose an optimization procedure that minimizes the total variance in the estimate of snowpack thickness. The novelty of this work is to treat, for the first time, the problem of snow observation network optimization of an entire mountain range rather than for small catchments as done in previous studies. Taking into account the reduced data available, which is a common problem in many mountain ranges, the importance of a proper design of these observation networks is even larger.

Snowpack thickness is estimated by combining regression models to approach the effect of the explanatory variables and kriging techniques to consider the influence of the stakes location. We solve the optimization problems under different hypotheses, studying the impacts of augmentation and reduction, both one by one and in pairs. We also analyse the sensitivity of results to non-snow measurements deduced from satellite information. Finally, we design a new optimal network by combining the reduction and augmentation methods. The methodology has been applied to the Sierra Nevada mountain range (southern Spain), where very limited resources are employed to monitor snowfall and where an optimal snow network design could prove critical. An optimal snow observation network is defined by relocating some observation points. It would reduce the estimation variance by around 600 cm² (15%).

Keywords: snow stakes, regression kriging snow depth estimation, estimation uncertainty, snow observation network optimization, satellite information, Sierra Nevada (southern Spain)

1. Introduction

Monitoring and estimation of snow depth in alpine catchments is important for a proper assessment of the available water resources (Liu et al., 2012), which in turn is necessary to analyse management alternatives (Pulido-Velazquez et al., 2011; Escriba-Bou et al., 2017). Although snow cover area may be estimated from satellite data (Pardo-Igúzquiza et al., 2017), an assessment of the distribution of the thickness of the snowpack in alpine areas requires additional information. Satellite products to describe Snow Water Equivalent (SWE) exist but these still do not provide a proper assessment of snowpack in alpine regions (Dawson et al., 2018). Table 4.1 summarizes the available SWE products for Europe. These products have a coarse spatial resolution for studying water resources in catchments or small mountain systems. For example, the main mountain system in southern Spain (Sierra Nevada) is represented by one or two cells when the usual product of the 25 x 25 km spatial resolution is considered.

Airborne-based Light Detection and Ranging (LiDAR) can be also applied to measure snow depth at high spatial resolution over large areas (Harpold et al., 2014). However, while it improves the ability to make accurate estimates of snow melt water resources in these areas, it is not used in the majority of regions due to its cost (requiring significant economic investment to perform the flights).

Snowpack distribution is also traditionally approached by using in-situ data and applying interpolation procedures or hydrological models that include estimates of snow processes (e.g., accumulation and fusion) (Collados-Lara et al., 2017; Zeinivand and De Smedt, 2009). SWE is normally measured using snow pillows based on the hydrostatic pressure created by overlying snow (e.g., SNOTEL system (Fassnacht et al., 2003, 2018)). Field survey data to measure snow depth is collected using hand probes and snow samples from a given number of locations (snow courses) that constitute the monitoring network. In some places there are permanent infrastructures (snow stakes) that support these monitoring activities.

In the scientific literature we can find various approaches to the design of snow observation networks. They are summarized in Table 4.2. All of them aim to select an optimal network as a subset of the existing spatial observations, which sometimes comes from detailed field surveys or snow course data (Butcher and McManamon, 2011; Welch et al., 2013; Molotch and Bales, 2005; Galeati et al., 1986; Saghafian et al., 2016), or LiDAR images (Oroza et al., 2016; Kerkez et al., 2012). We are not aware of previous work that addresses the problem of expanding an observation network in areas where scarce snow depth spatial information is available, which presents an interesting problem to solve in areas with limited economic resources.

Some of the previous studies are based on cluster techniques to identify homogeneous areas, and/or Principal Components Analysis technique to identify representative stations that explain the modes of variability (Galeati et al., 1986; Butcher and McManamon, 2011; Welch et al., 2013). Other studies are based on optimization procedures to minimize the difference between estimates and observations (Molotch and Bales, 2005; Oroza et al., 2016).

The majority of the snow network optimization studies have focused on small catchments (López-Moreno et al., 2015; Molotch et al., 2005; Butcher et al., 2011; Oroza et al., 2016). Some cover part of a mountain range (Galeati et al., 1986; Kerkez et al., 2012; Welch et al., 2013), but none analyses an entire mountain range to optimize the snow monitoring network.

Research has also been published that is oriented towards designing observation networks for other meteorological and hydrological variables (e.g., ice (Vance et al., 2016), rainfall (Pardo-Igúzquiza., 1998a) and temperature (Amorim et al., 2012)).

In the current study we propose a novel approach to design snow observation network infrastructures (both reducing or expanding existing networks) based on a multivariate snow depth model (a regression-kriging model) in order to obtain the best possible estimate of snowpack over an entire alpine mountain range, using the available economic resources. An optimization procedure is applied to design an observation network that minimizes the total standard deviation in the estimate of snowpack thickness. The methodology was applied in Sierra Nevada mountain range (southern Spain), where very limited resources are employed to monitor the snow and where an optimal snow network design could be crucial. The main novelties of the work are (1) the scarce snow depth spatial information available in the pilot area due to the limited economic resources, (2) the use of RK technique to optimize the snow monitoring network that allows an optimal estimation of snow depth in a further step, and (3) the application of the methodology to an entire mountain range.

The paper is organized as follows. Section 2 describes the method. It includes the description of the proposed procedure to estimate snowpack thickness by a regression-kriging (RK) approach (section 2.1) and the optimization approach and hypothesis assumed for the network design (section 2.2). We study the case of modifying an existing observation network by enlarging or reducing the number of snow stakes one by one, the case of pairwise reduction; we also analyse the sensitivity of the results if we consider non-snow measurements deduced from satellite information along the boundary of the snow cover area. We design a new optimal observation network combining the reduction and augmentation approaches. Finally, we summarize the hypothesis assumed (section 2.3). Section 3 describes the case study and the data employed. The results, discussion and limitations are included in Section 4, while Section 5 presents our conclusions.

2. Method

The steps that define the method are represented in Figure 4.1. All the calculations have been performed with our own Fortran codedeveloped for the case study. Nevertheless, the proposed methodology can be applied to any case study to obtain an optimal snow depth monitoring network, being easy to adapt the cited code to make them applicable to other case studies. The methodology is divided into two main activities: definition of a regression model to estimate snow thickness (section 2.1), and optimization procedure (section 2.2).

2.1. Snow depth estimation from snow stakes by Regression Kriging

Multiple regression models have been extensively applied to estimate snow depth and its uncertainty (López-Moreno and Nogués-Bravo, 2006; Fassnacht et al., 2013, Collados-Lara et al., 2017). They can be calibrated using different model structures and explanatory variables. These regression model estimates can be improved by applying kriging to the regression residuals, resulting in a RK estimate. The RK technique allows consideration of several explanatory variables to calculate the target variable and it has been widely used to estimate precipitation fields (e.g., Pardo-Igúzquiza 1998b; Collados-Lara et al., 2018) but its results are also useful for estimating snow depth fields (e.g., Collados-Lara et al., 2017; Liu et al., 2018). In this study a RK approach is applied to estimate error fields of snow depth. The RK error is calculated as the sum of the estimated errors produced in the regression and kriging approaches. This error can be used to optimize the observation network as we explain in the following section.

2.2. Optimization approach

A simple procedure based on minimizing the estimation errors was used to design the snow observation network. In this optimization procedure two sources of uncertainty should be considered to quantify the standard deviation of the estimate: (1) the standard deviation of regression to model the effect of the explanatory variables and (2) the kriging standard deviation to consider the influence of the locations of the snow stakes in the interpolation process. The summation of the two sources of uncertainty provides an assessment of the uncertainty in the RK estimation procedure. The objective of the optimization is to find the combination of stakes locations that minimize the total estimation uncertainty fixing a number of stakes.

The area of interest is discretized into cells (with a variable size depending the study case) where the total standard deviation is calculated. The candidate sites for the location of new stakes are the centers of the cells that comprise the study area. The area of interest can be defined by applying statistical criteria to the Snow Cover Area (SCA) data available for study case. For example, in this study we propose the definition of an area of interest as the domain above a certain elevation covered by snow for at least 90% of the days during the snow season (October to May). Note that the area defined by this condition is obtained from the statistical analyses of SCA information within the historical period for. This condition avoids locating stakes in zones that are snow-free for the majority of the time. In order to solve the optimization problem we assume the following hypotheses:

- One-by-one augmentation and reduction cases

In the augmentation case the initial stakes cannot be removed and we add one stake in each calculation step at the location that minimizes the total standard deviation of the estimate. The optimization problem can be solved by applying a uniform mesh method in which the potential locations (cells considered in the area of interest) are tested. The calculation is made considering an additional stake at each cell, generating a new standard deviation surface. At the end of this process a new stake location is proposed.

The added stake modifies the map of the estimated standard deviation. This procedure is repeated until the desired number of stakes is reached. The reduction case can be useful if we want to remove some of the initial stakes (for example, due to economic restrictions). In these cases, the potential solutions to be tested depend on the number of existing stakes, which usually is significantly smaller than the alternatives to be checked in the augmentation problem, since that depends on the number of cells in the mesh.

- Pairwise augmentation and reduction case

The optimization procedure can also be performed by removing or adding two stakes in each calculation step; the results can differ with respect to the one by one optimization. Normally, the pairwise reduction problem can be solved by comparing the solutions for all potential alternatives, which depend on the initial number of stakes. On the other hand, when the number of potential locations (cells) in the augmentation problems is significant it cannot be solved by applying the uniform mesh method because of an excessive computational cost. In these cases another search algorithm, such as simulation annealing, should be applied.

In this study we tested the pairwise reduction case in order to assess the sensitivity of the location of the eliminated stakes and the reduction in error compared to the one-by-one solution.

- Augmentation case considering the zeros along the boundary

Another test is to consider the zero data along the boundary of the area of interest. It will move optimal locations away from the boundary. The idea of introducing zero snow pixels to make the network more robust was introduced previously by other authors (e.g. Foppa et al., 2007; Jonas et al., 2009; Sturm et al., 2010). The RK approaches employed by Collados-Lara et al. (2017) were calibrated without considering the zeros present in the satellite observations, since this would have modified the statistics of the data set and introduced errors in the estimates of snow depth at the stakes. The information of the zeros was employed when applying a mask with the satellite image (indicating presence or absence of snow) to the estimated thickness. However, in the present study considering zeros does not introduce errors, but rather moves the optimal locations away from the boundary where snow cover is shallower or even absent. This possibility allows a comparison of the optimal locations with and without the zeros along the boundary.

- Combination of the one-by-one reduction and augmentation cases

When the initial locations of the stakes are not optimal and we want to replace them by others at optimal locations, it is necessary to combine the reduction and augmentation cases. This procedure has two phases: (1) reduction of the number of stakes as far as any desired number (fulfilling a minimum of four as a numerical

constraint) and (2) augmentation of the number of stakes back up to the desired number.

2.3. Simplifications

In order to make the methodology feasible we have made various assumptions about the optimization methodology. The most relevant simplifications are as follows:

- A single regression model has been used in this study to characterize the snow depth distribution over the whole mountain.
- The kriging standard deviation depends on both the variance of residuals and the location of the stakes. We fixed the variance of the residuals to be the average of the known measurements because in the new locations we do not know the snow depth. However, the second term, namely the location of the stakes, is the more important one in the optimization procedure.
- In the reduction case we only can reduce down to four stakes because the kriging systems need at least four data to be solved. We assume at least four of the stakes in the initial configuration are well placed.
- In the augmentation case that considers boundary zeros, we assume that the area of interest is the area covered by snow, even though the snow cover area changes over time. We consider the area of interest as a representative, snow-covered part of the case study where the boundary delineates areas with lower or null thickness.

3. Case study and data employed

We applied the described methodology to the Sierra Nevada (southern Spain), which is a very important mountain massif from the point of view of water resources in the southern Iberian Peninsula (see Figure 4.2.A). The Sierra Nevada is around 80 Km long and between 15 to 30 Km wide and covers an area of more than 2000 Km². It is a high elevation zone where the elevation varies from around 1000 to 3478.6 m a.s.l. (Mulhacén Peak, the highest point on the Iberian Peninsula). Figure 4.2.B shows a digital elevation map of the zone. The case study has two well differentiated periods corresponding to presence/absence of snow, with snow cover normally present from October to May.

In this study we employed a snow depth estimation regression model from the study carried out by Collados-Lara et al. (2017) in order to optimize the snow observation network. The snow depth variable is estimated by a RK technique using snow depth data from the ERHIN program (“Evaluation of Water Resources from Snowfall”) of the Spanish Ministry for Agriculture, Food and Environment. This snow depth observation network comprises 23 stakes (see Figure 4.2.A). Most of times the snow depth was measured by visual inspection from helicopter with a measurement error around 10 cm. A more complete description of the data can be found in Collados-Lara et al. (2017). Note that in this study the measurements are not important because we used the regression model obtained by Collados-Lara et al. (2017). However the locations of the stakes (showed in Figure 4.2.A) and the new potential locations

can configure the estimation uncertainty and therefore the optimization procedure. In our case study, ten regression models were obtained as optimal models for eleven surveys (two of the surveys shared the same optimal regression model) using multiple regression from eight general linear regression model structures. These models give estimates of snow depth for the whole mountain range for each survey. These estimates were improved by kriging the residuals. The model structures employed by Collados-Lara et al. (2017) related the target variable (snow depth) with nine explanatory variables (elevation, slope, profile curvature, longitude, latitude, eastness, northness, maximum upwind slope and radiation) and their transformations (logarithm, inverse, square, and square root). The ten optimal regression models obtained for each survey were tested for the other surveys in order to find a single regression model (Eq. 1) that can explain the snow depth dynamics over the entire mountain range for all surveys (in different years and seasons).

$$Y = \beta_0 + \beta_1 \cdot H + \beta_2 \cdot S^2 + \beta_3 \cdot E^2 \cdot C^2 \quad (1)$$

where Y is the target variable, snow depth, H is the elevation, S is the slope, E is eastness and C is the curvature in a determined cell.

We then employed this model to optimize the snow observation network using the optimization approach described in the next section. This model has a relatively good mean correlation coefficient (0.73) but in some surveys this coefficient is around 0.65. These values were obtained changing the coefficients of the model for each survey and maintaining the explanatory variables and their interactions.

SCA information was obtained from the dataset dubbed MODIS/Terra Snow Cover Daily Global 500 m Grid (Data Set ID: MOD10A1), which has a spatial resolution of about 460 m at the latitude of the study area and a temporal resolution of 1 day. We used the same mesh as the MODIS product to perform the calculations. The size of the cells in our discretization is 460 m too.

The area of interest was defined as lying above a certain elevation using the condition proposed in the methods section and the SCA information from satellite MODIS data (see Figure 4.2.A).

The results obtained for the various hypotheses considered in the methodology and their respective limitations are presented in the following section.

4. Results and discussion

As noted above, the optimization procedure is performed to minimize the estimation error. Figure 4.3 shows the standard deviation for the three alternatives of regression, kriging and the sum of both for the case study in the initial situation. The error of estimation of regression (Figure 4.3.a) indicates a spatial distribution that is markedly influenced by elevation. Higher elevations give a lower estimation error. In contrast, the smallest error using the kriging procedure (Figure 4.3.b) are in the influence area where the stakes are located. The remaining areas have a homogeneous estimation error. The sum of the two estimation errors (regression

and kriging) represents the total estimation error (Figure 4.3.c), which is influenced by the combination of elevation and stake locations.

4.1. Augmentation and reduction cases

The optimization procedure (augmentation or reduction) minimizes the total estimation error in each step. In the augmentation procedure a new stake is tested in all available positions (cells) of the area of interest until the lowest error configuration is found. Figure 4.4 shows how the standard deviation of estimation changes as we add five optimal stakes to the initial situation. At first sight the maps look very similar but closer inspections reveals a reduction in the total standard deviation, especially in the area around the new stakes. This area appears due to the kriging procedure (Chiles and Delfiner, 1999) that minimizes the estimation error around the experimental locations and is directly related with range of the variogram which is estimated to be 1200 m in this study. The same explanation is valid for the reduction case (Figure 4.5) but instead a smaller standard deviation, a higher total standard deviation is obtained in each step and the areas with lower error around the experimental locations disappear. Figure 4.6 shows the evolution of the mean variance of estimation as well as the mean standard deviation for the two cases from the initial situation (23 stakes). Two points of inflection in the slope are observed: the first point is when the number of stakes is fewer than eight, when the estimation error increases more quickly. The second point is located between the lines that represent each case (23 stakes) where a sharp inflection in slope is observed, indicating that the initial 23 stakes are not located optimally. Thus a combination of the reduction and augmentation case proves useful (section 4.4). The locations of the added stakes and the eliminated stakes in the two cases can be observed in Figure 4.7.a and 4.7.b, respectively.

Some of the added stakes are located close to the boundary of the area of interest due to the higher standard deviation of regression (Figure 4.3.c) at lower elevations. In section 4.3 zeros located along the boundary are considered in the optimization procedure in order to assess the sensitivity of the stake locations.

4.2. Pairwise reduction case

In this case two stakes are eliminated in each step. Figure 4.8 shows the evolution of mean variance and mean standard deviation of estimation for this and the previous case (one-by-one reduction). The rate of increment of the estimation error is practically the same for the two cases. Thus the sensitivity of the estimation error to the number of stakes eliminated in each step (1 or 2) is very low. With respect to the order of the eliminated stakes some differences are observed. In Figure 4.9 the eliminated stakes in the pairwise reduction case is represented. A comparison with Figure 4.7.b reveals the differences between the two cases.

The pairwise augmentation method was not considered due to its very high computational requirements (we have a large area of interest and a fine mesh) and to the very low sensitivity of the estimation error to the number of stakes eliminated in each step (one-by-one versus pairwise reduction). The pairwise augmentation case requires a more computationally efficient technique than the uniform mesh method.

4.3. Augmentation case considering the zeros of the boundary

In order to avoid an excessive number of new locations for stakes close to the boundary of the area of interest we considered a set of zeros values located along the boundary. As noted above, this procedure requires that we assume that the area of interest is representative in terms of snow cover over the whole of the study zone. If we consider zeros the virtual total estimation error is lower, and is very low along the boundary (Figure 4.10). The same procedure was performed from this initial configuration. The evolution of estimation error in the various augmentation steps is shown in Figure 4.11. The slope of the error reduction curve is practically the same in the two cases (without and with zeros) but the total error is lower when we consider zeros. However it is not a real error reduction because the experimental locations considered were virtual. Figure 4.12 shows the added stakes in this case. When zeros are not considered, 13 of the 20 new stakes are placed close to the border, while when we do consider zeros 6 of the 20 stakes lie close to the border. We have reduced the number of stakes close to the border but in the eastern part of the case study area any new potential location is considered with this configuration. On the other hand the boundary is a zone where snow can be present or not over time. As a result, estimation errors are bound to be larger along the boundary and so new stakes are located close to the border when we do not consider zeros as virtual experimental locations. Thus placing new stakes close to the border will contribute to reducing this uncertainty.

4.4. Combination of the one-by-one reduction and augmentation cases

This approach provides useful information if we want to define an optimal observation network by replacing some original stakes. In this case, the reduction problems must be solved before analyzing the augmentation problem. We have considered a reduction phase from 23 to 4 stakes and an augmentation phase from 4 to 23 stakes. Figure 4.13 shows the evolution of the estimation error for the reduction and augmentation phases. A total reduction of the variance to around 600 cm² is observed. Nevertheless, further stakes can be added with this procedure if funds are available. The final configuration of the snow depth observation network can be seen in Figure 4.14. Figure 4.14.a shows the order of eliminating stakes while Figure 4.14.b shows the order or adding replacement ones.

4.5. Limitations and future work

Although we have presented a general method (that is applicable to any case study) to optimize the snow depth observation network under different hypotheses in an alpine area, we want to highlight certain limitations and potential future work:

- We have considered a unique regression model to explain the spatial variability of the snow depth dynamics in the study area. This model shows good results for the 11 surveys considered but it might be useful to consider different regression models for different months or days in order to consider the temporal variability.
- The proposed method does not consider accessibility or cost criteria in the optimization procedure. These two criteria are very important from the operational and

economic point of view and could be incorporated in future studies: a secondary optimization procedure taking into account the operational and economics criteria could be done in each cell in order to determine the precise location of the stakes.

5. Conclusions

A systematic procedure to optimize the snow observation network to estimate snow depth in alpine systems is proposed. This procedure requires a regression model that explains snow depth from several explanatory variables. The proposed method minimizes the total estimation error assessed by a RK approach for the alpine system under consideration. Two sources of uncertainty have been considered to quantify the total estimation error: the standard deviation of regression to model the effect of the explicative variables and the kriging standard deviation to consider the influence of location in kriging estimation. Different optimization cases are presented: one-by-one and pairwise augmentation, one-by-one and pairwise reduction, augmentation considering virtual stations with zero values and a combination of the reduction and augmentation cases. These procedures were applied to the whole of the Spanish Sierra Nevada mountain range. Interesting results were obtained that indicate that the existing snow observation network is not optimally located from the point of view of estimation and could be improved applying any of the cases presented. For example, if we consider a combination of reduction and augmentation that maintains the initial number of stakes, the total estimation variance of the snow depth observation network is reduced by around 600 cm² (some 15%) and is better distributed in the area of interest. Due to its generality, the proposed methodology can be easily implemented in other areas.

The operational and economic optimization of the precise locations in the defined cells is left open for future research.

Acknowledgments

This research was partially supported by the research projects CGL2013-48424-C2-2-R and CGL2015-71510-R from the Spanish Ministry of Economy and Competitiveness and the European ESSEM COST Action ES1404. We would also like to acknowledge the ERHIN program and NASA DAAC for the data provided for this study.

References

- Amorim, A.M.T., Goncalves, A.B., Nunes, L.M., Sousa, A.J., 2012. Optimizing the location of weather monitoring stations using estimation uncertainty. *International Journal of Climatology* 32 (6), 941–52. doi: 10.1002/joc.2317.
- Armstrong, R., M.J. Brodzik, K. Knowles, M. Savoie, 2005. Global Monthly EASE-Grid Snow Water Equivalent Climatology, Version 1. [Data Set ID: NSIDC-0271]. Boulder, Colorado USA. NASA National Snow and Ice Data Center Distributed Active Archive Center. doi: 10.5067/KJVERY3MIBPS.

- Brown, R.D., 2002. Reconstructed North American, Eurasian, and Northern Hemisphere Snow Cover Extent, 1915-1997, Version 1. [Data Set ID: G02131]. Boulder, Colorado USA. NSIDC: National Snow and Ice Data Center. doi: 10.7265/N5V985Z6.
- Brown, R.D., B. Brasnet, 2010, updated annually. Canadian Meteorological Centre (CMC) Daily Snow Depth Analysis Data, Version 1. [Data Set ID: NSIDC-0447]. Boulder, Colorado USA. NASA National Snow and Ice Data Center Distributed Active Archive Center. doi: 10.5067/W9FOYWH0EQZ3.
- Butcher, P., McManamon, A., 2011. Optimization of a Snow Observation Network via Principal Component Analysis. American Geophysical Union, Fall Meeting 2011, abstract id. H43G-1305.
- Chiles, J.P., Delfiner, P., 1999. Geostatistics: Modelling Spatial Uncertainty. Wiley, New York.
- Collados-Lara, A.J., Pardo-Iguzquiza, E., Pulido-Velazquez, D., 2017. Spatio-temporal estimation of snowpack thickness using point data from snow stakes, digital terrain models and satellite data. *Hydrological Processes* 31, 1966–1982. doi: 10.1002/hyp.11165.
- Collados-Lara, A.J., Pardo-Iguzquiza, E., Pulido-Velazquez, D., 2018. Precipitation fields in an alpine Mediterranean catchment: Inversion of precipitation gradient with elevation or undercatch of snowfall?. *International Journal of Climatology*. doi: 10.1002/joc.5517.
- Dawson, N., Broxton, P., Zeng, X., 2018. Evaluation of Remotely Sensed Snow Water Equivalent and Snow Cover Extent over the Contiguous United States. *Journal of Hydrometeorology* 19(11), 1777–1791. doi:10.1175/jhm-d-18-0007.1
- Escriva-Bou, A., Pulido-Velazquez, M., Pulido-Velazquez, D., 2017. The economic value of adaptive strategies to global change for water management in Spain's Jucar Basin. *Journal of Water Resources Planning and Management* 143. doi: 10.1061/(ASCE)WR.1943-5452.0000735
- Fassnacht, S.R., K.A. Dressler, R.C. Bales, 2003. Snow water equivalent interpolation for the Colorado River Basin from snow telemetry (SNOWTELE) data. *Water Resour. Res.* 39, 1208. doi:10.1029/2002WR001512.
- Fassnacht, S.R., Lopez-Moreno, J.I., Toro, M., Hultstrand, D.M., 2013. Mapping snow cover and snow depth across the Lake Limnopolar watershed on Byers Peninsula, Livingston Island, Maritime Antarctica. *Antarctic Science*, 252, 157–166. doi: 10.1017/S0954102012001216.
- Fassnacht, S.R., Venable, N.B., McGrath, D., Patterson, G.G., 2018. Sub-Seasonal Snowpack Trends in the Rocky Mountain National Park Area, Colorado, USA. *Water*, 10, 562. doi: 10.3390/w10050562.

- Foppa, N., Stoffel, A., Meister, R., 2007. Synergy of in situ and space borne observation for snow depth mapping in the Swiss Alps. International Journal of Applied Earth Observation and Geoinformation 9, 294–310. doi: 10.1016/j.jag.2006.10.001.
- Galeati, G., Rossi, G., Pini, G. Zilli, G., 1986. Optimization of a snow network by multivariate statistical analysis. Hydrol. Sci. J. 31, 93–108. doi: 10.1080/02626668609491030.
- Harpold, A.A., Guo, Q., Molotch, N., Brooks, P.D., Bales, R., Fernandez-Diaz, J.C., Musselman, K.N., Swetnam, T.L., Kirchner, P., Meadows, M.W., Flanagan, J., Lucas, R., 2014. LIDAR derived snowpack data sets from mixed conifer forests across the Western United States. Water Resour. Res. 50, 2749–2755. doi:10.1002/ 2013WR013935.
- Jonas, T., Marty, C., Magnusson, J., 2009. Estimating the snow water equivalent from snow depth measurements in the Swiss Alps. Journal of Hydrology 378, 161-167. doi: 10.1016/j.jhydrol.2009.09.021.
- Kerkez, B., Glaser, S.D., Bales, R.C., Meadows, M.W., 2012. Design and performance of a wireless sensor network for catchment-scale snow and soil moisture measurements. Water Resour. Res. 48. doi: 10.1029/2011WR011214.
- Liu, Y., Li, L., Chen, X., Yang J.M, Hao J.S., 2018. Spatial distribution of snow depth based on geographically weighted regression kriging in the Bayanbulak Basin of the Tianshan Mountains, China. Journal of Mountain Science 15 (1), 33-45. doi:10.1007/s11629-017-4564-z.
- Liu, Y., Weerts, A.H., Clark, M., Hendricks Franssen, H.-J., Kumar, S., Moradkhani, H., Seo, D.-J., Schwanenberg, D., Smith, P., van Dijk, A.I.J.M., van Velzen, N., He, M., Lee, H., Noh, S J., Rakovec, O., Restrepo, P., 2012. Advancing data assimilation in operational hydrologic forecasting: Progresses, challenges, and emerging opportunities. Hydrology and Earth System Sciences 16 (10), 3863–3887. doi: 10.5194/hess-16-3863-2012
- López-Moreno, J.I., Nogués-Bravo, D., 2006. Interpolating local snow depth data: An evaluation of methods. Hydrological Processes 20 (10), 2217–2232. doi:10.1002/hyp.6199.
- López-Moreno J.I., Revuelto J., Fassnacht S.R., Azorín-Molina C., Vicente-Serrano S.M., Morán-Tejeda E., Sexstone G.A, 2015. Snowpack variability across various spatio-temporal resolutions. Hydrol. Process. 29 (6), 1213–1224 doi: 10.1002/hyp.10245.
- Molotch, N. P., R.C. Bales, 2005. Scaling snow observations from the point to the grid element: Implications for observation network design. Water Resour. Res. 41, W11421. doi:10.1029/2005WR004229.
- Oroza, C.A., Zheng, Z., Glaser, S.D., Tuia, D., Bales, R.C., 2016. Optimizing Embedded Sensor Network Design for Catchment-scale Snow-depth Estimation Using LiDAR and Machine Learning. Water Resour. Res. 52 (10), 8174–8189. doi: 10.1002/2016WR018896

- Pardo-Igúzquiza, E., 1998a. Optimal selection of number and location of rainfall gauges for areal rainfall estimation using geostatistics and simulated annealing. *J. Hydrol.* 210 (1-4), 206–220. doi: 10.1016/S0022-1694(98)00188-7.
- Pardo-Igúzquiza, E., 1998b. Comparison of geostatistical methods for estimating the areal average climatological precipitation mean using information of precipitation and topography. *Int. J. Climatol.* 18 (9), 1031-1047. doi: 10.1002/(SICI)1097-0088(199807)18:9<1031::AID-JOC303>3.0.CO;2-U.
- Pulido-Velazquez, D., Garrote, L., Andreu, J., Martin-Carrasco, F. J., Iglesias, A., 2011. A methodology to diagnose the effect of climate change and to identify adaptive strategies to reduce its impacts in conjunctive-use systems at basin scale. *Journal of Hydrology* 405 (1-2), 110–122. doi:10.1016/j.jhydrol.2011.05.014
- Saghafian, B., Davtalab, R., Rafieeinab, A. and Ghanbarpour, M.R., 2016. An Integrated Approach for Site Selection of Snow Measurement Stations. *Water*, 8 (11), 539. doi: 10.3390/w8110539.
- Sturm, M., B. Taras, G.E. Liston, C. Derksen, T. Jonas, J. Lea, 2010. Estimating Snow Water Equivalent Using Snow Depth Data and Climate Classes. *J. Hydrometeor.*,11, 1380-1394. doi: 10.1175/2010JHM1202.1
- Takala, M., K. Luojus, J. Pulliainen, C. Derksen, J. Lemmetyinen, J. Kärnä, J. Koskinen, B. Bojkov, 2011. Estimating Northern Hemisphere Snow Water Equivalent for Climate Research through Assimilation of Space-Borne Radiometer Data and Ground-Based Measurements. *Remote Sensing of Environment* 115, 3517-3529. doi: 10.1016/j.rse.2011.08.014.
- Tedesco, M., R. Kelly, J.L. Foster, A.T. Chang, 2004. AMSR-E/Aqua Daily L3 Global Snow Water Equivalent EASE-Grids, Version 2. [Data Set ID: AE_DySno]. Boulder, Colorado USA. NASA National Snow and Ice Data Center Distributed Active Archive Center. doi: 10.5067/AMSR-E/AE_DYSNO.002.
- Vance, T.R., Roberts, J.L., Moy, A.D., Curran, M.A.J., Tozer, C.R., Gallant, A.J.E., Abram, N.J., van Ommen, T.D., Young, D.A., Griman, C., Blankenship, D.D., Siegert, M.J., 2016. Optimal site selection for a high-resolution ice core record in East Antarctica, *Climate of the Past* 12, 595-610. doi:10.5194/cp-12-595-2016.
- Welch, S.C., Kerkez, B., Bales, R.C., Glaser, S.D., Rittger, K., Rice, R.R., 2013. Sensor placement strategies for snow water equivalent (swe) estimation in the american river basin. *Water Resources Research* 49 (2), 891–903. doi: 10.1002/wrcr.20100.
- Zeinivand, H., De Smedt, F., 2009. Hydrological modeling of snow accumulation and melting on river basin scale. *Water Rersour. Manage.* 23 (11), 2271–2287. doi: 10.1007/s11269-008-9381-2.

Tables of the Chapter 4

Product	Spatial resolution	Temporal resolution	Spatial coverage	Temporal coverage	Reference
Canadian Meteorological Centre (CMC) Daily Snow Depth Analysis Data	24 km x 24 km	Monthly	Northern Hemisphere	1 August 1998 to 31 December 2016 (updated annually)	Brown and Brasnett, 2010
Global Monthly EASE-Grid Snow Water Equivalent Climatology	25 km x 25 km	Monthly	Global	1 January 1978 to 31 December 2007	Armstrong et al., 2005
AMSR-E/Aqua Daily L3 Global Snow Water Equivalent EASE-Grids	25 km x 25 km	Daily	Global	19 June 2002 to 3 October 2011	Tedesco et al., 2004
Reconstructed North American, Eurasian, and Northern Hemisphere Snow Cover Extent	Varies	Monthly	North American, Eurasian, and Northern Hemisphere	1 January 1915 to 31 December 1997	Brown, 2002
ESA GlobSnow Snow Water Equivalent (SWE)	25 km x 25 km	Daily	Northern Hemisphere	11 September 1979 to present	Takala et al., 2011

Table 4.1. Available SWE products for Europe.

Work	Problem to solve	Mathematics techniques	Spatial scale
Galeati et al., 1986	To select a reduced number of measurement stations	Cluster methods and principal component analysis	River basin
Molotch and Bales, 2005	To identify the optimal location for measuring SWE	Binary regression tree models	2 x 2 km zones
Butcher and McManamon, 2011	To identify optimal snow course sites for conversion to snow pillow sites.	Principal component analysis	Portion of river basin
Kerkez et al., 2012	To optimize a wireless sensor network	Statistical analysis	1 x 1 km zone
Welch et al., 2013	Near-optimal sensor placement methodology for real-time SWE estimation	Rank-based clustering and geographically based clustering	River basin
Oroza et al., 2016	To optimize ground-based sensor placements for snow measurements	Machine-learning algorithm	River basin
Saghafian et al., 2016	Site selection of snow measurement stations	Combination of meteorological, hydrological and satellite information criteria.	River basin

Table 4.2. Previous works on snow observation network optimization.

Figures of the Chapter 4

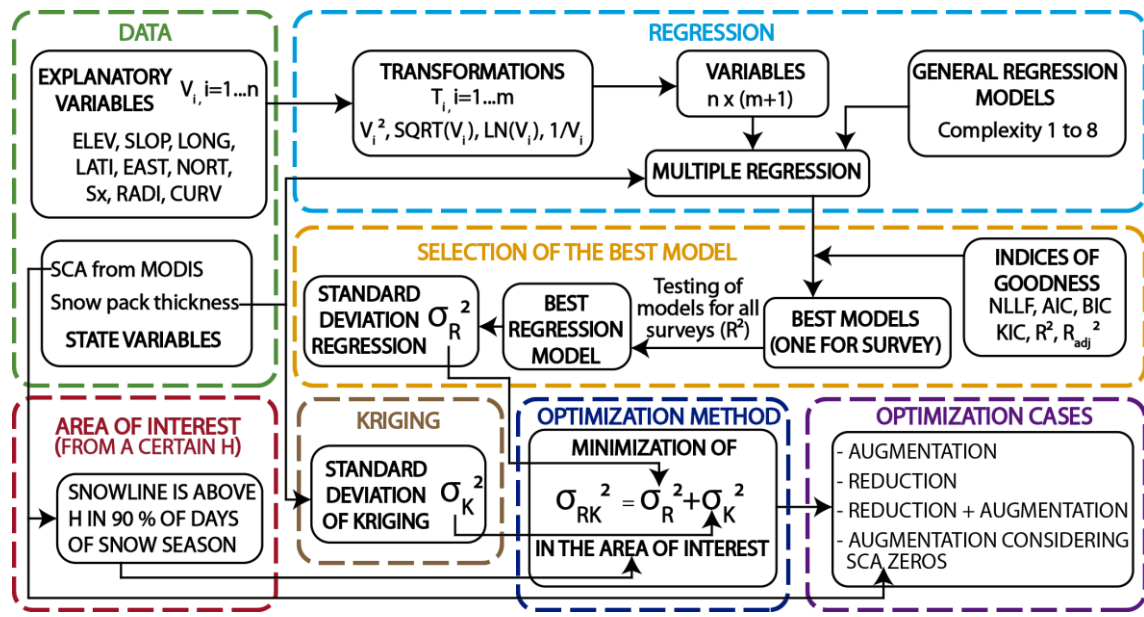


Figure 4.1. Flow chart of the proposed methodology.

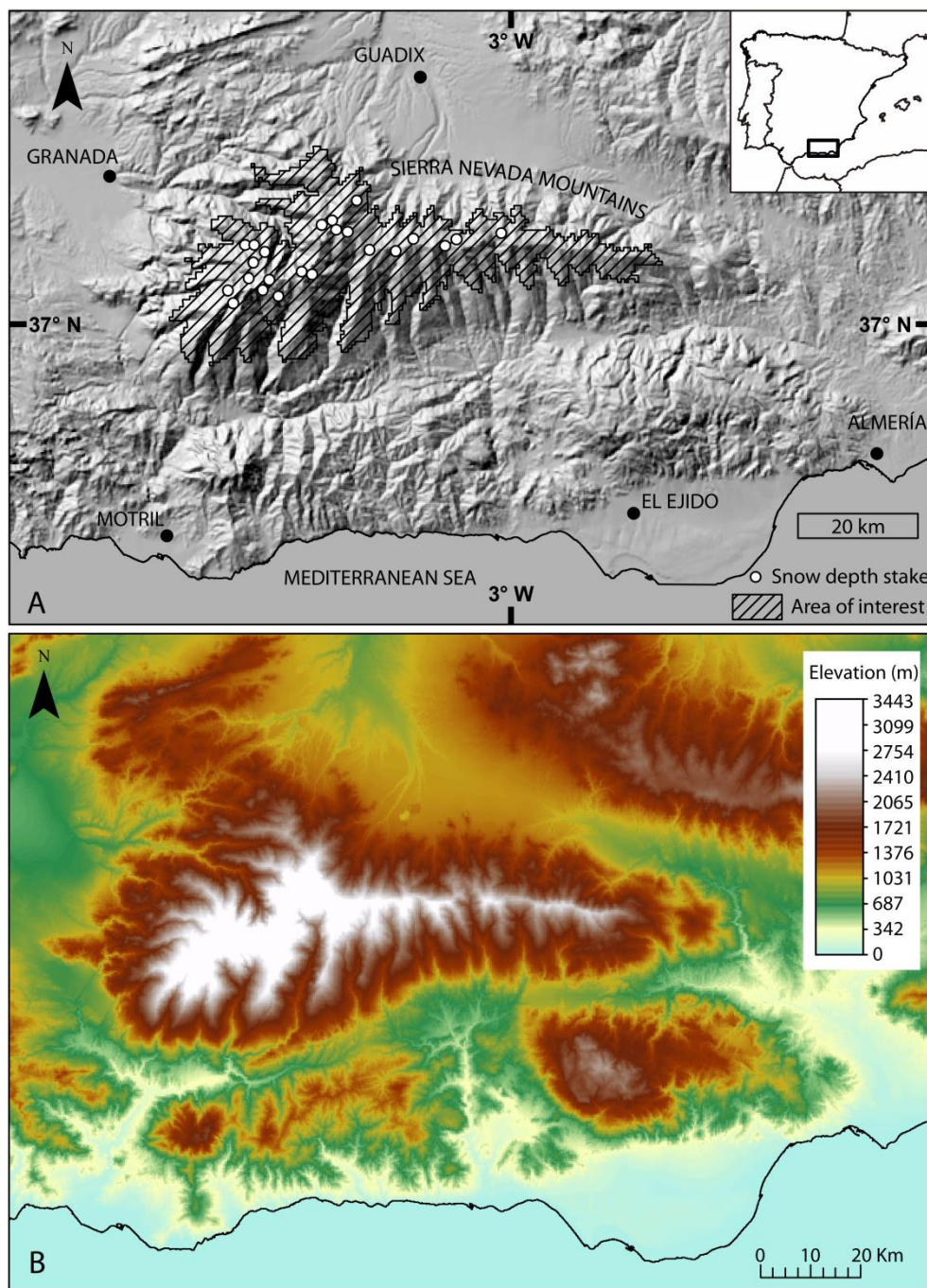


Figure 4.2. A) Location of the case study area. B) Digital elevation map of the case study.

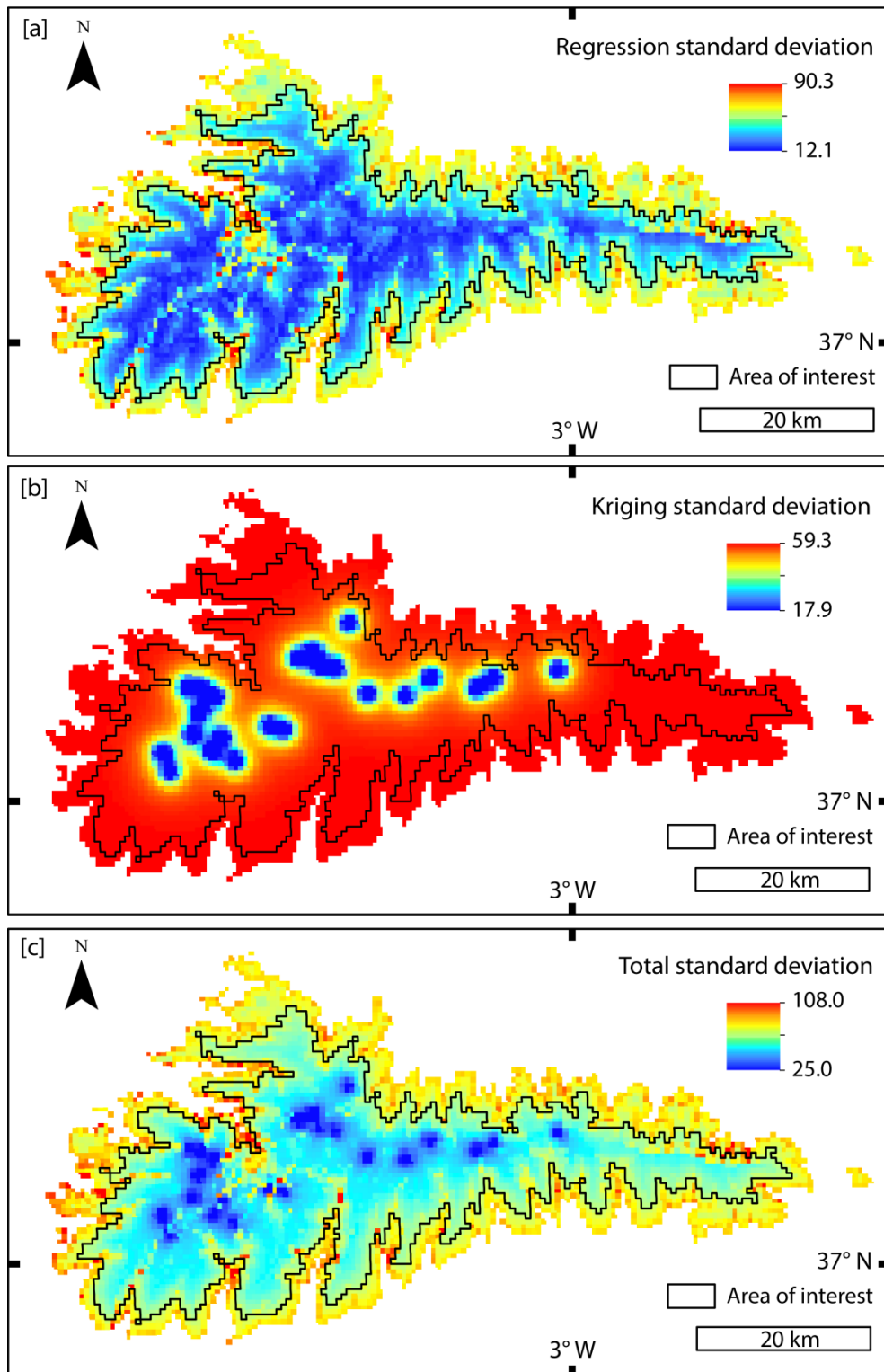


Figure 4.3. Standard deviation of estimates from the initial situation using regression (a), kriging (b) and the total standard deviation (c).

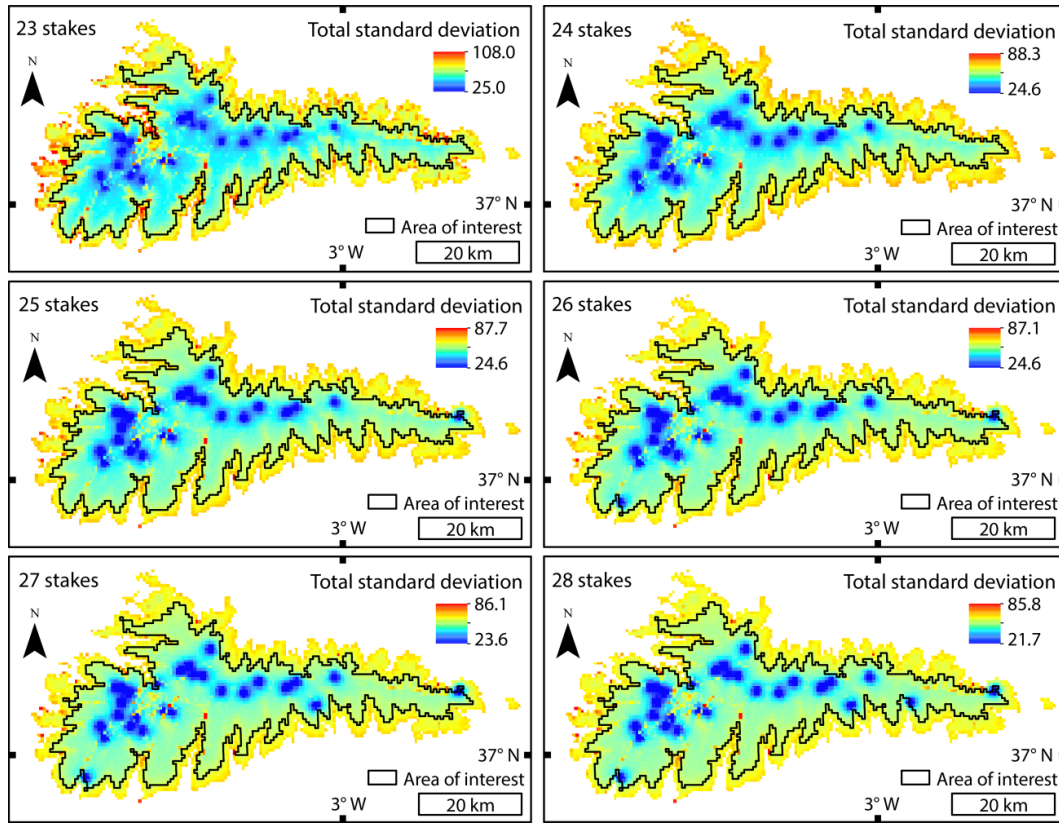


Figure 4.4. Spatial evolution of the total standard deviation in the augmentation steps.

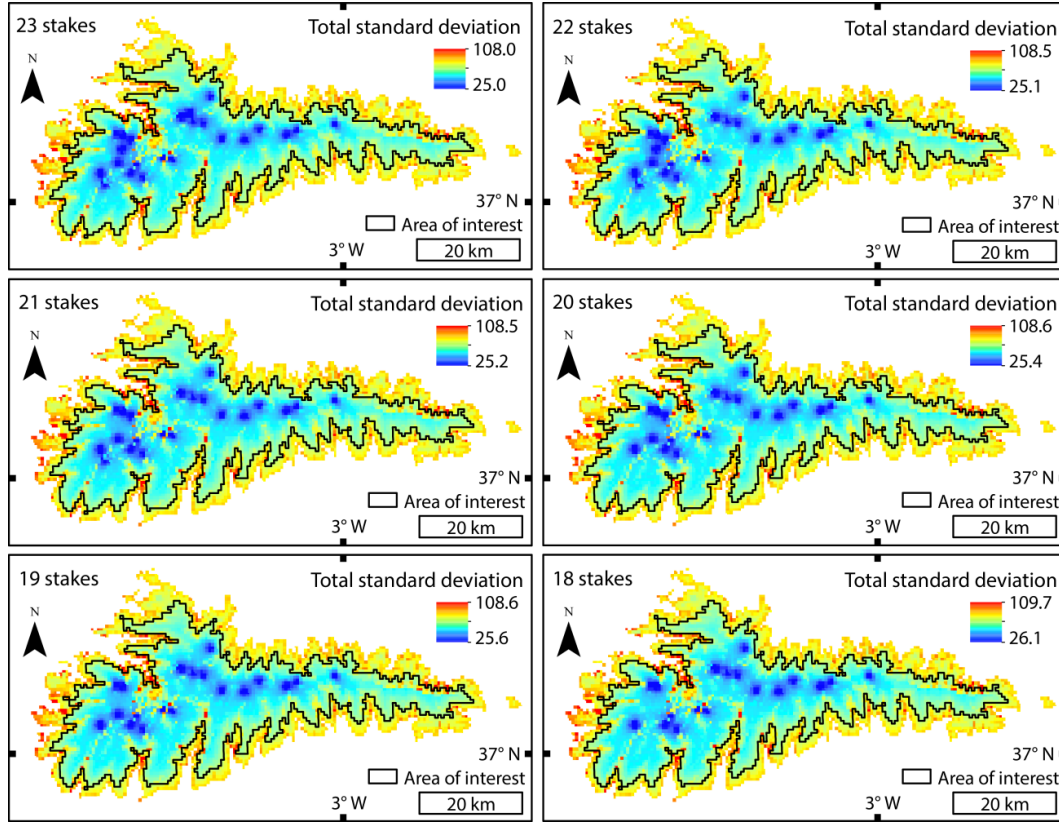


Figure 4.5. Spatial evolution of the total standard deviation in the reduction steps.

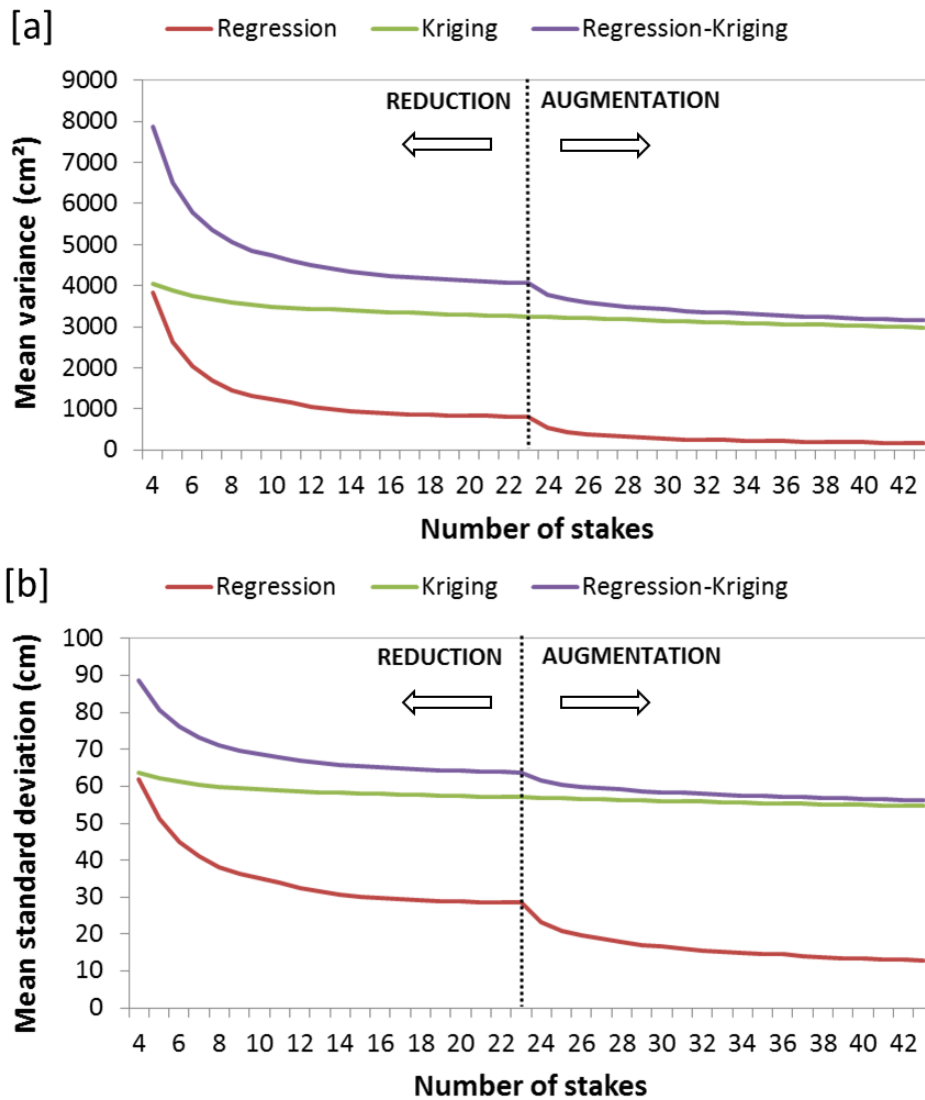


Figure 4.6. Mean variance and standard deviation (a and b, respectively) for the augmentation and reduction cases.

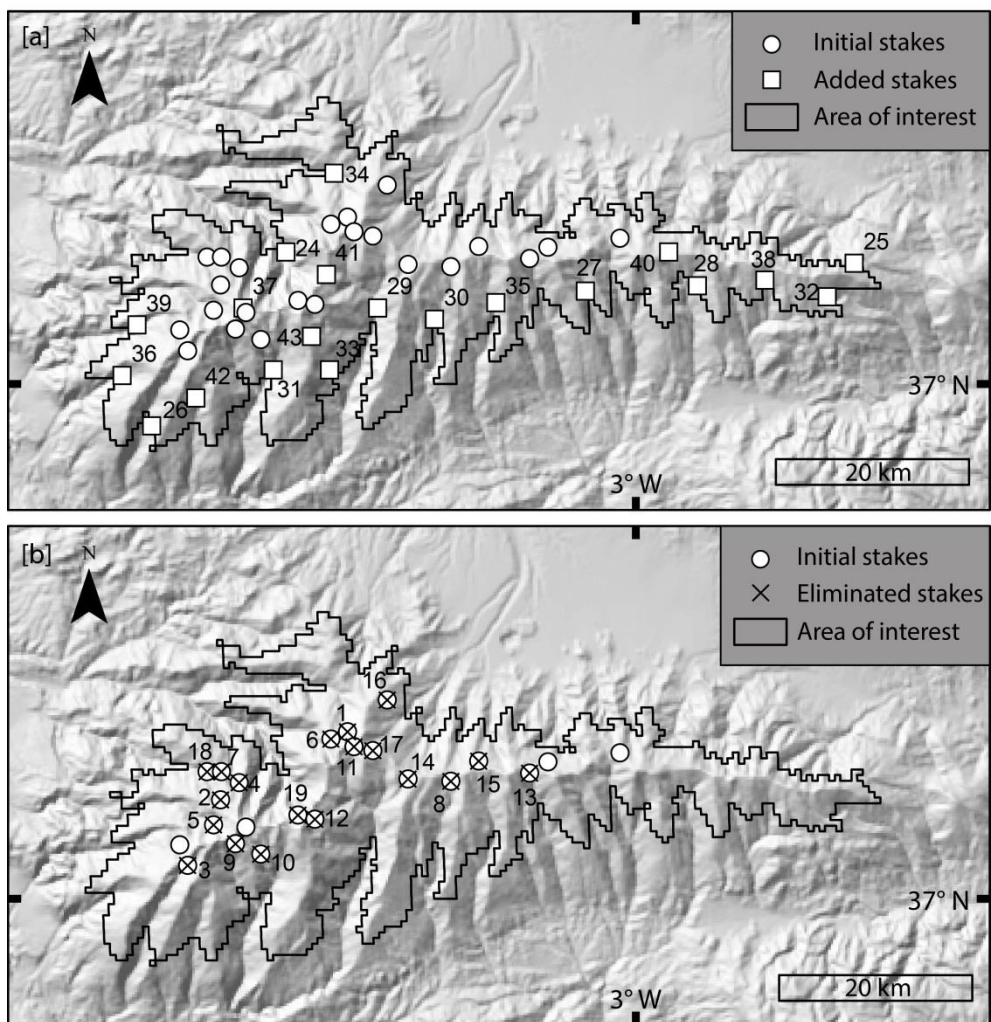


Figure 4.7. Location of the added stakes (a) and eliminated stakes (b) in the augmentation and reduction cases.

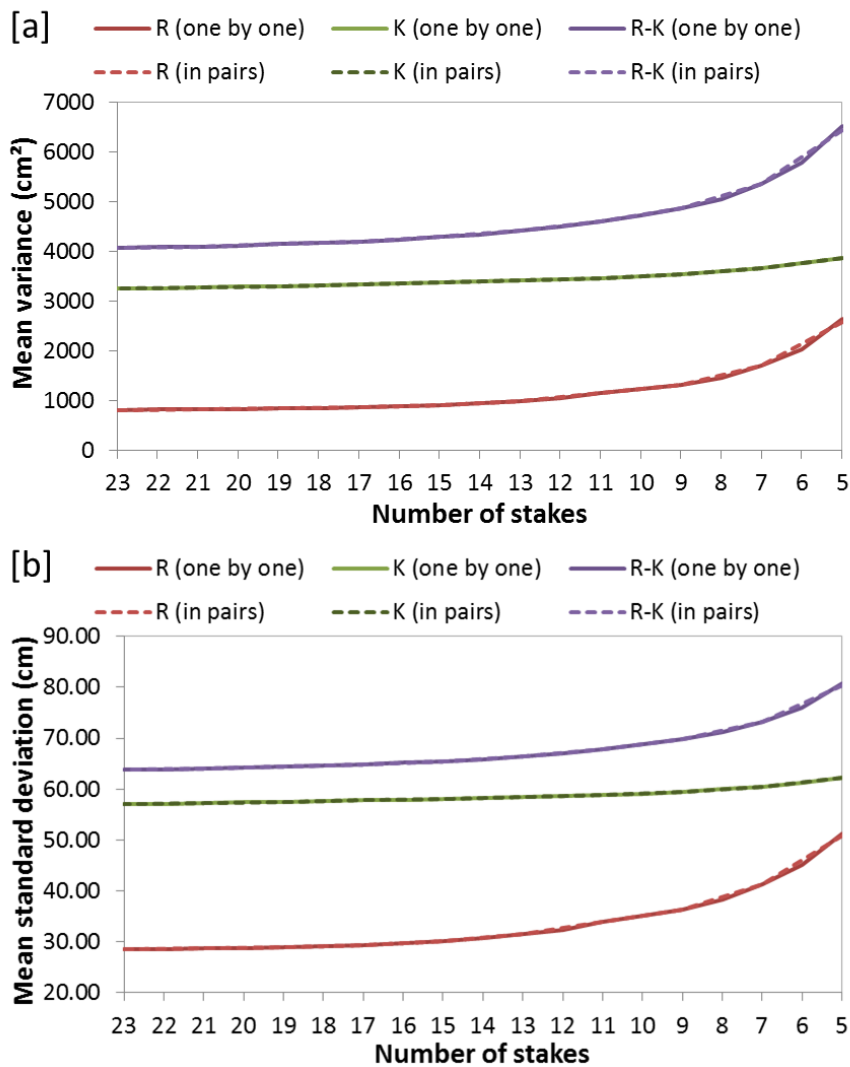


Figure 4.8. Mean variance and standard deviation (a and b, respectively) for the one-by-one and pairwise reductions.

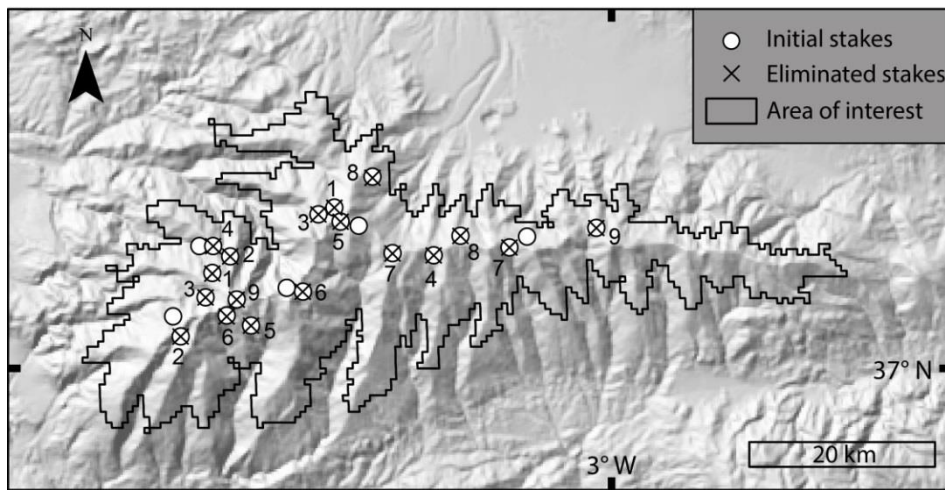


Figure 4.9. Location of the eliminated stakes for the pairwise reduction case.

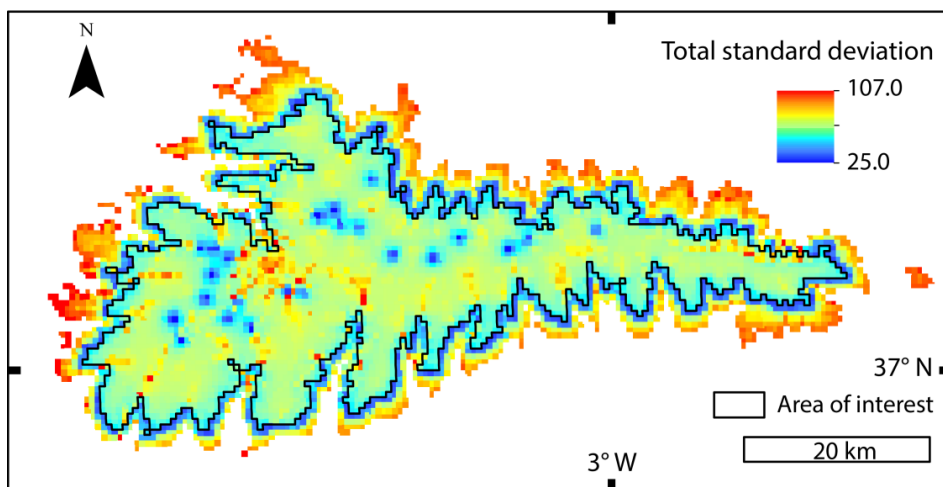


Figure 4.10. Total standard deviation of estimation considering SCA zeros.

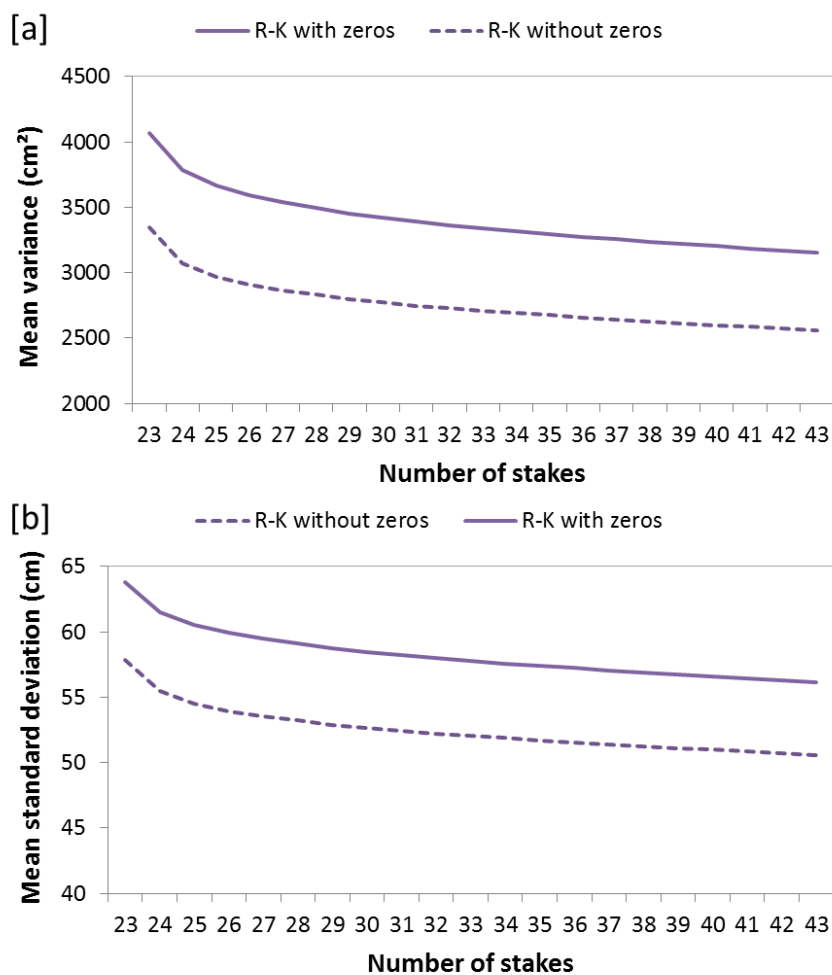


Figure 4.11. Mean variance and standard deviation (a and b, respectively) without considering SCA zeros and considering SCA zeros.

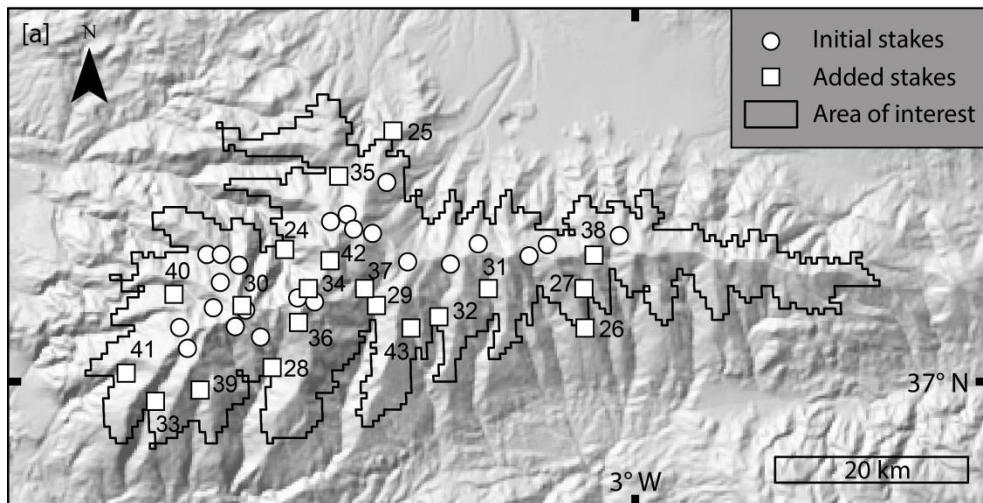


Figure 4.12. Location of the added stakes considering SCA zeros.

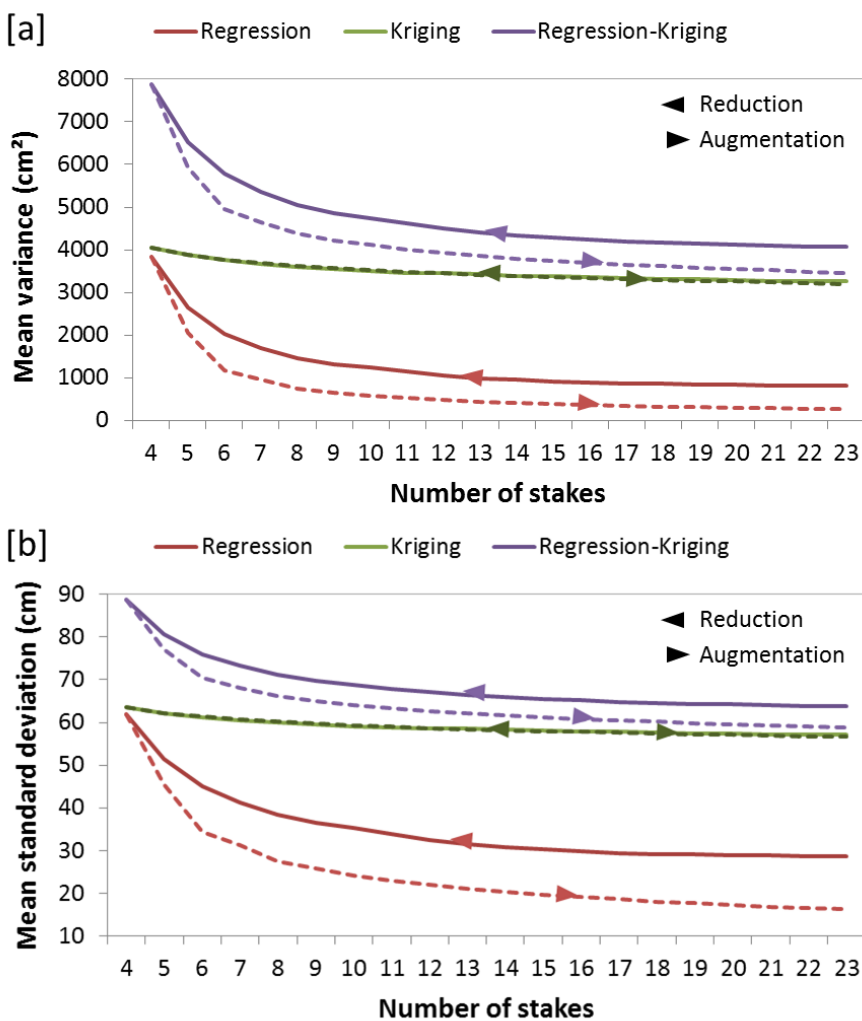


Figure 4.13. Mean variance and standard deviation (a and b, respectively) for the combination of augmentation and reduction cases.

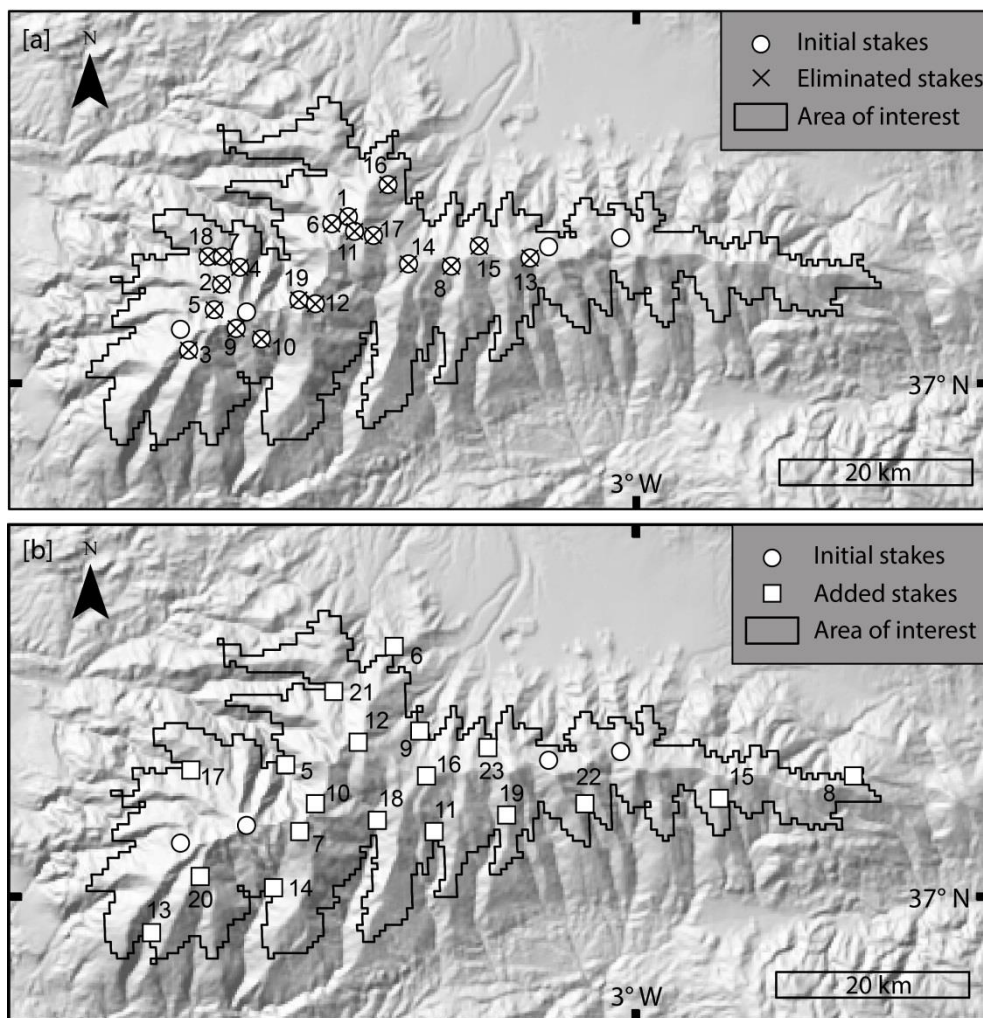


Figure 4.14. Location of the eliminated stakes in the reduction phase (a) and added stakes in the augmentation phase (b).

Chapter 5: Estimation of the spatiotemporal dynamics of snow covered area by using cellular automata models

Journal of Hydrology 550 (2017) 230–238

Contents lists available at [ScienceDirect](#)

Journal of Hydrology

journal homepage: www.elsevier.com/locate/jhydrol



Research papers

Estimation of the spatiotemporal dynamics of snow covered area by using cellular automata models

Eulogio Pardo-Igúzquiza^a, Antonio-Juan Collados-Lara^{b,*}, David Pulido-Velazquez^{b,c}



Eulogio Pardo-Igúzquiza⁽¹⁾, Antonio-Juan Collados-Lara^(2,*) and David Pulido-Velazquez^(2, 3)

(1) Instituto Geológico y Minero de España (IGME), Ríos Rosas, 23. 28003 Madrid (Spain).
E-mail address: e.pardo@igme.es

(2) Instituto Geológico y Minero de España (IGME), Urb. Alcázar del Genil, 4, bajo. Edificio Zulema. 18006, Granada (Spain). E-mail address: ajcollados@gmail.com, d.pulido@igme.es

(3) Departamento de Ciencias Politécnicas, Escuela Universitaria Politécnica, UCAM
Universidad Católica San Antonio de Murcia, Murcia, Spain

* Corresponding author

Abstract

Given the need to consider the cryosphere in water resources management for mountainous regions, the purpose of this paper is to model the daily spatially distributed dynamics of snow covered area (SCA) by using calibrated cellular automata models. For the operational use of the calibrated model, the only data requirements are the altitude of each cell of the spatial discretization of the area of interest and precipitation and temperature indexes for the area of interest. For the calibration step, experimental snow covered area data are needed. Potential uses of the model are to estimate the snow covered area when satellite data are absent, or when they provide a temporal resolution different from the operational resolution, or when the satellite images are useless because they are covered by clouds or because there has been a sensor failure. Another interesting application is the simulation of SCA dynamics for the snow covered area under future climatic scenarios. The model is applied to the Sierra Nevada mountain range, in southern Spain, which is home to significant biodiversity, contains important water resources in its snowpack, and contains the most meridional ski resort in Europe.

Key words: snowline, cellular automata, elevation, climatological indexes, Sierra Nevada

1. Introduction

Water resources management and operational river forecasts in river basins that enclose high mountainous regions must take into account the cryosphere (i.e. the snowpack). The amount of snow and its spatial and temporal distribution as well as the outflow of water from the snowpack must be estimated from available information. The problem is three-fold: (i) estimation of the snow covered area (SCA); (ii) estimation of the snowpack thickness and (iii) estimation of the snow density. The three variables (covered area, thickness and density) are needed to estimate the snow water equivalent, however estimating each variable is a problem in and of itself. Each variable can be approached by applying different modelling techniques: interpolation methods (e.g. Richer *et al.*, 2012; Mir *et al.*, 2015 to estimate SCA; Collados-Lara *et al.*, 2017 to estimate snow pack thickness; Bormann *et al.*, 2013 and Lopez-Moreno *et al.*, 2013 to estimate snow density; Sexstone and Fassnacht, 2014 and Elder *et al.*, 1998 to estimate snow water equivalent), conceptual methods (e.g. HBV (Lindström *et al.*, 1997); Snowmelt Runoff Model (SRM) (Martinec *et al.*, 2008; Sensoy and Uysal, 2012) or physically-based models (e.g. CROCUS (Bruland *et al.*, 2001); ECHAM (Foster *et al.*, 1996)). Under standard circumstances, SCA can be estimated using satellite data, such as from the Moderate Resolution Imaging Spectroradiometer (MODIS) (Hall *et al.*, 2006; Hall and Riggs, 2007). The question we aim to answer in this work is how to estimate the snow covered area when satellite data are unavailable. Satellite data may be unavailable for different reasons. For instance it could be because the satellite was not launched yet or because the temporal resolution of the satellite data is larger than the temporal resolution of interest. Also satellite data may be useless because the area of interest was covered by clouds or because there was a failure in the sensor. Furthermore, future scenarios of precipitation and temperature could be defined from the simulation performed with different Regional Climatic Models (RCM) for the emission scenarios defined by IPCC (Jacob *et al.*, 2013). These future scenarios of climate in an area, defined by applying a downscaling technique from the RCM simulations, could be used to feed the SCA model in order to assess future SCA scenarios. This is a method commonly applied to assess future scenarios of other hydrological variables from hydrological balance models (Pulido-Velazquez *et al.*, 2011; 2015). These hydrological model predictions could also be improved by incorporating SCA using the data assimilation technique (Thirel *et al.*, 2013, Alvarado Montero *et al.*, 2016).

In addition to the physically-based or conceptual approaches (Molotch *et al.* 2004), we can also find examples of regression techniques (Richer *et al.*, 2012; Mir *et al.*, 2015) and learning algorithms (artificial neural networks) to estimate Snow Cover Fraction Mapping (Hou and Huang, 2014; Mishra *et al.*, 2014). In this study we propose a novel approach to the problem: the application of an evolutionary algorithm, as the cellular automaton, to estimate SCA. The estimation of SCA fits perfectly in the kind of problems that can be analysed with cellular automata techniques, as they are complex, dynamic systems that can be approached in a discrete way. Cellular automata models are good for simulating complex discrete dynamics by using simple rules that define the interaction between neighbour cells that discretize the study area. They have been applied to different problems in geosciences like urban growth dynamics (Kumar *et al.*, 2014), snow crystal growth (Reiter, 2005) or simulation of snow

avalanches (Barpi, 2007), among others. Cellular automata have also been used to simulate snow cover dynamics (Leguizamón, 2006). However the latter reference offers only a preliminary study that had significant limitations: (i) it only uses a small synthetic area rather than a real study area, (ii) it simulates a simple dynamic situation of reduction of the snowpack from a starting condition with an existing snowpack, (iii) the simulation is for a short time interval, (iv) the simulation does not introduce driving climatological indexes (precipitation and temperature) in order to guide the dynamics, (v) the procedure cannot start a snowpack in an image where all the cells are without snow. In this paper we extend the idea of using cellular automata to estimate the snow covered area. The extension deals with overcoming each of the aforementioned limitations. We used a real case study so that the cellular automata could be calibrated and validated but the methodology is completely general and can be applied to any area of interest because the data requirements are minimal. The methodology is described in the next section.

2. Methodology

Cellular automata are discrete dynamic models introduced by Wolfram (1984) in order to simulate complex dynamics using simple rules of interaction. The two-dimensional area of interest (i.e. a geographical region projected on a plane) is divided into a finite number of cells or pixels. Time is also discretized in time steps. The shape and size of the study area can be arbitrary, but for the sake of presentation one can think of a rectangular grid of cells: $\{(i,j); i = 1, \dots, N_x; j = 1, \dots, N_y\}$. The size of the cell can be any of interest; for example in the case study we will use square cells measuring approximately 460 m x 460 m, which is the spatial resolution of a MODIS image for the latitude of the study area. As was already mentioned, there is also a discretization of time; for example in the case study the time step is one day. Next, each cell (i,j) can be, at each time, t , in one of two possible states (1 or 0):

$$S(i,j,t) = \begin{cases} 1 & \text{if cell } (i,j) \text{ is covered by snow at time } t \\ 0 & \text{if cell } (i,j) \text{ is free of snow at time } t \end{cases} \quad (1)$$

The state $S(i,j,t)$ depends, in general, on:

- The state of the cell (i,j) at the previous time step: $S(i,j,t - 1)$.
- The states, at the previous time step, of the cells of a given configuration of neighbour cells. For example for an 8-neighbourhood, the states of the cells $(i - 1, j - 1)$, $(i, j - 1)$, $(i + 1, j - 1)$, $(i + 1, j)$, $(i + 1, j + 1)$, $(i, j + 1)$, $(i - 1, j + 1)$ and $(i - 1, j)$ at time $t - 1$ are involved.
- A given set of transition rules. In classic cellular automaton models, the transition rules depend on the state of the cell at the previous step and the states of the neighbour cells at the previous step. However, in order to simulate realistic snow dynamics, we must introduce transition rules defined by some driving variables. This can be defined as a mixed cellular automaton. We have chosen a couple climatological indexes as driving variables: precipitation and temperature, $P(t)$ and $T(t)$, respectively, and a terrain variable: the altitude $H(i,j)$ of each cell (i,j) . This allows the cellular automaton to evolve even if all the cells of the study area are at state zero. The altitude

index in the calculation cells has been obtained as the mean altitude from a digital elevation model which has a spatial resolution of 5 meters (the highest DEM resolution available from the National Geographic Institute of Spain). Temperature and precipitation indices are used in the form of two time series: a time series of daily temperature and a time series of daily precipitation. These time series could be measured at a weather station or obtained from a given estimation product. The absolute values of these indices are not important in this problem because they are calibrated for a specific problem. The truly important feature of these indices is that they capture the temporal climatological variability of the case study.

The cellular automata model is calibrated with experimental snow covered area data for a particular period of time. For example, in our case study the experimental data are daily binary images of snow/no snow cells obtained from MODIS images (Hall et al., 2006) and the calibration period lasts three years. Furthermore, in our case study (next section), the estimation time starts on 1 July of the first year of the calibration period when the state of every cell in the study area is equal to zero (there is no snow in the study area). Hence, a pure cellular automaton cannot work because all the cells have the same state of zero, or equivalently the snowline is at an arbitrarily high altitude, which is larger than the largest altitude in the study area. Thus by introducing the driving variables, the discrete system can follow the realistic dynamics of the snowpack by changing the snowline, which is defined as the altitude above which the terrain can have snow. Thus new transition rules are introduced by using the climatological indexes and the digital elevation model is:

- If the precipitation is larger than or equal to a given threshold, $P(t) \geq P_0$, and the altitude of the cell (i,j) is above the snowline $H(i,j) > H_k(t)$, the state of the cell will be 1 (that is, by remaining at state 1 if it was already 1 or by changing from state 0 to state 1). The snow line H_k is defined, discretized in K values, by the temperature index $T(t)$:

$$\text{If } T(t) < T_1 \text{ then } H_k(t) = H_1$$

$$\text{If } T(t) < T_2 \text{ then } H_k(t) = H_2$$

...

$$\text{If } T(t) < T_K \text{ then } H_k(t) = H_K$$

$$\text{With } T_1 > T_2 > \dots > T_K \text{ and } H_1 > H_2 > \dots > H_K.$$

- If precipitation at day t is below the threshold $P(t) < P_0$ and the temperature has decreased or has increased by an amount smaller than a given threshold:

$$T(t) - T(t-1) \leq T_c > 0 \quad (2)$$

then the state of each cell remains at the state of the previous time step.

- Otherwise, if precipitation at day t is below the threshold $P(t) < P_0$ and the temperature has increased by an amount larger than a given threshold

$$T(t) - T(t-1) > T_c > 0 \quad (3)$$

the state of a pixel in state 0 remains at state 0, and a pixel at state 1 changes to state 0 (fusion of snow) if the number of neighbour cells $N(i,j)$ with state 1 is smaller than a given threshold N_m :

$$N(i,j) \leq N_m \quad (4)$$

Thus $P_0, K, T_1, T_2, \dots, T_K, H_1, H_2, \dots, H_K, T_c, N_m$ are parameters to calibrate.

When representing the discretized snowline defined by the data pairs $(T_1, H_1; T_2, H_2; \dots; T_K, H_K)$ they result in a straight line, thus the calibration can be simplified from $2K$ parameters to just two parameters, the slope b and the intercept a of the straight line:

$$H(t) = a + bT(t) \quad (5)$$

Thus the parameters to calibrate are P_0, a, b, T_c, N_m , which is a more amenable number of parameters. They are assigned optimal values using an optimization approach (search using the uniform mesh method) in which values are given to the parameters. The set of values which result in a minimum value for the mean squared error between experimental data and simulated snowpack for the calibration period are chosen as the parameters for the model.

3. Case study

Our case study is located in the Sierra Nevada mountain range, a Mediterranean high altitude mountain range in southern Spain (Figure 5.1.A). The area of interest is the domain in which we find the main snow pack of the Sierra Nevada mountain range. Nevertheless, for simplicity, the domain employed to simulate the SCA evolution was defined by using a rectangular portion of the MODIS mesh that includes the aforementioned area of interest. The final adopted mesh covers an area significantly wider than the main snowpack in the Sierra Nevada. Outside of this area within the mesh we can occasionally find some snow but it disappears in a few days. Figure 5.1.A shows the area of interest, where the probability of having snow is higher than six days every snow season. It has been obtained by using historical MODIS satellite data.

The domain dimensions are around 80 km in length (E-W direction) and between 15 and 30 km wide (N-S direction), giving a surface area of approximately 2000 km². The Sierra Nevada is a national park with significant biodiversity and it is home to the most meridional ski resort in Europe. The Sierra Nevada is also an important source of water resources, mainly from the accumulation of snow during the winter. The aim of this study is to estimate the daily dynamics of the snow covered area on a grid with square cells approximately 460 m long on each side, which correspond to the pixels of the MODIS image that covers the region. NASA has been collecting SCA information since 1966 at various temporal resolutions (1 day, 8 days and 1 month) and with an approximate spatial resolution of 463 m since 2000, using MODIS (Hall *et al.*, 2006).

The daily SCA from MODIS provides the fractional covered area (in % for example). Because the automaton provides binary results for each pixel (snow or non-snow), in order to

facilitate the comparison of snow spatial distribution with the satellite observation maps, we decided to use a binary satellite product to calibrate and validate the model. Nevertheless, instead of directly using the binary MODIS product (Hall *et al.*, 2006) we used the fractional snow cover product in order to define our own binary product. We did this because we wanted to complete the snow information for pixels with cloudy conditions to define the satellite maps. We employed an interpolation method to estimate those “cloudy pixels” that can be only applied with the fractional snow covered area product before translating it into our binary product.

For cloudy days, the fractional snow cover in a pixel covered by clouds was estimated using a linear interpolation between the closest prior and next cloudless days. In our case, this provided a close enough approximation, taking into account that, in the historical period, the number of consecutive cloudy days in a pixel was quite small (the mean length of consecutive cloudy dates in a pixel is 2.2 days in the calibration period and 1.6 in the validation period) and the inertia of the snowpack in this alpine region is sufficient.

Finally, we transformed the completed fractional SCA product to a daily binary SCA image by using the unbiased transformation:

$$B(i,j,t) = \begin{cases} 1 & \text{if } F(i,j,t) \geq 50\% \\ 0 & \text{if } F(i,j,t) < 50\% \end{cases} \quad (6)$$

Where $F(i,j,t)$ is the fractional SCA (in %) of the cell (i,j) at day t and $B(i,j,t)$ is the binary SCA of the cell (i,j) at day t . Thus the daily dynamics of SCA, that is the area covered by the snowpack, can be represented as a time series of the number of cells of SCA versus time.

In this study, a three year time span, from 1 July 2000 to 30 June 2003, was used for calibration purposes and another three year time span, from the 1 July 2003 to 30 June 2006, was used for validation purposes. As an example of the snow area dynamics for a given year, Figure 5.2 shows the daily dynamics of the SCA for three consecutive years, from 1 July 2000 to 30 June 2003. From Figure 5.2, it can be seen how the time series starts in the summer when there is no snow pack. The SCA is represented as number of cells where each cell has a surface area of 460 m x 460 m or 0.2116 km². For this particular time period, it can be seen how the dynamics may be very different from year to year with a different number of maxima each year. At the beginning of the snow season the SCA peaks are asymmetrical with rapid growth and a slower decrease but in the middle of the snow season the peaks are more symmetrical and show quick dynamics. The driving variables of precipitation and temperature can be calculated from many different sources, such as from the dataset SPAIN02 (Herrera *et al.*, 2012, 2016). The Spain02 dataset is a daily temperature and precipitation estimation from the observational data (around 2500 quality-controlled stations) collected by the Spanish Meteorological Agency in the period 1971 to 2010. An assessment of the validation of some Spanish datasets, including Spain02, was recently carried out by Quintana *et al.* (2016). We have employed version 4 (v4) of the SPAIN02 project dataset (<http://www.meteo.unican.es/en/datasets/spain02>), which includes daily field estimations with a spatial resolution of 0.11° in rotated coordinates matching Euro-CORDEX grids. The

SPAIN02 dataset has already been employed in many research studies (Escriva-Bou *et al.*, Fernandez-Montes *et al.*, 2015).

Even for this single dataset, different indices can be calculated, for example by using the mean precipitation of stations that have a certain altitude (a.s.l.). The altitude thresholds of 1000, 1500, 2000, 2500 and 3000 m (a.s.l.) have been used. For temperature, there are even more possibilities, as the minimum, mean or maximum temperature could be used. Also, with regard to precipitation, the mean temperatures above 1000, 1500, 2000, 2500 and 3000 m (a.s.l.) have been considered. Figure 5.3 shows, for one year and for illustrative purposes, the daily temperature index calculated as the mean of the minimum temperatures above 1000 and 3000 m (Figure 5.3.A) and the mean of the maximum temperatures above 1000 and 3000 m (Figure 5.3.B). After trying the different combinations of precipitation indices (5 possibilities) and temperature indices (15 possibilities) the combination of precipitation above 1000 m and maximum temperature above 1000 m have been shown to be the best choice as climatological indices for the study area. The procedure used to choose the best climatological indices was to obtain a first best estimation of the model parameters P_0, a, b, T_c, N_m and then compare the results with each pair of indices as explained below. These indices are shown with the experimental SCA in Figure 5.4. Once the climatological driving variables are chosen, calibration is performed by selecting the optimal values of the parameters P_0, a, b, T_c, N_m that provide unbiased and minimum squared error estimation by comparing the experimental SCA given in Figure 5.2, $SCA(t)$, and the estimated SCA from the automata model, $SCA^*(t)$. The estimate is unbiased if the mean error is close to zero and the estimate with minimum squared error is preferred, where the mean error (ME) is defined as:

$$ME = \frac{1}{N} \sum_{t=1}^N (SCA^*(t) - SCA(t)) \quad (7)$$

And the mean squared error (MSE) is defined as:

$$MSE = \frac{1}{N} \sum_{t=1}^N (SCA^*(t) - SCA(t))^2 \quad (8)$$

Because the number of calibration variables P_0, a, b, T_c, N_m is relatively low (five variables), it is possible to obtain the first estimates by doing an exhaustive search in a coarse grid. Using 10 possibilities for each variable there are 10^5 combinations of parameters to evaluate. Next the search is refined by using a finer grid for each parameter while keeping the rest of the parameters fixed at their best estimates. The best estimate for T_c is 0 and the best estimate for N_m is 14 when a neighbourhood of 24 cells (that is a 5x5 neighbourhood) is considered. The best estimate for P_0 is 6.80 mm while the best estimates for a and b are 1170 and 80 respectively. Figure 5.5 shows the ME and MSE as a function of the temperature threshold T_c , while the rest of the parameters are kept to their optimal values. It can be seen how the lowest MSE is given by the value of 0 °C which gives also an acceptable ME. Figure 5.6 shows the ME and MSE as a function of the precipitation threshold P_0 , while the rest of the parameters are kept to their optimal values. It can be seen how the lowest MSE is given by values of P_0 equal to 6.8 mm which also results in an acceptable ME. Figure 5.7 shows the ME and MSE as a function N_m when a neighbourhood of 24 cells (that is a 5x5 neighbourhood) is

considered. The estimated value is 14, which gives the minimum MSE and a reasonable ME. Figure 5.8 shows the ME and MSE as a function of the calibration parameters a and b respectively. Thus the best calibration values for the variables P_0, a, b, T_c, N_m are 6.8, 1170, 80, 0 and 14 respectively.

When the cellular automaton model is applied with these parameters, the estimated dynamics of daily SCA are obtained and have been represented in Figure 5.9. The mean error is 62 cells and the mean squared error is 264896. It can be seen from Figure 5.9 that the main discrepancy is that the maximum experimental SCA with very fast dynamics is only partially captured. One explanation for this may be that the change in the snowline over time does not follow a straight line for the whole year but two different straight lines, one for the winter months and another for the rest of the year. We have observed this when the data are averaged for a large number of years. However, for the three year period the relationship is not as clear, as may be seen in Figure 5.10. Thus, this issue is left open for future research to improve the cellular automaton. Nevertheless, Figure 5.10 shows how the linear relationship between snowline altitude and temperature obtained from the experimental data (MODIS binary images, the digital elevation model and the temperature driving variable) is similar to the optimal values obtained by calibration and minimization of the mean square error, which speaks to the robustness of the methodology.

The utility of the calibrated model is that it can be applied in operational mode to another time interval that was not used in the calibration and where there are not experimental SCA data. However in this study where the main task was to present the methodology and its performance, the method has been applied to another time interval not used in calibration, but where the SCA is known so it can be compared to the model's prediction. This process is shown in Figure 5.11, which shows the experimental SCA from 1 July 2003 to 30 June 2006 and the estimated evolution of the SCA. The ME is -49 cells and the MSE is 451212. Obviously the MSE is worse than in the calibration period but it can be seen how the bulk of the evolution has been captured and could provide useful results for application. Finally, Figure 5.12 shows the spatial evolution of the daily SCA for the 8 days from 19 to 26 December 2005, which correspond to the main peak in Figure 5.11 around day 177. It can be seen how the main features of the SCA are captured in the values estimated using the cellular automaton model.

The cellular automaton model may be modified in different ways so as to improve its final performance. Some are left for future research but one that should be examined here is the following. The rule described in equations (2) and (3) seems to have less of an explanation than a global rule as follows:

- If precipitation at day t is below the threshold $P(t) < P_0$ and the temperature has decreased or has increased by an amount smaller than a given threshold:

$$T(t) > T_{cc} \quad (9)$$

By calibrating the cellular automaton with this new rule the optimal value of T_{cc} is 13°C (Figure 5.13). Although this rule seems to make more physical sense than the other rule, the

results of MSE of 308760 for calibration (Figure 5.14) and 580121 for validation (Figure 5.15) are clearly worse than the rules in equations (2) and (3).

4. Conclusions

Cellular automata models have been presented to estimate daily snow cover dynamics in the Sierra Nevada mountain range in southern Spain. The area has been discretized with a cell size equal to the size of the MODIS pixel. The snow covered area from the MODIS snow covered area product was used to calibrate the cellular automaton model. Lumped climatological indexes were introduced in order to reproduce realistic dynamics in the study area, given that in summer the snow covered area is null (thus the whole area has a constant value of zero) and therefore a pure cellular automaton would fail. The model must be calibrated using five parameters: a precipitation threshold, the parameters of a straight line that define the snowline altitude as a function of temperature, and two pure cellular automata parameters. Of the latter, the first parameter is the size of the neighbourhood considered in the dynamics of each cell and it has been set as a 5x5 neighbourhood so the central pixel has 24 neighbours. The second parameter is the number N_m of neighbours with snow, which controls if a pixel with snow will change to the state of no snow when the temperature increases and there is no precipitation. The optimal number N_m was 14. The results obtained with the calibrated model when it is applied in operational mode to a different time period can be judged as satisfactory, as the main events of the dynamics are captured by the calibrated model. The introduction of spatially distributed climatological indices is left open for future research.

Acknowledgements

This research was funded by the research projects CGL2013-48424-C2-2-R and CGL2015-71510-R from the “Ministerio de Economía y Competitividad” of Spain. We would also like to thank the NASA DAAC for the SCA data and the Spain02 project (Herrera *et al.* 2012) for the climatic data employed in this project. We would like to thank the anonymous reviewers for providing constructive criticism.

References

- Alvarado Montero, R., Schwanenberg, D., Krahe, P., Lisniak, D., Sensoy, A., Sorman, A.A., Akkol, B., 2016. Moving horizon estimation for assimilating H-SAF remote sensing data into the HBV hydrological model. *Advances in Water Resources* 92: 248-247. <http://dx.doi.org/10.1016/j.advwatres.2016.04.011>.
- Barpi, F., Borri-Brunetto, M., Delli Veneri, L., 2007. Cellular-Automata Model for Dense-Snow Avalanches. *Journal of Cold Regions Engineering* 21(4), 121–140.
- Bormann K.J., Westra, S., Evans, J.P., McCabe, M.F., 2013. Spatial and temporal variability in seasonal snow density. *Journal of Hydrology* 484: 63-73.

- Bruland, O., Maréchal, D., Sand, K., Killingtveit, Å., 2001. Energy and water balance studies of a snow cover during snowmelt period at a high arctic site. *Theoretical and Applied Climatology* 70: 53–63.
- Collados-Lara, A.J., Pardo-Iguzquiza, E., Pulido-Velazquez, D., 2017. Spatio-temporal estimation of snowpack thickness using point data from snow stakes, digital terrain models and satellite data. *Hydrological Processes*. DOI: 10.1002/hyp.11165.
- Elder, K., Rosenthal, W., Davis, R.E., 1998. Estimating the spatial distribution of snow water equivalence in a montane watershed. *Hydrological Processes* 12 10-11: 1793-1808.
- Escriva-Bou, A., Pulido-Velazquez, M., Pulido-Velazquez, D., 2017. The Economic Value of Adaptive Strategies to Global Change for Water Management in Spain's Jucar Basin. *Journal of Water Resources Planning and Management*. DOI: 10.1061/(ASCE)WR.1943-5452.0000735.
- Fernandez-Montes, S., Rodrigo, F.S., 2015. Trends in surface air temperatures, precipitation and combined indices in the southeastern Iberian Peninsula (1970-2007). *CLIMATE RESEARCH* 63(19): 43-60. DOI: 10.3354/cr01287.
- Foster, J.L., Hall, D.K., Eylander, J.B., Riggs, G.A., Nghiem, S.V., Tedesco, M., Kim, E., Montesano, P.M., Kelly, R.E.J., Case, K.A., Choudhury, B., 2011. A blended global snow product using visible, passive microwave and scatterometer satellite data. *Int. J. Remote Sens.* 32: 1371–1395.
- Hall, D. K., G. A. Riggs, V. V. Salomonson, 2006. MODIS/Terra Snow Cover 5-Min L2 Swath 500m. Version 5. Boulder, Colorado USA: NASA National Snow and Ice Data Center Distributed Active Archive Center. <http://dx.doi.org/10.5067/ACYTYZB9BEOS>.
- Hall, D.K., G.A. Riggs, 2007. Accuracy assessment of the MODIS products. *Hydrological Processes* 21:1534-1547.
- Herrera, S., Gutiérrez, J.M., Ancell, R., Pons, M.R., Frías, M.D. and Fernández, J., 2012. Development and analysis of a 50-year high-resolution daily gridded precipitation dataset over Spain (Spain02). *International Journal of Climatology*, 32, 74–85.
- Herrera, S., Fernández, J., Gutiérrez, J.M., 2016. Update of the Spain02 Gridded Observational Dataset for Euro-CORDEX evaluation: Assessing the Effect of the Interpolation Methodology. *International Journal of Climatology*, 36:900–908. DOI: 10.1002/joc.4391.
- Hou, J.L., Huang, C.L., 2014. Improving Mountainous Snow Cover Fraction Mapping via Artificial Neural Networks Combined With MODIS and Ancillary Topographic Data. *IEEE Transactions on Geoscience and Remote Sensing* 52 9: 5601-5611
- Jacob, D., Petersen, J., Eggert, B., Alias, A., Christensen, O. B., Bouwer, L., Braun, A., Colette, A., Déqué, M., Georgievski, G., Georgopoulou, E., Gobiet, A., Menut, L., Nikulin, G., Haensler, A., Hempelmann, N., Jones, C., Keuler, K., Kovats, S., Kröner, N., Kotlarski,

S., Kriegsmann, A., Martin, E., Meijgaard, E., Moseley, C., Pfeifer, S., Preuschmann, S., Radermacher, C., Radtke, K., Rechid, D., Rounsevell, M., Samuelsson, P., Somot, S., Soussana, J.-F., Teichmann, C., Valentini, R., Vautard, R., Weber, B., Yiou, P. EURO-CORDEX: new high-resolution climate change projections for European impact research Regional Environmental Change, Springer Berlin Heidelberg, 2013, 1-16

Kumar U., C. Mukhopadhyay, Ramachandra, T.V., 2014. Cellular automata calibration model to capture urban growth. Boletín Geológico y Minero, 125 (3), 285-299.

Leguizamón, S., 2006. Simulation of Snow-cover Dynamics Using the Cellular Automata Approach. 8th International Symposium on High Mountain Remote Sensing Cartography, 41: 87-92.

Lindström, G., Johansson, B., Persson, M., Gardelin, M., Bergström, S., 1997. Development and test of the distributed HBV-96 hydrological model. Journal of Hydrology 201: 272–288.

Lopez-Moreno, J.I., Fassnacht, S.R., Heath, J.T., Jonas, T., 2013. Small scale spatial variability of snow density and depth over complex alpine terrain: Implications for estimating snow water equivalent. Advances in Water Resources 55:40–52. DOI: 10.1016/j.advwatres.2012.08.010

Martinec, J., Rango, A., Roberts, R., 2008. Snowmelt Runoff Model SRM User's Manual. New Mexico State University 178 pp.

Mir, R.A., Jain, S.K., Saraf, A.K., Goswami, A., 2015. Accuracy assessment and trend analysis of MODIS-derived data on snow-covered areas in the Sutlej basin, Western Himalayas. International Journal of Remote Sensing 36 15: 3837-3858.

Mishra, B., Tripathi, N.K., Babel, M.S., 2014. An artificial neural network based snow cover predictive modeling in the higher Himalayas. Journal of Mountain Science 114: 825-837.

Molotch, N.P., Fassnacht, S.R., Bales, R.C., Helfrich, S.R., 2004. Estimating the distribution of snow water equivalent and snow extent beneath cloud cover in the Salt–Verde River basin, Arizona. Hydrological Processes 18(9):1595-1611.

Pulido-Velazquez, D., Garrote, L., Andreu, J., Martin-Carrasco, FJ, Iglesias, A., 2011. A methodology to diagnose the effect of climate change and to identify adaptive strategies to reduce its impacts in conjunctive-use systems at basin scale. Journal of Hydrology 405: 110–122 doi:10.1016/j.jhydrol.2011.05.014.

Pulido-Velázquez, D., García-Aróstegui, J.L., Molina, J.L., Pulido-Velázquez, M., 2015. Assessment of future groundwater recharge in semi-arid regions under climate change scenarios (Serral-Salinas aquifer, SE Spain). Could increased rainfall variability increase the recharge rate? Hydrol. Process. 29 (6), 828–844. DOI: 10.1002/hyp.10191

- Quintana-Seguí, P., Turco, M., Herrera, S., and Miguez-Macho, G., 2016. Validation of a new SAFRAN-based gridded precipitation product for Spain and comparisons to Spain02 and ERA-Interim, *Hydrol. Earth Syst. Sci. Discuss.*, doi:10.5194/hess-2016-349.
- Reiter, C.A., 2005. A local cellular model for snow crystal growth. *Chaos, Solitons and Fractals*, 23, 1111-1119.
- S.K., Fassnacht, S.R., Moore, C.C., 2013. Spatiotemporal index for analyzing controls on snow climatology: application in the Colorado Front Range. *Physical Geography* 342: 85-107.
- Sensoy, A., Uysal, G., 2012. The Value of Snow Depletion Forecasting Methods Towards Operational Snowmelt Runoff Estimation Using MODIS and Numerical Weather Prediction Data. *Water Resources Management* 2612: 3415-3440.
- Sexstone, G.A., Fassnacht, S.R., 2014. What drives basin scale spatial variability of snowpack properties in northern Colorado?. *Cryosphere* 82: 329-344.
- Thirel, G., Salamon, P., Burek, P., Kalas, M., 2013. Assimilation of MODIS Snow Cover Area Data in a Distributed Hydrological Model Using the Particle Filter. *Remote Sens* 5: 5825-5850. doi:103390/rs5115825.
- Wolfram, S., 1984. Cellular automata: a model of complexity. *Nature*, 31, 419-424.

Figures of the Chapter 5

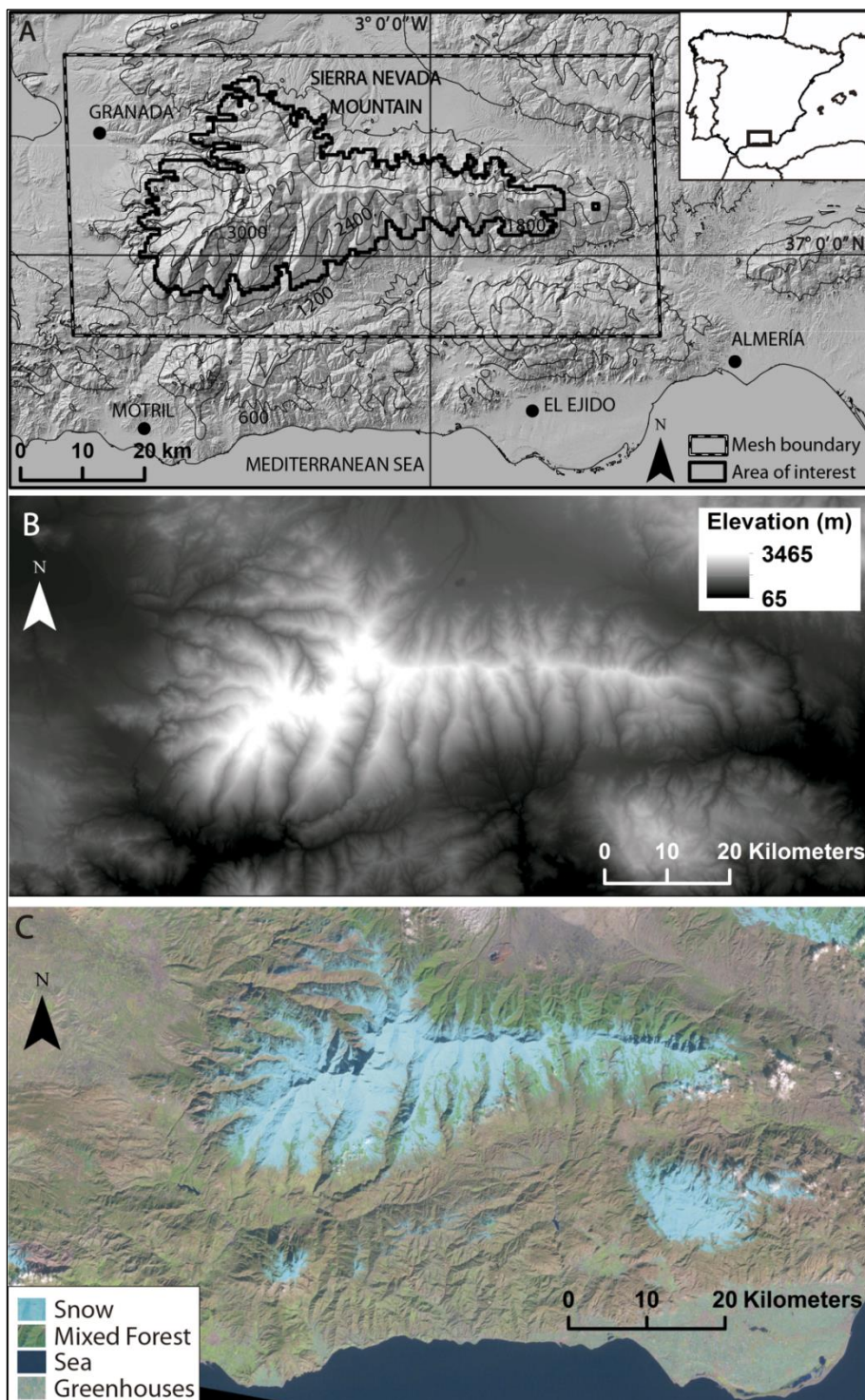


Figure 5.1. A: Location of the Sierra Nevada mountain range in Southern Spain. B: the digital elevation model of the study area. C: Landsat image, provided by the USGS, that shows the snow covered area in Sierra Nevada for the date 20/01/2000.

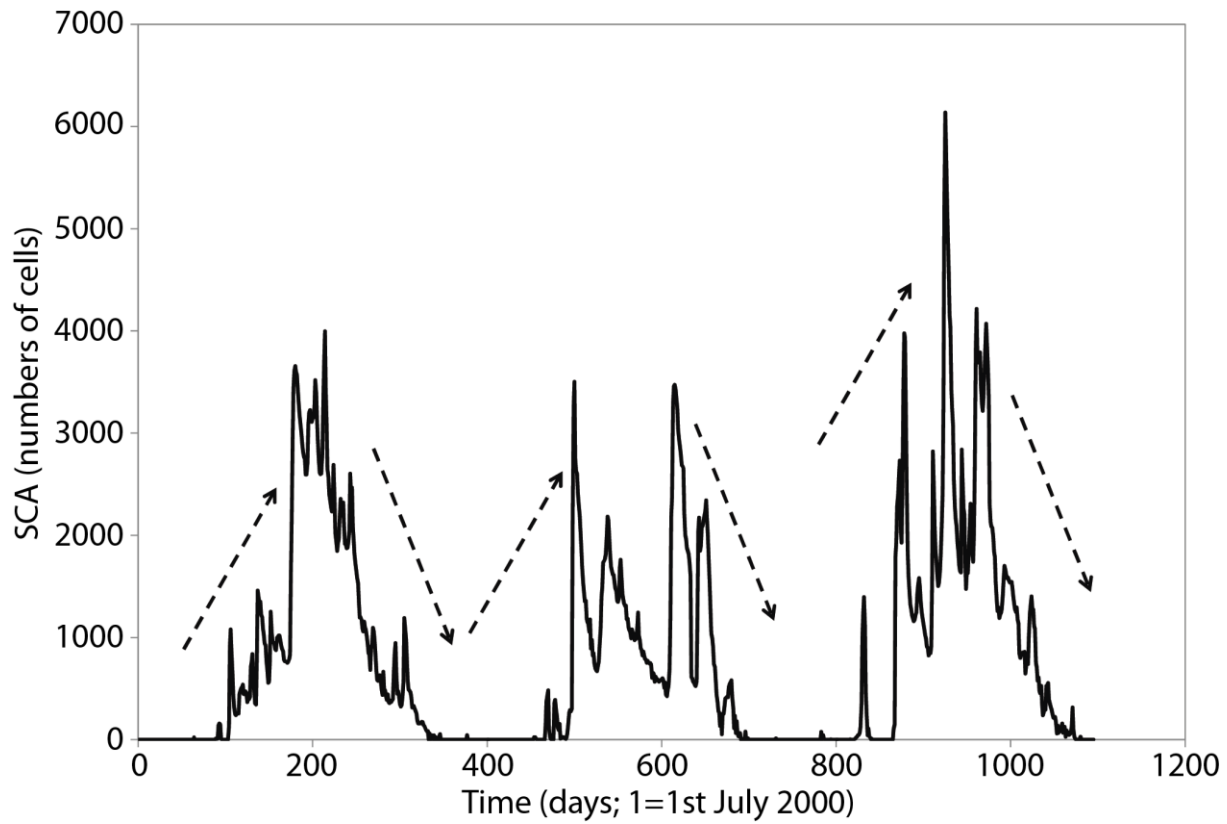


Figure 5.2. Daily dynamics of the snow covered area for three consecutive years, from the 1st of July of 2000 to the 30th of June 2003.

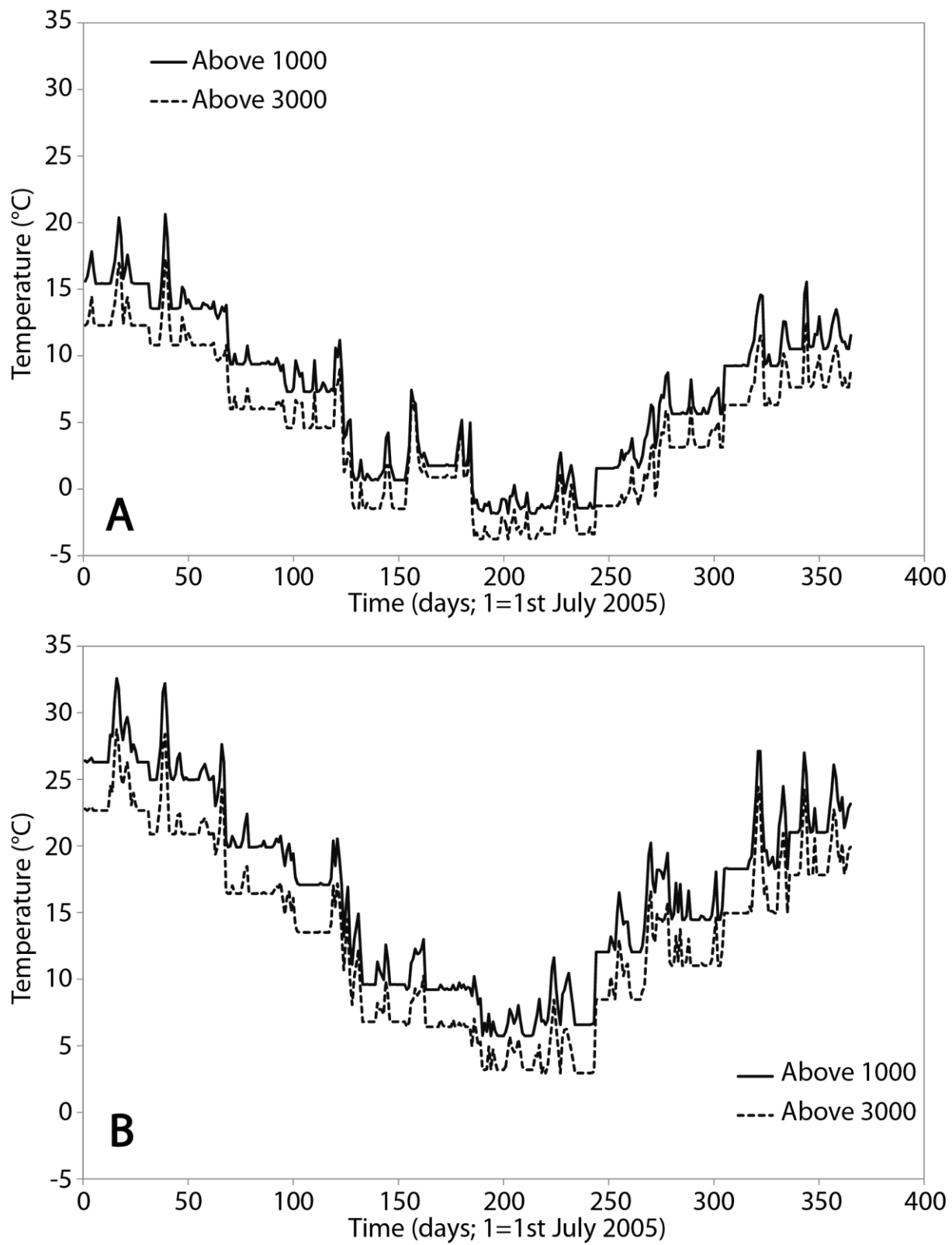


Figure 5.3. Daily temperature indexes calculated as A: the mean of the minimum temperatures of the stations of SPAIN02 that are above 1000 and 3000 m and B: the mean of the maximum temperatures of the stations of SPAIN02 that are above 1000 and 3000 m.

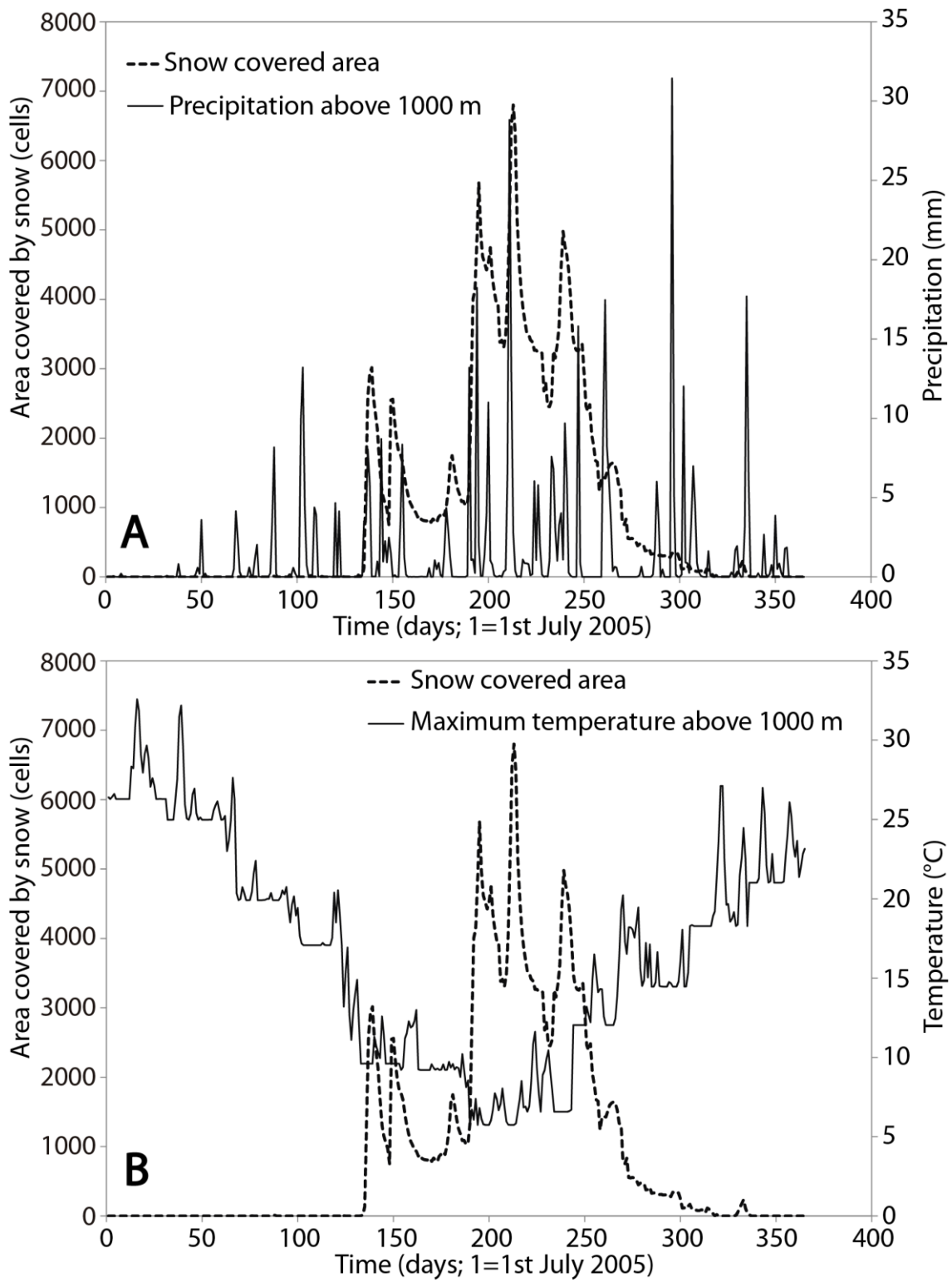


Figure 5.4. A: Daily precipitation index (calculated as the mean precipitation from stations of SPAIN02 above 1000 m) and the SCA time series, and B: Daily precipitation index (calculated as the mean maximum temperature from stations from SPAIN02 above 1000 m and SCA) and the SCA time series.

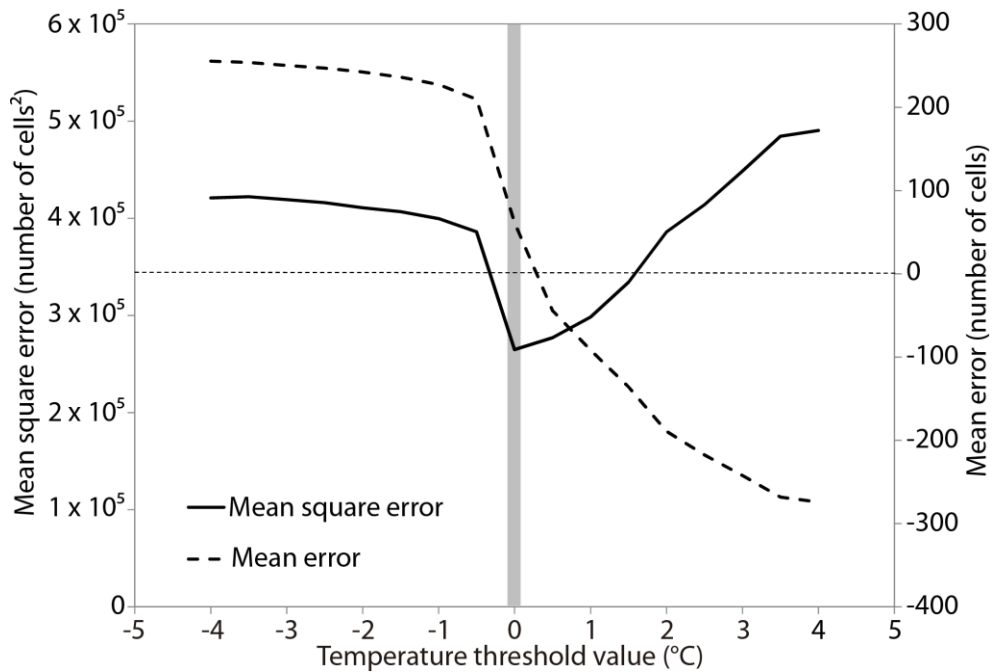


Figure 5.5. Mean square error (solid line) and mean error (dashed line) when the only varying parameter is the temperature threshold T_c while the rest of the parameters are hold at their optimal values. It may be seen how the lowest MSE is given by the value of 0°C which gives also an acceptable ME.

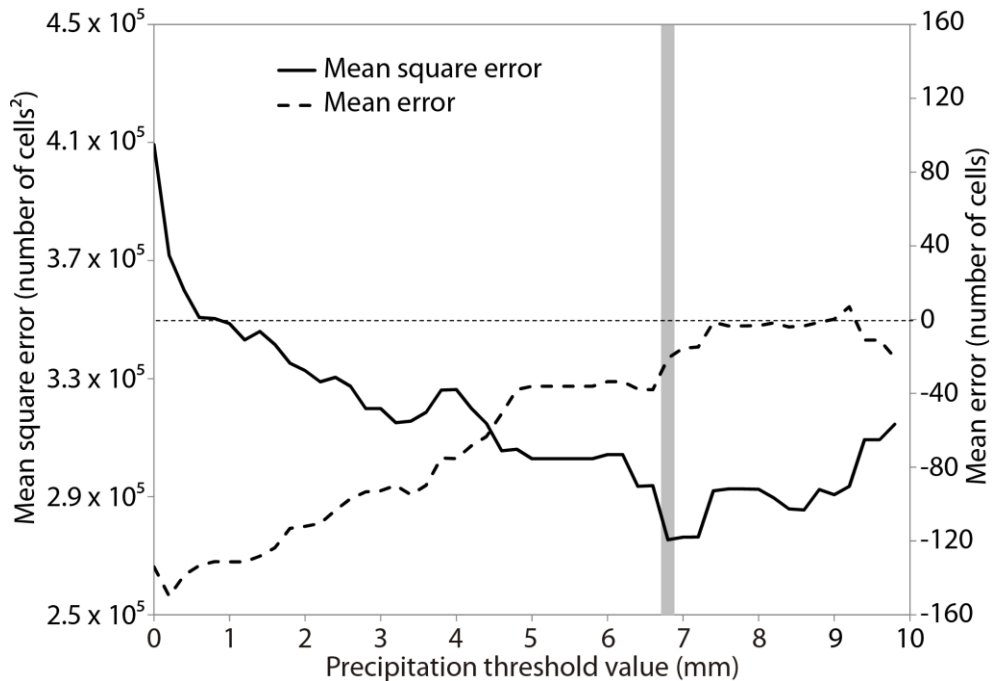


Figure 5.6. Mean square error (solid line) and mean error (dashed line) when the only varying parameter is the precipitation threshold while the rest of the parameters are hold at their optimal values. The precipitation threshold with minimum mean square error statistic is 6.8 mm (vertical gray bar) which gives an acceptable mean error of -20 cells.

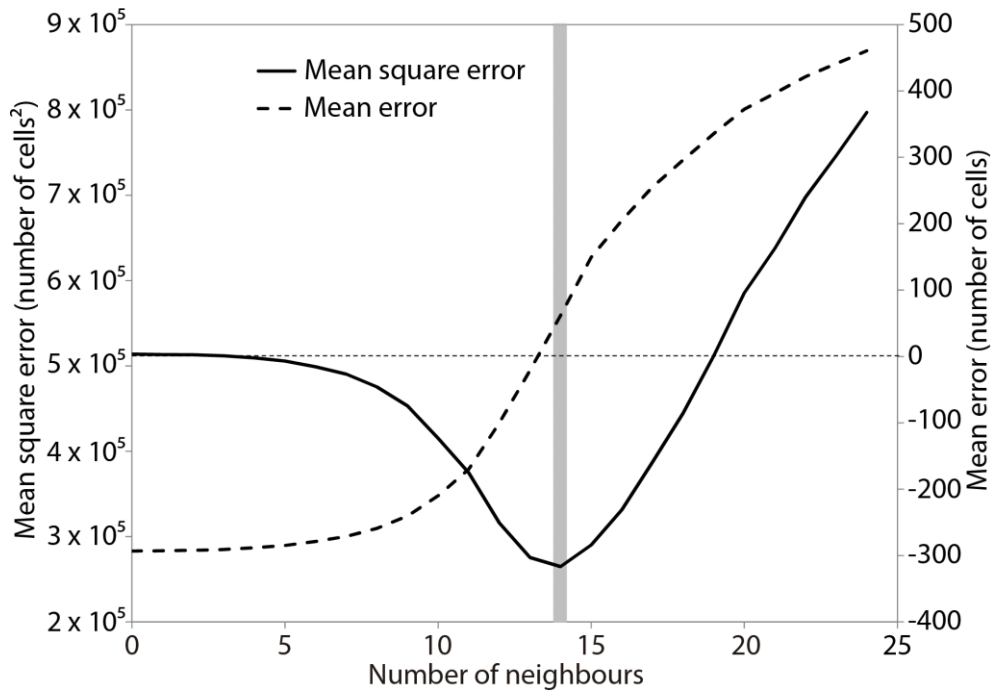


Figure 5.7. Mean square error (solid line) and mean error (dashed line) when the only varying parameter is the number N_m of neighbours with snow which controls if a pixel with snow will change to the state of no snow when temperature increases and there is no precipitation. The N_m with minimum mean square error statistic is 14 (vertical gray bar) which gives an acceptable mean error.

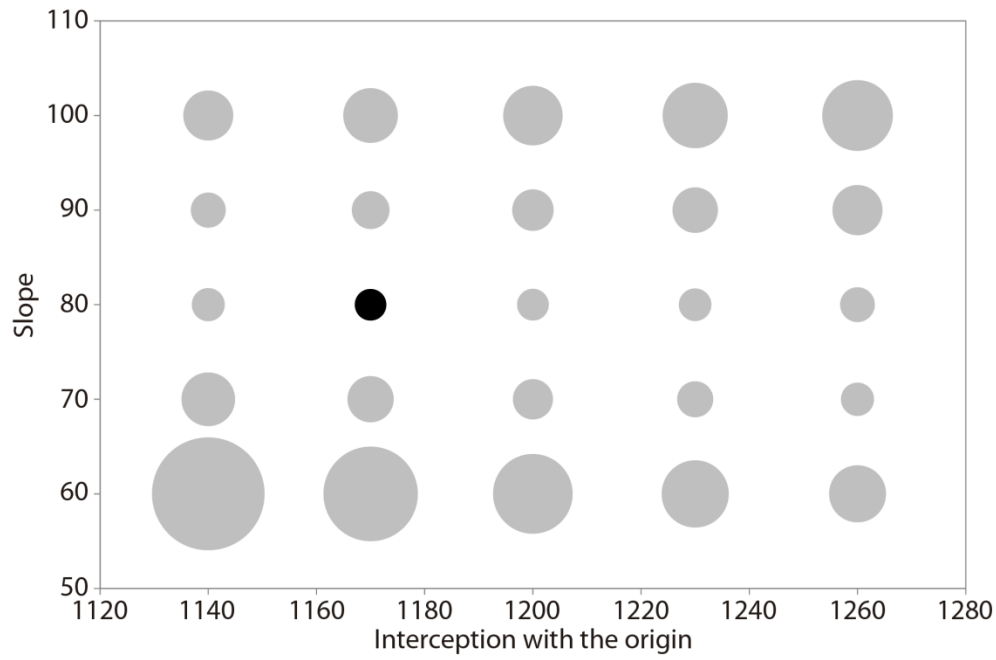


Figure 5.8. Mean square error (proportional to the width of the circles) when the only varying parameters are a (interception with the origin) and the parameter b (slope) of the straight line between temperature and altitude of the snow line. The values of 1170 and 80, for a and b respectively, provides the minimum mean square error (solid black circle).

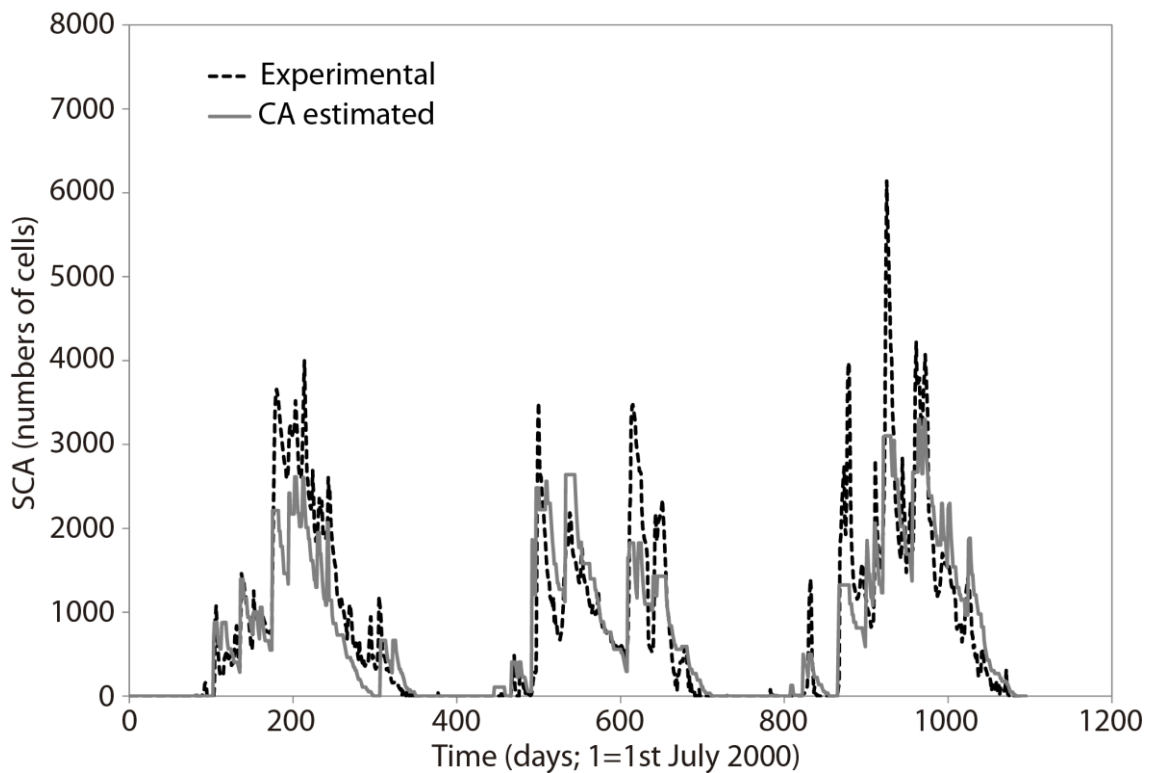


Figure 5.9. Experimental SCA and estimated SCA by the calibrated cellular automata model.

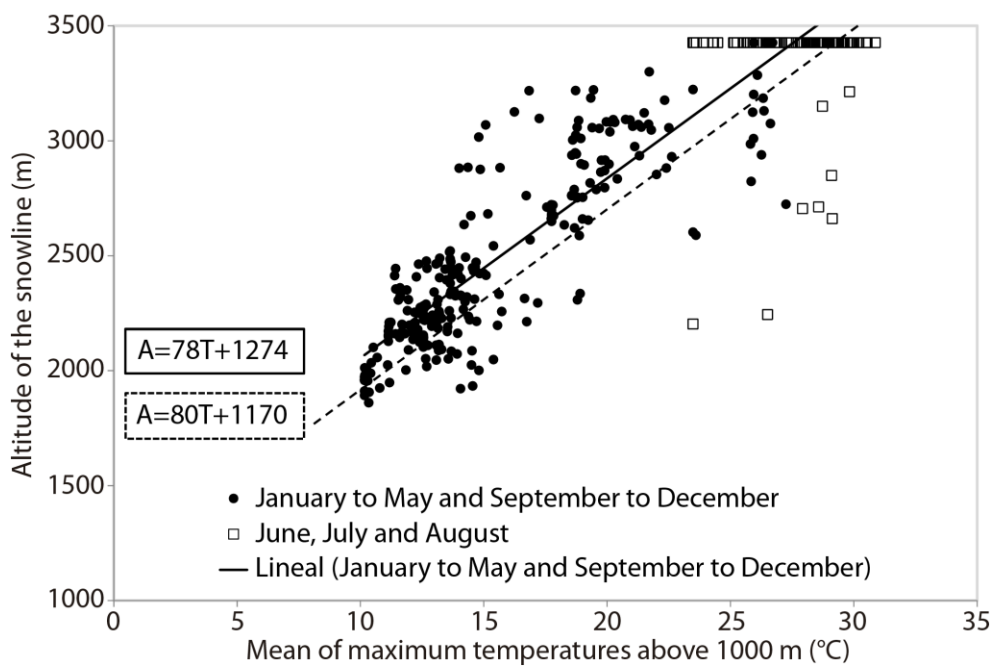


Figure 5.10. Experimental lineal relation between temperature and altitude of the snow line for the three years calibration period (dots and solid line) and the independent lineal relation obtained from model calibration (dashed line).

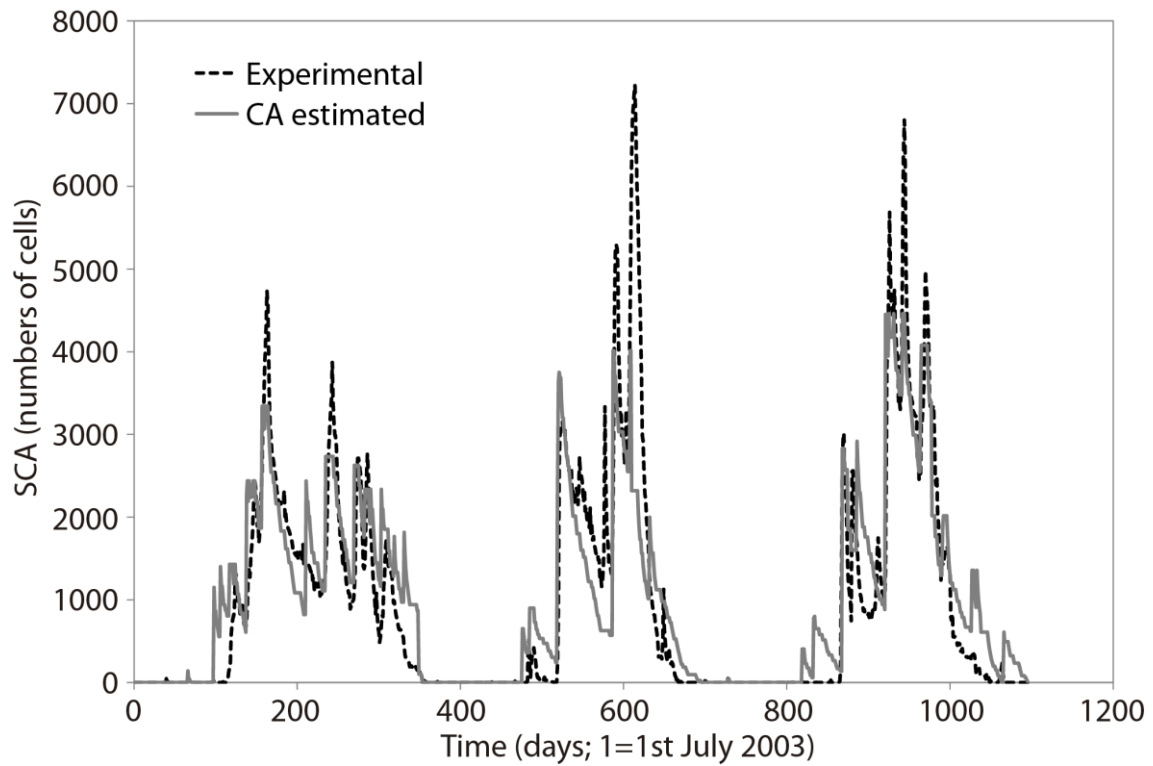


Figure 5.11. Experimental SCA and estimated SCA by the calibrated cellular automaton model.

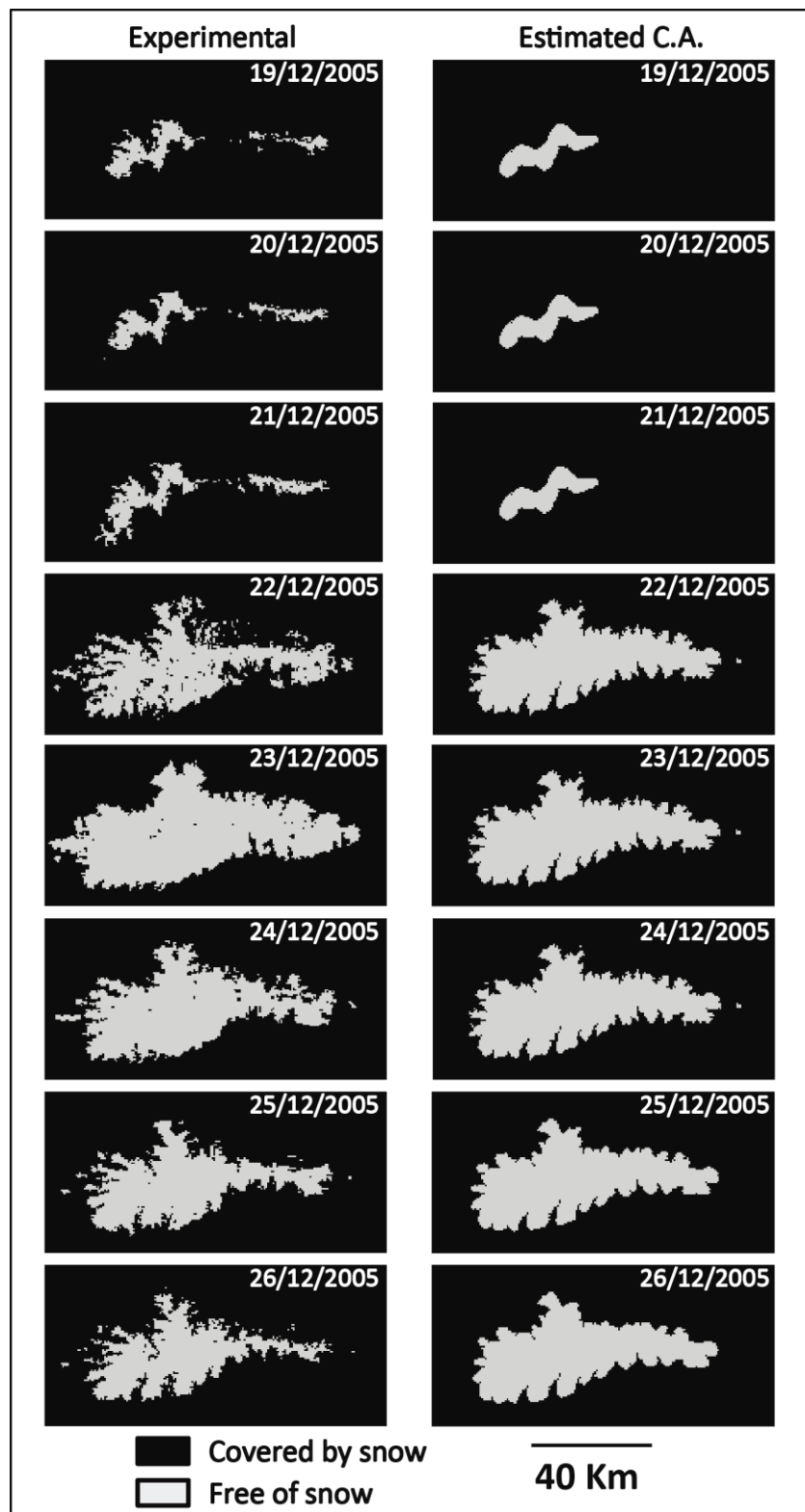


Figura 5.12. Spatial daily evolution of the experimental (left) and the estimated by the cellular automaton (right) from the 19th of December 2005 (top) to the 26th of December 2005 (bottom).

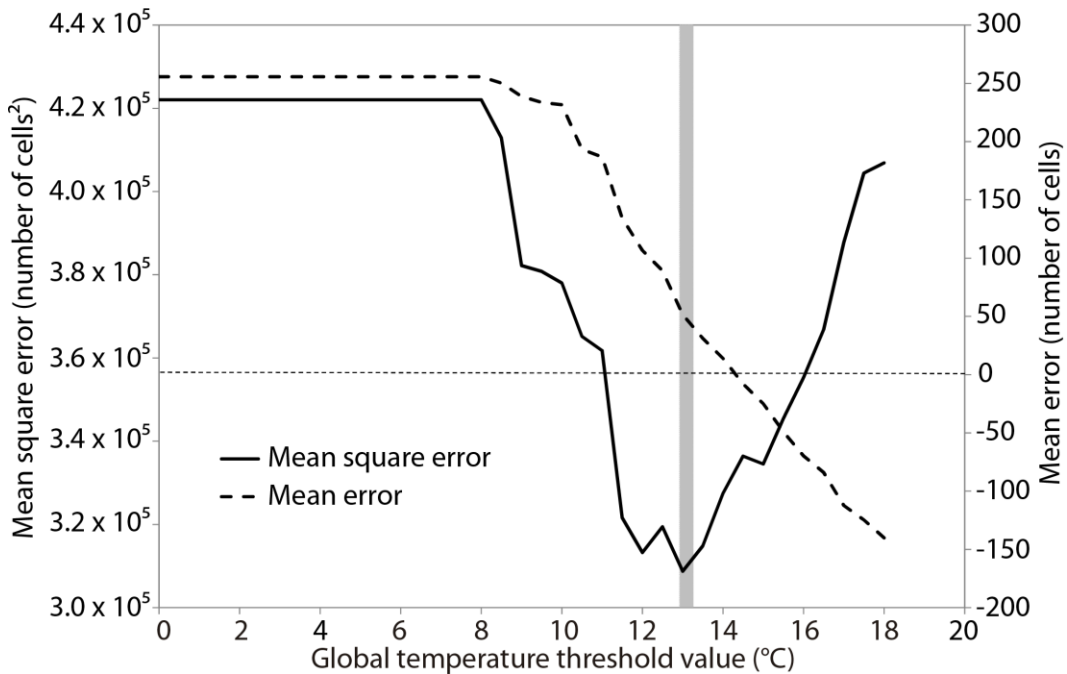


Figure 5.13. Mean square error (solid line) and mean error (dashed line) when the only varying parameter is the global temperature threshold T_{cc} while the rest of the parameters are hold at their optimal values. It may be seen how the lowest MSE is given by the value of 13 $^{\circ}\text{C}$ which gives also an acceptable ME.

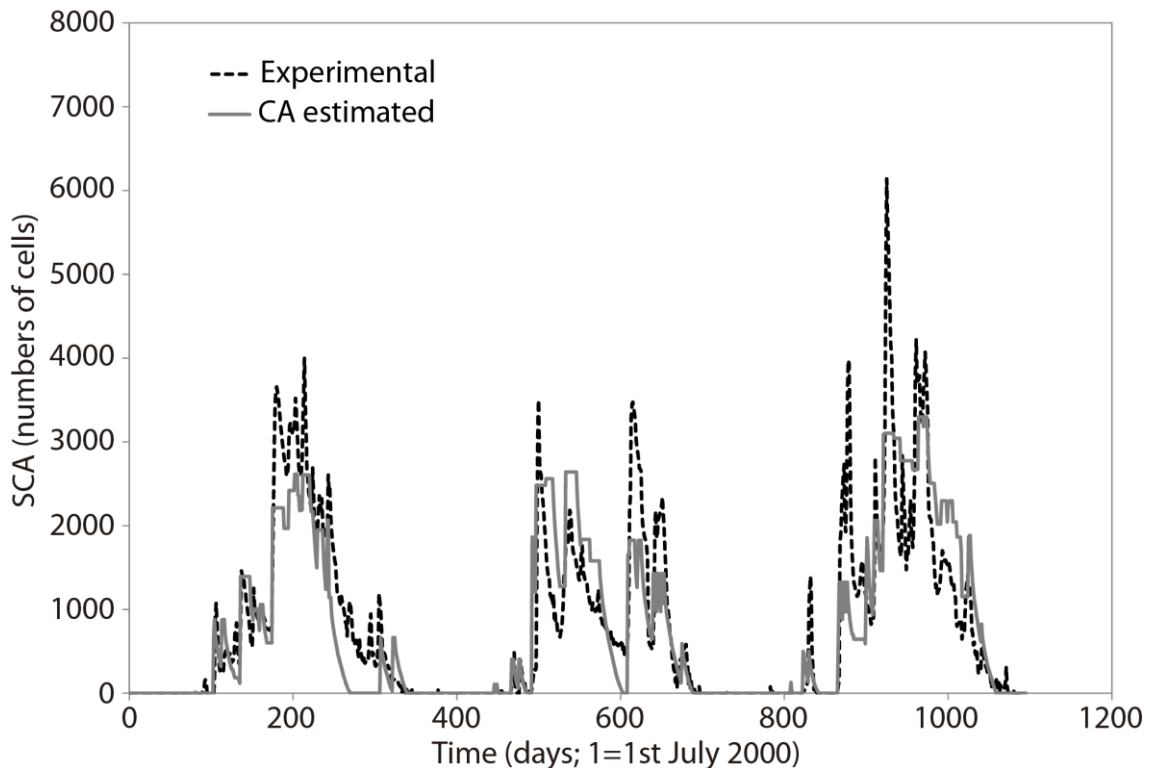


Figure 5.14. Experimental SCA and estimated SCA by the calibrated cellular automata model with the global criterion given in Equation (9).

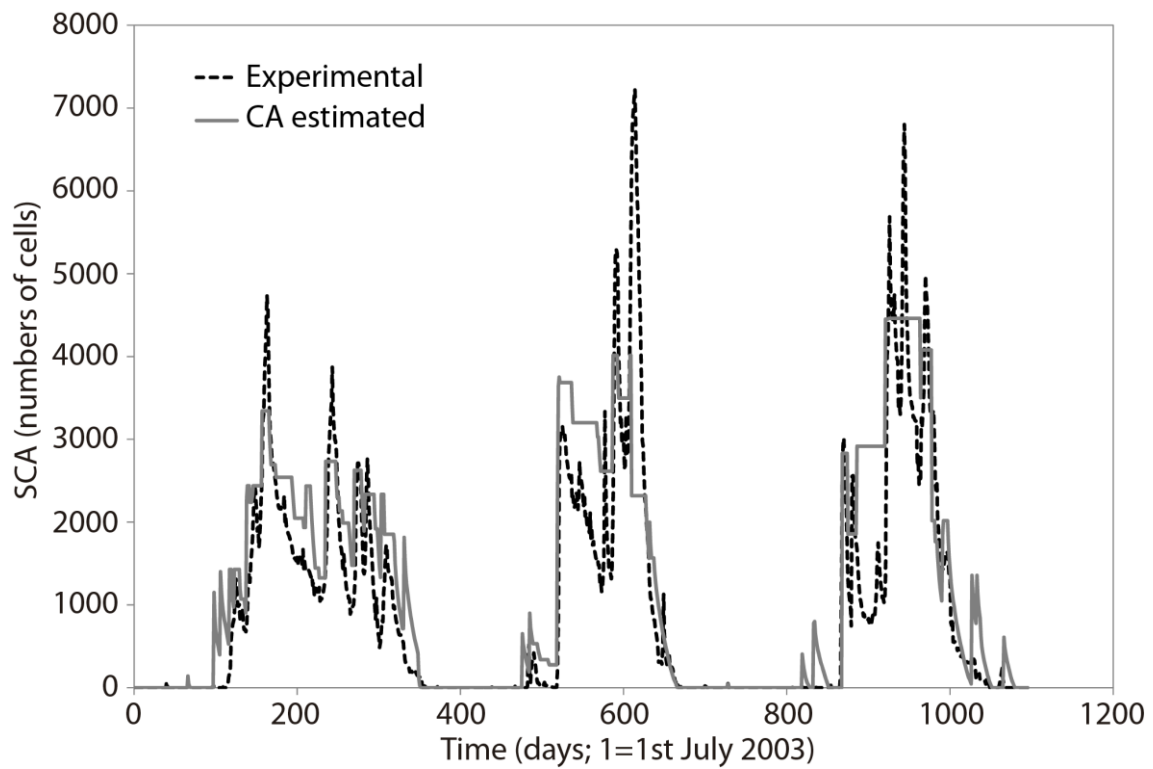


Figure 5.15. Experimental SCA and estimated SCA by the calibrated cellular automaton model with the global criterion given in Equation (9).

Chapter 6: An Integrated Statistical Method to Generate Potential Future Climate Scenarios to Analyse Droughts



Article

An Integrated Statistical Method to Generate Potential Future Climate Scenarios to Analyse Droughts

Antonio-Juan Collados-Lara ^{1,*}, David Pulido-Velazquez ^{1,3} and Eulogio Pardo-Igúzquiza ²

Antonio-Juan Collados-Lara ^(1,*), David Pulido-Velazquez ^(1, 3), Eulogio Pardo-Igúzquiza ⁽²⁾

(1) Instituto Geológico y Minero de España, Departamento de Investigación en Recursos Geológicos, Urb. Alcázar del Genil, 4. Edificio Zulema Bajo, 18006 Granada, Spain; d.pulido@igme.es

(2) Instituto Geológico y Minero de España, Departamento de Investigación en Recursos Geológicos, Ríos Rosas, 23, 28003 Madrid, Spain; e.pardo@igme.es

(3) Universidad Católica de Murcia, Departamento de Ingeniería Civil, Campus de los Jerónimos s/n, 30107 Guadalupe, Murcia, Spain.

* Correspondence: ajcollados@gmail.com

Abstract

The objective of this paper is to investigate different methods to generate future potential climatic scenarios at monthly scale considering meteorological droughts. We assume that more reliable scenarios would be generated by using regional climatic models (RCMs) and statistical correction techniques that produce better approximations to the historical basic and drought statistics. A multi-objective analysis is proposed to identify the inferior approaches. Different ensembles (equifeasible and non-equifeasible) solutions are analysed, identifying their pros and cons. A sensitivity analysis of the method to spatial scale is also performed. The proposed methodology is applied in an alpine basin, the Alto Genil (southern Spain). The method requires historical climatic information and simulations provided by multiple RCMs (9 RCMs are considered in the proposed application) for a future period, assuming a potential emission scenario. We generate future series by applying two conceptual approaches, bias correction and delta change, using five statistical transformation techniques for each. The application shows that the method allows improvement of the definition of local climate scenarios from the RCM simulation considering drought statistics. The sensitivity of the results to the applied approach is analysed.

Keywords: climate change; droughts analysis; statistical corrections; multi-objective analysis; ensemble of scenarios; Alto Genil catchment

1. Introduction

Water-scarce areas frequently suffer severe drought periods and their optimal operation is crucial for sustainable management of their water resources systems. Over the last thirty years, Europe has been affected by a series of major droughts: in 1976, 1989, 1991, and 2003 [1]. The drought of 2005 has been the most marked in the Iberian Peninsula. In addition, the latest studies on climate change expect significant decreases in resources in the Mediterranean river catchments, with significant environmental, economic, and social impacts [2]. In most of these areas, the problem will be exacerbated in the future, due to climate change [3], which is associated with an increment in the occurrence of extreme events [4].

In recent years, the number of studies assessing the impacts of climate change on droughts (through appropriate indices and techniques) in water resources systems [5,6], which is a major concern of climate change, has increased [7–9]. Some authors point out that the global climate models (GCMs) and regional climatic models (RCMs) are generally able to reproduce the observed pattern of droughts [10,11]. There are some works that directly use climate model simulations to assess droughts (e.g., [12,13]). However, other authors show cases where there is significant bias between the historical and modelled precipitation [14,15], which requires further analysis.

Future scenarios of climatic variables can be generated by applying statistical correction techniques to the output of physical climate models (control and future scenarios), taking into account the statistics of the historical series [16–18]. RCMs provide a dynamic approach, with a spatial resolution of tens of kilometres. They are nested with GCMs that have a coarser spatial resolution (hundreds of kms). In most cases, the statistics generated by these physical models show a significant bias with respect to the “real” values, and the application of appropriate correction techniques is required to analyse climate change impacts in these systems. There are several correction techniques with various degrees of complexity and accuracy: correction of first and second order moments, regression approach, quantile mapping (QM), etc. They can be applied assuming two different conceptual approaches: bias correction and delta change techniques [19,20]. The bias correction techniques apply a perturbation to the control series to obtain another one whose statistics are more similar to the historical ones. They assume that the bias between statistics of real data and model scenarios (control scenarios) will be maintained invariant, into the future (e.g., [21–24]). The delta change techniques assume that the RCMs provide an accurate assessment of the relative changes between the present and future statistics, but do not adequately assess their absolute values. They use the relative difference in the statistics of future and control simulations to create a perturbation in the historical series in accordance with these estimated changes (e.g., [25–27]).

When future scenarios are generated from RCMs nested to GCM, an important aspect to take into account is the assessment of uncertainties, which play a big role in the definition of future climate projections [28]. In order to reduce the modelling uncertainty, different RCM

simulations should be considered. On the other hand, the generation of potential future scenarios, based on a selection of the most reliable RCMs, could reduce the uncertainty of the future predictions, which would be important for the assessment of extreme events, such as droughts [29]. From individual climate change projections, different authors (e.g., [26,30]) have proposed defining ensemble scenarios, which coalesce and consolidate the results of individual climate projections, thus allowing for more robust climate projections that are more representative than those based on a single model [31].

In this study, we perform an analysis of several statistical approaches and RCMs, to generate future potential scenarios at a monthly scale, which is the usual timescale for the analysis of water resource management problems. We assess different solutions, taking into account basic and drought statistics of the historical series and the climatic model simulations. A multi-objective analysis is proposed to identify the inferior approaches. The elimination of the inferior approaches in the definition of ensemble scenarios would also help to reduce the uncertainties associated with the generation of scenarios. Different ensembles (equifeasible and non-equifeasible) solutions are analysed, identifying their pros and cons. A sensitivity analysis of the method to the spatial resolution employed in the assessment is also performed. The proposed methodology is applied to the Alto Genil Basin (southern Spain).

The paper is structured as follows. In Section 2, we describe the methodology, which includes the sequential application of different statistical techniques (correction techniques; multi-objective analysis, and predictions of ensembles). Section 3 describes the case study and available data, including historical and climatic simulations. Section 4 includes the results and the discussion, Section 5 presents limitations of this study and, finally, Section 6 summarises the main conclusions.

2. Method

The steps of the proposed methodology to generate potential monthly future climate scenarios (precipitation and temperature) are represented in Figure 6.1. This includes the analysis of data and generation of future individual projections, a multi-objective analysis to identify inferior models, and different ensembles of predictions (described in Sections 2.1, 2.2, and 2.3, respectively).

2.1. Generation of Future Individual Projections

An analysis of historical data and RCM simulations allows for identifying the necessity of applying statistical correction techniques to generate future scenarios. These techniques can be employed under two different approaches:

- (1) For each RCM model, we can represent the differences between the statistics (basic and drought statistics) of the control scenarios simulations and the “historical” values. These usually reveal significant bias, which justifies correcting them. The set of techniques to address this issue are known as bias correction approaches, since they apply a perturbation to the control series with the aim of forcing some of their statistics to get closer to the historical ones. In order to generate future series, they assume that the bias

between the statistics of real data and model scenarios (control scenarios) will remain invariant into the future (e.g., [22,32]).

- (2) We can also represent and analyse the relative differences between control and future scenario statistics for the climatic model simulation for specific emission scenarios. Based on this information, future scenarios can be also generated by assuming that the RCMs provide accurate assessment of the relative changes in the statistics between present and future scenarios, but that they do not adequately assess the absolute values. These approaches, known as delta change solutions, use the relative difference in the statistics of control and future simulations to create a perturbation in the historical series, in accordance with these estimated changes (e.g., [25–27]).

Both approaches, bias correction and delta change, use the same time series (historical and control and future simulation from RCMs) to generate future climatic scenarios. In the bias correction approach, a transformation function is calibrated to modify the RCM control series, in order to obtain a corrected one whose statistics are similar to the historical ones. The calibrated correction function is applied to the future RCM simulation series to generate potential future scenarios. In the delta change approach, the transformation function is defined, taking into account the difference between future and control RCM simulations. They assume that the changes described by these transformation functions can be applied directly to the historical series to obtain potential future series. For both conceptual approaches, bias correction models and delta change solutions, we intend to test several statistical techniques with various degrees of complexity and accuracy that intend to preserve different statistics: correction of first- and second-order moments, regression approach, and QM, which are described below.

In the first-moment correction techniques, the transformation function only intends to provide a good approximation to the mean values. It is the simplest correction technique and has been extensively used for delta change [33] and bias correction [34] approaches. The second-moment correction technique is focused on the approximation of the mean and standard deviation to define the transformation function. We will apply the transformation function proposed by Pulido-Velazquez et al. [25]. The regression technique defines the transformation function by adjusting a regression function. Usually, a linear function can provide reliable results in the adjustment. This technique has been extensively applied using the bias correction approach (e.g., [35,36]). The QM is another correction technique commonly employed. The transformation is elaborated using the cumulative distribution function of the series. In this study, we will consider two QM techniques [37]: the distribution-derived transformations and empirical quantiles. The two techniques were applied using the qmap package developed by Gudmundsson et al. [37]. We will use the Bernoulli–gamma distribution to adjust precipitation data and the normal distribution for temperature series. The cumulative distribution function is approximated using tables of empirical percentiles, while values between the percentiles are approximated using linear interpolation in the case of empirical quantiles. Table 6.1 shows a brief summary of advantages and disadvantages of each correction technique.

In the bias correction approaches, a correction function will be calibrated to modify the control series to make the statistics of the new corrected series equal or similar to the historical ones. Since the bias correction is focused on the statistics of the series, we need to use long-enough historical and control series with invariant statistics, in order to be representative of the system climate. In cases in which these historical series can be divided into two long-enough series, one should be employed for the calibration and the other for the validation. It can be achieved through a “traditional split sample test” or a “differential split sample test” [38]. The first has earlier been used to evaluate bias correction methods for stationary conditions [39,40], while the second is used for non-stationary conditions [41]. If the series are not long enough, they might include drought or wet periods that modify the statistics of the series, making them not representative of the climate. In those cases, we need to assume the hypotheses of climate stationarity, the statistic of the representative series being invariant. In this case, the validation is not possible, and we need to assume that those inferiors in calibration would also be inferiors in a hypothetical validation. The adopted calibrated bias model will be applied to the future series to generate the corrected future scenarios.

We also analyse the statistics of the corrected series (corrected control and corrected future in the bias correction approach and future series generated by perturbation of the historical series in the delta change approach) in order to discuss and draw conclusions about the pros and cons of each statistical technique applied under different conceptual approaches.

We analyse not only classic but also drought statistics (duration, magnitude, and intensity) [42,43]. The Standard Precipitation index (SPI) was adopted to perform the drought analysis [44,45]. From the SPI series, the statistics were obtained by applying run theory [46,47]. Note that the probability of occurrence of precipitation for the SPI calculation, in the control and future simulations, was obtained using parameters calibrated from the observed series, in order to perform an appropriate comparison [9].

2.2. Multi-Objective Analysis of the Main Statistics (Basic and Drought Statistics)

A multi-objective analysis based on the goodness-of-fit to some statistics is proposed to identify the approaches that provide more reliable approximations to basic (mean, standard deviation, and asymmetry coefficient) and drought statistics (duration, magnitude, and intensity). The criteria employed to identify the inferior approaches is the next one: An approach is inferior if any other approach provides approximations significantly better for all the cited statistics (basic and drought statistics). In this analysis of the goodness-of-fit, we do not provide a higher relevance to any of the selected statistics. A homogeneous criteria (threshold) has been adopted to consider an approach significantly better than others with respect to a specific statistic. It is defined by a maximum value of the relative difference with respect to the historical statistic. This maximum threshold will be discussed in the application to the case study.

It allows discrimination of the inferior RCMs (in delta change solutions) and combinations of RCM models and correction techniques (in bias correction approaches). Note that in bias

correction approaches, each technique generates a corrected control simulation, whose statistics can be compared with the historical ones, and, therefore, the goodness-of-fit for each technique can be assessed. However, delta change approaches do not generate corrected control series and the goodness-of-fit with respect to the historical statistics can only be assessed for the RCMs and not for the correction techniques.

A multi-objective analysis, somewhat similar to the one proposed here, was performed in an earlier study of an aquifer, but it was focused only on basic statistics (mean, standard deviation, and asymmetry coefficient) [26] of “delta change” solutions for two different corrections (first and second moment corrections). It aimed to identify reliable RCM models in terms of goodness-of-fit for the first and second statistics of the control scenario simulations of the historical data. The inferior RCM models (in terms of goodness-of-fit) were identified (“dominated solutions”, using the terminology of multiple-objective analysis) and eliminated. In this way, a model is eliminated if any other RCM model provides a more accurate approximation for all the cited historical statistics. In the present study, we propose a more general and complete multi-objective analysis, in which drought statistics (duration, magnitude, and intensity) are also included in the selection objective.

The application is also extended to consider bias correction approaches. This allows us to identify the best combination of RCM models and bias correction technique, in terms of the goodness-of-fit of the corrected control scenarios to the main statistics of the historical data. These multi-objective analyses should be performed in accordance with the results obtained when validating the correction model. Nevertheless, if the information cannot be divided into two long-enough series representative of the climate whose statistics are nearly invariant, we cannot perform, explicitly, a validation of the correction model. In these cases, assuming that the statistics of any long-enough period remain invariant, the calibration implicitly could be considered validated, due to the fact that the same results would be obtained under this hypothesis for any other period representatives of the climate conditions. Therefore, in these cases, the results of the calibration periods should be used to perform the multi-objective analyses.

2.3. Ensembles of Predictions to Define More Representative Future Climate Scenarios

We will study different options to define ensemble of potential future series from the results obtained in the multi-objective analysis. Some authors suggest that the ensembles of predictions produce more robust climate projections than those based on a single model [31]. We compare equifeasible solutions (considering all the RCMs simulations) and non-equifeasible solutions (considering only those RCMs, or combination of RCMs and techniques that are not inferior according to the multi-objective analysis).

Two ensemble scenarios were defined by combining, as equifeasible members, all the future series (that correspond to different RCMs simulations) generated by applying delta change (scenario E1) or bias correction (scenario E2) approaches. Note that, in the equifeasible ensembles, the number of members employed to define the future scenarios can be obtained by multiplying the number of RCMs and the number of techniques. Two other options were defined by combining only the uneliminated models (E3) (in delta change approach) or the

uneliminated combinations of models and correction techniques (E4) (bias correction techniques), assuming that we do not trust the eliminated ones. As we already commented on in the previous section, in the delta change approaches, we eliminate RCM simulations, instead of series obtained by the combinations of RCM and correction technique. Therefore, when we eliminate an RCM simulation, we remove all the series generated with this RCM by applying different correction techniques. This will allow us to perform a sensitivity analysis of the goodness-of-fit of the future ensemble scenarios generated with or without any previous selection. From a methodological point of view, the proposed ensembles (E3 and E4) defined with the uneliminated models are based exclusively in those that provide better approximations of both basic and drought statistics.

The sensitivity of the solutions to the spatial scale has been also analysed for the selected case study. The Alto Genil Basin (southern Spain) extends over a wide range of altitudes and may, therefore, produce greater spatial variability with respect to the impacts of climate change on precipitation [48]. The distributed approaches are defined by applying the correction techniques (Section 2.1) to generate the future series in each cell by using the historical and RCM series available for the cell. The multi-objective analyses (Section 2.2) in the distributed approaches is defined by using, for each statistic, the weighted average for all the cells in the domain (taking into account the surface area of each) of the square relative differences, with respect to the historical one. The final ensemble of predictions obtained for the distributed approaches (Section 2.3) allows us to analyse the spatial heterogeneity of the climate change impacts. We will also analyse the sensitivity of the overall results obtained at catchment scale from using a lumped or a distributed procedure.

3. Study Area: Description and Available Data

3.1. Location and Description of the Alto Genil Basin

The study basin has an area of 2596 km², and it is situated in the south of Spain (see Figure 6.2). The basin varies substantially in elevation, from 528 m to 3471 m. The main river of the basin is the river Genil, which is the most important in the province of Granada, and one of the most important in Andalusia. The main contributions to the river come from Sierra Nevada Mountains in the melt season. The spatial resolution applied to perform a distributed approach is defined by the grid represented in Figure 6.2, in which the cell size is 12.5 km.

3.2. Historical Climate Data

We used historical data provided by the Spain02 project [49,50] for the period 1971–2000. It includes daily temperature and precipitation estimates from observations (around 2500 quality-control stations) of the Spanish Meteorological Agency. An assessment of the validation of some Spanish datasets (including Spain02) was recently made by Quintana-Seguí et al. [51]. We used version 4 (v4) of the Spain02 project dataset (<http://www.meteo.unican.es/en/datasets/spain02>). The project uses the same grid as the EURO-CORDEX project [52] (see Figure 6.2) with a spatial resolution of 0.11° (approximately 12.5 km). The Spain02 dataset has already been employed in many research studies [53,54]. Figure 6.3 shows the lumped historical monthly temperature and precipitation

for the catchment and the distributed mean temperature and precipitation. The areas of higher elevation (see Figure 6.2) produce higher precipitation and lower temperatures.

3.3. Climate Model Simulation Data. Control and Future Scenarios

The most pessimistic emission scenario of the CORDEX project [52] was considered (RCP8.5). For this scenario, we analysed nine climate-change scenarios corresponding to four different GCMs. To assess potential future climate scenarios (for the period 2071–2100) we used the output series (control and future simulations available from the CORDEX EU Project) from five RCMs (CCLM4-8-17, RCA4, HIRHAM5, RACMO22E, and WRF331F) nested inside each of the GCMs considered. The RCM simulations considered are summarised in Table 6.2.

In order to show the bias between historical data and the control simulation, Figure 6.4 shows the monthly mean and standard deviation of the historical and control series from RCMs (precipitation and temperature) for the mean year in the reference period (1971–2000). All RCMs show significant biases with historical data for the basic statistics. The mean relative differences in precipitation are significant (54% for the mean and 36% for the standard deviation). They are lower, though also significant, for temperature (22% for the mean and 11% for the standard deviation). Figure 6.5 shows the drought statistics of the historical and control series of the RCM in the reference period (1971–2000). The RCM drought statistics also show significant biases with historical data.

Significant bias in the basic (Figure 6.4) and drought (Figure 6.5) statistics, also pointed out by several authors in different case studies [3,23], forces us to apply a correction technique to generate future scenarios (see Section 2.1). These techniques use the relative changes between the control and future simulation to perturb the historical series, in order to generate future climatic series. Figure 6.6 shows the relative monthly change between mean and standard deviation of the future (2071–2100) and control (1971–2000) series (precipitation and temperature) for each RCM. This information is used directly in the delta change approach to generate the future series. However, the bias correction approach, as commented in Section 2.1, uses the changes between the historical and the control simulations. The mean relative changes in mean temperature and mean precipitation predicted by the different RCMs were –27% and 1.5%, and the mean relative changes in the standard deviation of temperature and precipitation were –9% and 16%, respectively.

4. Results and Discussion

4.1. Application of Different Correction Techniques

In order to apply statistical techniques to generate future scenarios, we assume that our 30-year period of historical data is long enough to summarise the climate conditions in our system, being similar to those obtained with any other previous historical time series. However, if we split this period in two series, the statistics of these two periods are significantly different, and we cannot perform an explicit calibration and validation of the representative climate statistics with these data. For this reason, we have used the statistics of

the calibration period to assess the combinations of correction technique—RCMs under the bias correction approach and RCMs under the delta change approach, instead of using a “split sample test”.

Different correction techniques under the two considered approaches (bias correction and delta change) have been applied to the nine RCMs considered. In this section, we only present results for one of them. The results concerning all the RCMs are presented in Sections 4.2 (multi-objective analysis) and 4.3 (ensembles of scenarios).

In the bias correction approach, we correct the control simulation in order to assess what combination of RCM technique provides the smallest difference compared to the historical data. If we focus on the mean, all the techniques provide accurate results. Figure 6.7 shows the control simulation, the corrected control simulation generated with each correction technique, and the historical data for the lumped approaches obtained for one of the nine RCMs used (HIRHAM5 RCM model nested in the EC-EARTH GCM).

The corrected control simulations for all the techniques considered reproduce, almost exactly, the monthly means of the historical data. For precipitation, there are very small differences in means for some months because the correction procedure may produce some values lower than zero, which have to be moved to zero to have physical meaning. This has been pointed out in earlier work (e.g., [25]). In terms of standard deviation, most of the techniques provide accurate results for temperature and acceptable results for precipitation, except for the first-moment correction, which maintains the same standard deviation as the control simulation. In the precipitation case, the results are not as accurate as in the temperature case because the correction procedure produces values lower than zero, which are moved to zero. For the asymmetry coefficient, QM using empirical quantiles provides the most accurate results. QM using empirical quantiles corrects this statistic, and using parametric distribution provides acceptable results. Again, these conclusions cannot be fully affirmed. With respect to the drought statistics (presented in Figure 6.8) for lumped approaches obtained using the HIRHAM5 RCM model nested in the EC-EARTH GCM, they still show important bias with respect to the historical droughts. As commented on in Section 1, several authors have previously pointed out that, in some cases, RCMs are not capable of reproducing the drought statistics of the observed series [14,15]. All the bias techniques provide considerable improvement in the drought statistic. However, since we are not proposing bias correction techniques that specifically correct drought statistics, we still have significant biases (see Figure 6.8). Nevertheless, we will apply a multi-objective analysis in order to eliminate, in the definition of potential future scenarios, the approaches that provide inferior approximations in terms of goodness-of-fit to the cited statistics.

The basic and drought statistics of the future series generated (obtained using the HIRHAM5 RCM model nested in the EC-EARTH GCM) by the five correction techniques considered under the two approaches (bias correction and delta change) can be observed in Figures 6.9 and 6.10, respectively. All of the generated future series provide similar monthly means, especially for temperature. First-moment correction provides the same means for the two approaches, although the generated series are different. The same happens with the second-

moment correction regarding the mean and standard deviation. However, the generated series show reduced precipitation and higher temperature for all techniques and approaches. The drought analysis indicates a significant increase in duration, magnitude, and intensity of droughts (see Figure 6.10).

Figure 6.10 shows some SPI values lower than -4 , which are too small, even for the Mediterranean area impacted by the extreme climate changes. In other studies, these values are commonly considered as outliers. Why do we obtain such small values? We should take into account that they are obtained from the simulation with a single specific RCM model in a long-term future horizon (2071–2100) under the most pessimistic emission scenario (RCP 8.5). On the other hand, we should also take into account that the probability of occurrence of precipitation for the SPI calculation, in the control and future simulations, was obtained using parameters calibrated from the observed series, in order to perform an appropriate comparison [9]. Nevertheless, these results show that, using a single model, we could obtain some “strange” values. For this reason, we recommend performing the analyses of potential future scenarios considering several RCMs and correction techniques. In order to reduce the uncertainty due to the RCM employed, many authors recommend using an ensemble of several approaches coming from different RCM models. In our methodology, we also propose the analyses of different ensemble solutions, which would be described for our case study in the next subsections, where we will see if we still obtain values smaller than -4 .

4.2. Multi-Objective Analysis of Basic and Drought Statistics

A multi-objective analysis taking into account basic statistics (mean, standard deviation, and asymmetry coefficient) and drought statistics (duration, magnitude, and intensity) has been performed in accordance with the methodology explained in Section 2.2. Since most of the combinations of model and bias correction technique provide accurate approximations to the first and second moments, a relative error threshold was defined for each statistic to define, as inferior approaches, only those whose corrected control is significantly worse. This threshold allows us to assume certain differences in some statistics as not significant. For a given statistic, we assumed that, when the relative difference of the estimated corrected control to the historical ones is smaller than 3%, the approach is labelled accurate enough, and not considered inferior to other approaches that provide slightly better estimates. If we do not apply this threshold to the analyses of bias correction approaches, a technique producing very reliable results for certain statistics, but poor results in the others, could not be eliminated by other techniques, with reliable results in all the statistics.

Table 6.3 shows the eliminated (inferior models in terms of goodness-of-fit) and uneliminated models for the delta change approaches for the lumped and distributed cases. As described in Section 2, the lumped approaches are derived from single series for the whole case study, while the distributed approaches are defined by applying the correction techniques in each cell by using the historical and RCM series available for the cell. In these distributed approaches, the multi-objective analyses is defined by using, for each statistic, the weighted average (taking into account the surface area of each) for all the cells in the domain of the square relative differences, with respect to the historical one. In the lumped case only, the RCM

RCA4 nested with the GCM MPI-ESM-LR provides results inferiors to the others. In the distributed case, two models are inferior (HIRHAM5 nested to EC-EARTH and RCA4 nested to EC-EARTH). On the other hand, the multi-objective analysis allows us to identify the inferior combinations of RCM and correction technique in the bias correction approach. Table 6.4 shows the eliminated and uneliminated combinations of models and correction technique for the bias correction approach. The approaches obtained with the first-moment correction technique are eliminated independently of the RCM employed. The approaches coming from the model RCA4, nested to EC-EARTH, are removed independently of the correction technique employed. The data presented in Table 6.4 were used to elaborate Figure 6.11. It shows the number of times that the approaches defined with each technique or RCM are not eliminated in the multi-objective analysis under the bias correction approach. The first-moment correction technique, which is the most basic one, is always eliminated. Although it provides very accurate results in terms of the mean, its bias regarding other statistics is quite high. These simple first-moment correction approaches were also identified by other authors as the less accurate solutions [27]. The approaches obtained by regression and QM empirical quantile techniques show better agreement between historical and corrected control statistics (see Figures 6.7 and 6.8), and yield a greater number of uneliminated approaches. Regarding RCMs, CCLM4-8-17 (MPI-ESM-LR) and HIRHAM5 (EC-EARTH) are the most participative models in the ensembles, though the other models have considerable participation, with the exception of RCA4 (MPI-ESM-LR) and RACMO22E (EC-EARTH).

In general, the sensitivity of the multi-objective analyses, with respect to using distributed approaches instead of lumped ones, depends on the model and the applied correction technique. Figure 6.11 shows that the results are not sensitive for the approaches obtained from the models MPI-ESM-LR nested to CCLM4-8-17, and IPSL-CM5A-MR nested to WRF331F. On the other hand, the approaches obtained with the correction technique “QM empirical quantile” are the only ones that are not sensitive. In general, the distributed approaches are eliminated a higher number of times than the lumped approaches, which makes sense, due to the higher complexity that supposes to fulfil the different objectives with distributed approaches.

4.3. Ensembles of Predictions to Define More Representative Future Climate Scenarios

We considered four options to define the most representative future scenarios by applying different ensembles of potential scenarios deduced from the available climate models. Two ensemble scenarios were considered by combining all future series (under different RCMs simulations and correction techniques) generated by delta change (E1) or bias correction (E2). This combination was done as equifeasible members. From the multi-objective analysis, two other combinations were defined using only the uneliminated models (E3) (in delta change approach) or the uneliminated combinations of models and correction techniques (E4) (in bias correction approach), assuming that we do not trust the eliminated ones.

In terms of future temperature statistics, the ensemble scenarios defined with the lumped approach (Figure 6.12) show practically the same increment in monthly means. The standard

deviation estimated using delta change approaches are quite similar to the historical, but both ensembles defined by applying bias correction show significantly lower values.

In terms of future precipitation statistics, almost the same reduction in future mean values are predicted by all the ensembles for every month (Figure 6.12). The standard deviation of the future precipitation predicted using the delta change approaches are more similar to the historical (as for temperature variable) than those defined by applying bias correction, whose values are significantly lower. The scenarios under the same approach provide very similar statistics.

The future ensemble precipitation scenarios were analysed in terms of drought statistics (Figure 6.13). All four ensembles predict considerable increases in length, magnitude, and intensity of droughts as others authors pointed out for different Mediterranean zones [8,9]. Note that, although for a specific RCM model (Figure 6.10) we obtained some “strange” SPI values, smaller than -4 (see Section 4.1), which are usually considered as outliers, we do not obtain values smaller than -4 for any the considered ensemble scenarios in our case study. In our case study, the sensitivity of the ensemble scenarios to the multi-objective selection is low, but some differences are observed. The statistics are relatively similar in pairs considering the bias correction approach (E2 and E4 ensembles) and delta change approach (E1 and E3 ensembles). For example, for the threshold -0.84 SPI, the statistic with higher changes between the two bias correction scenarios (E2 and E4) is the magnitude with a relative change equal to 24.6% . For the two delta change ensembles (E1 and E3) the statistic with higher changes is the length with a relative change of 1.5% . Nevertheless, the results are more sensitive to the selection of bias correction or delta change approaches. The delta change approach produces more extreme droughts, reaching intensity values of around -4 SPI, while the bias correction approach does not produce droughts with SPIs higher than -2.9 (similar to the maximum historical intensity).

Nevertheless, an important con of using these ensemble scenarios, instead of multiple single projections, is that we lose information about future climate uncertainties and their potential propagation.

4.4. Sensitivity of Results to Spatial Scale

The results were also obtained in a distributed way. Figure 6.14 shows the spatial heterogeneity of the climate change impacts on precipitation and temperature obtained using the distributed approaches. It shows, in accordance with previous work [55], that significantly greater changes are predicted at higher altitude.

We also analysed the sensitivity of the overall results at the catchment scale calculated using the lumped or distributed procedures. Table 6.5 shows the mean reduction in precipitation and the overall mean rise in temperature for the four scenarios considered.

Changes in temperature are more homogeneous than in precipitation. The largest difference between the distributed and lumped cases is 1.50% for temperature in scenario E4, and 1.35% for precipitation in scenario E2. Changes in the overall mean between the various future

ensemble scenarios with respect to mean historical data are small. Figure 6.15 shows the monthly mean relative change of the lumped case compared to the distributed case in an average year, in terms of mean and standard deviation.

The equifeasible ensembles (E1 and E2) yields the relative changes closest to zero. The maximum relative changes for the E1 scenario are -4.12% , 0.41% , -4.07% , and 0.64% for mean precipitation, mean temperature, standard deviation of precipitation, and standard deviation of temperature, respectively. For the E2 scenario, the corresponding values are -4.25% , -1.16% , -5.64% , and -3.97% . Therefore, considering an equifeasible ensemble, the differences between the lumped and distributed cases can be considered insignificant. However, in the multi-objective ensemble, these differences are considerable, since the uneliminated models and techniques are different (see Tables 6.3 and 6.4). The maximum relative changes for the E3 scenario are 12.43% , 1.06% , 15.98% , and -3.21% for mean precipitation, mean temperature, standard deviation of precipitation, and standard deviation of temperature, respectively. The corresponding values for the E4 scenario are 11.63% , -2.33% , -28.17% , and -23.70% .

5. Limitations and Future Research Works

This work is focused on the assessment of potential future scenarios of climate change, taking into account drought statistics. From a methodological point of view, the proposed approach is an important step to define scenarios in a systematic and coherent way, taking into account meteorological drought statistics. On the other hand, the proposed statistical correction of precipitation and temperature does not preserve the energy balance when modifying the results from the RCM simulation, which could have some drawbacks as other authors previously pointed out. They reduce the uncertainty of simulations without providing a satisfactory physical justification, which can reduce the advantages of RCMs [56]. On other hand, the reduction of uncertainty could not have importance when the hydrological models have their own sources of uncertainty [57]. Nevertheless, the benefit of these new scenarios when propagating meteorological droughts to hydrological, agricultural, and operational drought have not been assessed yet. More research is required to study their propagation by using hydrological, agronomical, and management models.

In the application performed, the available data are not long enough to perform, explicitly, a calibration and a validation of the model. This work shows how to proceed in these cases, assuming stationarity of the series for an implicit validation of the model. Nevertheless, in the future, it should be also interesting to test other cases where long-enough information allows for performing an explicit validation of the model.

The proposed methodology is applied to the Alto Genil Basin (southern Spain), but could be extended to other basins in different climatic regimes and with longer periods of data, in order to draw more general conclusions.

6. Conclusions

In this research study, we propose a novel method to generate future potential climate scenarios to analyse meteorological droughts. It is based on a non-equifeasible ensemble of scenarios generated by correcting RCMs (using bias correction and delta change approaches), giving more weight to solutions that provide better approximations of the historical statistics identified in multi-objective analyses. We intend to provide consistent pictures of plausible future monthly scenarios, taking into account basic statistics (mean, standard deviation, and asymmetry coefficient) and drought statistics (duration, magnitude, and intensity) of the historical series and climatic model simulations. The drought statistics are obtained by applying run theory to the associated SPI series.

An appropriate approximation of these statistics may significantly influence the analysis of climate change impacts. A detailed analysis of the results obtained combining different hypotheses (correction techniques, conceptual approaches, equifeasible or non-equifeasible ensemble, spatial resolution) was performed for the Alto Genil Catchment.

All the RCMs considered in this study show important bias between control simulation series and historical series, in terms of basic and drought statistics. The correction techniques analysed in this work considerably reduce this bias. With the exception of the mean values, the statistics (basic and drought) of the generated scenarios are quite sensitive to the conceptual approach assumed for the correction (bias correction or delta change). If we only use a single model to generate the potential future scenarios, we might obtain some “strange” results (for example, SPI values smaller than -4) which do not appear when we use an ensemble of approaches based on different models. In order to reduce the uncertainty due to the RCM employed, several approaches coming from different RCM models should be considered. We propose the analyses of different equifeasible and non-equifeasible ensemble solutions based on a multi-objective analysis.

A multi-objective analysis based on the goodness-of-fit to some statistics is proposed to identify the approaches that provide more reliable approximations to basic (mean, standard deviation, and asymmetry coefficient) and drought statistics (duration, magnitude, and intensity). It allows discrimination of the inferior RCMs (in delta change solutions) and combinations of RCM models and correction techniques (in bias correction approaches). The approaches obtained with the first-moment correction technique, which is the most basic one, are always eliminated. Although it provides very accurate results in terms of the mean, its bias regarding other statistics is quite high. The approaches obtained by regression and QM empirical quantile techniques show better agreement between historical and corrected control statistics, and yield a greater number of uneliminated approaches.

In our application, we also conclude that the sensitivity to the hypothesis assumed to define the ensembles (equifeasible or non-equifeasible) is higher in the bias correction approach. Spatial heterogeneity of the climate change impacts on precipitation is high in our case study. Significantly greater changes are predicted in higher altitude areas. Nevertheless, the sensitivity of the overall results at catchment scale, obtained by applying lumped or distributed procedures to perform the calculations, is quite low. The four ensembles of

projections for the future horizon 2071–2100 under the emission scenario RCP 8.5, show considerable increases in length, magnitude, and intensity of droughts. The average changes predicted using the four ensembles of scenarios for precipitation and temperature are quite similar for lumped and distributed cases. They are around –27% in precipitation and +32% in temperature.

Author Contributions: D.P.-V. and E.P.-I. conceived and designed the research; A.-J.C.-L. analysed the data and conducted the experiments. All authors contributed to writing the manuscript.

Acknowledgments

We would like to thank the Spain02 and CORDEX projects for the data provided for this study and the R package qmap. This research was partially funded by the GeoE.171.008-TACTIC project from GeoERA organization funded by European Union's Horizon 2020 research and innovation program. It has been also partially funded by the PMAFI/06/14 project with UCAM funds.

Conflicts of Interest: The authors declare no conflict of interest.

References

1. Feyen, L.; Dankers, R. Impact of global warming on streamflow drought in Europe. *J. Geophys. Res.* 2009, **114**, D17116, doi:10.1029/2008JD011438.
2. Iglesias, A.; Garrote, L.; Flores, F.; Moneo, M. Challenges to manage the risk of water scarcity and climate change in the Mediterranean. *Water Resour. Manag.* 2007, **21**, 227–288, doi:10.1007/s11269-006-9111-6.
3. Blenkinsop, S.; Fowler, H.J. Changes in drought characteristics for Europe projected by the PRUDENCE regional climate models. *Int. J. Climatol.* 2007, **27**, 1595–1610, doi:10.1002/joc.1538.
4. Skaugen, T.; Astrup, M.; Roald, L.A.; Førland, E. Scenarios of extreme daily precipitation for Norway under climate change. *Hydrol. Res.* 2004, **35**, 1–13.
5. Mishra, A.K.; Singh, V.P. A review of drought concepts. *J. Hydrol.* 2010, **391**, 202–216, doi:10.1016/j.jhydrol.2010.07.012.
6. Mishra, A.K.; Singh, V.P. Drought modeling—A review. *J. Hydrol.* 2011, **403**, 157–175, doi:10.1016/j.jhydrol.2011.03.049.
7. Pedro-Monzonís, M.; Solera, A.; Ferrer, J.; Estrela, T.; Paredes-Arquiola, J. A review of water scarcity and drought indexes in water resources planning and management. *J. Hydrol.* 2015, **52**, 482–493, doi:10.1016/j.jhydrol.2015.05.003.

8. Lopez-Nicolas, A.; Pulido-Velazquez, M.; Macian-Sorribes, H. Economic risk assessment of drought impacts on irrigated agriculture. *J. Hydrol.* 2017, *550*, 580–589, doi:10.1016/j.jhydrol.2017.05.004.
9. Marcos-Garcia, P.; Lopez-Nicolas, A.; Pulido-Velazquez, M. Combined use of relative drought indices to analyze climate change impact on meteorological and hydrological droughts in a Mediterranean basin. *J. Hydrol.* 2017, *554*, 292–305, doi:10.1016/j.jhydrol.2017.09.028.
10. Herweijer, C.; Seager, R.; Cook, E. North American droughts of the mid to late nineteenth century: A history, simulation and implication for Mediaeval drought. *Holocene* 2006, *16*, 159–171, doi:10.1191/0959683606hl917rp.
11. Seager, R.; Kushnir, Y.; Herweijer, C.; Naik, N.; Velez, J. Modeling of tropical forcing of persistent droughts and pluvials over western North America: 1856–2000. *J. Clim.* 2005, *18*, 4065–4088, doi:10.1175/JCLI3522.1.
12. Lloyd-Hughes, B.; Shaffrey, L.C.; Vidale, P.L.; Arnell, N.W. An evaluation of the spatiotemporal structure of large-scale European drought within the HiGEM climate model. *Int. J. Climatol.* 2013, *33*, 2024–2035, doi:10.1002/joc.3570.
13. Zhang, X.; Tang, Q.; Liu, X.; Leng, G.; Li, Z. Soil moisture drought monitoring and forecasting using satellite and climate model data over Southwest China. *J. Hydrometeorol.* 2017, *18*, 5–23, doi:10.1175/JHM-D-16-004.
14. Cook, B.; Miller, R.; Seager, R. Dust and sea surface temperature forcing of the 1930s “Dust Bowl” drought. *Geophys. Res. Lett.* 2008, *35*, L08710, doi:10.1029/2008GL033486.
15. Seager, R.; Burgman, R.; Kushnir, Y.; Clement, A.; Cook, E.; Naik, N.; Miller, J. Tropical Pacific forcing of North American medieval megadroughts: Testing the concept with an atmosphere model forced by coral-reconstructed SSTs. *J. Clim.* 2008, *21*, 6175–6190, doi:10.1175/2008JCLI2170.1.
16. Chen, J.; Brissette, F.P.; Leconte, R. Uncertainty of downscaling method in quantifying the impact of climate change on hydrology. *J. Hydrol.* 2011, *401*, 190–202, doi:10.1016/j.jhydrol.2011.02.020.
17. Chen, J.; Brissette, F.P.; Chaumont, D.; Braun, M. Performance and uncertainty evaluation of empirical downscaling methods in quantifying the climate change impacts on hydrology over two North American river basins. *J. Hydrol.* 2013, *479*, 200–214, doi:10.1016/j.jhydrol.2012.11.062.
18. Chen, J.; Brissette, F.P.; Leconte, R. Assessing regression-based statistical approaches for downscaling precipitation over North America. *Hydrol. Process.* 2014, *28*, 3482–3504, doi:10.1002/hyp.9889.

19. Räty, O.; Räisänen, J.; Ylhäisi, J. Evaluation of delta change and bias correction methods for future daily precipitation: Intermodal cross-validation using ENSEMBLES simulations. *Clim. Dynam.* 2014, *42*, 2287–2303, doi:10.1007/s00382-014-2130-8.
20. Sunyer, M.A.; Hundecha, Y.; Lawrence, D.; Madsen, H.; Willems, P.; Martinkova, M.; Vormoor, K.; Bürger, G.; Hanel, M.; Kriauciuniene, J.; et al. Inter-comparison of statistical downscaling methods for projection of extreme precipitation in Europe. *Hydrol. Earth Syst. Sci.* 2015, *19*, 1827–1847, doi:10.5194/hess-19-1827-2015.
21. Piani, C.; Haerter, J.O.; Coppola, E. Statistical bias correction for daily precipitation in regional climate models over Europe. *Theor. Appl. Clim.* 2010, *99*, 187–192, doi:10.1007/s00704-009-0134-9.
22. Watanabe, S.; Kanae, S.; Seto, S.; Yeh, P.J.-F.; Hirabayashi, Y.; Oki, T. Intercomparison of bias-correction methods for monthly temperature and precipitation simulated by multiple climate models. *J. Geophys. Res.* 2012, *117*, D23114, doi:10.1029/2012JD018192.
23. Teutschbein, C.; Seibert, J. Bias correction of regional climate model simulations for hydrological climate-change impact studies: Review and evaluation of different methods. *J. Hydrol.* 2012, *456–457*, 12–29, doi:10.1016/j.jhydrol.2012.05.052.
24. Seaby, L.P.; Refsgaard, J.C.; Sonnenborg, T.O.; Højberg, A.L. Spatial uncertainty in bias corrected climate change projections and hydrogeological impacts. *Hydrol. Process.* 2015, *29*, 4514–4532, doi:10.1002/hyp.10501.
25. Pulido-Velazquez, D.; Garrote, L.; Andreu, J.; Martin-Carrasco, F.J.; Iglesias, A. A methodology to diagnose the effect of climate change and to identify adaptive strategies to reduce its impacts in conjunctive-use systems at basin scale. *J. Hydrol.* 2011, *405*, 110–122, doi:10.1016/j.jhydrol.2011.05.014.
26. Pulido-Velazquez, D.; García-Aróstegui, J.L.; Molina, J.L.; Pulido-Velázquez, M. Assessment of future groundwater recharge in semi-arid regions under climate change scenarios (Serral-Salinas aquifer, SE Spain). Could increased rainfall variability increase the recharge rate? *Hydrol. Process.* 2015, *29*, 828–844, doi:10.1002/hyp.10191.
27. Räisänen, J.; Räty, O. Projections of daily mean temperature variability in the future: Cross-validation tests with ENSEMBLES regional climate simulations. *Clim. Dyn.* 2013, *41*, 1553–1568, doi:10.1007/s00382-012-1515-9.
28. Rupp, D.E.; Abatzoglou, J.T.; Hegewisch, K.C.; Mote, P.W. Evaluation of CMIP5 20th century climate simulations for the Pacific Northwest USA. *J. Geophys. Res. Atmos.* 2013, *118*, 10–884, doi:10.1002/jgrd.50843.
29. Ahmadalipour, A.; Rana, A.; Moradkhani, H.; Sharma, A. Multi-criteria evaluation of CMIP5 GCMs for climate change impact analysis. *Theor. Appl. Climatol.* 2015, *128*, 71–87, doi:10.1007/s00704-015-1695-4.

30. Hashmi, M.Z.; Shamseldin, A.Y.; Melville, B.W. Statistically downscaled probabilistic multi-model ensemble projections of precipitation change in a watershed. *Hydrol. Process.* 2013, *27*, 1021–1032, doi:10.1002/hyp.8413.
31. AEMET (Spanish Meteorological Agency). Generación de Escenarios Regionalizados de Cambio Climático Para España; Agencia Estatal de Meteorología (Ministerio de Medio Ambiente y Medio Rural y Marino): Madrid, Spain, 2009.
32. Haerter, J.O.; Hagemann, S.; Moseley, C.; Piani, C. Climate model bias-correction and the role of timescales. *Hydrol. Earth Syst. Sci.* 2011, *15*, 1065–1079, doi:10.5194/hess-15-1065-2011.
33. Prudhomme, C.; Reynard, N.; Crooks, S. Downscaling of global climate models for flood frequency analysis: Where are we now? *Hydrol. Process.* 2002, *16*, 1137–1150, doi:10.1002/hyp.1054.
34. Lafon, T.; Dadson, S.; Buys, G.; Prudhomme, C. Bias correction of daily precipitation simulated by a regional climate model: A comparison of methods. *Int. J. Climatol.* 2013, *33*, 1367–1381, doi:10.1002/joc.3518.
35. Hellström, C.; Chen, D.; Achberger, C.; Räisänen, J. Comparison of climate change scenarios for Sweden based on statistical and dynamical downscaling of monthly precipitation. *Clim. Res.* 2001, *19*, 45–55, doi:10.3354/cr019045.
36. Hessami, M.; Gachon, P.; Ouarda, T.; St-Hilaire, A. Automated regression-based statistical downscaling tool. *Environ. Model. Softw.* 2008, *23*, 813–834, doi:10.1016/j.envsoft.2007.10.004.
37. Gudmundsson, L.; Bremnes, J.B.; Haugen, J.E.; Engen-Skaugen, T. Technical Note: Downscaling RCM precipitation to the station scale using statistical transformations—A comparison of methods. *Hydrol. Earth Syst. Sci.* 2012, *16*, 3383–3390, doi:10.5194/hess-16-3383-2012.
38. Klemeš, V. Operational testing of hydrological simulation models/Vérification, en conditions réelles, des modèles de simulation hydrologique. *Hydrol. Sci. J.* 1986, *31*, 13–24, doi:10.1080/0262668609491024.
39. Bennett, J.C.; Ling, F.L.N.; Graham, B.; Grose, M.R.; Corney, S.P.; White, C.J.; Holz, G.K.; Post, D.A.; Gaynor, S.M.; Bindoff, N.L. *Climate Futures for Tasmania: Water and Catchments: Technical Report*; Antarctic Climate & Ecosystems Cooperative Research Centre: Hobart, Tasmania, Australia, 2010.
40. Terink, W.; Hurkmans, R.T.W.L.; Torfs, P.J.J.F.; Uijlenhoet, R. Evaluation of a bias correction method applied to downscaled precipitation and temperature reanalysis data for the Rhine basin. *Hydrol. Earth Syst. Sci.* 2010, *14*, 687–703, doi:10.5194/hess-14-687-2010.

41. Teutschbein, C.; Seibert, J. Is bias correction of regional climate model (RCM) simulations possible for non-stationary conditions? *Hydrol. Earth Syst. Sci.* 2013, *17*, 5061–5077, doi:10.5194/hess-17-5061-2013.
42. McKee, T.B.; Doesken, N.J.; Kleist, J. The relationship of drought frequency and duration to time scale. In Proceedings of the Eighth Conference on Applied Climatology, Anaheim, CA, USA, 17–22 January 1993; American Meteorological Society: Boston, MA, USA, 1993.
43. McKee, T.B.; Doesken, N.J.; Kleist, J. Drought monitoring with multiple timescales. In Proceedings of the Ninth Conference on Applied Climatology, Dallas, TX, USA, 15–20 January 1995; Boston American Meteorological Society: Boston, MA, USA, 1995; pp. 233–236.
44. Bonaccorso, B.; Bordi, I.; Cancelliere, A.; Rossi, G.; Sutera, A. Spatial Variability of Drought: An Analysis of the SPI in Sicily. *Water Resour. Manag.* 2003, *17*, 273–296, doi:10.1023/A:1024716530289.
45. Livada, I.; Assimakopoulos, V.D. Spatial and temporal analysis of drought in Greece using the Standardized Precipitation Index (SPI). *Theor. Appl. Climatol.* 2007, *89*, 143–153, doi:10.1007/s00704-005-0227-z.
46. Mishra, A.K.; Singh, V.P.; Desai, V.R. Drought characterization: A probabilistic approach. *Stoch. Environ. Res. Risk Assess.* 2009, *23*, 41–55, doi:10.1007/s00477-007-0194-2.
47. González, J.; Valdés, J.B. New drought frequency index: Definition and comparative performance analysis. *Water Resour. Res.* 2006, *42*, W11421, doi:10.1029/2005WR004308.
48. Barnett, T.P.; Adam, J.C.; Lettenmaier, D.P. Potential impacts of a warming climate on water availability in snow-dominated regions. *Nature* 2005, *438*, 303–309, doi:10.1038/nature04141.
49. Herrera, S.; Gutiérrez, J.M.; Ancell, R.; Pons, M.R.; Frías, M.D.; Fernández, J. Development and analysis of a 50-year high-resolution daily gridded precipitation dataset over Spain (Spain02). *Int. J. Climatol.* 2012, *32*, 74–85, doi:10.1002/joc.2256.
50. Herrera, S.; Fernández, J.; Gutiérrez, J.M. Update of the Spain02 Gridded Observational Dataset for Euro-CORDEX evaluation: Assessing the Effect of the Interpolation Methodology. *Int. J. Climatol.* 2016, *36*, 900–908, doi:10.1002/joc.4391.
51. Quintana-Seguí, P.; Turco, M.; Herrera, S.; Miguez-Macho, G. Validation of a new SAFRAN-based gridded precipitation product for Spain and comparisons to Spain02 and ERA-Interim. *Hydrol. Earth Syst. Sci.* 2017, *21*, 2187–2201, doi:10.5194/hess-21-2187-2017.

52. CORDEX PROJECT. The Coordinated Regional Climate Downscaling Experiment CORDEX. Program Sponsored by World Climate Research Program (WCRP). 2013. Available online: <http://www.cordex.org/> (accessed on 8 September 2018).
53. Escriva-Bou, A.; Pulido-Velazquez, M.; Pulido-Velazquez, D. The Economic Value of Adaptive Strategies to Global Change for Water Management in Spain's Jucar Basin. *J. Water Resour. Pl. Manag.* 2016, *143*, 04017005, doi:10.1061/(ASCE)WR.1943-5452.0000735.
54. Fernandez-Montes, S.; Rodrigo, F.S. Trends in surface air temperatures, precipitation and combined indices in the southeastern Iberian Peninsula (1970–2007). *Clim. Res.* 2015, *63*, 43–60, doi:10.3354/cr01287.
55. Pepin, N.C.; Lundquist, J.D. Temperature trends at high elevations: Patterns across the globe. *Geophys. Res. Lett.* 2008, *35*, L14701, doi:10.1029/2008GL034026.
56. Ehret, U.; Zehe, E.; Wulfmeyer, V.; Warrach-Sagi, K.; Liebert, J. HESS Opinions “Should we apply bias correction to global and regional climate model data?”. *Hydrol. Earth Syst. Sci.* 2012, *16*, 3391–3404, doi:10.5194/hess-16-3391-2012.
57. Muerth, M.J.; Gauvin St-Denis, B.; Ricard, S.; Velázquez, J.A.; Schmid, J.; Minville, M.; Caya, D.; Chaumont, D.; Ludwig, R.; Turcotte, R. On the need for bias correction in regional climate scenarios to assess climate change impacts on river runoff. *Hydrol. Earth Syst. Sci.* 2013, *17*, 1189–1204, doi:10.5194/hess-17-1189-2013.

Tables of the Chapter 6

Correction Technique	Pros	Cons
First-moment correction	- Does not generate negative values for P	- Only preserve the mean
Second-moment correction	- Preserve mean and standard deviation	- Generates some negative values for P
Regression	- Allow to use different regression models - Preserve mean and standard deviation	- Generates some negative values for P
Quantile mapping	- Preserve mean and standard deviation - No generates negative values of P - Variety of methods (theoretical distribution, parametric, non-parametric, empirical, splines)	- Required more complex transformations (application to the probability distribution of data)

Table 6.1. Summary of advantages and disadvantages of each correction technique (P stands for precipitation).

RCM \ GCM	CNRM-CM5	EC-EARTH	MPI-ESM-LR	IPSL-CM5A-MR
CCLM4-8-17	X	X	X	
RCA4	X	X	X	
HIRHAM5		X		
RACMO22E		X		
WRF331F				X

Table 6.2. Regional climatic models (RCMs) and global climate models (GCMs) considered.

RCM	GCM	ELIMINATED?	
		Lumped Cases	Distributed Case
CCLM4-8-17	CNRM-CM5	NO	NO
CCLM4-8-17	EC-EARTH	NO	NO
CCLM4-8-17	MPI-ESM-LR	NO	NO
HIRHAM5	EC-EARTH	NO	YES
RACMO22E	EC-EARTH	NO	NO
RCA4	CNRM-CM5	NO	NO
RCA4	EC-EARTH	NO	YES
RCA4	MPI-ESM-LR	YES	NO
WRF331F	IPSL-CM5A-MR	NO	NO
CCLM4-8-17	CNRM-CM5	NO	NO

Table 6.3. Eliminated and uneliminated models in the multi-objective analysis of the delta change approaches for the lumped and distributed cases.

RCM	GCM	Technique	Lumped Case	Distributed Case
CCLM4-8-17	CNRM-CM5	1st moment correc.	YES	YES
CCLM4-8-18	CNRM-CM6	2nd moment correc.	NO	YES
CCLM4-8-19	CNRM-CM7	Regression	YES	YES
CCLM4-8-20	CNRM-CM8	QM Parametric dist.	NO	YES
CCLM4-8-21	CNRM-CM9	QM Empirical quant.	YES	NO
CCLM4-8-17	EC-EARTH	1st moment correc.	YES	YES
CCLM4-8-18	EC-EARTH	2nd moment correc.	YES	YES
CCLM4-8-19	EC-EARTH	Regression	NO	YES
CCLM4-8-20	EC-EARTH	QM Parametric dist.	YES	YES
CCLM4-8-21	EC-EARTH	QM Empirical quant.	NO	NO
CCLM4-8-17	MPI-ESM-LR	1st moment correc.	YES	YES
CCLM4-8-17	MPI-ESM-LR	2nd moment correc.	NO	NO
CCLM4-8-17	MPI-ESM-LR	Regression	NO	NO
CCLM4-8-17	MPI-ESM-LR	QM Parametric dist.	NO	NO
CCLM4-8-17	MPI-ESM-LR	QM Empirical quant.	NO	NO
HIRHAM5	EC-EARTH	1st moment correc.	YES	YES
HIRHAM5	EC-EARTH	2nd moment correc.	NO	NO
HIRHAM5	EC-EARTH	Regression	NO	NO
HIRHAM5	EC-EARTH	QM Parametric dist.	NO	YES
HIRHAM5	EC-EARTH	QM Empirical quant.	NO	YES
RACMO22E	EC-EARTH	1st moment correc.	YES	YES
RACMO22E	EC-EARTH	2nd moment correc.	YES	YES
RACMO22E	EC-EARTH	Regression	NO	YES
RACMO22E	EC-EARTH	QM Parametric dist.	YES	YES
RACMO22E	EC-EARTH	QM Empirical quant.	YES	YES
RCA4	CNRM-CM5	1st moment correc.	YES	YES
RCA4	CNRM-CM5	2nd moment correc.	NO	YES
RCA4	CNRM-CM5	Regression	NO	YES
RCA4	CNRM-CM5	QM Parametric dist.	YES	YES
RCA4	CNRM-CM5	QM Empirical quant.	NO	NO
RCA4	EC-EARTH	1st moment correc.	YES	YES
RCA4	EC-EARTH	2nd moment correc.	YES	YES
RCA4	EC-EARTH	Regression	YES	YES
RCA4	EC-EARTH	QM Parametric dist.	YES	YES
RCA4	EC-EARTH	QM Empirical quant.	YES	YES
RCA4	MPI-ESM-LR	1st moment correc.	YES	YES
RCA4	MPI-ESM-LR	2nd moment correc.	YES	YES
RCA4	MPI-ESM-LR	Regression	YES	NO
RCA4	MPI-ESM-LR	QM Parametric dist.	NO	NO
RCA4	MPI-ESM-LR	QM Empirical quant.	YES	YES
WRF331F	IPSL-CM5A-MR	1st moment correc.	YES	YES
WRF331F	IPSL-CM5A-MR	2nd moment correc.	YES	YES
WRF331F	IPSL-CM5A-MR	Regression	YES	YES
WRF331F	IPSL-CM5A-MR	QM Parametric dist.	YES	YES
WRF331F	IPSL-CM5A-MR	QM Empirical quant.	NO	NO

Table 6.4. Eliminated and uneliminated combinations of model and bias correction technique for the lumped and distributed cases.

Scenario	Lumped Case		Distributed Case	
	P	T	P	T
Absolute Changes (mm or °C)				
E1	-147.9	4.5	-142.4	4.5
E2	-139.0	4.5	-131.9	4.6
E3	-143.4	4.5	-149.4	4.5
E4	-139.1	4.4	-141.9	4.6
Relative Changes (%)				
E1	-28.21	31.94	-27.16	31.66
E2	-26.51	31.59	-25.16	32.05
E3	-27.35	31.74	-28.50	31.79
E4	-26.53	30.99	-27.06	32.49

Table 6.5. Changes of overall mean values for precipitation and temperature scenarios compared to historical data.

Figures of the Chapter 6

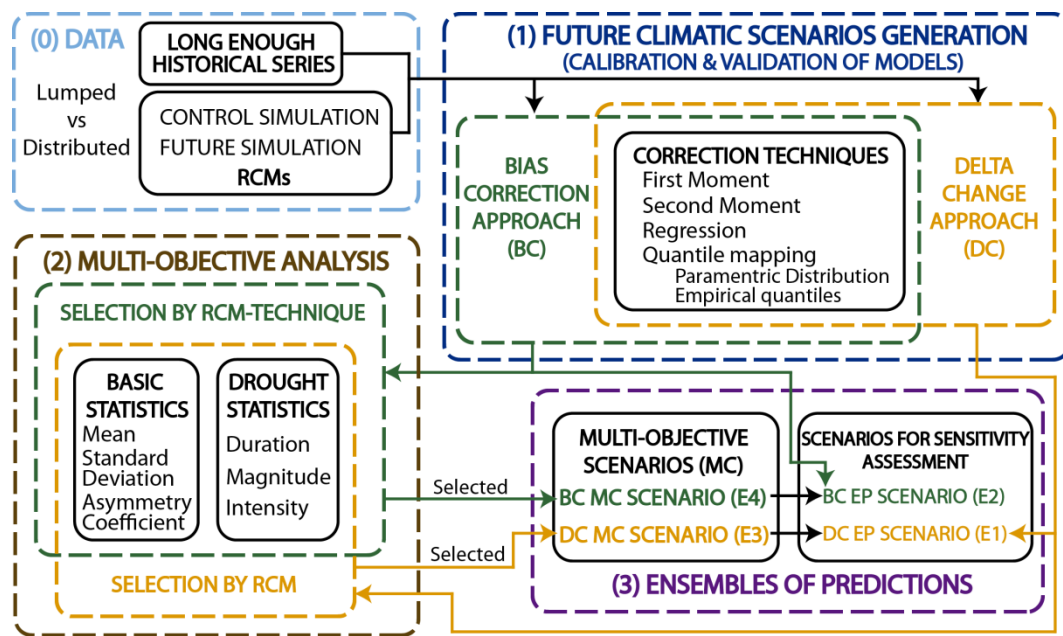


Figure 6.1. Flow chart of the proposed methodology.

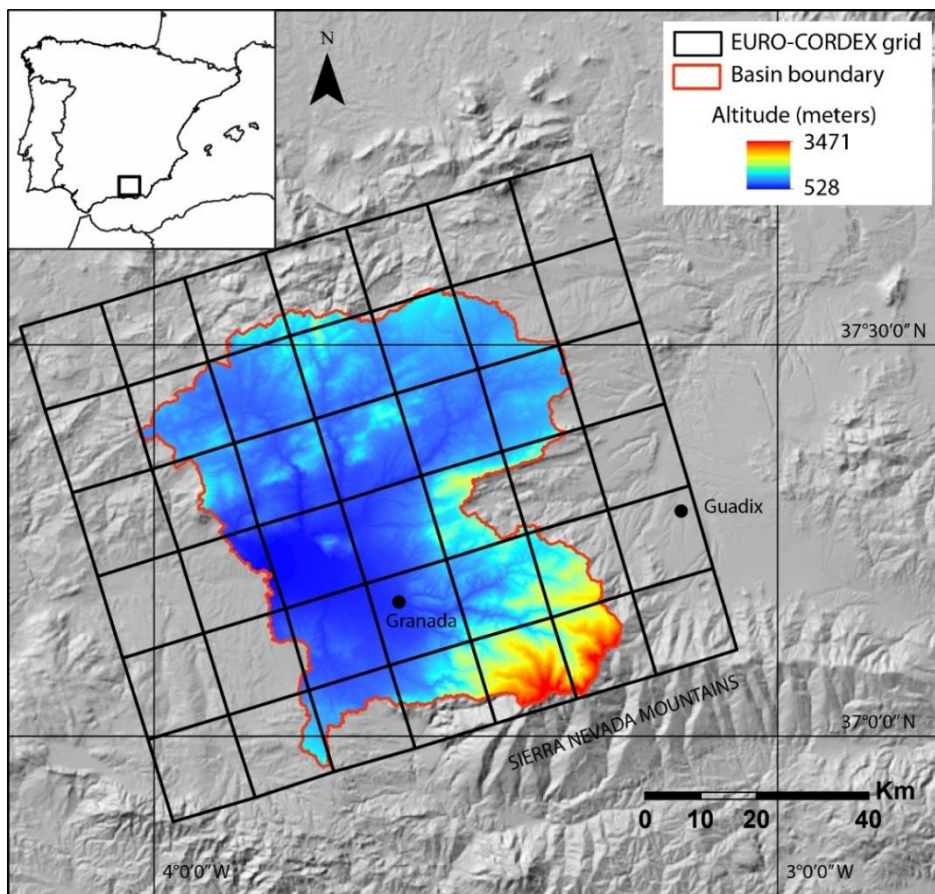


Figure 6.2. Location of the case study.

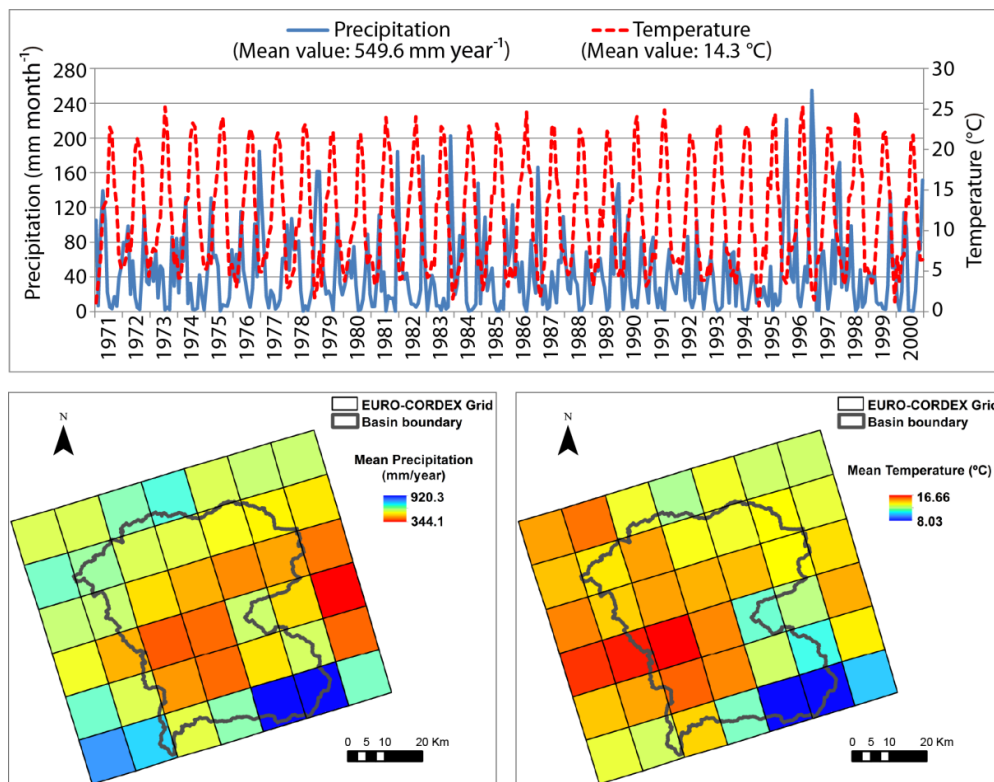


Figure 6.3. Historical precipitation and temperature in Alto Genil basin. Above: Monthly precipitation and temperature time series. Below: Spatial distribution of mean precipitation and temperature.

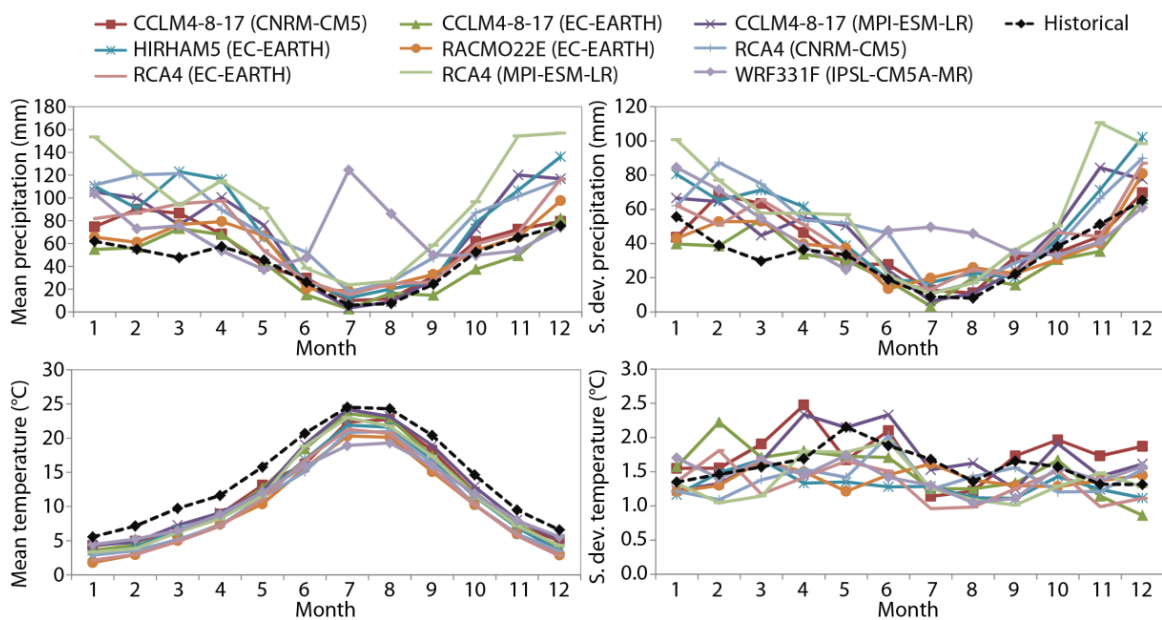


Figure 6.4. Monthly mean and standard deviation for the historical and control series (precipitation and temperature) for the mean year in the period 1971–2000—lumped approaches.

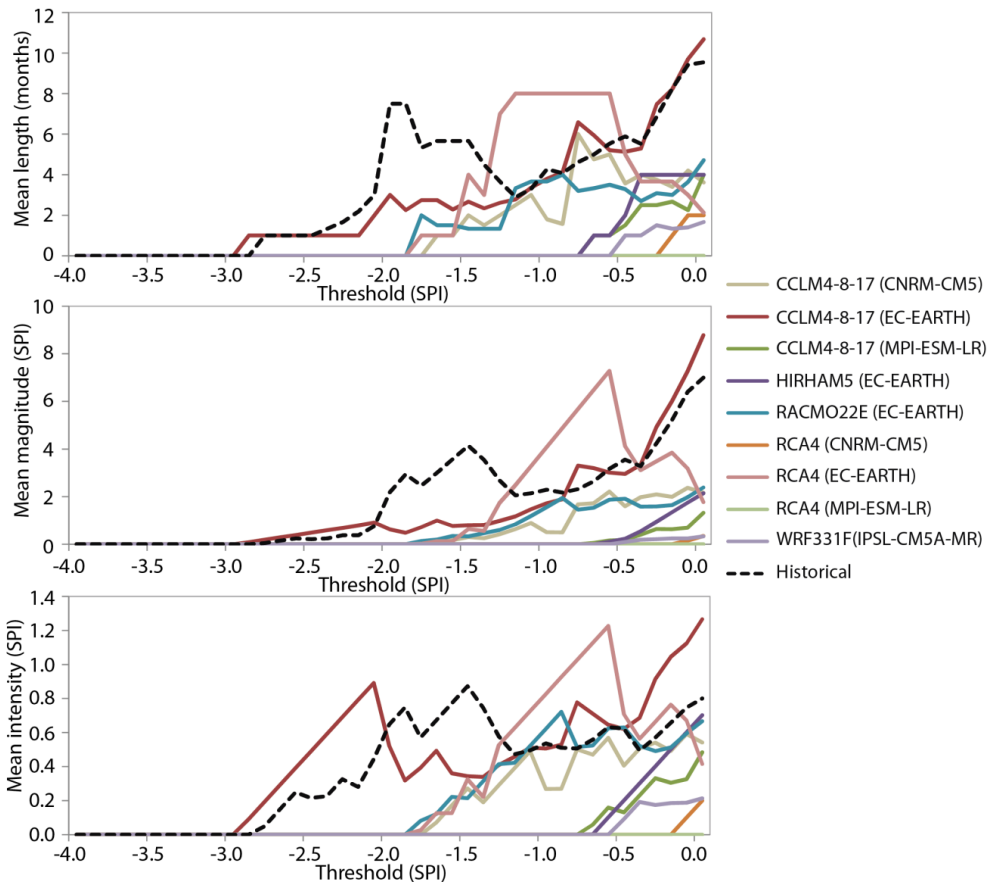


Figure 6.5. Drought statistics for the historical and control series in the period 1971–2000—lumped approaches.

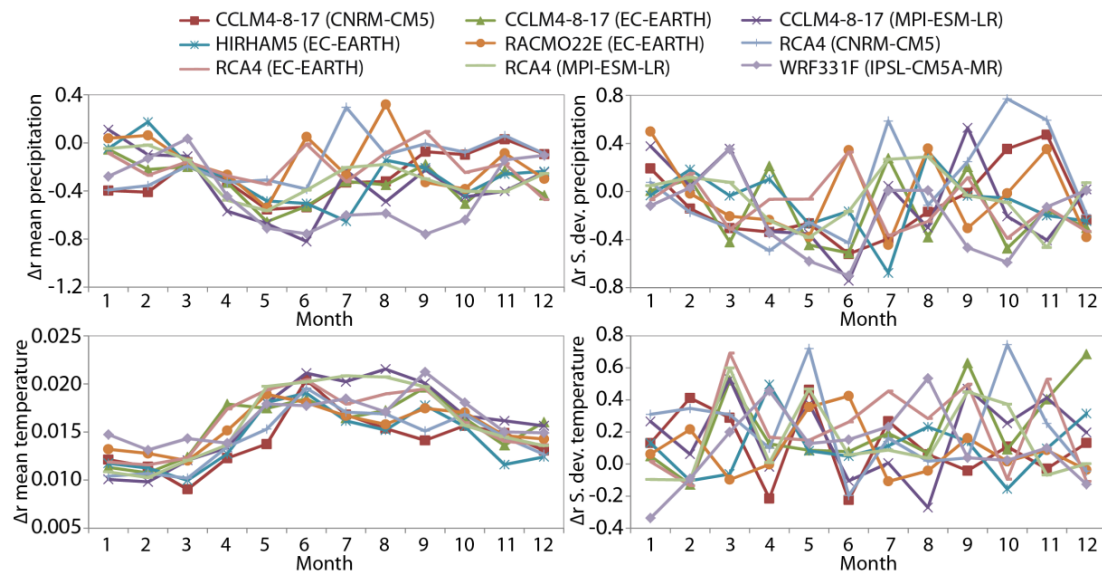


Figure 6.6. Dimensionless relative monthly change in mean and standard deviation of the future P and T series (2071–2100) with respect to the control series (1971–2000)—lumped approaches. Relative changes calculated as $(F - C)/C$ where F stands for future model projections and C control model simulations.

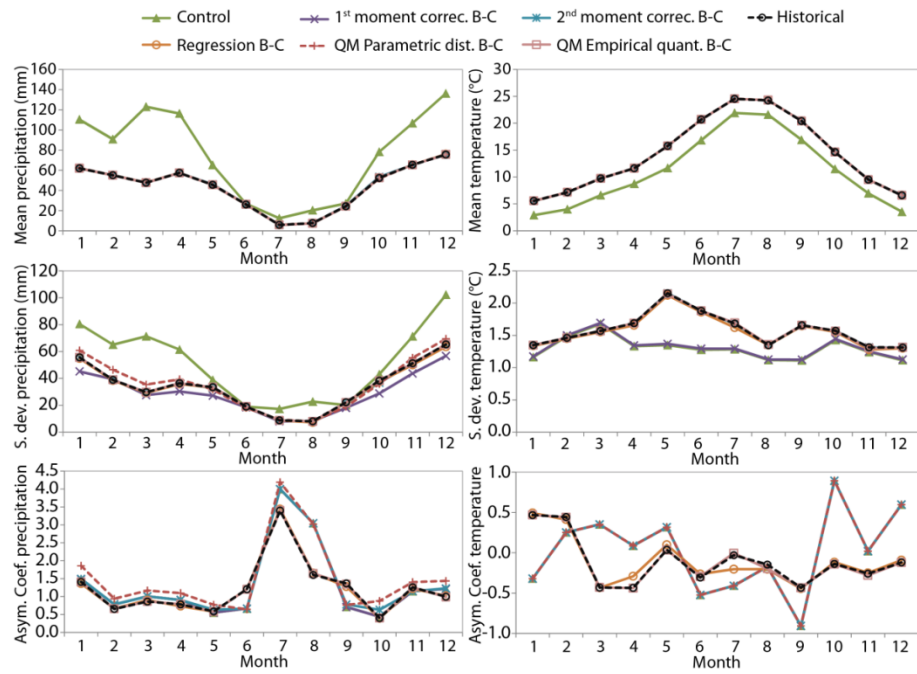


Figure 6.7. Mean, standard deviation, and asymmetry coefficients of the corrected control scenario (1971–2000) for precipitation (left column) and temperature (right column). Average year for HIRHAM5 RCM model nested inside EC-EARTH GCM—lumped approaches.

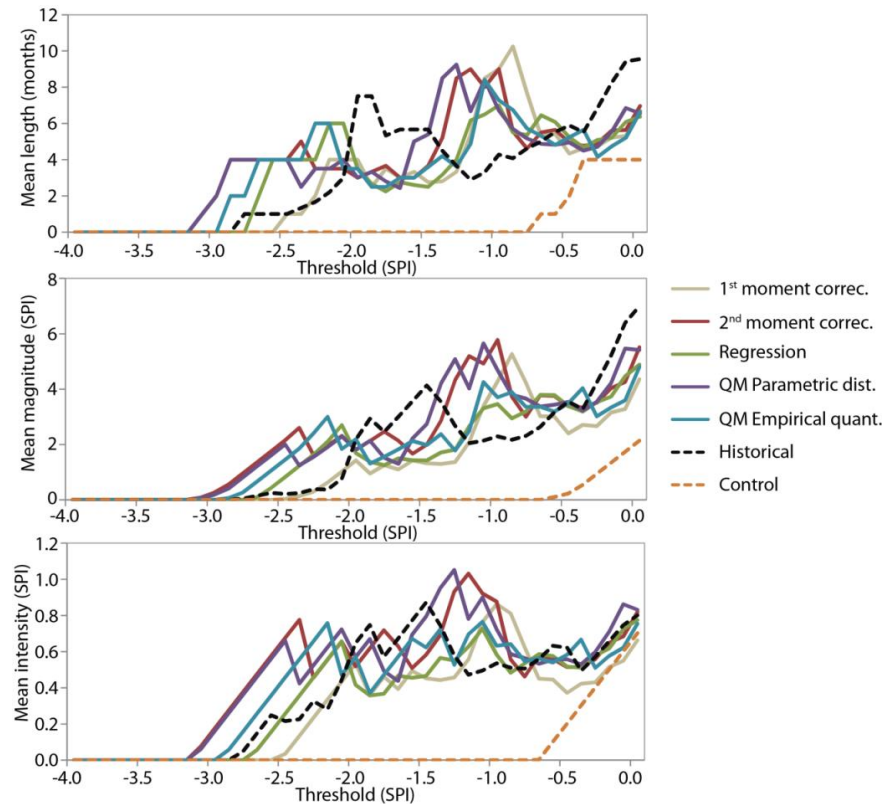


Figure 6.8. Drought statistics of the corrected precipitation control scenario (1971–2000) for the HIRHAM5 RCM model nested inside EC-EARTHGCM—lumped approaches.

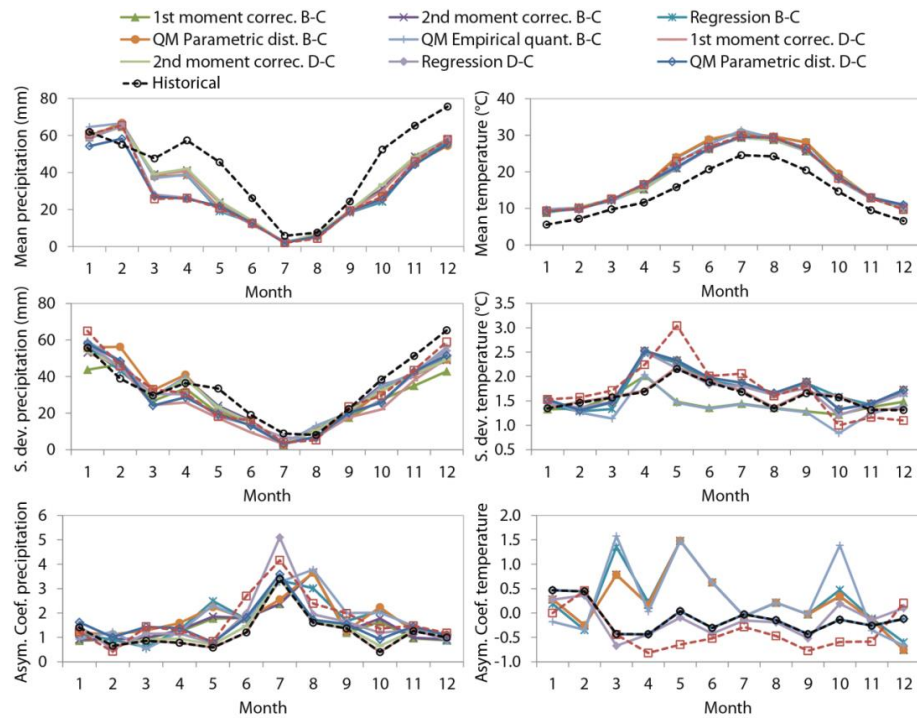


Figure 6.9. Mean, standard deviation and asymmetry coefficients of future precipitation (left column) and temperature series (right column). Average year for HIRHAM5 RCM model nested inside EC-EARTH GCM—lumped approaches.

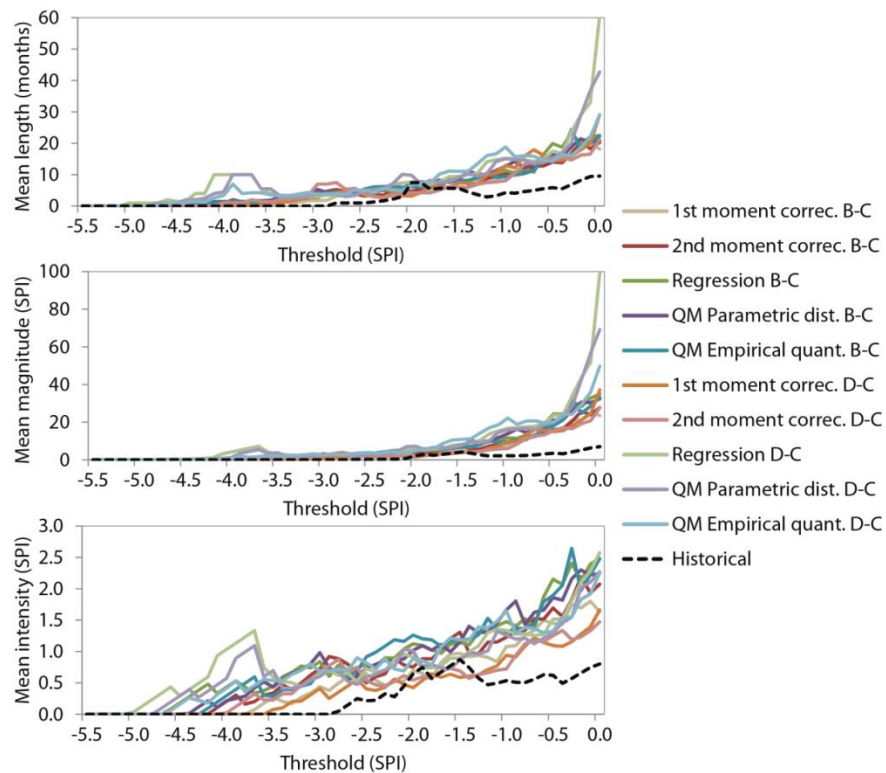


Figure 6.10. Drought statistics of future precipitation series for the HIRHAM5 RCM model nested inside EC-EARTH GCM—lumped approaches.

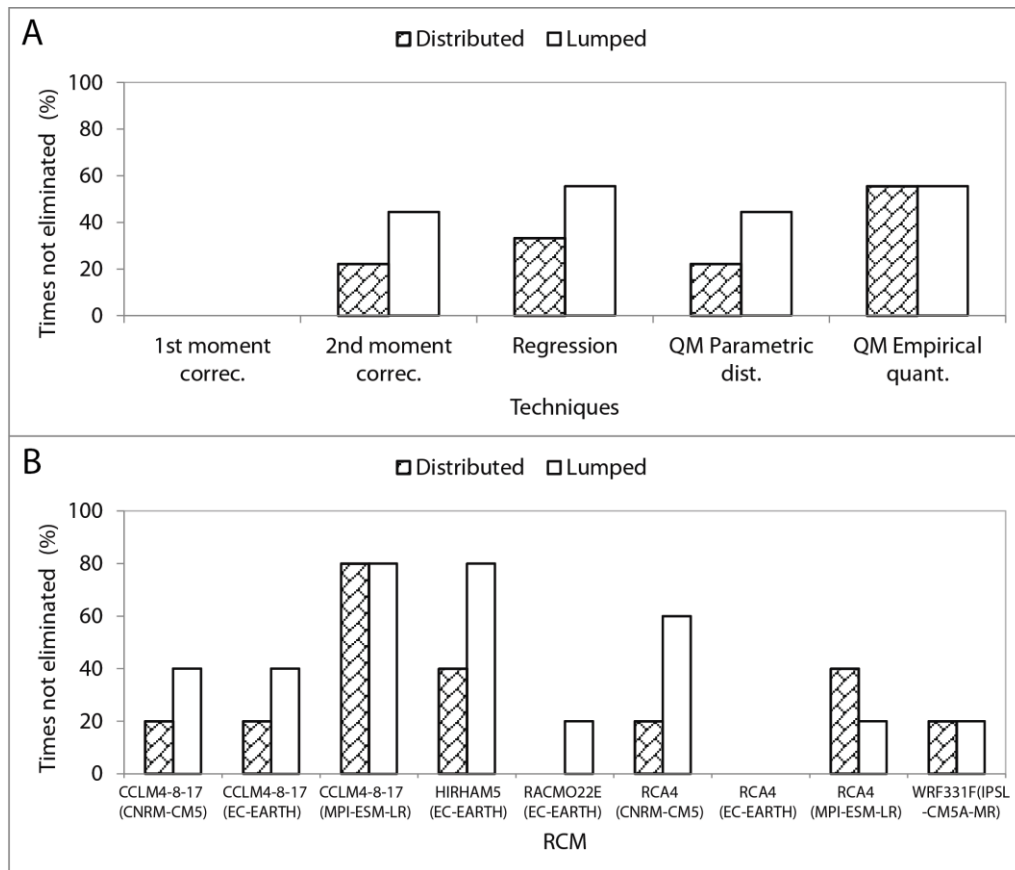


Figure 6.11. (A) Times that the techniques are not eliminated in the multi-objective analysis (bias correction approach); (B) Times that the RCMs are not eliminated in the multi-objective analysis (bias correction change approach).

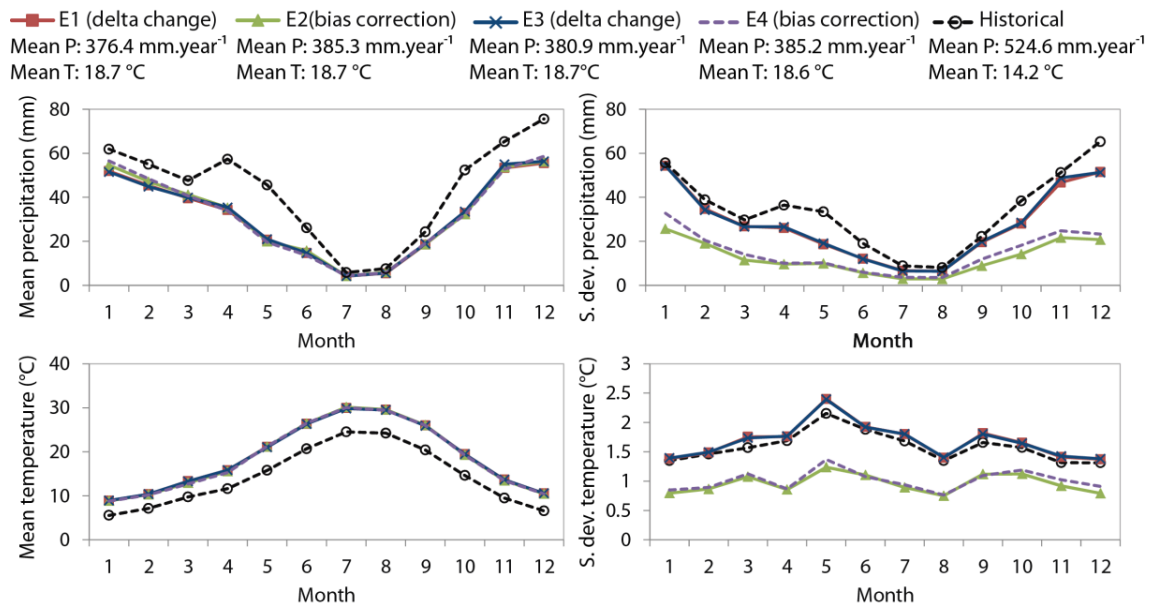


Figure 6.12. Mean and standard deviation of future precipitation and temperature series obtained by the four ensemble options (E1, E2, E3, and E4)—lumped approaches.

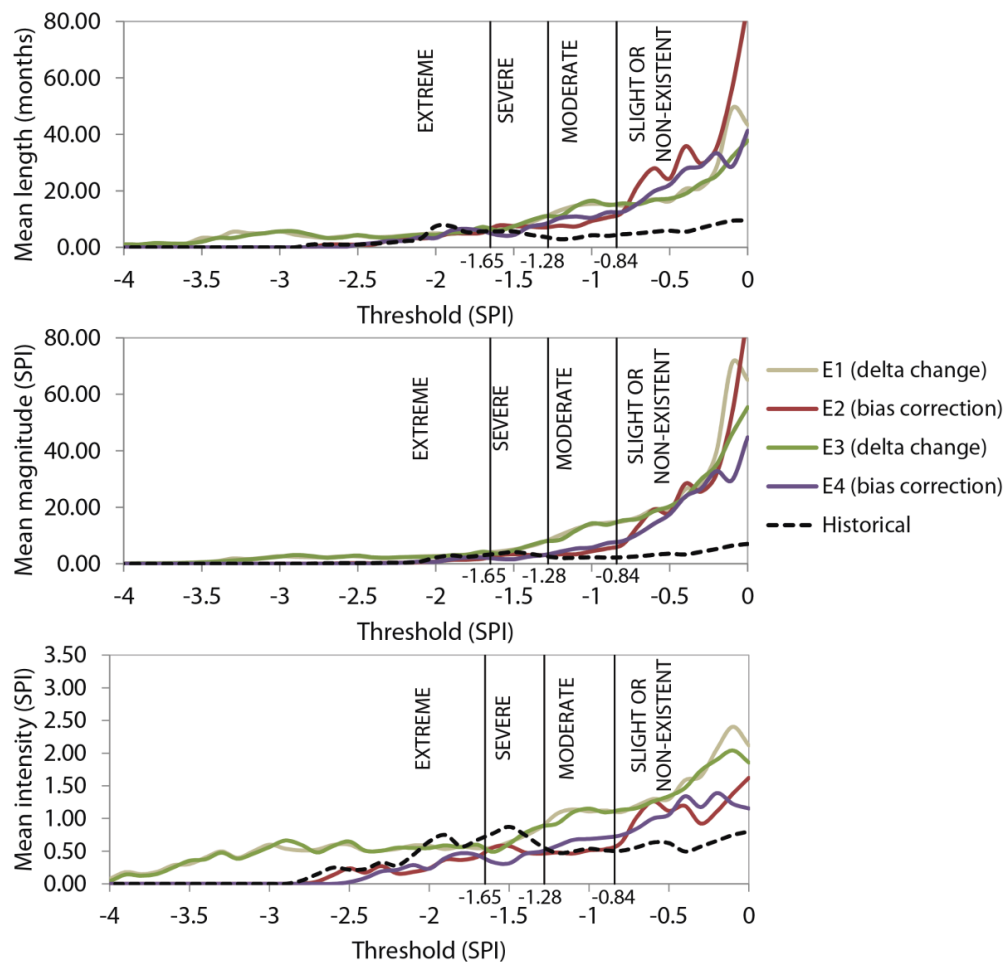


Figure 6.13. Drought statistics of future precipitation series obtained by the four ensemble options (E1, E2, E3, and E4)—lumped approaches.

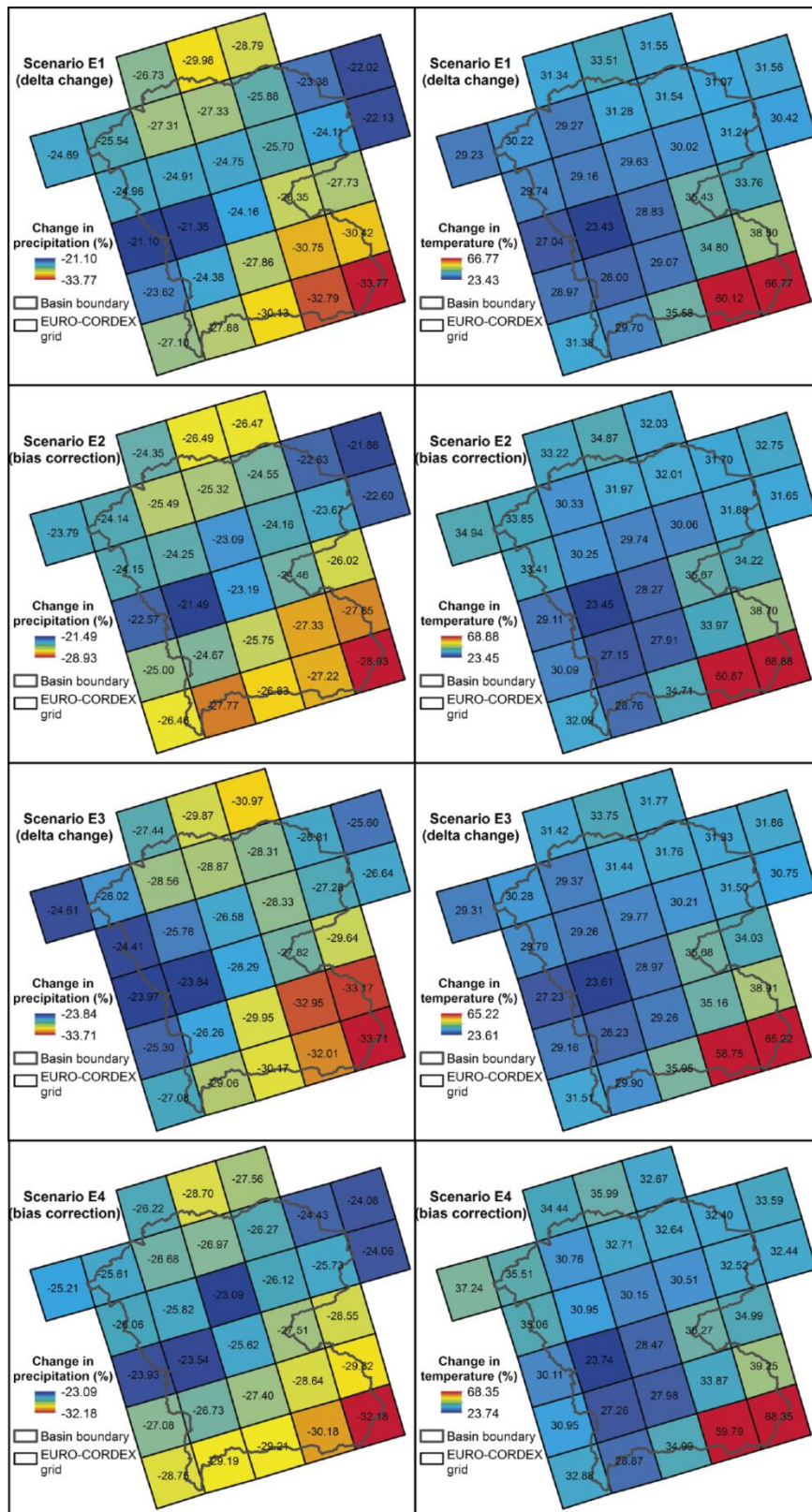


Figure 6.14. Spatial distribution of the mean relative change (expressed in %) in precipitation and temperature obtained by the four ensemble options (E1, E2, E3, and E4)—distributed approaches.

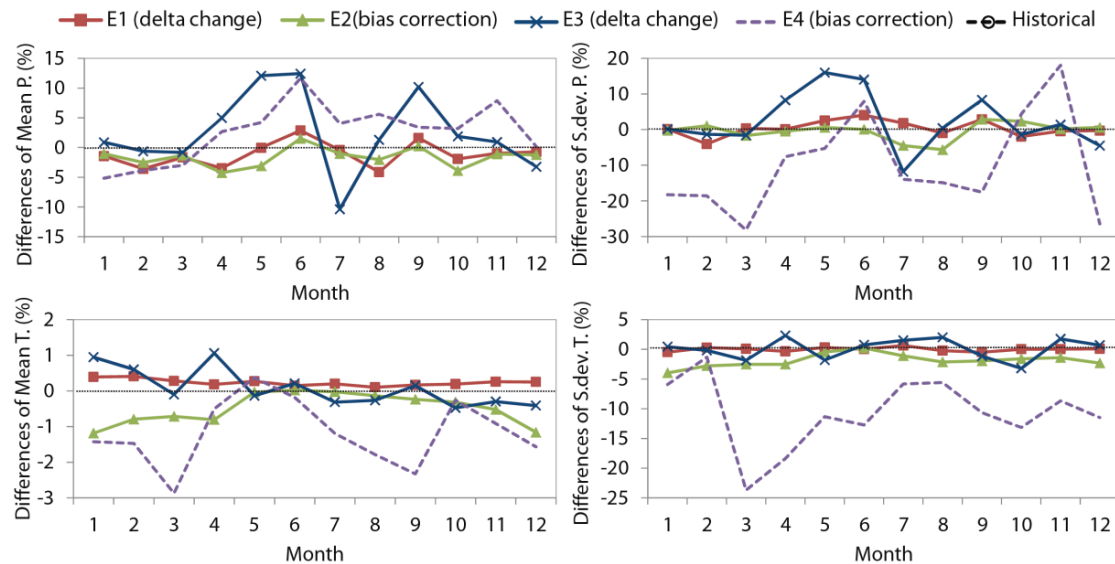


Figure 6.15. Monthly differences in mean and standard deviation in an average year between distributed (D) and lumped (L) approaches $((L - D)/D \times 100)$ for the four ensembles scenarios (E1, E2, E3 and E4).

Chapter 7: A distributed cellular automata model to simulate potential future impacts of climate change on snow cover area

Advances in Water Resources 124 (2019) 106–119

Contents lists available at ScienceDirect

Advances in Water Resources

journal homepage: www.elsevier.com/locate/advwatres



A distributed cellular automata model to simulate potential future impacts of climate change on snow cover area

Antonio-Juan Collados-Lara ^{a,*}, Eulogio Pardo-Igúzquiza ^b, David Pulido-Velazquez ^a

Antonio-Juan Collados-Lara^(1,*), Eulogio Pardo-Igúzquiza⁽²⁾, David Pulido-Velazquez⁽¹⁾

(1) Instituto Geológico y Minero de España, Urb. Alcázar del Genil, 4. Edificio Zulema Bajo, 18006, Granada (Spain). E-mails: ajcollados@gmail.com, d.pulido@igme.es

(2) Instituto Geológico y Minero de España, Ríos Rosas, 23, 28003 Madrid (Spain). E-mail: e.pardo@igme.es

* Corresponding author

Abstract

Snow dynamics in alpine systems play an important role in water resources management. One of the main variables that characterises the snowpack is snow cover area. In this paper, we present a novel methodology to assess the impact of climate change scenarios on snow cover area in alpine systems. The methodology calibrates and validates a distributed cellular automata (CA) model. Potential climate change scenarios can be generated to feed the CA model in order to assess the potential impact of climate change on snow cover area. The methodology has been applied to the Sierra Nevada mountain range in southern Spain, an area with a Mediterranean climate, which is valuable in terms of both its ecology and the tourism industry. Snow falls on the mountains from October to May, but this snow season may vary in the future due to climate change. We analysed the influence of elevation on the potential impact of climate change on the area covered by snow. The size of the potential changes associated with climate change increase with elevation in the case of temperature and decrease in the case of precipitation. These potential changes will modify snow dynamics, causing an important reduction in the area covered by snow (mean 60.4%) for the future horizon considered (2071–2100).

Key words: cellular automata, climate change, snow cover area, Spanish Sierra Nevada

1. Introduction

Climate change will modify the availability of water resources in the future (Arnell and Lloyd-Hughes, 2013; Pulido-Velazquez *et al.*, 2017). Alpine systems where the majority of precipitation is solid could be very sensitive to climate change (Horton *et al.*, 2006; Gobiet *et al.*, 2014). Snow dynamics govern ecosystems and so any variation in snow availability could bring significant changes to these ecosystems (Beniston 2003; Edwards *et al.*, 2007). From the point of view of water resources, an assessment of the impact of future potential climate change scenarios on snow is essential for appropriate water resources management (Barnett *et al.*, 2005, Arnell and Lloyd-Hughes, 2013). Accordingly, assessments of snow cover area (SCA) and potential changes to it become key to assessing climate change in alpine systems.

SCA is one of the main variables that characterises the snow dynamic, which is important for assessing water resources and their management. Snow Water Equivalent (SWE) quantifies the availability of water in the snow pack; if we want to obtain the SWE in a certain area we need to estimate snow depth and the snow density in the domain with snow, which is defined by the snow cover area (SCA).

Several studies have been done to estimate snow depth using snow stakes (*e.g.*, Kucerova and Jenicek, 2014; Collados-Lara *et al.*, 2017) and snow density (*e.g.*, Lopez-Moreno *et al.*, 2013; Bormann *et al.*, 2013). With regard to SCA, various agencies have developed products to estimate SCA based on satellite data (*e.g.*, Rutgers University Global Snow Lab, which uses NOAA satellite data; NASA Distributed Active Archive Centre, which uses MODIS satellite data), but sometimes we need information that covers a longer period or with higher spatiotemporal resolution to assess operational issues. Where such remote-sensing data is available, SCA estimates can be directly used as input for hydrological models (*e.g.*, Thirel *et al.*, 2013; Mir *et al.*, 2015). Elsewhere, however, SCA data may be unavailable, or have too crude a spatial resolution to assess the operational issues in question. Moreover, satellite data may be useless during certain periods if cloud cover obscures the view or if there has been a sensor failure (Ackerman *et al.*, 1998; Schmugge *et al.*, 2002). In such cases, alternative tools or models are required to estimate SCA.

To date, SCA has been analysed using various procedures, including physically-based models (Molotch *et al.*, 2004; Warscher *et al.*, 2013), regression techniques (Richer *et al.*, 2013; Mir *et al.*, 2015), artificial neural networks (Hou and Huang, 2014; Mishra *et al.*, 2014) and cellular automata (CA) models (Leguizamón, 2006; Pardo-Igúzquiza *et al.*, 2017).

Cellular Automata (CA) are infinite, regular lattices of simple finite state machines that change their states synchronously, according to a local update rule that specifies the new state of each cell based on the former states of its neighbours (Wolfram, 1984; Kari, 2005). CA models were first described by Wolfram (1983) to simulate complex dynamics using simple rules of interaction between cells that discretize the area of interest. In this paper we apply CA models to the field of hydrology, and in particular the role of SCA in water resources availability, since CA models are capable of capturing the dynamics of SCA. Moreover, there is great potential for using calibrated and validated CA models to estimate SCA in periods where no SCA data are available. Nevertheless, to date few studies have addressed this issue.

Leguizamón (2006) undertook a preliminary study, though this involved significant limitations. These limitations were pinpointed and overcome by Pardo-Igúzquiza *et al.* (2017) in a study that extended the idea of using CA models to estimate SCA. They proposed a novel algorithm to estimate SCA based on the state of the cell during the previous time step, the states of a given configuration of neighbouring cells at the previous time step, and a set of transition rules. These transition rules involve unique precipitation (P) and temperature (T) indices (driving variables) for the entire mountain range. Classic CA models do not require driving variables but they are needed in order to simulate realistic snow dynamics (Pardo-Igúzquiza *et al.*, 2017).

The climatic indices of the aforementioned CA models can be defined using potential future climatic scenarios of precipitation and temperature in order to assess potential future impacts on the target variable.

Potential scenarios of precipitation and temperature can be obtained using statistical correction techniques applied to simulations performed using different Regional Climatic Models (RCM) (Chen *et al.*, 2013, 2014). These models have spatial resolutions of tens of kilometres and they are nested inside General Circulation Models (GCM) with spatial resolutions of hundreds of kilometres. Generally RCMs cannot be applied directly to assess climate change because they show significant bias with respect to historical time series (Cook *et al.*, 2008; Seager *et al.*, 2008). Appropriate corrections are required to analyse the potential impacts of climate change in a particular system (Collados-Lara *et al.*, 2018). Statistical corrections can be applied using one of two conceptual approaches (bias correction or delta change) depending on the series used to perform the transformation function (Räty *et al.*, 2014; Sunyer *et al.*, 2015). Bias correction approaches apply a correction to the control simulations of RCM in order to fit them to a historical series; then they assume the same biases for the future period in question (*e.g.*, Piani *et al.*, 2010; Watanabe *et al.*, 2012).

Meanwhile, delta change approaches assume that the difference between control and future simulations of RCM are valid, and then use these differences (deltas) to correct the historical series in order to obtain potential future scenarios (*e.g.*, Pulido-Velazquez *et al.*, 2011; 2015; Räisänen and Räty, 2012).

In this paper, we propose a systematic methodology to estimate SCA dynamics in alpine systems that contains two new innovations: (1) the development of a spatially distributed CA model (for driving variables and parameters) to estimate SCA and (2) the use of the calibrated distributed CA model to assess the impacts of potential climate change scenarios on snowpack. To achieve this, we have extended the algorithm proposed by Pardo-Igúzquiza *et al.* (2017) to obtain a distributed approach with spatially distributed climatic indexes and spatially distributed parameters. We test different approaches to search for the optimal parameters and use spatially distributed indices to calibrate the CA algorithm. The calibrated CA models can then be fed with future potential precipitation and temperature scenarios in order to assess the expected changes in SCA.

The proposed methodology is applied to a Mediterranean alpine system where changes due to climate change are expected to be significant; however the method is general and could be applied to any alpine system for different purposes. The assessment of spatial and quantity changes in SCA are crucial to water resources management and ecosystem impact assessments (Beniston 2003; Edwards *et al.*, 2007). Thus, this tool has great potential to be used in operational environmental management due to its ability to estimate and predict the potential impacts of climate change on SCA. On the other hand, this tool could be useful to meteorological forecasts in alpine systems since albedo is an important variable in numerical weather prediction models and is closely related to SCA (Yucel, 2006; Moody *et al.*, 2008).

2. Methodology

In this work we propose a method for performing a sensitivity analysis of the SCA dynamic in potential future climate scenarios, assuming steady land use/land cover (LULC) in the historical and future scenarios. It is based on the CA model developed by Pardo-Igúzquiza *et al.* (2017), which uses five parameters and two driving variables (P and T) to estimate SCA. This relatively simple approach can be used in cases where daily SCA, precipitation and temperature data are available for calibration, but where only precipitation and temperature are available in the operational mode. The model estimates SCA as one of two possible binary states in each cell: snow cover represented by 1 or no snow cover represented by 0. It uses a set of interaction rules that involve the parameters, driving variables (precipitation (P), temperature (T) and elevation (H)), and approaches to the interaction between neighbouring cells. The parameters to be calibrated in this CA model are: P_0 is a precipitation threshold; a and b are the intercept and the slope that define the straight line that represents the discretized snowline (the altitude above which the terrain can have snow); T_c is a temperature threshold; and N_m is the threshold in the number of neighbour cells that produce a change in the cell state. In this study we propose calibrating the parameters in a distributed fashion in accordance with some climatic zones. They are areas in which we assume homogeneous climate conditions (P and T) and parameters of the CA model. Those climatic zones (k) are discretized in cells (i,j) to perform simulations with the objective of determining the state of the cell (0 if it is free of snow and 1 if it is covered by snow) following the below transition rules:

- (1) If $P(k, t) \geq P_0(k)$ and $H(i, j) > H_s(k, t)$ then $S(i, j, t) = 1$
- (2) If $P(k, t) < P_0(k)$
 - a. If $T(k, t) - T(k, t - 1) \leq T_c(k) > 0$ then $S(i, j, t) = S(i, j, t - 1)$
 - b. If $T(k, t) - T(k, t - 1) > T_c(k) > 0$ then
 - I. If $S(i, j, t - 1) = 0$ then $S(i, j, t) = 0$
 - II. If $S(i, j, t - 1) = 1$ then
 - i. If $N(i, j, t) \leq N_m(k)$ then $S(i, j, t) = 0$

ii. If $N(i, j, t) > N_m(k)$ then $S(i, j, t) = 1$

where $H_s(k, t)$ is the elevation of the snowline for climatic zone k and day t defined as $H_s(k, t) = a(k) + b(k) \cdot T(k, t)$, and $N(i, j, t)$ is the number of neighbour cells with $S(i, j, t - 1) = 1$, considering a neighbourhood of 24 cells in which all the cells are close enough to have the same influence on cell state.

Note that rules a. and b. could be replaced by more global rules in order to have a more physical explanation, as follows:

a'. If $T(k, t) \leq T_c(k) > 0$ then $S(i, j, t) = S(i, j, t - 1)$

b'. If $T(k, t) > T_c(k) > 0$ then

I. If $S(i, j, t - 1) = 0$ then $S(i, j, t) = 0$

II. If $S(i, j, t - 1) = 1$ then

i. If $N(i, j, t) \leq N_m(k)$ then $S(i, j, t) = 0$

ii. If $N(i, j, t) > N_m(k)$ then $S(i, j, t) = 1$

The main rule that defines the accumulation of snow in the CA model depends on the precipitation threshold and the snowline. The snowline is the altitude above which the terrain can have snow and it is approached by a straight line defined by parameters a and b and the temperature. It varies with the time and the climatic zone. If the elevation of a cell is above the snowline elevation and precipitation is sufficient, the state of the cell will be 1 (snow covered). The other two parameters, T_c and N_m are related to the snow melt processes, when a pixel at state 1 changes to state 0. A higher temperature with respect to the previous day (rules a. and b.) or with respect to the global threshold (rules a'. and b'.) are related to snowmelt. In the same way, a lower number of neighbour cells with snow is also related to snowmelt. That is, a large number of neighbour cells with snow imply more inertia in the cell to continue with the same state (i.e., with snow), while a small number of neighbour cells with snow implies that the cell is close to the border of the snowpack and has less inertia to change to the non-snow state .

In the model proposed by Pardo-Igúzquiza *et al.* (2017) the search for the parameters' optimal values in the calibration phase is done by varying one parameter and leaving the remaining ones fixed. In this study, we have modified the algorithm to vary all parameters simultaneously. An initial range of three values for each parameter is defined; then the ranges of all parameters are moved simultaneously until the optimal value is located in the middle of the range. The set of values yielding the minimum mean squared error (MSE) between the experimental and simulated SCA for the calibration period are chosen as the best parameters.

CA models are distributed if the driving variables and parameters are distributed spatially, or lumped if unique indices and parameters are used for the entire mountain range. In order to test distributed approaches, the calibration of a previous lumped CA model is used as a 'first

iteration', to identify and select the best driving variables and define the 'set-up' or initial values of parameters for the distributed case. The numerical experiment that uses lumped series and parameters allows several driving variables and parameters to be tested simultaneously and, due to its low computational cost, saves time compared to setting up the distributed case from zero; the optimal parameters for the lumped case provide an idea of the interval ranges to be used in the distributed case. For the distributed cases, climatic indices (P and T) can be defined over a grid containing different climatic zones. This grid can have a resolution that is the same or coarser than the SCA grid. A semi-distributed case can be developed if we use distributed climatic indices and lumped parameters. The computational cost of distributed approaches depends on the resolution of the grids. If a fine calculation grid is chosen in which several climatic zones are defined, the search for optimal parameters can be done in two phases in order to avoid excessive calculation times for the algorithm. Some parameters can be fixed in the first phase according the results of the lumped case, then varied in the second phase. Different distributed variants can be tested with respect to the driving variables (the climatic indices of each climatic zone can be used as driving variables for that climatic zone or for the whole mountain range) and the domain of minimization (parameters can be calibrated by minimising the MSE for each climatic zone in the entire mountain range). These different configurations need to be tested for each case study in order to find the best results in the calibration and validation phases.

With respect to the uncertainties of the CA model, it should be noted that the architecture of the CA is not probabilistic and thus it is impossible to evaluate the intrinsic uncertainty of the model. This uncertainty can be decreased by improving the approach provided in the initial CA model. Uncertainty in the parameters could be evaluated by considering the following assumptions:

- 1) The calibration process, where the mean square error is minimised, can be seen as a least squares estimation procedure.
- 2) The parameters are going to be considered as a set of joint Gaussian variables.
- 3) Given (2), the estimation procedure in (1) is equivalent to the maximum likelihood estimation.
- 4) An approximate variance–covariance matrix (C), assuming a Gaussian distribution of the parameters, is estimated by standard nonlinear inversion theory (Menke, 1984):

$$C \approx [J^T \cdot \Gamma^{-1} \cdot J]^{-1} \quad (1)$$

where J is the Jacobian or sensitivity matrix evaluated at the generalised least square estimates and Γ is the identity matrix multiplied by the MSE in the validation period. On the other hand, the uncertainty of the CA model outputs can be quantified by considering the MSE of the calibration period to be the variance in the validation period. This procedure allows for a representation of the uncertainty interval [$\text{SCA estimate} - \sigma$, $\text{SCA estimate} + \sigma$] for the validation period and for a comparison of the number of days with experimental data within this interval to the theoretical value, assuming a Gaussian distribution (68%).

The CA model presented in this study only considers three driving variables: elevation, which can be considered constant for the temporal scale used in hydrological studies, and

precipitation and temperature, which can be varied in accordance with climate change scenarios. Calibrated CA models allow the impact of potential climate change scenarios on SCA to be assessed using the future series generated for the driving variables selected. Also, if we consider distributed CA models, the spatial variation of climate change can be incorporated into the study. Note that the CA model presented is only able to assess the potential impacts of climate change due to precipitation and temperature. RCMs have significant bias with respect to the historical series. Statistical correction techniques (*e.g.*, first moment correction, second moment correction, regression, quantile mapping) can be used to reduce this bias. Bias correction and delta change correction techniques can be applied to the RCM to obtain the future precipitation and temperature series.

In this study we apply both bias and delta change approaches. The second moment correction technique is used in both cases. This technique corrects both mean and standard deviation to define the transformation function. We applied the transformation function proposed by Pulido-Velazquez *et al.* (2011) for the delta change method. Ensembles of the future series are proposed to obtain more representative potential future climate scenarios. We used equifeasible solutions (considering all RCM simulations) for the bias correction and delta change methods.

The future precipitation and temperature series generated were used as input for the selected distributed CA model (previously calibrated) to assess the potential changes in SCA.

3. Application to the case study and data employed

3.1. Case study

Our case study is the Sierra Nevada mountain range in southern Spain (see Figure 7.1.A). It extends over 80 km, is between 15 and 30 km wide and covers more than 2000 km². It includes the highest point on the Iberian Peninsula – Mulhacén Peak, which is 3,478.6 m a.s.l. The Sierra Nevada enjoys a high-mountain Mediterranean climate with relatively dry summers, and wetter winters, during which the majority of precipitation falls as snow. Thus, snowfall dynamics are essential to the availability of water in the Sierra Nevada catchments. The study of these dynamics and future potential changes in SCA is a key issue for the region from the point of view of the ski industry, which is an important economic driver, but also from a water resources standpoint. This study proposes a new methodology than could provide useful knowledge about the future impacts of climate change on sensitive, high-altitude landscapes, such as in this case of the alpine mountains of the Spanish Sierra Nevada. In our case study, LULC changes in the historical period employed for the calibration are not very significant. Note that the area of interest in this study is an alpine area where forest canopy is scarce (Figure 7.1.B). Assessing SCA dynamics in forested areas is more difficult due to the interaction between snow and vegetation and therefore it would be necessary to assess the suitability of the proposed method in these cases (see section 4).

3.2. Application to the case study

The CA model considered requires an input of SCA data, which can be collected from satellite images. In our case study, the experimental SCA data were taken from a MODIS satellite product. We used the MODIS/Terra Snow Cover Daily Global 500 m Grid (Data Set ID: MOD10A1), which has a spatial resolution of approximately 460 m for the latitude of the study area and a temporal resolution of 1 day. The SCA data were transformed to binary codes (1 = covered by snow; 0 = snow-free). The grid used by this product was also used for the calculations. There are around 4100 cells in a 460 m x 460 m grid inside the area of interest (Figure 7.1).

The CA model also requires climatic indices (P and T) as driving variables. These were obtained from the Spain02 project dataset (Herrera *et al.*, 2012, 2016). The Spain02 dataset contains daily temperature (maximum, mean and minimum) and precipitation estimates from historical data (around 2500 monitoring stations) collected by the Spanish Meteorological Agency over the period 1971–2010. We used version 4 (v4) of the Spain02 project dataset (<http://www.meteo.unican.es/en/datasets/spain02>), which includes daily field estimates with a spatial resolution of approximately 12.5 km using the Euro-CORDEX grid. In the case study, we have defined the climatic zones (introduced in the previous section) using the Euro-CORDEX grid (see Figure 7.1). The parameters and driving variables depend on the climatic zones in the distributed cases.

We applied the modified algorithm (varying the parameters simultaneously) to a three-year timespan (the calibration period was 1 July 2000 to 30 June 2003, whilst the validation period was 1 July 2003 to 30 June 2006). We have selected these periods due to the availability of data, but a comparison between different periods could be useful in order to assess the impact of selecting adjacent years.

For the case study we have tested different numerical experiments (approaches) with respect to the spatial distribution of driving variables and parameters (lumped or distributed), the tested variables (different variables and elevation thresholds), the calibration procedure (minimization of error and searching for optimal parameters) and temperature threshold (global or linked to the previous day). All of these numerical experiments are summarised in the following lines.

As a first approach, we tested lumped driving variables (mean precipitation, and maximum, mean and minimum temperatures above 1000, 1500, 2000, 2500 and 3000 m a.s.l.) [numerical experiment A1]. Figure 7.2 shows the MSE for the various combinations of elevations and variables. From numerical experiment A1, we selected precipitation and maximum temperature above 1000 meters as the driving variables. Better approximations were obtained – in the sense that a smaller MSE was achieved – than for numerical experiment AA (performed by Pardo-Igúzquiza *et al.* (2017)) (MSE of 259,750 cells² versus 264,896 cells²), while the validation results were slightly worse (MSE of 457,804 cells² versus 451,212 cells²). The optimal parameters obtained for numerical experiment A1 were ($P_0 = 6.8$; $a = 1140$; $b = 80$; $T_c = 0$; $N_m = 14$) while for numerical experiment AA the results were ($P_0 = 6.8$; $a = 1170$; $b = 80$; $T_c = 0$; $N_m = 14$). Also, this lumped CA approach (numerical

experiment A1) has been compared to a logistic regression alternative. For this application, we considered the same explanatory variables as in the CA approach. The logistic regression provided worse results (MSE of 571,406 cells² in the calibration case and 1,019,121 cells² in the validation case), underestimating SCA in winter and overestimating SCA in summer. Note that techniques based on regression are performed using the mean of the dependent and independent variables. Therefore they are more sensitive to outliers and less able to capture spatiotemporal variability. In addition, the absence of snow in summer is not properly approached by the regression model. Therefore, the CA methodology provides better approximations than standard regression approaches. For these reasons, the great interest in studying distributed numerical CA solutions is justified.

The variables selected for numerical experiment A1 were used as driving variables for all the distributed numerical experiments (A2, D1, D2, D3). In these distributed numerical experiments, the parameters N_m and T_c from numerical experiment A1 remained fixed, while the remainder were varied, due to the high computational cost of the distributed approaches. Nevertheless, in a subsequent procedure, these parameters were also calibrated for the numerical experiment that had the best results in the first stage. Numerical experiment D2 produced the best results, so a second numerical experiment (D2.1) was performed based on D2 (now varying N_m and T_c and having all other variables remain fixed). This numerical experiment yielded an improvement with respect to the lumped approach developed by Pardo Igúzquiza *et al.* (2017) (-6.6% MSE for the calibration period and -10.1% MSE for the validation period). Like Pardo Igúzquiza *et al.* (2017), in the current study, we tested the possibility of using an absolute temperature threshold instead of a threshold that depends on the previous day (rules a' and b' of the formulation), because it seems to be more reasonable physically (numerical experiments D4 and D4.1), but the approximations obtained were poorer than in Pardo Igúzquiza *et al.* (2017). Table 7.1 shows a summary of the CA model numerical experiments performed and their results.

In light of the results, numerical experiment D2.1 was selected to perform the next analysis. In this numerical experiment, the CA parameters were calibrated by minimising the MSE for each climatic zone where the driving variables are defined (Euro-CORDEX grid). For each climatic zone we calibrated the CA model using the climatological indices of the climatic zone as driving variables for the entire mountain range. We repeated this procedure for all climatic zones in order to obtain distributed parameters. The optimal value of the parameters in the various climatic zones was plotted against the mean elevation of each climatic zone in order to test for possible correlations (Figure 7.3).

All parameters, with the exception of T_c , show significant correlations to elevation. Parameters P_0 , a and b increase with elevation, while N_m decreases. When the CA model is applied using these parameters, the best estimated dynamics of daily SCA are obtained. This configuration shows the lowest MSE, which implies the smallest differences between estimated and experimental SCA. In order to assess the performance of the CA model, we calculated the SCA for each day for the entire mountain range and the experimental and estimated datasets. These results are shown in Figure 7.4.

In general, extreme snowfall events are underestimated, but general SCA dynamics are captured. We further calculated the number of cells where snow cover exceeded 5, 15, 25 and 35% of days in order to assess the spatial distribution of snowfall. Figure 7.5 shows that experimental and estimated SCA have a very similar pattern.

Thus, we demonstrate that the CA model applied is able to reproduce the spatial dynamics of SCA for the calibration period. In the same way, the validation results are shown in Figures 7.6 and 7.7. Again, the temporal SCA dynamics are captured but extreme snowfall events are underestimated.

We have also compared the estimates to experimental data cell by cell for the calibration and validation data, obtaining the failure probability of the CA model in two situations: errors when the cell is covered, and when there is no snow (see Figure 7.8). Note that the model is more likely to fail when the cell is covered by snow ($S(i, j, t) = 1$) at lower elevations where snow dynamics change more quickly. From the point of view of water resources quantification, these errors are not very important because at those elevations snow thickness is lower. With respect to spatial distribution, the probability of failure is similar for the two periods and the two cases (snow covered or snow-free).

Furthermore, we have evaluated the uncertainty of parameters using the procedure explained in section 2 (Equation 1) for the lumped CA model. The standard deviations of the calibrated parameters are shown in Table 7.2. The uncertainty of the CA model outputs has been quantified by considering the MSE of the calibration period as explained in section 2. The experimental data and the uncertainty interval defined by estimates \pm standard deviations of SCA are shown in Figure 7.9. For the case study, on 69.1% of the days the experimental data are within the uncertainty interval. This value is similar to the theoretical value assuming a Gaussian distribution, represented by 68%.

As noted in the methodology section, the climate change information used to generate potential future scenarios can be taken from the RCM. In our case study, we used nine RCMs from the CORDEX PROJECT (2013). We selected the most pessimistic emissions scenario of the project, Representative Concentration Pathways 8.5 (RCP8.5). Table 7.3 shows the RCMs used and the GCM in which they are nested.

We considered the historical period 1971-2000 and the future period 2071-2100 to perform the statistical transformations used to generate the potential future scenarios. The method was systematically applied to all cells of the Euro-Cordex grid inside the study area to obtain the future precipitation and maximum temperature series (the driving variables selected for the CA model). We considered two precipitation and temperature climate change scenarios, depending on which approach was employed – delta change (E1) or bias correction (E2). These two scenarios, E1 and E2, are equi-feasible solutions obtained from the nine RCMs considered. These two future scenarios are used as the driving variables for the calibrated CA model in order to obtain potential future scenarios of snow cover area due to climate change. An example of the precipitation and temperature time series generated for a particular cell is presented in Figure 7.10.

There is a significant reduction in precipitation and a significant increase in temperature. The means of the series generated for the two scenarios are similar in the case of precipitation and the same in the case of maximum temperature. Theoretically, the means must be the same in the two scenarios, even though the time series are different, so that the two scenarios have different behaviour when they are fed into the CA model. However, in the case of precipitation, the small differences are due to negative values generated in the statistical process that are corrected to zero.

In order to evaluate potential climate change spatially, we calculated the relative changes in precipitation and maximum temperature for all cells, plotting them with respect to elevation (see Figure 7.11).

Figure 7.11 shows that climate change leads to an increase in maximum temperature and a decrease in precipitation with elevation. So, in this alpine system the potential climate change will be greater in the case of temperature and smaller in the case of precipitation for higher elevations.

The CA model was fed with the series generated for the two scenarios. This yielded significant reductions in SCA (59.0% for E1 and 61.7% for E2). The size of the reduction depends on the month (Table 7.4).

Figures 7.12 and 7.13 shows the mean monthly and daily historical and future SCA, respectively. Graphically, we verified that potential reductions in SCA are highly significant. Figure 7.14 shows the cells with snow cover on more than 5, 15, 25 and 35% of days for the historical and future potential scenarios; again, the potential reductions are significant.

4. Limitations and future research

It should be noted that when hydrological models, especially those defined at a regional scale covering an extensive area with heterogeneous conditions (as in our case), are employed to simulate conditions and that are very different from those used to calibrate and validate the model, uncertainty in the assessment increases. For this reason, all the models should be validated again when new information is available. This occurs even with physical hydrological models (e.g. groundwater flow models, rainfall-runoff models, etc.). Our model, although it is not based on such physical models, provides coherent solutions with the capability to predict very extreme conditions; for example, if snow is not present, it does not show any values of SCA.

Nevertheless, as explained above, in all models uncertainty grows when they are used to simulate very different conditions. The patterns and variability of future climate conditions may be considerably different from the historical/current climate data used to calibrate and validate the model's parameters (the model's rules in our approach) (IPCC, 2007; 2013). However, despite the inevitable uncertainty in predicting the impact of climate change (an uncertainty that also exists in many other aspects analysed by the scientific community, both within physical and non-physical processes, and which is also inherent to the definition of potential climate change scenarios), there is a clear need to provide a quantitative assessment

of potential hydrological impacts. This will allow scientists to rationally evaluate potential adaptation strategies for maintaining sustainable management of water resources systems, which may be very vulnerable to climate change. Due to the importance to society of understanding the potential impacts of climate change, although there may be uncertainties involved in this impact assessment, scientific production on this issue is very relevant (*e.g.*, Brown and Mote, 2009; Vorosmarty *et al.*, 2000).

In this work we assume a steady LULC in historical and future scenarios in order to perform a sensitivity analysis of the SCA dynamics to potential future climate scenarios. Therefore, representative SCA results can be provided for long-term future climate periods if we assume that LULC will remain quite similar to its historical data, or that the changes do not have an important influence on the snow dynamic. The CA model has been calibrated and validated with P and T time series from recent years and it only requires P and T time series in order to assess the impact on the future evolution of SCA. Suppose we take the P and T time series projected for the year 2100. There will be, on average, less rainfall and higher temperatures. Suppose that these time series are taken to be the record from a recent abnormally dry and hot year. We would think that the output of the model is valid for this recent year, although we are using the projections for the year 2100. Thus, as long as we assume that the calibration is robust in accordance with the validation performed, and make the hypothesis that the parameters (rules, in our approach) will remain invariable in the future, as they depend on P and T only (because topographic parameters may be considered constant at a timescale of one hundred years), the use of CA will be valid for addressing SCA dynamics in the future. The spatial change in the global circulation of the atmosphere has already been taken into account in the P and T time series projections for the future.

New research would be needed to use the same CA model to study a historical period with significant LULC changes, or to simulate potential future impacts that also include future LULC changes. Most likely, such models would need to include other spatial variables influenced by LULC in the rules.

Additionally, different parameter sets can lead to similar responses in the SCA dynamics (principle of equifinality). The analysis of parameters in this deterministic model cannot be used to draw conclusions about the factors that influence snow dynamics. As a future line of research, a new approach would be required to perform a more complete analysis of the factors that influence SCA, combining stochastic and physical-based models.

5. Conclusions

A CA model to estimate SCA has been calibrated and validated with good results for the Sierra Nevada mountain range (southern Spain). We implemented several lumped and distributed numerical experiments (varying the driving variables, algorithm parameters, minimisation procedure, search for optimal parameters and temperature) based on a lumped CA model developed by Pardo-Igúzquiza *et al.* (2017). The best implementation (numerical experiment D2.1) reduced the MSE by 6.6% and 10.1% in the calibration and validation periods, respectively, compared to the initial lumped CA model. Subsequently, we used this

best CA model numerical experiment to assess the impacts of climate change on snow cover dynamics using future precipitation and temperature scenarios as driving variables.

When the relative changes in the future precipitation and maximum temperature time series generated (with respect to the historical series) are plotted against mean elevation in each grid, we conclude that, in this alpine case study, potential climate change at higher altitudes will result in higher temperatures and lower precipitation.

The future series generated was used as an input for the calibrated CA model, leading to the worrying result that there will be a drastic reduction in snow cover area in the future. Using the future precipitation and temperature scenarios as driving variables for the period 2071–2100, we obtain a significant reduction in snow cover area using the calibrated CA model (59.0% for E1 and 61.7% for E2).

Thus, the distributed CA developed is proved to be a useful tool for predicting the future evolution of snowpack. This tool can be applied to various management tasks, including water resources management, operational river forecasts and landscape management.

Acknowledgements

This research was funded by the research projects CGL2013-48424-C2-2-R and CGL2015-71510-R from the Spanish ‘Ministerio de Economía y Competitividad’ and the European ESSEM COST Action ES1404. We would also like to acknowledge NASA’s DAAC for the SCA data, the Spain02 project for the precipitation and temperature data and the CORDEX project for the climatic change information. Valuable comments and suggestions by an editor, associate editor and two anonymous referees are greatly appreciated.

References

- Ackerman, S. A., Strabala, K. I., Menzel, P. W. P., Frey, R. A., Moeller, C. C., Gumley, L. E., 1998. Discriminating clear sky from clouds with MODIS. *J. Geophys Res.*, 103, 32141–32157.
- Arnell, N.W., Lloyd-Hughes, B., 2013. The global-scale impacts of climate change on water resources and flooding under new climate and socio-economic scenarios. *Clim. Chang.* 122, 127–140.
- Beniston, M., 2003. Climatic Change in Mountain Regions: A Review of Possible Impacts. *Climatic Change* 59. doi: 10.1023/A:1024458411589.
- Barnett, T. P., Adam, J.C., Lettenmaier, D.P., 2005. Potential impacts of a warming climate on water availability in snow-dominated regions. *Nature* 438, 303–309. doi:10.1038/nature04141.
- Bormann, K.J., Westra, S., Evans, J.P., McCabe, M.F., 2013. Spatial and temporal variability in seasonal snow density. *Journal of Hydrology* 484, 63–73.
- Brown, R.D., Mote, P.W., 2009. The response of northern hemisphere snow cover to a

- changing climate. *J. Clim.* 22 (8), 2124–2145. doi: 10.1175/2008JCLI2665.1.
- Chen, J., Brissette, F.P., Chaumont, D., & Braun, M., 2013. Performance and uncertainty evaluation of empirical downscaling methods in quantifying the climate change impacts on hydrology over two North American river basins. *J. Hydrol.* 479(0), 200-214. doi:10.1016/j.jhydrol.2012.11.062.
- Chen, J., Brissette, F. P. & Leconte, R., 2014. Assessing regression-based statistical approaches for downscaling precipitation over North America. *Hydrol. Process.* 28, 3482–3504. doi:10.1002/hyp.9889
- Collados-Lara, A.J., Pardo-Iguzquiza, E., Pulido-Velazquez, D., 2017. Spatio-temporal estimation of snowpack thickness using point data from snow stakes, digital terrain models and satellite data. *Hydrol. Process.* 31, 1966-1982. doi: 10.1002/hyp.11165.
- Collados-Lara, A.J., Pulido-Velazquez, D., Pardo-Iguzquiza, E., 2018. An integrated statistical method to generate potential future climate scenarios to analyse droughts. *Water* 10, 1224. doi:10.3390/w10091224.
- Cook, B., Miller, R., Seager, R., 2008. Dust and sea surface temperature forcing of the 1930s “Dust Bowl” drought. *Geophys. Res. Lett.* 35(8), L08, 710.
- CORDEX PROJECT. 2013. The Coordinated Regional Climate Downscaling Experiment CORDEX. Program sponsored by World Climate Research Program (WCRP). Available at: <http://wcrp-cordex.ipsl.jussieu.fr/>
- Edwards, A.C., Scalenghe, R., Freppaz, M., 2007. Changes in the seasonal snow cover of alpine regions and its effect on soil processes: a review. *Quaternary Int.* 172,162–163.
- Gobiet, A., Kotlarski S., Beniston, M., Heinrich, G., Rajczak, J., Stoffel, M., 2014. 21st century climate change in the European Alps-a review. *Sci. Total Environ.* 493,1138–1151. doi: 10.1016/j.scitotenv.2013.07.050.
- Herrera, S., Gutiérrez, J.M., Ancell, R., Pons, M.R., Frías, M.D., Fernández, J., 2012. Development and analysis of a 50-year high-resolution daily gridded precipitation dataset over Spain (Spain02). *Int. J. Climatol.* 32, 74–85.
- Herrera, S., Fernández, J., Gutiérrez, J.M., 2016. Update of the Spain02 gridded observational dataset for Euro-CORDEX evaluation: assessing the effect of the interpolation methodology. *Int. J. Climatol.* 36, 900–908. doi: 10.1002/joc.4391.
- Horton, P., Schaeefli, B., Mezghani, A., Hingray, B., and Musy, A., 2006. Assessment of climate-change impacts on alpine discharge regimes with climate model uncertainty. *Hydrol. Process.* 20, 2091–2109. doi:10.1002/hyp.6197, 2006.
- Hou, J.L., Huang, C.L., 2014. Improving mountainous snow cover fraction mapping via artificial neural networks combined with MODIS and ancillary topographic data. *IEEE Trans. Geosci. Remote Sens.* 52 (9), 5601–5611.

- Intergovernmental Panel on Climate Change (IPCC), 2007. Climate Change 2007: The Physical Science Basis. Contribution of Working Group I to the Fourth Assessment Report of the Intergovernmental Panel on Climate Change [S. Solomon, D. Qin, M. Manning, Z. Chen, M. Marquis, K. Averyt, M.M.B Tignor, H.L. Miller Jr, and Z. Chen (eds.)]. Cambridge University Press, Cambridge, United Kingdom and New York, NY, USA, 996 pp.
- Intergovernmental Panel on Climate Change (IPCC), 2013. Climate Change 2013: The Physical Science Basis. Contribution of Working Group I to the Fifth Assessment Report of the Intergovernmental Panel on Climate Change [Stocker, T.F., D. Qin, G.-K. Plattner, M. Tignor, S.K. Allen, J. Boschung, A. Nauels, Y. Xia, V. Bex and P.M. Midgley (eds.)]. Cambridge University Press, Cambridge, United Kingdom and New York, NY, USA, 1535 pp.
- Kucerova, D., Jenicek, M., 2014. Comparison of selected methods used for the calculation of the snowpack spatial distribution, Bystrice river basin, Czechia. *Geografie* 119 (3), 199-217.
- Kari, J., 2005. Theory of cellular automata: A survey. *Theoretical Computer Science* 334 (1-2), 3-33. doi: 10.1016/j.tcs.2004.11.021.
- Leguizamón, S., 2006. Simulation of snow-cover dynamics using the cellular automata approach. In: 8th International Symposium on High Mountain Remote Sensing Cartography, 41, pp. 87–92.
- Lopez-Moreno, J.I., Fassnacht, S.R., Heath, J. T., Jonas, T., 2013. Small scale spatial variability of snow density and depth over complex alpine terrain: Implications for estimating snow water equivalent. *Advances in Water Resources* 55, 40-52. doi:10.1016/j.advwatres.2012.08.010.
- Menke,W., 1984. Geophysical data analysis: Discrete inverse theory: Academic Press, San Diego, CA, 285 p.
- Mir, R.A., Jain, S.K., Saraf, A.K., Goswami, A., 2015. Accuracy assessment and trend analysis of MODIS-derived data on snow-covered areas in the Sutlej basin, Western Himalayas. *International Journal of Remote Sensing* 36 (15), 3837-3858.
- Mishra, B., Tripathi, N.K., Babel, M.S., 2014. An artificial neural network based snow cover predictive modeling in the higher Himalayas. *J. Mt. Sci.* 114, 825–837.
- Molotch, N.P., Fassnacht, S.R., Bales, R.C., Helfrich, S.R., 2004. Estimating the distribution of snow water equivalent and snow extent beneath cloud cover in the Salt-Verde River basin, Arizona. *Hydrol. Process.* 18 (9), 1595–1611.
- Moody, E. G., King, M.D., Schaaf, C. B., Platnick, S., 2008. MODIS derived spatially complete surface albedo products: Spatial and temporal pixel distribution and zonal averages. *J. Appl. Meteor. Climatol.* 47, 2879–2894.

- Pardo-Iguzquiza, E., Collados-Lara, A.J., Pulido-Velazquez, D., 2017. Estimation of the spatiotemporal dynamics of snow covered area by using cellular automata models. *Journal of hydrology* 550, 230-238. doi: 10.1016/j.jhydrol.2017.04.058.
- Piani, C., Haerter, J.O., Coppola, E., 2010. Statistical bias correction for daily precipitation in regional climate models over Europe. *Theor. and Appl. Clim.* 99, 187. doi:10.1007/s00704-009-0134-9.
- Pulido-Velazquez, D, Collados-Lara, A.J., Alcalá, F.J., 2017. Assessing impacts of future potential climate change scenarios on aquifer recharge in continental Spain. *Journal of hydrology*. doi: 10.1016/j.jhydrol.2017.10.077
- Pulido-Velazquez, D., García-Aróstegui, J.L., Molina, J.L., Pulido-Velázquez, M., 2015. Assessment of future groundwater recharge in semi-arid regions under climate change scenarios (Serral-Salinas aquifer, SE Spain). Could increased rainfall variability increase the recharge rate? *Hydrol. Process.* 29 (6), 828-844. doi:10.1002/hyp.10191.
- Pulido-Velazquez, D., Garrote, L., Andreu, J., Martin-Carrasco, F.J., Iglesias, A., 2011. A methodology to diagnose the effect of climate change and to identify adaptive strategies to reduce its impacts in conjunctive-use systems at basin scale. *Journal of Hydrology* 405, 110-122. doi:10.1016/j.jhydrol.2011.05.014.
- Räisänen, J., Räty, O., 2012. Projections of daily mean temperature variability in the future: cross-validation tests with ENSEMBLES regional climate simulations. *Climate Dynamics*. doi:10.1007/s00382-012-1515-9.
- Räty, O., Räisänen, J., Ylhäisi, J., 2014. Evaluation of delta change and bias correction methods for future daily precipitation: intermodal cross-validation using ENSEMBLES simulations. *Clim. Dynam.* 42, 2287-2303.
- Richer, E.E., Kampf, S.K., Fassnacht, S.R., Moore, C.C., 2013. Spatiotemporal index for analyzing controls on snow climatology: application in the Colorado Front Range. *Phys. Geogr.* 342, 85–107.
- Seager, R., Burgman, R., Kushnir, Y., Clement, A., Cook, E., Naik, N., & Miller J., 2008. Tropical Pacific forcing of North American medieval megadroughts: testing the concept with an atmosphere model forced by coral-reconstructed SSTs. *J. Climate* 21(23), 6175-6190.
- Schmugge, T.J., Kustas, W.P., Ritchie, J.C., Jackson, T.J., Rango, A., 2002. Remote sensing in hydrology. *Adv. Water Resour.* 25, 1367–1385.
- Sunyer, M.A., Hundecha, Y., Lawrence, D., Madsen, H., Willems, P., Martinkova, M., Vormoor, K., Bürger, G., Hanel, M., Kriauciuniene, J., Loukas, A., Osuch, M., Yücel, I., 2015. Inter-comparison of statistical downscaling methods for projection of extreme precipitation in Europe. *Hydrology and Earth System Sciences* 19 (4), 1827-1847.

- Thirel, G., Salamon, P., Burek, P., Kalas, M., 2013. Assimilation of MODIS snow cover area data in a distributed hydrological model using the particle filter. *Remote Sensing* 5, 5825-5850. doi:10.3390/rs5115825.
- Vorosmarty, C.J., Green, P., Salisbury, J., Lammers, R.B., 2000. Global water resources: vulnerability from climate change and population growth. *Science* 289, 284–288. doi:10.1126/science.289.5477.284.
- Warscher, M., Strasser, U., Kraller, G., Marke, T., Franz, H., Kunstmann, H., 2013. Performance of complex snow cover descriptions in a distributed hydrological model system: A case study for the high Alpine terrain of the Berchtesgaden Alps. *Water Resour. Res.* 49, 2619-2637. doi:10.1002/wrcr.20219.
- Watanabe, S., Kanae, S., Seto, S., Yeh, P.J.F., Hirabayashi, Y., Oki, T., 2012. Intercomparison of bias-correction methods for monthly temperature and precipitation simulated by multiple climate models. *Journal of Geophysical Research* 117, D23114. doi:10.1029/2012JD018192.
- Wolfram, S. Statistical mechanics of cellular automata. *Reviews of modern physics* 55(3), 601, 1983.
- Wolfram, S., 1984. Cellular automata: a model of complexity. *Nature* 31, 419–424
- Yucel, I., 2006. Effects of implementing MODIS land cover and albedo in MM5 at two contrasting U.S. regions. *J. Hydrometeor.* 7, 1043–1060.

Tables of the Chapter 7

Numerical experiments	Series	Calibration			Results of Validation		
		Parameters	Tested Variables	Elevation (m)	Minimization	Parameters threshold	Temperature ME (cells) MSE (cells ²)
AA*	Lumped	Lumped	- P and Tmin 1000,1500, - P and Tmed 2000, 2500 - P and Tmax and 3000	For the entire mountain range	Varying one and fixing the rest	Relative to t-1 62	264896 -49 451212
AB*	Lumped	Lumped	- P and Tmin 1000,1500, - P and Tmed 2000, 2500 - P and Tmax and 3000	For the entire mountain range	Varying one and fixing the rest	Absolute	308760 580121
AI	Lumped	Lumped	- P and Tmin 1000,1500, - P and Tmed 2000, 2500 - P and Tmax and 3000	For the entire mountain range	Varying one and simultaneously	Relative to t-1 9	259750 -115 457804
A2	Distributed (the series of each climatic zone are the driving variables for that Lumped climatic zone)	- P and Tmax 1000 (from AI)	For the entire mountain range (from AI)	Varying a, b, Po Fixing Nm,Tc (from AI)	Relative to t-1 -23	288672 -128	467104
DI	Distributed (the series of each climatic zone are the driving variables for the Distributed whole mountain range)	- P and Tmax 1000 (from AI)	For the entire mountain range (from AI)	Varying a, b, Po Fixing Nm,Tc (from AI)	Relative to t-1 II	260778 -150	422191
D2	Distributed (the series of each climatic zone are the driving variables for the Distributed whole mountain range)	- P and Tmax 1000 (from AI)	For each climatic zone (from AI)	Varying a, b, Po Fixing Nm,Tc (from AI)	Relative to t-1 8	258764 -185	412152
D2.I	Distributed (the series of each climatic zone are the driving variables for that Distributed zone)	- P and Tmax 1000 (from AI)	For each climatic zone (from AI)	Varying a, b, Po Fixing Nm,Tc (from D2)	Relative to t-1 3I	247473 -129	405806
D3	Distributed (the series of each climatic zone are the driving variables for the Distributed whole mountain range)	- P and Tmax 1000 (from AI)	For each climatic zone (from AI)	Varying a, b, Po Fixing Nm,Tc (from AI)	Relative to t-1 -9	259539 -198	424324
D4	Distributed (the series of each climatic zone are the driving variables for the Distributed whole mountain range)	- P and Tmax 1000 (from AI)	For each climatic zone (from AA)	Varying a, b, Po Fixing Nm,Tc (from AA)	Absolute 4I	292164 -285	575346
D4.I	Distributed (the series of each climatic zone are the driving variables for the Distributed whole mountain range)	- P and Tmax 1000 (from AI)	For each climatic zone (from D4)	Varying Nm,Tc Fixing a, b, Po (from D4)	Absolute 35	285639 -296	609799

*From Pardo-Iguzquiza et al. (2017)

Table 7.1. Summary of the CA numerical experiments carried out in this study.

Parameter	Optimal value	σ
Po	6.8 mm	0.20 mm
a	1140	34.35
b	80	2.77
Tc	0 °C	0.10 °C
Nm	14	0.18

Table 7.2. Optimal values of parameters and standard deviations for the lumped CA model.

RCMs \ GCMs	CNRM-CM5	EC-EARTH	MPI-ESM-LR	IPSL-CM5A-MR
CCLM4-8-17	X	X	X	
RCA4	X	X	X	
HIRHAM5		X		
RACMO22E		X		
WRF331F				X

Table 7.3. Regional Climatic Models (RCMs) and General Circulation Models (GCMs) considered for simulations.

Month	Relative changes in SCA (%)	
	Scenario E1	Scenario E2
October	-50.8	-69.7
November	-61.4	-52.5
December	-60.9	-57.8
January	-58.9	-59.8
February	-57.0	-60.8
March	-63.6	-67.2
April	-51.3	-65.3
May	-54.8	-86.6

Table 7.4. Potential relative changes in SCA for the two scenarios considered

Figures of the Chapter 7

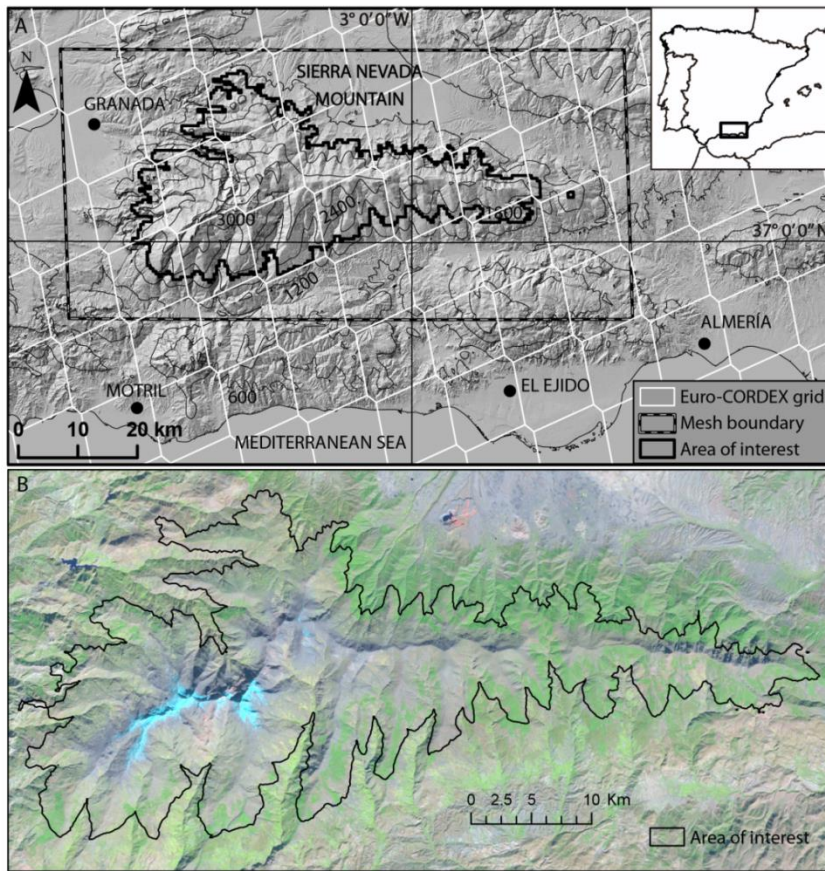


Figure 7.1. A) Location of the study area. B) Land cover of the area of interest (Day image from 01/11/1999 from the Landsat 7 satellite).

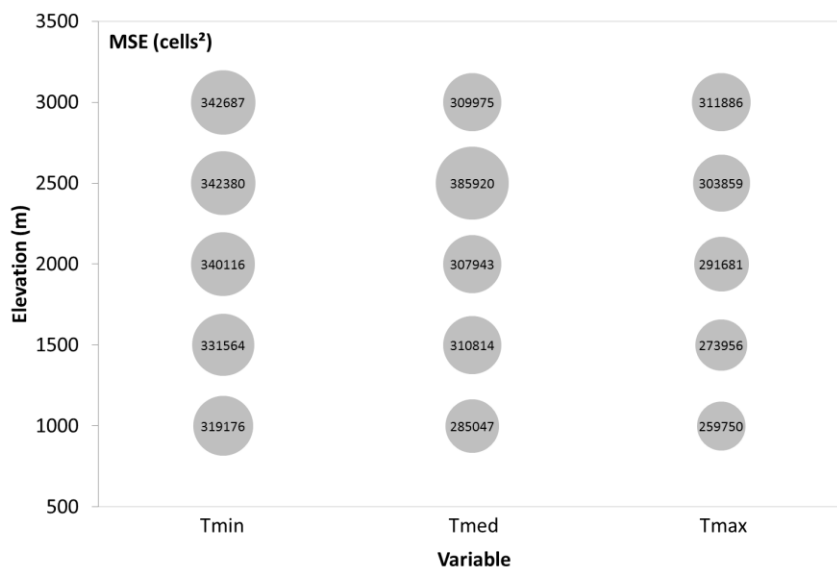


Figure 7.2. Mean squared error estimated from the number of errors in cells in the area in the calibration period for numerical experiment A1.

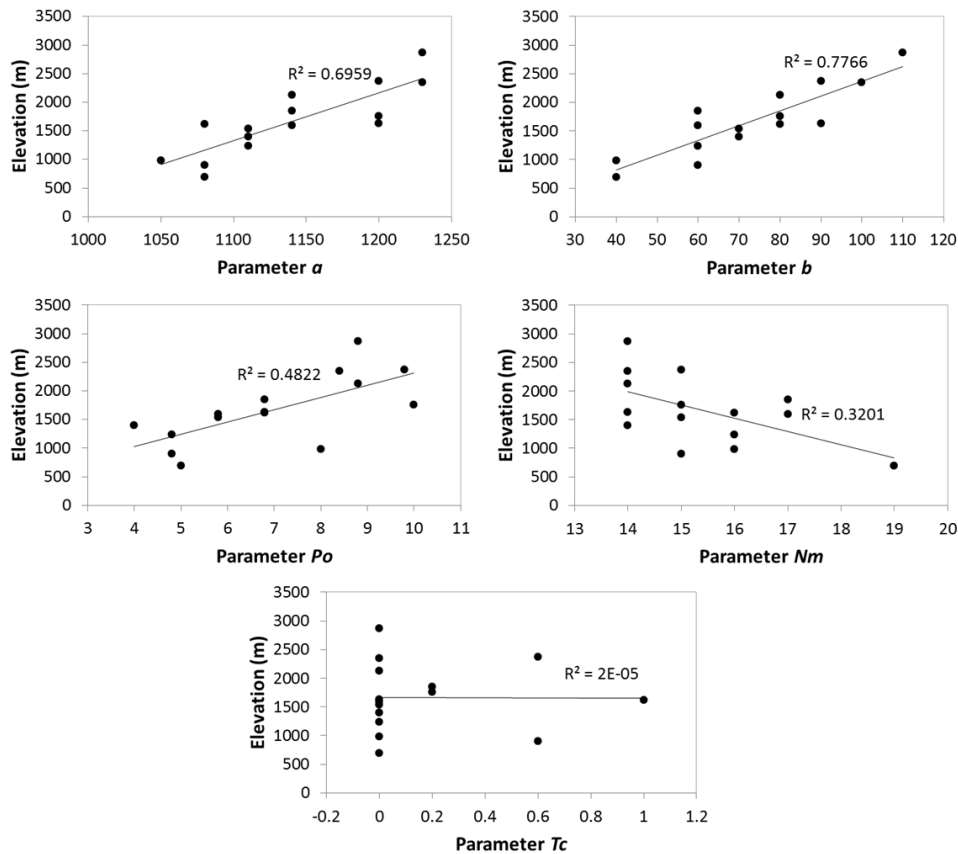


Figure 7.3. Value of the calibrated parameters in the various climatic zones compared to the mean elevation of each climatic zone.

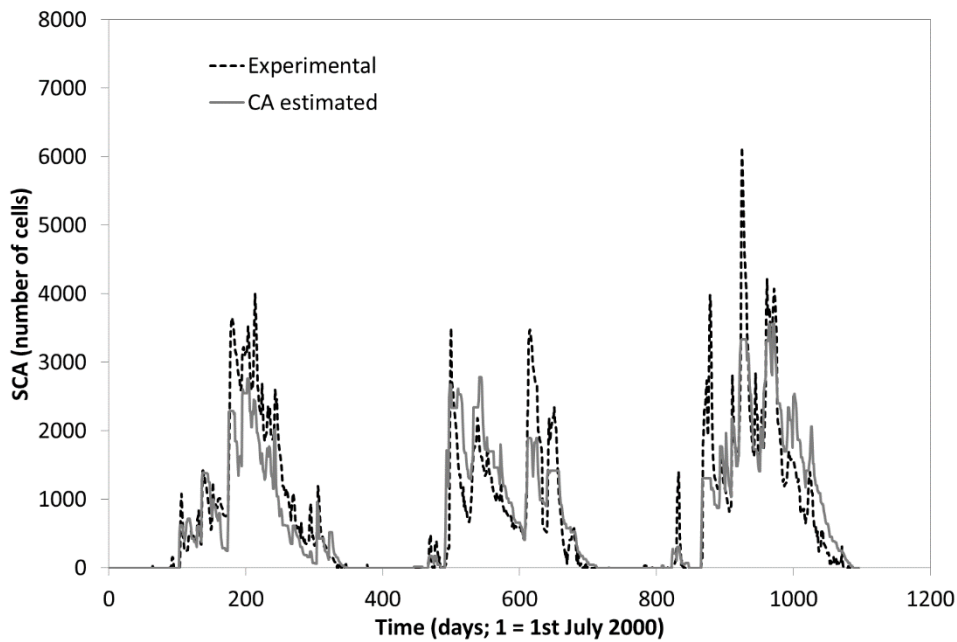


Figure 7.4. Experimental SCA and SCA estimated by the calibrated CA model over the calibration period.

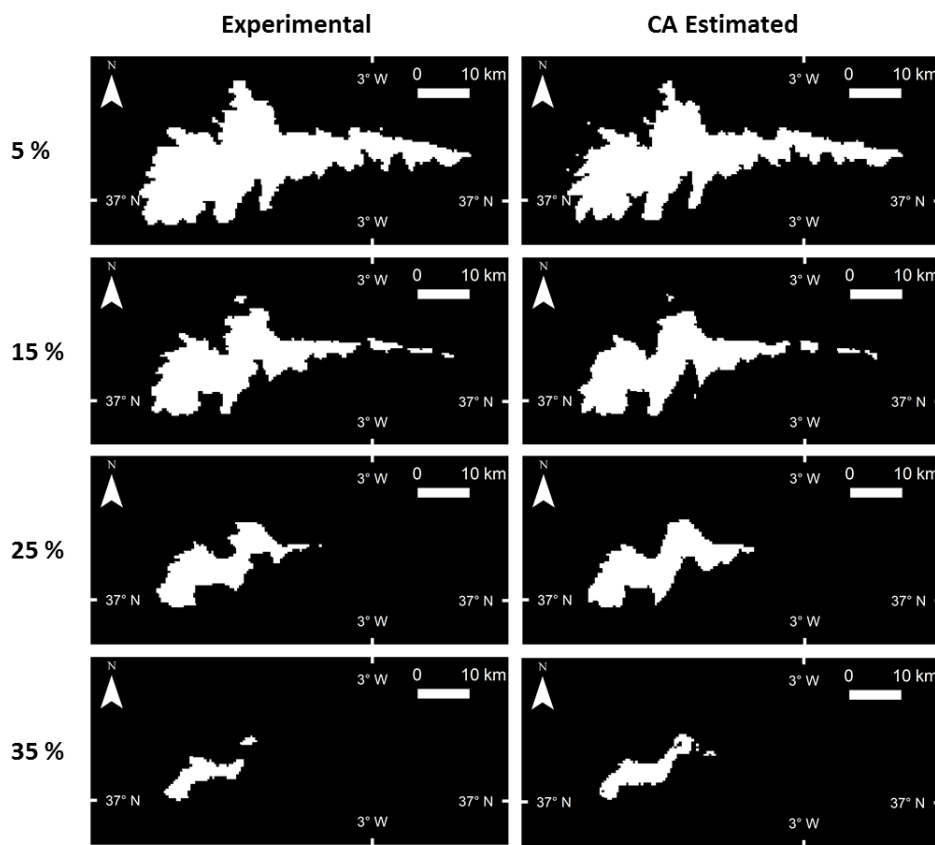


Figure 7.5. Cells where snow cover exceeds 5, 15, 25 and 35% of days for experimental and estimated SCA using the calibrated cellular automata model over the calibration period.

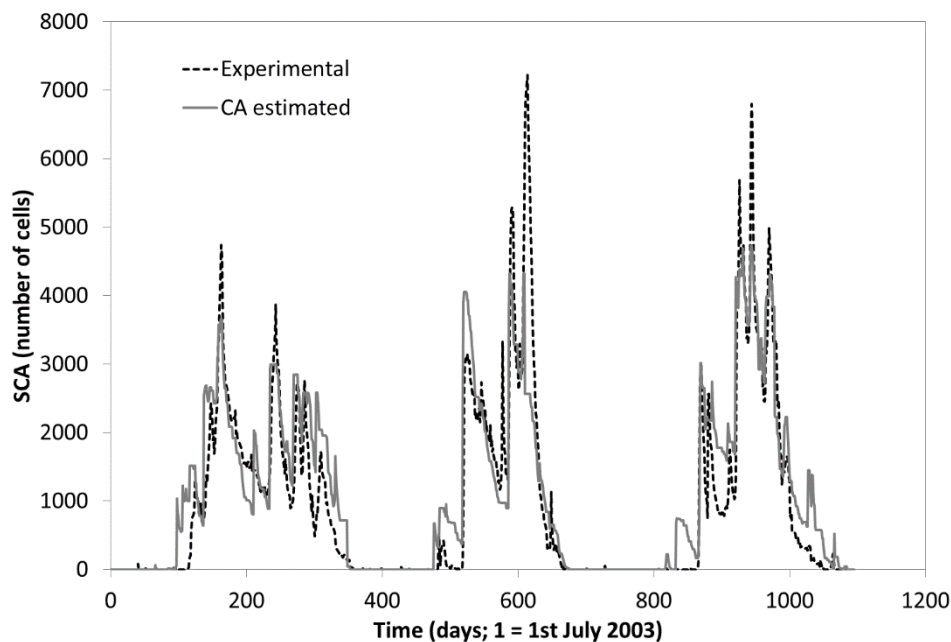


Figure 7.6. Experimental SCA and SCA estimated by the calibrated CA model for the validation period.

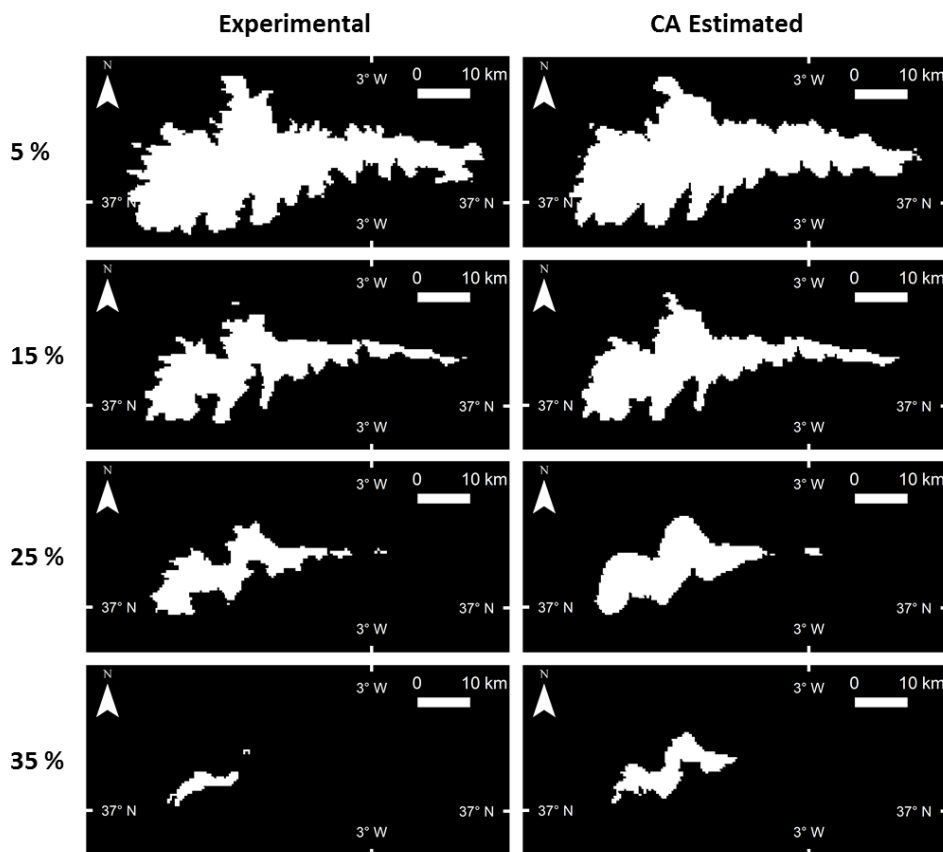


Figure 7.7. Cells where snow cover exceeds 5, 15, 25 and 35% of days for the experimental and estimated SCA using the calibrated CA model for the validation period.

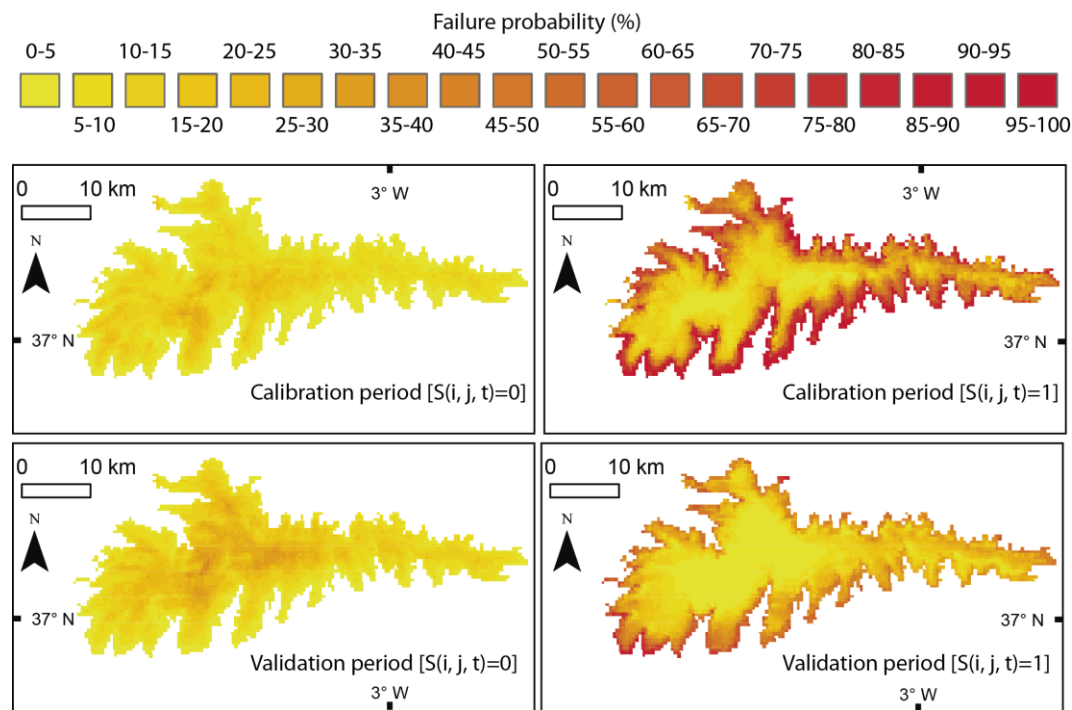


Figure 7.8. Failure probability of the CA model in the calibration and validation periods.

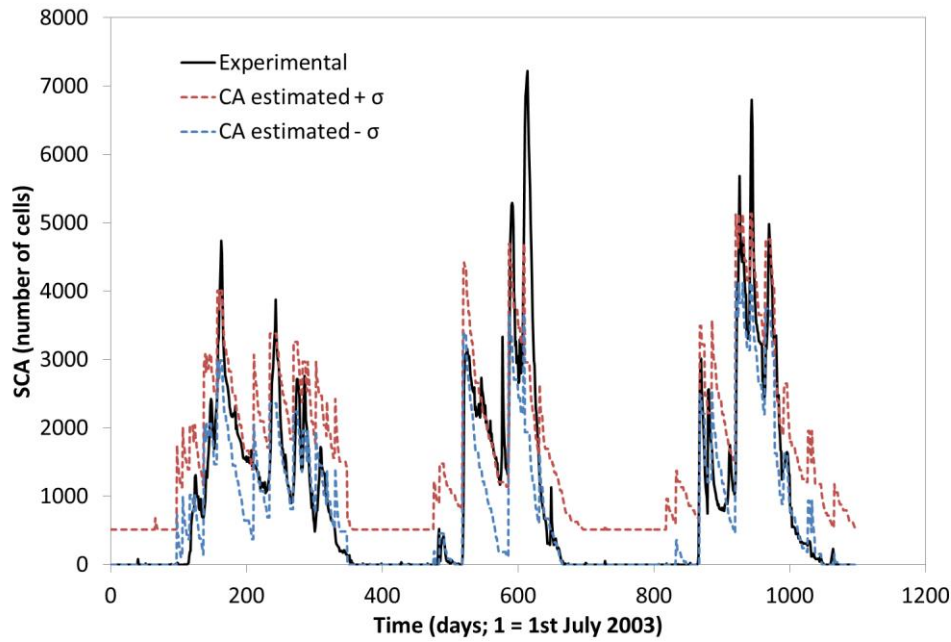


Figure 7.9. Experimental and estimates \pm standard deviation of SCA using lumped CA model for the validation period.

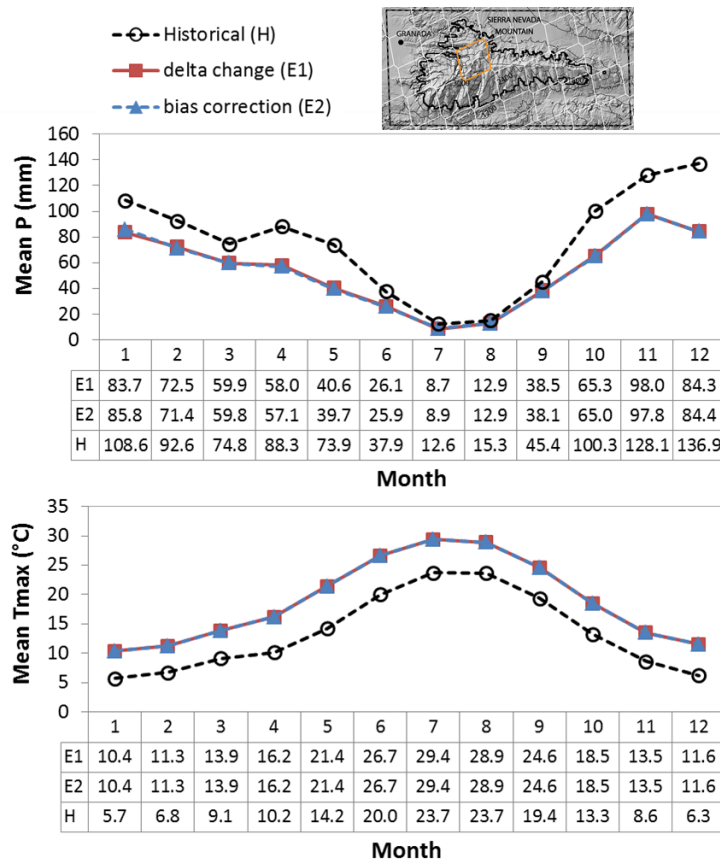


Figure 7.10. Historical and ensemble of future precipitation and maximum temperature series for the bias correction and delta change approaches for a given climatic zone.

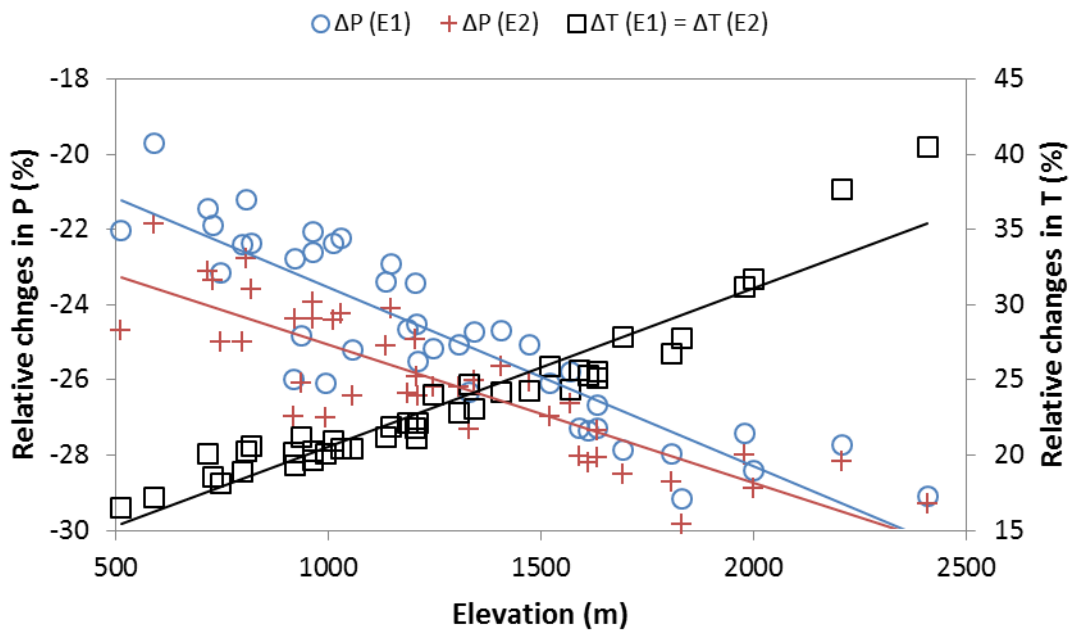


Figure 7.11. Relative changes in precipitation and temperature with respect to the elevation of each climatic zone.

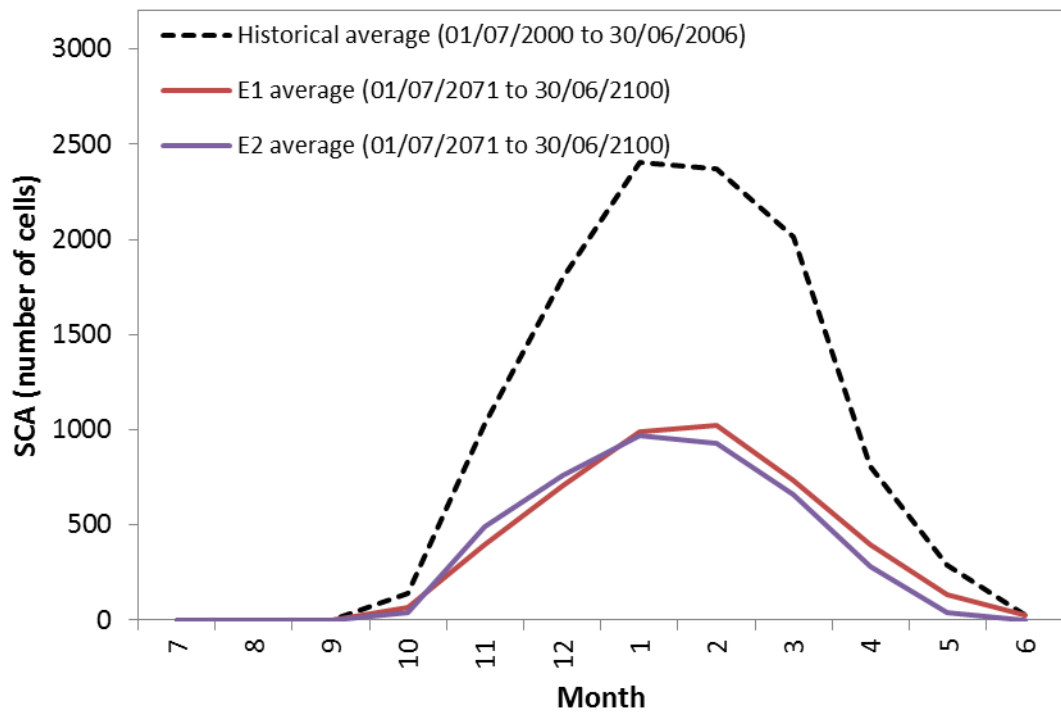


Figure 7.12. Historical and future monthly estimated SCA using the calibrated cellular automata model.

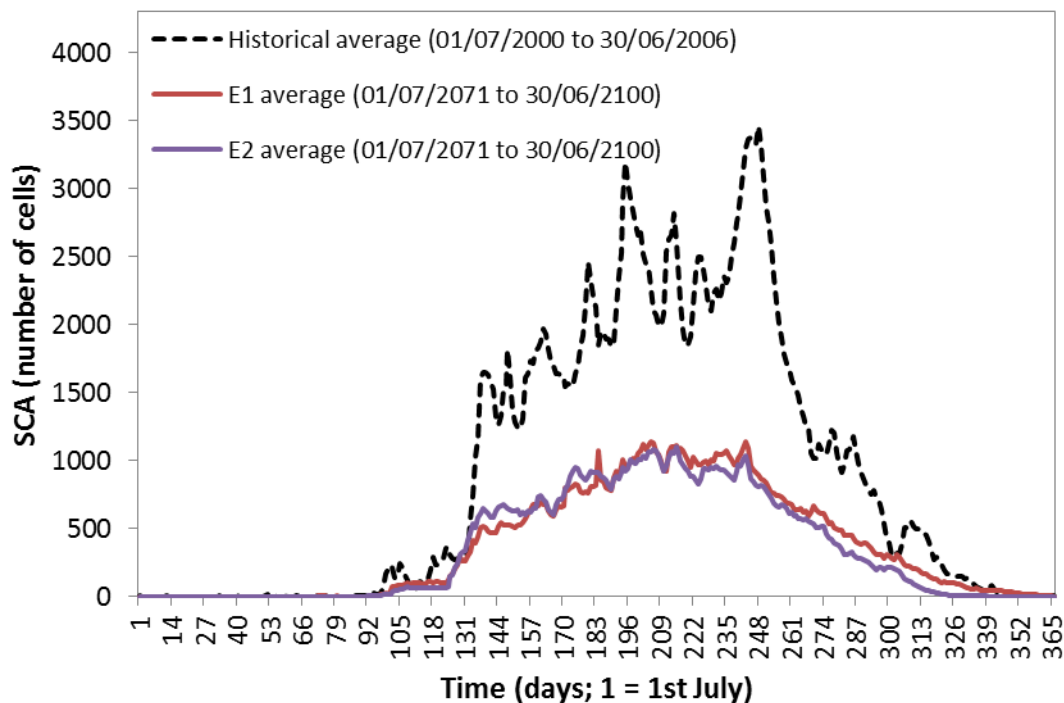


Figure 7.13. Historical and future daily estimated SCA using the calibrated cellular automata model.

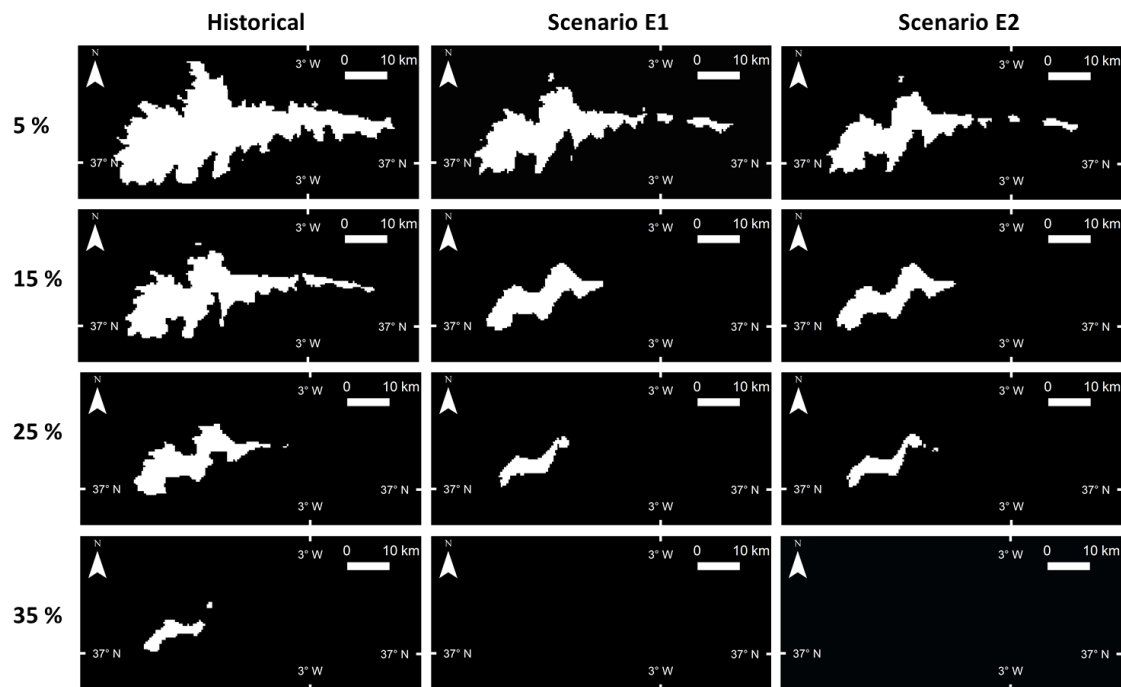


Figure 7.14. Cells with snow cover for more than 5, 15, 25 and 35% of days for the historical and future scenarios.

Chapter 8: Assessing impacts of future potential climate change scenarios on aquifer recharge in continental Spain

Journal of Hydrology 567 (2018) 803–819

Contents lists available at [ScienceDirect](#)

Journal of Hydrology

journal homepage: www.elsevier.com/locate/jhydrol

Research papers

Assessing impacts of future potential climate change scenarios on aquifer recharge in continental Spain

David Pulido-Velazquez ^{a,b}, Antonio-Juan Collados-Lara ^{a,*}, Francisco J. Alcalá ^{b,c}

 CrossMark

David Pulido-Velazquez ^(1,2), Antonio-Juan Collados-Lara ^(1,*) and Francisco J. Alcalá ^(2,3)

(1) Instituto Geológico y Minero de España (IGME), Ríos Rosas 23, 28003 Madrid (Spain).
E-mail address: d.pulido@igme.es, aj.collados@igme.es

(2) Departamento de Ciencias Politécnicas, Escuela Universitaria Politécnica, Universidad Católica San Antonio de Murcia (UCAM), 30107 Murcia (Spain). E-mail address: d.pulido@igme.es, fjalcala@ucam.edu

(3) Instituto de Ciencias Químicas Aplicadas, Facultad de Ingeniería, Universidad Autónoma de Chile, 7500138 Santiago (Chile). E-mail address: francisco.alcala.fa01@gmail.com

* Corresponding author

Abstract

Climate change will modify the availability of groundwater resources in the future. Thus the evaluation of average aquifer recharge from precipitation, and its uncertainty, becomes a key subject in determining suitable countrywide water policies. The confident prediction of renewable groundwater resources requires an accurate evaluation of aquifer recharge over time and space, especially in large territories with varied conditions for aquifer recharge such as continental Spain. This study assesses impacts of future potential climatic change scenarios on distributed net aquifer recharge (NAR) from precipitation over continental Spain. For this, the used method (1) generates future time series of climatic variables (precipitation, temperature) spatially distributed over the territory for potential aquifer recharge (PAR), and (2) simulates them within previously calibrated spatial PAR or NAR recharge models from the available historical information to provide distributed PAR or NAR time series. The information employed comes from the Spain02 project for the historical climatic data, from Alcalá and Custodio (2014, 2015) for the historical spatial NAR, and from the CORDEX EU project regional climate models (RCMs) simulations for the future climate scenarios. A distributed empirical precipitation-recharge model is defined by using a regular 10 km × 10 km grid, and

assuming that precipitation (P) and temperature (T) are the most important climatic variables determining PAR, while their spatiotemporal variabilities determine the impacts of future potential climatic scenarios on renewable groundwater resources. Potential plausible pictures of future climate scenarios are defined by combining information coming from different RCMs and General Circulation models (GCMs), downscaling techniques, and ensemble hypothesis. These scenarios were simulated within the used precipitation-recharge model to estimate impacts on NAR. The results show that global mean NAR decreases by 12% on average over continental Spain. Over 99.8% of the territory, a variable degree of recharge reduction is obtained; the reduction is quite heterogeneously distributed in line with the variety of conditions for aquifer recharge over continental Spain. The standard deviation of annual mean NAR will increase by 8% on average in the future. The dependence of these changes regarding potential explanatory variables, such as elevation and latitude was also analysed.

Key words: aquifer recharge, climate change scenarios, hydrological impacts, continental Spain

1. Introduction

The evaluation of aquifer recharge from precipitation is essential to make a quantitative evaluation of renewable groundwater resources, required to implement appropriate countrywide water policies (Freeze and Cherry, 1979; National Ground Water Association, 2004). Potential and net aquifer recharge can be evaluated. From a hydrological point of view, ‘potential’ aquifer recharge (PAR) refers to the fraction of precipitation (P) that infiltrates into the soil and percolates below the root zone. It is expected to be greater than ‘net’ aquifer recharge (NAR) (De Vries and Simmers, 2002; Andreu et al., 2011; España et al., 2013), which is the fraction of recharge that reaches the water table after some delay, smoothing out the variability inherent to precipitation events (Lerner et al., 1990; Batelaan and de Smedt, 2007). Note that precipitation events include all the atmospheric water phases reaching the land surface, such as rain, snow, dew, fog, etc. For the purpose of assessing renewable groundwater resources, the NAR fraction is what matters (Alcalá and Custodio, 2014).

Aquifer recharge evaluation is a complex task subjected to significant uncertainties inferred by governing weather and physical variables, as well as the choosing of appropriate techniques to cover different physical processes determining recharge (Milly and Eagleson, 1987; De Vries and Simmers, 2002; Clark et al., 2011). Aquifer recharge varies over space and time. So, the NAR timing may vary from daily to weekly when the water table is shallow (Andreu et al., 2011) to monthly to yearly in areas having a thick vadose zone (Alcalá et al., 2011). For example, the snow melting seasonal cycles may determine recharge rates and timing in mountainous areas (Simpson et al., 1972; Winograd et al., 1998; Earman et al., 2006).

The complexity of aquifer recharge evaluation increases when we intend to estimate potential impacts of long-term climate variability. Aquifer recharge may be subjected to variation due to global driving forces such as climate change and local human actions such as land-use transitions, and this adds to the overall uncertainty in planning future evaluations under

different climate scenarios. The main statistics (mean and standard deviation) of natural recharge from precipitation over a long enough period should not change substantially, unless they were influenced by climate or land-use changes. The steady behaviour of the cited main statistics declines when there is evidence of climate change (Milly et al., 2008; Pulido-Velazquez et al., 2015).

Due to this complexity in evaluating aquifer recharge, and taking into account that its direct measure is often unreliable over large spatial scales, several techniques have been developed to evaluate aquifer recharge at different temporal and spatial scales, ranging widely in complexity and cost (Scanlon et al., 2002; Lerner et al., 1990). Recharge estimates can be classified according to the hydrological zone to which recharge refers (soil, vadose zone, and saturated zone) and the technique employed (physical, tracer, numerical modelling, and empirical) (Lerner et al., 1990; Scanlon et al., 2002, 2006; Coes et al., 2007; McMahon et al., 2011). On aquifer or catchment scales, water-balance techniques applied in the soil and in the vadose zone provide PAR estimates while tracer techniques, hydrodynamic methods based on Darcy's Law, and groundwater numerical models applied in the saturated zone provide NAR estimates (Lerner et al., 1990; Batelaan and de Smedt, 2007; Alcalá and Custodio, 2014).

For large-scale applications, geographical information system (GIS) can be coupled with lumped and distributed hydrological models to determine the spatial distribution of PAR or NAR (Barthel 2006; Minor et al., 2007; Batelaan and de Smedt, 2007; Pulido-Velázquez et al., 2015). Several examples combine different techniques to establish the different timing of PAR and NAR associated to the use of different techniques at different spatial scales (Nolan et al., 2007; Coes et al., 2007; Alcalá et al., 2011; McMahon et al., 2011).

The choice of one of these techniques depends on the objective of the study and the available data (Lerner et al., 1990; Scanlon et al., 2002; Islam, 2015). In this paper, the selection was based on the available distributed historical information about climatic variables (Spain02 project; Herrera et al., 2016) for PAR and existing databases for NAR (Alcalá and Custodio, 2015) in continental Spain. We will propose to apply an empirical modeling approach to assess yearly recharge for future potential climate scenarios in large-scale areas, such as Continental Spain.

The impact of climate change scenarios on Groundwater is a topic that has produced a continuous interest in the research community since 1990's (cf. Vaccaro, 1992; Edmunds and Gaye, 1994; Bouraoui et al., 1999; Eckhardt and Ulbrich, 2003; Chen et al., 2004; Scibek and Allen, 2006; Jyrkama and Sykes, 2007). In recent years the number and relevance of the studies has shown a sharp increase (cf. Di Matteo et al., 2011; Green et al., 2011; Treidel et al., 2012; Klove et al., 2013; Taylor et al., 2013; Cotterman et al., 2017; Di Matteo et al., 2017; Gemitzi et al., 2017; Huang et al., 2017; Kidd, 2017; McIntyre, 2017). Regarding the spatial scale, most of the studies assessed the impacts of climate change on a specific groundwater flow system (Dragoni and Sukhija, 2008; Molina et al., 2013; Pulido-Velazquez et al., 2015), while a few encompassed regional groundwater flow systems. Impacts on groundwater were considered in some basin-scale studies (e.g., Pulido-Velazquez et al., 2011; Escriba-Bou et al., 2016; Herrmann et al., 2016) as well as for countries (Polemio, 2016) or

entire continents (Earman and Dettinger, 2011; Panwar and Chakrapani, 2013; Adhikari et al., 2015; Hartmann et al., 2015).

In this paper we propose a new systematic method to assess yearly impacts of future potential climate change scenarios on net aquifer recharge (NAR) in large scale areas. Future potential climate scenarios are generated with a non-equifileable ensemble of downscaling projections coming from different RCMs simulations. These scenarios are propagated with a new distributed empirical recharge model to estimate NAR from climatic fields. It has been applied in Continental Spain, an extensive and varied territory where no previous research work of this type has been performed. The results, which intend to be indicators of potential future plausible scenarios, are obtained under a set of hypotheses that are listed and discussed within the paper.

This paper is organized as follows. Section 2 describes the case study and available data. Section 3 presents the method used to assess potential impacts of future climatic scenarios on NAR. Subsection 3.1 defines an empirical precipitation-recharge model to simulate hydrological impacts from climatic variables (P, T). Subsection 3.2 describes the generation of future potential climatic scenarios. Subsection 3.3 describes the assessment of climate change impacts by simulating future potential climatic scenarios within a previously calibrated recharge model. Section 4 shows the results and discusses them. Finally, section 5 presents the main conclusions.

2. Materials: Description of the case study and available data

2.1 Case study: continental Spain

Continental Spain, lying between latitudes 36° and 44° N (Figure 8.1), occupies most (493,519 km²) of the Iberian Peninsula, the rest belonging to continental Portugal. A large proportion of the territory is occupied by the relatively high-elevation plains (*mesetas*), which lie at about 900 m a.s.l. in the northern half of the country and about 700 m a.s.l. in the southern half; the mountain ranges that enclose them may exceed 2500 m of elevation. The mesetas are characterised by a continental climate (MIMAM, 2000), which means hot, dry summers and cold, relatively wet winter-spring seasons.

Due to its varied geology, continental Spain has many relatively small yet high-yielding aquifers. The most important aquifers lie in Plio-Quaternary sedimentary formations in the large river valleys, and the quite extensive but compartmentalized Triassic to Tertiary carbonate massifs (Figure 8.1). The former consist of groundwater bodies surrounded by mountain ranges, small alluvial and piedmont units, and deltaic formations on infilled estuaries in coastal areas. Carbonate massifs are common, occurring in quite extensive but compartmentalised areas along the northern, eastern, and southern mountain ranges (IGME, 1993). In addition, the weathered and fissured granite and Palaeozoic shale formations in the northern, southern, and north-eastern mountain ranges contain small aquifers of local significance. The wide lithological, orographic, edaphic, and climatic diversity of continental Spain gives rise to a wide range of conditions for net aquifer recharge (NAR) (Alcalá and Custodio, 2014, 2015).

2.2 Historical climatic data

For the period 1976-2005, historical climatic (precipitation and temperature) time series were taken from the Spain02 project (Herrera et al., 2016), which includes a large database of meteorological data covering continental Spain. Precipitation (P) and temperature (T) show significant spatial heterogeneity due to the very different climatic conditions (Figure 8.2). Mean P ranges from 2000 mm year⁻¹ in the northern mountainous areas, to about 500-600 mm year⁻¹ over the northern *meseta*, and 380-500 mm year⁻¹ in the southern *meseta* (Figure 8.2.a). In the semiarid south-eastern coastal areas and north-eastern inland areas, P is around 300 mm year⁻¹ or less, and sometimes as low as 180 mm year⁻¹ (MIMAM, 2000). Precipitation occurs mainly in late autumn and winter (November to March), associated with the circulation of cold air masses from the North Atlantic Ocean and deep pressure lows that travel eastwards and generate an inflow of air masses from the Subtropical Atlantic Ocean (Trigo et al., 2004). The eastern coast of Spain may also receive precipitation from humid air masses over the western Mediterranean Sea, especially in late summer and autumn, which generally do not penetrate far inland (Martín-Vide and López-Bustins, 2006). The annual mean T varies from 4.6 to 21.1 °C (Figure 8.2.b) with minimums in January and maximums in August; the daily T amplitude on a year may be as high as 50 °C in the southern *meseta* and river valleys. There is a pronounced gradient of T with elevation in mountain areas, thus favouring the seasonal snow-melting contribution to surface and groundwater bodies (MIMAM, 2000).

2.3 Historical recharge data

The CMB method was recently used for determining spatial mean NAR from precipitation and its uncertainty over continental Spain, by assuming long-term steady conditions of the CMB variables: atmospheric chloride bulk deposition, chloride export flux by runoff, and recharge water chloride content (Alcalá and Custodio, 2014, 2015). Other sources of natural recharge such as groundwater transferences among aquifers, external runoff contribution, and snow melting coming from others areas were not considered (Alcalá and Custodio, 2014, 2015). Alcalá and Custodio (2014, 2015) analysed the influence of hydraulic properties (permeability and aquifer storage) of different aquifer lithologies on NAR estimates. For local usage, the hydrological meaning and reliability of distributed NAR was determined by comparing them with local, assumed trustable NAR values. The CMB variables were regionalised using ordinary kriging at the same 4976 nodes of a 10 km × 10 km grid to estimate a mean NAR value in each grid node. Two main sources of uncertainty affecting recharge, induced by the inherent natural variability of the variables and from mapping of the CMB variables, were identified and estimated (Alcalá and Custodio, 2014). While uncertainty from mapping may be reduced with better data coverage, the part of the natural uncertainty inferred by the variable length of yearly data series was corrected by comparing them to existing long time series. A data-correction procedure was implemented to improve mean annual NAR and its natural uncertainty deduced from variable-length data series (Alcalá and Custodio, 2015).

The critical balance period to reach comparable steady CMB averages and uncertainties was

defined as around 10 years. This period coincides with the decadal global climatic cycles acting over the Iberian Peninsula, with imperfect ~5-year positive and negative phases that follow the North Atlantic Oscillation trend (Hurrell, 1995; Trigo et al., 2004). Taking into account that (1) a minimum 10-year balance period is needed for reliable steady evaluations; and (2) the CMB databases covered preferably the period 1994-2007, the historical 1996-2005 period covering a 10-year long NAO climatic cycle with two successive 5-year long dry and wet phases was selected. Corrected CMB averages and natural uncertainties were regionalised. Mean annual NAR varied from 14 to 813 mm year⁻¹, with 90% ranging from 35 to 300 mm year⁻¹ (Figure 8.3.a), and the standard deviation of mean annual NAR varied from 4 to 281 mm year⁻¹ (Figure 8.3.b).

2.4 Climatic model simulation data. Control and future scenarios

Several series of climatic data generated with different climatic model simulations performed in the CORDEX EU project were employed. The most pessimistic emission scenario of the project, Representative Concentration Pathways 8.5 (RCP8.5), was selected. The simulations selected include results from five RCMs (CCLM4-8-17, RCA4, HIRHAM5, RACMO22E, and WRF331F) nested inside four different General Circulation Models (GCM), as shown in Table 8.1.

Dimensionless spatial monthly mean relative differences between the control simulation and the historical P time series for an average year over the reference period (1976-2005) were obtained by means of an equi-feasible ensemble of all RCMs simulations (Figure 8.4). The relative difference distribution is negatively biased overall, with a central set of values in the ±0.7 range and extreme values of -0.87 in August and +1.33 in May. Except for October (with a slightly positive average relative difference) all months show negative differences, which justifies applying some correction to the time series obtained from the RCMs simulations. The negative differences reach -0.4 in March in the northern half of the territory, but not until July and August in southern and south-eastern highlands areas, characterised by dry continental and semiarid climates with evidence of active desertification (Martínez-Valderrama et al., 2016).

The summary of the spatial distribution of the mean impacts of climate change on P is represented using the dimensionless monthly relative differences between future (2016-2045) and control (1976-2005) time series by assuming equi-feasible ensembles of all RCMs simulations (Figure 8.5). The relative difference distribution is positively biased overall, with central values in the ±0.1 range and extreme values of -0.44 in June and 0.2 in October. Except for January (with a slightly positive average relative difference), each month shows negative or close-to-average differences, with a very heterogeneous distribution. The negative relative differences decrease to below -0.1 in spring and summer (April to August) in the southern and south-western highlands.

3. Methods

The methodology used to assess impacts of future potential climatic change scenarios on aquifer recharge (NAR) from precipitation over continental Spain is described in three steps:

(1) definition of an empirical distributed precipitation-recharge model; (2) generation of future potential time series of climatic variables (P, T) spatially distributed over the territory; and (3) assessment of future hydrological impacts on aquifer recharge.

3.1 Precipitation-recharge model

A distributed empirical precipitation-recharge model is defined by using the 10 km x 10 km grid, to generate NAR series from climate series in each grid cell. The model, instead of assessing recharge series by using exclusively P, which is an approximation commonly applied (Kirn et al., 2016, for example applying an infiltration coefficient to P) is defined from the historical PAR time series estimated as difference in P and actual evapotranspiration (AET) time series (PR recharge time series hereafter).

Taking the positive relationship of temperature (T) and AET into account (Arora, 2002; Gerrits et al., 2009), changes in T will determine the available non-evaporative fraction of P available for aquifer recharge. Other factors susceptible to control AET in the future are not considered. For instance, evaporation is expected to increase with warming temperatures, while transpiration may actually decline in some cases if the warming results from increased CO₂ due to CO₂ fertilization (Bazzaz and Sombroek, 1996; Ward et al., 1999; Green et al., 2007) and the vegetation cover transitions toward a more degraded condition, as expected in the western Mediterranean region (Martínez-Valderama et al., 2018) and other mid-terrestrial latitudes (Sun et al., 2017). On the other hand, warming climate can shift multiple days per year of snowfall to rain, potentially altering recharge.

Different non-global empirical models could be applied to estimate the historical AET from P and T time series (e.g., Turc, 1954, 1961; Coutagne, 1954; Budyko, 1974; amongst others) as described in Beven (1997), Arora (2002), Gerrits et al. (2009), and España et al. (2013). In this study, the Turc (1954, 1961) model, in which annual AET depends on annual T and P, is applied in each grid cell as:

$$AET = \frac{P}{\sqrt{0.9 + \frac{P^2}{L^2}}} \quad (1)$$

where AET and P are in mm year⁻¹, and $L = 300 + 25T + 0.05T^3$ is a dimensionless parameter function of annual T.

The NAR series are obtained in each cell by applying a model whose target is to produce a perturbation of the historical PR series to obtain a new series whose mean and standard deviation is equal to the NAR series. The model is defined with a correction function that is calibrated forcing that the perturbation of the historical PR series produces a new series whose mean and standard deviation is equal to the historical NAR series data provided by Alcalá and Custodio (2014). The calibrated function will be applied to correct future PR series to obtain future NAR series assuming that the bias correction or correction function will not change in the future. The procedure involves the next steps:

(1) Average change of mean and standard deviation of the PR and NAR series for the same

historical period:

$$\Delta\mu = \frac{\mu(NAR) - \mu(PR)}{\mu(PR)} \text{ and } \Delta\sigma = \frac{\sigma(NAR) - \sigma(PR)}{\sigma(PR)} \quad (2)$$

Where $\Delta\mu$ is the change in mean and $\Delta\sigma$ is the change in standard deviation.

(2) Standardization of the PR series (historical and future)

$$PRn_i = \frac{PR_i - \bar{PR}}{\sigma_{PR}} \quad (3)$$

(3) Generation of NAR series from PR series

$$NAR_i = \sigma_c \cdot PRn_i + \mu_c \quad (4)$$

$$\text{Where } \mu_c = \mu(PR) \cdot (1 + \Delta\mu) \text{ and } \sigma_c = \sigma(PR) \cdot (1 + \Delta\sigma) \quad (5)$$

When Equation (4) is applied to the historical PR series the generated NAR series have the same mean and standard deviation to the historical NAR series of data provided by Alcalá and Custodio (2016). If it is applied to the future PR series future NAR series will be obtained assuming that the bias correction remain invariant in the future.

The NAR model was calibrated using PR recharge time series from historical climatic data (section 2.2) and historical NAR data from the CMB method (section 2.3) for the period 1996-2005. Two different hypotheses are assumed regarding the length of the PR recharge time series used to calibrate the precipitation-recharge model (the transformation function) (1) the same period of recharge time series (1996-2005; called mod_1996-2005); or (2) a longer historical period (1976-2005; called mod_1976-2005). This hypothesis assumes that the statistics (mean and standard deviation) of NAR time series from the CMB method for the period 1996-2005 and PAR time series generated from a longer historical period 1976-2005 do not differ substantially, and can be considered identical. This assumption is supported by assuming steady-state conditions of the mean and standard deviation of the balance variables determining the historical recharge when simulating the period 1976-2005 with both mod_1976-2005 and mod_1996-2005 models. The distributed mean annual recharge was 139 mm and 144.4 mm, respectively, thus the relative difference was less than 4% on average (Figure 8.6). The maps show a quite similar spatial distribution despite the mod_1976-2005 providing a slightly more smoothed estimate with lower maximum values.

3.2 Generation of future potential climatic scenarios

We introduce a method to generate potential future short-term-horizon (2016-2045) climatic scenarios from the historical data (1976-2005) and the available climatic models simulations performed in the CORDEX EU project, taking the uncertainty linked to these future scenarios into account. For this, a multi-criteria analysis of the time series obtained by applying different correction techniques (bias correction and delta change) for downscaling the values obtained with the climatic model simulations was performed to identify the best fits to the historical data. Assuming equifeasible members or non-equifeasible members (see Christensen and Lettenmaier, 2007; Lopez et al., 2009; Pulido-Velazquez et al., 2015),

different ensembles of the obtained time series are used to achieve more-representative future potential climate scenarios for assessing impacts on aquifer recharge.

3.2.1 Application of downscaling techniques: bias correction and delta change approaches

Future scenarios of climatic variables for distributed PAR or NAR over a territory have usually been generated by applying statistical downscaling techniques to the outputs of climatic models (control and future scenarios), and taking the values of these variables in the historical period into account. RCMs provide dynamic approaches with a spatial resolution of tens of kilometres. They are nested inside General Circulation models that have coarser spatial resolution (hundreds of km of grid side). In most cases the statistics of the series generated by RCMs showed a bias regarding the ‘real’ values, and appropriate downscaling techniques are required to analyse impacts at the groundwater flow system scale. Depending on the problem, several downscaling techniques of varying complexity and accuracy (correction of first- and second-order moments, regression approach, quantile mapping, etc.) were applied by assuming different conceptual approaches, such as bias correction and delta change techniques (Räisänen and Räty, 2012).

Bias correction techniques aim to define a perturbation of the control time series to force some of their statistics closer to the historical ones. They assume that the bias between statistics of the model and data will remain invariant in the future (e.g., Haerter et al., 2011; Watanabe et al., 2012, Stigter et al., 2012). The delta change techniques assume that the RCMs provide good assessments of the relative changes in the statistic between present and future, but they do not thoroughly assess the absolute values. They use the relative difference in the statistic of future and control simulations to perform a perturbation of the historical time series in accordance with these estimated changes (e.g., Pulido-Velázquez et al., 2011, 2015; Räisänen and Räty, 2012).

However, the spatio-temporal resolution between the historical and the control time series (from RCMs) often differs. Usually, the spatial resolution of historical datasets is greater than the spatial resolution of the RCMs dataset. So the transformations of both bias correction and delta change techniques indirectly produce downscaling approximations to the system (the spatial resolution of the RCMs is increased through the historical series in the case study). This is the reason they are commonly known as downscaling transformations.

In this research, two downscaling approaches were used, correction of first and second order moments, for both bias correction and delta change techniques. These were applied to all the RCMs simulations described in Section 2.2 (Table 8.1).

3.2.2 Multi-criteria analysis of the main statistic

A multi-criteria analysis analogous to those described in Pulido Velazquez et al. (2011) (Escriva-Bou et al., 2016), was used to identify the RCMs simulations that provide the best approximation to the main statistics (mean, standard deviation) of the historical time series. It aims to identify the best RCMs in terms of goodness of fit of the statistics of the control series to the historical ones. To assess it we define an error index (ES , see Equation 6) that is applied

to the main statistics (mean and Standard deviation) for each RCM and climatic variable (precipitation and temperature).

$$ES = \frac{1}{N} \sum_N \left(\frac{s_c - s_h}{s_h} \right)^2 \quad (6)$$

where ES is the error of the considered statistic, N is the length of the statistical time series, c is the control simulation, and h is the historical. Table 8.2 shows eliminated and non-eliminated RCMs.

After assessing Es it in each cell we estimate the mean lumped value for our case study (Continental Spain), which will be employed to perform the multicriteria analysis. It intends to find models that were “inferior” to others in terms of fitting the historical dataset (‘dominated solutions’, in the terminology of multi-objective analyses). The models are then compared and those ones that were worse than any other model in all the statistics, i.e., strictly dominated are the “inferior” one.

It has been also applied to identify the best combination of models and bias correction techniques in terms of goodness of fit of the corrected control scenarios to the basic statistics of the historical time series. Due to the fact that most combinations of models and bias correction techniques provide good approximations to the first and second moments, a relative error threshold (percentage difference with respect to the historical statistics) was defined; only significant differences were used to decide when a corrected control is worse than other ones. Table 8.3 shows the inferior and non-inferior combinations of models and bias-correction techniques for a 3% threshold of the mean relative error.

3.2.3 Prediction ensembles to define more representative future climatic scenarios

Four options to define more representative future scenarios by applying different ensembles of the potential scenarios deduced from the available climatic models were considered. Two ensemble scenarios were considered by combining as equifeasible members all the future series (corresponding to different RCMs simulations) generated by bias correction (E1) or delta change (E2). Two other options were defined by combining only the non-inferior models using the 3% threshold [E3] (in bias correction approach) or the non-inferior combinations of model and correction technique [E4] (delta change techniques), by assuming that the inferior ones are untrusted.

Despite the temporal series being different, the two equi-feasible ensembles E1 (applying bias correction techniques) and E2 (applying delta change techniques) produced identical future mean temperature maps (Figure 8.7). There are very small differences in mean values between the equi-feasible projections and the two other alternatives. In terms of precipitation, there are very small differences between the two equi-feasible ensembles E1 and E2 due to a reduced number of negative values appearing in some cells when correcting using the second moment approach (Figure 8.8). Larger differences appear between the mean values of these equi-feasible predictions and the two other alternatives, although they are not significant. Therefore, the sensitivity of the means of climatic variables to the hypothesis assumed to define the ensemble is quite low.

3.3 Assessment of future climate impacts on aquifer recharge

The analysis of climate change impacts required to simulate various climatic scenarios (E_i) within the precipitation-recharge models defined in section 3.2. The results obtained are summarised and discussed in next section. Note that other variables affecting recharge, such as soil properties, vegetation patterns, and land use are considered steady, despite there being expected to change according to global climate driving forces and new human actions on a local scale that will be induced by adaptation to climate and water resource availability (Martínez-Valderrama et al., 2016, 2018). How these variables will change through time over the territory is not considered in this paper.

4. Results and discussion

4.1. Future aquifer recharge scenarios

Eight potential future mean NAR scenarios for the period 2011-2045 were obtained by combining future potential climatic scenarios defined by the four ensemble options (E1, E2, E3, and E4) and two precipitation-recharge models (mod_1976-2005 and mod_1996-2005) (Figure 8.9). As pointed out for the historical time series, the results obtained with the mod_1976-2005 are slightly smoother (with lower maximum values) than those ones obtained with the mod_1996-2005, as shown in the maps and graphs in Figure 8.9. Note that significant differences in the temporal evolution of the annual future recharge time series are found when the assumed hypothesis are used. Scenarios E1 and E3 obtained by applying bias correction are similar to each other scenarios E2 and E4 obtained by using the delta-change perturbation technique. The recharge models used do not introduce large differences into the annual time series distribution, despite the mod_1976-2005 produces slightly more smoothed result with lower extreme values. The year-to-year distribution of recharge values for scenarios E2 and E4 is similar to that obtained by using the historical time series, though the mean value is slightly lower. This is due to the fact that the delta-change technique (E2 and E4) perturbs the historical time series while the bias-correction technique perturbs the future time series from the RCMs.

Nevertheless, in statistical terms, both the mean and the median values of the aggregate NAR for the various scenarios and recharge models applied do not differ substantially, varying in the 98.5–106.9 mm year⁻¹ and 120.8–128.3 mm year⁻¹ ranges, respectively. The spatial distribution of mean NAR for each of the four scenarios is also quite similar (Figure 8.9). The sensitivity of the mean NAR and its distribution using both perturbation techniques (bias or delta change) and the ensemble hypothesis of the models (equi-feasible or not) is low; this is in agreement with what is observed by generating the future scenarios of P and T. The sensitivity of P and T maps to the recharge model employed (i.e., the transformation adopted) is also quite low; this is also expected given the small differences in mean in the simulations of the historical scenarios. A summary of basic statistics of governing variables P, T, and R for the historical period and future projections is included in Table 8.4.

The absolute differences of mean values between historical and future NAR time series obtained for the various scenarios oscillate between -11.5 and -22.8 mm year⁻¹ (Figure 8.10).

These figures highlight the differences between results obtained by using the various scenarios and recharge models. In terms of the means and medians, the differences are small, thus indicating that both time series are normally distributed and suitable for statistical comparisons. The model is more sensitive to which recharge model is applied (differences of 4.6 mm year⁻¹ and 3.8 mm year⁻¹ in the mean and median, respectively) than to the ensemble type (differences of 2.8 mm year⁻¹ and 2.6 mm year⁻¹ in the mean and median, respectively). There is intermediate sensitivity to the rescaling technique (differences of 3.9 mm year⁻¹ and 3.8 mm year⁻¹ in the mean and median, respectively). With respect to the extremes of mean P maps, the differences are small but the results are somewhat more sensitive to the rescaling correction technique (bias or delta change) than to the ensemble hypothesis (equi-feasible or not) or the recharge model applied (mod_1976-2005 and mod_1996-2005). Although this representation of absolute change also highlights that differences were almost unappreciable for the entire recharge dataset, the spatial distribution and statistics of values (Table 8.4) are very similar in all cases represented.

As far as standard deviation goes (Figure 8.11), the ensemble scenarios are sensitive to the downscaling technique (bias or delta change). However, the sensitivity both to the recharge model and the ensemble hypothesis (equi-feasible or not) is low.

The results that would be obtained by using an equi-feasible ensemble of the eight scenarios in terms of mean NAR, standard deviation, and relative variation of the future mean NAR compared to the historical ones are showed in Figure 8.12. One can see that although a small reduction in mean NAR is expected over 99.8% of continental Spain, there are two small north-eastern (600 km²) and eastern (100 km²) areas of the territory where a small increase is expected. A largest reduction in mean NAR in the centre and south-east of the territory is expected, dropping 28% in some areas. Only 6.6% of continental Spain corresponds to reductions of more than 20% in mean NAR. Nevertheless, 52.3% of the territory would suffer mean NAR reductions between 10% and 20%, while the reduction would be between 0% and 10% over 40.9% of the territory. In the case of the standard deviation on mean NAR, an increment of 41% on average is expected over 71.5% of the territory, being particularly marked in localized southern areas, with 36.7% of this area showing more than 50% increase. There would also be a significant reduction in the standard deviation in northern areas, with 6.9% of this area showing reductions greater than 30%.

Finally, relationships between the dimensionless relative differences in mean and standard deviation of mean NAR and some possible explanatory variables (elevation, latitude) is showed in Figure 8.13. A poor linear correlation coefficient between relative differences and elevation is found, despite some general trends are observed. For instance, the range in relative differences in standard deviation of mean NAR decreases in the -0.3–0 range as elevation increases, especially above 1700 m a.s.l. in the main mountains ranges. While the standard deviation decreases at higher elevations, at lower elevations (0 to 200 m a.s.l.) a greater dispersion of the relative differences in standard deviation in the -0.3–0.8 range is found. The linear correlation coefficient between the relative differences and latitude is higher, of 0.30 for the mean and 0.56 for the standard deviation. The relative differences in the mean NAR increase with elevation, while the relative differences in standard deviation of

mean NAR decrease with elevation. Other relationships with longitude were analyzed but, finding none, these analyses are omitted.

This work is the first one that assesses potential impacts of climate change on aquifer recharge in continental Spain. The limitations, uncertainties, and usefulness of the results are discussed below.

4.2 Limitations: assumptions, uncertainties, and usefulness of the results

The assumption of hypothesis and simplifications to apply the method presented in this work introduces different kinds of uncertainty which propagate in the final results. The more relevant hypotheses have been grouped into the two main methodological steps used, as follows:

(1) Generation of future potential climatic scenarios

- Total precipitation was used instead of differencing between rainfall and snowfall. Although most of continental Spain receive snowfall rarely (if ever), there are some areas in Pyrenees and Sierra Nevada ranges that receive significant snowfall. A great uncertainty in those areas is expected because snowmelt acts as a more 'efficient' recharge agent than rainfall (Simpson et al., 1972; Winograd et al., 1998; Earman et al., 2006) and warming climate can shift multiple days per year of snowfall to rain, potentially altering recharge.
- The research focus on the analysis of future short-term-horizon (2016-2045). Other future horizons, such as mid-term and long-term scenarios have not been considered. For those mid-term and long-term scenarios, due to they are further away in time we will expect to have higher impacts on NAR. There should be also higher uncertainties for them.
- Only the most severe IPCC scenario was analysed (RCP 8.5) to assess the most pessimistic potential impacts on NAR in the future short-term scenario. The impacts of other potential future scenarios (RCP2.6, RCP4.5, RCP6) on NAR should be less intensive.
- Two downscaling approaches (correction of first and second order moments) under two different hypotheses (bias correction and delta change techniques) were applied to generate future climatic series in accordance with RCMs simulations. Note that, depending on the problem and the target solution, several downscaling techniques of varying complexity and accuracy (correction of first- and second-order moments, regression approach, quantile mapping, etc.) can be applied by assuming different conceptual approaches, such as bias correction and delta change techniques (Räisänen and Räty, 2012). By combining both approaches we cover a wider range of solutions assessing the potential impacts of Climate Change, giving a better picture of the potential variability of the solutions.
- Potential plausible pictures of future climate scenarios are defined by combining information coming from different Regional Climatic Models (RCMs) and General

Circulation models (GCMs). The ‘ensembles’ coalesce and consolidate the results of individual climate projections, thus allowing for more robust climate projections that are more representative than those based on a single model (Spanish Meteorological Agency, AEMET, 2009).

- Two different hypotheses, equifeasible members or non-equifeasible members, were applied to define ensembles of the obtained future series for each RCM. They help to achieve more representative future potential climate scenarios for assessing impacts on aquifer recharge.

(2) Hydrological propagation of the climatic impact. Simulation of future climatic scenarios with a precipitation-recharge model.

- A simple empirical precipitation-recharge model has been adopted; whose inputs are P and E, being the outputs NAR time series. We have not tested other hydrological models, for example, based on a more physically based or detailed representation of the processes involved in the hydrological balance (Eg. Snowmelt processes) and the geological structures. We assume that precipitation (P) and temperature (T) are the variables determining NAR, and their spatiotemporal variability determines the impacts of future potential climatic scenarios on renewable groundwater resources. We do not consider the changes in other variables affecting recharge, such as soil properties, vegetation patterns and land-use. They are considered steady, despite there being expected to change according to global climate driving forces and new human actions on a local scale that will be induced by human adaptation to climate and water resource availability (Martínez-Valderrama et al., 2016). The assessment of these adaptation strategies developed to reduce the impacts on aquifer recharge is out of the scope of this research work.
- We assume that the climatic fields (P and T) taken from the Spain02 project (Herrera et al., 2016) and used as inputs of our model are good enough to approximate the historical climate. An assessment of the validation of some Spanish datasets, including Spain02, was recently carried out by Quintana-Seguí et al. (2017). The SPAIN02 dataset has already been employed in many research studies (Escriva-Bou et al., 2017; Pardo-Igurquiza et al., 2017).
- The Turc’s model (1954, 1961) was applied to estimate E. Its results depend on mean annual T and P. Different non-global empirical models could be applied to assess the historical AET from T and P time series. The applications of different methods would allow to assess uncertainties in this variable.
- The NAR series obtained by applying the chloride mass balance (CMB) method (Alcalá and Custodio, 2014, 2015) were used to calibrate the recharge model. The mean and standard deviation of the historical NAR for the period 1996-2005 were assumed representative of the steady-state condition, despite no longer than 40-year time series of the CMB variables are available in continental Spain to draw definitive conclusions (Alcalá and Custodio, 2014, 2015).
- The spatial resolution of the model, a regular 10 km x 10 km grid, is quite coarse because input data used to define the model were not available for smaller cells. Nevertheless it allows to obtain a first approach to identify areas where more detailed analyses should be

performed.

The results will be obtained under a set of hypotheses, and they are only indicators of potential plausible scenarios that may happen. Nevertheless, they give us an idea of the potential intensity of the climate change impacts under the most pessimistic emissions scenario in the analysed domain in a future short-term horizon (2016-2045). In spite of the uncertainties, the results also allow us to identify areas where the impact of climate change will be stronger. In these regions, there is the need for carrying out specific further research (using different detailed conceptual tools, etc) to provide a more detailed assessment of future values and uncertainties.

5. Conclusions

This work is the first one that assesses future potential impacts of climate change on aquifer recharge in continental Spain. A methodology is presented and used to estimate net aquifer recharge (NAR) over a regular 10 km x 10 km grid in two steps (1) generation of future potential climatic scenarios; and (2) hydrological propagation of the climatic impact by simulating future climatic scenarios with a precipitation-recharge model. The results, which are obtained assuming different hypotheses in each methodological step, are only indicators of potential plausible scenarios that may happen. They estimate the potential intensity of the climate change impacts for the horizon 2016-2045 under the most pessimistic emissions scenario. A reduction of mean NAR around 12% on average over continental Spain is deduced. A variable degree of NAR reduction over 99.8% of the territory is estimated; the reduction is quite heterogeneously distributed in line with the variety of conditions for aquifer recharge over continental Spain. The estimated standard deviation of mean NAR would increase by 8% on average in this future scenario. In spite of the uncertainties, the results are also useful to identify areas where the impact of climate change will be stronger. In these regions, we will need to perform more specific further research (using different detailed conceptual tools, etc) to provide a more detailed assessment of future values and uncertainties. The dependence of these changes regarding typical potential explanatory variables, such as elevation and latitude, was also analyzed. More significant relationships were found for the standard deviation than for the mean NAR values. The magnitude and range of standard deviation decrease at higher elevations and lower latitudes.

Acknowledgments

This research work was partially supported by the GESINHIMPADAPT project (CGL2013-48424-C2-2-R) with Spanish MINECO funds. We would like to thank the Spain02 and CORDEX projects for the data provided for this study. We appreciate the valuable comments and suggestions provided by three anonymous referees.

References

AEMET, 2009. Generación de escenarios regionalizados de cambio climático para España, Agencia Estatal de Meteorología, Mto, Medio Ambiente, Medio Rural y Marino.

Adhikari, U., Nejadhashemi, A.P., Herman, M.R., 2015. A review of climate change impacts

- on water resources in East Africa. *Transactions of the ASABE* 58(6), 1493-1507.
- Alcalá, F.J., Cantón, Y., Contreras, S., Were, A., Serrano-Ortiz, P., Puigdefábregas, J., Solé-Benet, A., Custodio, E., Domingo, F., 2011. Diffuse and concentrated recharge evaluation using physical and tracer techniques: results from a semiarid carbonate massif aquifer in southeastern Spain. *Environmental Earth Sciences* 63, 541–557.
- Alcalá, F.J., Custodio, E., 2014. Spatial average aquifer recharge through atmospheric chloride mass balance and its uncertainty in continental Spain. *Hydrological Processes* 28, 218–236.
- Alcalá, F.J., Custodio, E. 2015. Natural uncertainty of spatial average aquifer recharge through atmospheric chloride mass balance in continental Spain. *Journal of Hydrology* 524, 642-661.
- Andreu, J.M., Alcalá, F.J., Vallejos, Á., Pulido-Bosch, A., 2011. Recharge to aquifers in SE Spain: different approaches and new challenges. *Journal of Arid Environments* 75, 1262-1270.
- Arora, V.K., 2002. The use of the aridity index to assess climate change effect on annual runoff. *Journal of Hydrology* 265, 164-177.
- Barthel, R., 2006. Common problematic aspects of coupling hydrological models with groundwater flow models on the river catchment scale. *Advances in Geosciences*, European Geosciences Union 9, 63-71.
- Batelaan, O., De Smedt, F., 2007. GIS based recharge estimation by coupling surface-subsurface water balances. *Journal of Hydrology* 337, 337-355.
- Bazzaz, F., Sombroek, W., 1996. Global climate change and agricultural production: direct and indirect effects of changing hydrological soil and plant physiological processes, Food and Agriculture Organization of the United Nations/John Wiley & Sons, Chichester, UK.
- Beven, K., 2007. Towards integrated environmental models of everywhere: uncertainty, data and modelling as a learning process. *Hydrology and Earth System Science* 11(1), 460-467.
- Bouraoui, F., Vachaud, G., Li, L.Z.X., Le Treut, H., Chen, T., 1999. Evaluation of the impact of climate changes on water storage and groundwater recharge at the watershed scale. *Clim Dynam* 15(2), 153-161
- Budyko, M.I., 1974. Climate and Life. Academic Press, New York, 508pp.
- Chen, Z., Grasby, S.E., Osadetz, K.G., 2004. Relation between climate variability and groundwater levels in the upper carbonate aquifer, southern Manitoba, Canada. *Journal of Hydrology* 290(1-2), 43-62. doi: 10.1016/j.jhydrol.2003.11.029.
- Christensen, N.S., Lettenmaier, D.P., 2007. A multimodel ensemble approach to assessment of climate change impacts on the hydrology and water resources of the Colorado River Basin.

Hydrol. Earth Sys. Sci. 11(4), 1417-1434.

Clark, M.P., Kavetski, D., Fenicia, F., 2011. Pursuing the method of multiple working hypotheses for hydrological modeling. Water Resour. Res. 47(9), W09301. doi:10.1029/2010WR009827.

Coes, A.L., Spruill, T.B., Thomasson, M.J., 2007. Multiple-method estimation of recharge rates at diverse locations in the North Caroline Coastal Plains, USA. Hydrogeology Journal 15, 773–788.

CORDEX PROJECT. 2013. The Coordinated Regional Climate Downscaling Experiment CORDEX. Program sponsored by World Climate Research Program (WCRP). Available at: <http://wcrp-cordex.ipsl.jussieu.fr/>

Cotterman, K.A., Kendall, A.D., Basso, B., Hyndman D.W., 2017. Groundwater depletion and climate change: future prospects of crop production in the Central High Plains Aquifer. Climatic Change. doi:10.1007/s10584-017-1947-7.

Coutagne, A., 1954. Quelques considérations sur le pouvoir évaporant de l'atmosphère, le déficit d'écoulement effectif et le déficit d'écoulement maximum. La Houille Blanche, 360-369.

De Vries, J.J., Simmers, I., 2002. Groundwater recharge: an overview of processes and challenges. Hydrogeology Journal 10, 5–17.

Di Matteo L., Valigi, D., Cambi, C., 2011. Climatic characterization and response of water resources to climate change in limestone areas: some considerations on the importance of geological setting. [https://doi.org/10.1061/\(ASCE\)HE.1943-5584.0000671](https://doi.org/10.1061/(ASCE)HE.1943-5584.0000671).

Di Matteo, L., Dragoni, W., Maccari, D., Piacentini, S.M., 2017. Climate change, water supply and environmental problems of headwaters: The paradigmatic case of the Tiber, Savio and Marecchia rivers (Central Italy). Sci Total Environ 598, 733-748. doi: 10.1016/j.scitotenv.2017.04.153.

Dragoni, Walter, and Sukhija, B.S., 2008. Climate change and groundwater—A short review, in Dragoni, W., and Sikhija, B.S., eds., Climate change and groundwater: London, Geological Society, Special Publications 288, 1-12.

Earman, S., Campbell, A.R., Newman, B.D., Phillips, F.M., 2006. Isotopic exchange between snow and atmospheric water vapor: Estimation of the snowmelt component of groundwater recharge in the southwestern United States, Journal of Geophysical Research 111, D09302.

Earman, S., Dettinger, M., 2011. Potential impacts of climate change on groundwater resources - a global review. Journal of Water and Climate Change 2(4), 213-229.

Eckhardt, K., Ulbrich, U., 2003. Potential impacts of climate change on groundwater recharge and streamflow in a central European low mountain range. J. Hydrol. 284(1-4), 244-252. doi:10.1016/j.jhydrol.2003.08.005.

- Edmunds, W.M., Gaye, C.B., 1994. Estimating the variability of groundwater recharge in the Sahel using chloride. *J. Hydrol.* 106 (1-2), 55-78.
- Escriva-Bou, A., Pulido-Velazquez, M. and Pulido-Velazquez, D., 2016. The Economic Value of Adaptive Strategies to Global Change for Water Management in Spain's Jucar Basin. *Journal of Water Resources Planning and Management*. doi:10.1061/(ASCE)WR.1943-5452.0000735.
- España, S., Alcalá, F.J., Vallejos, A., Pulido-Bosch, A., 2013. A GIS tool for modelling annual diffuse infiltration on a plot scale. *Computers & Geosciences* 54, 318-325.
- Estrela, T., Cabezas, F., Estrada, F., 1999. La evaluación de recursos hídricos en el Libro Blanco del Agua en España. *Ing. Agua* 6(2), 125–138.
- Freeze, R. A., Cherry, J.A., 1979. *Groundwater*, Prentice Hall, Inc., Upper Saddle River, NJ.
- Garrido, A., Llamas, M.R., 2009. Water policy in Spain. John Wiley & Sons, Boca Raton, FL. 254 pp.
- Gemitzi, A., Ajami, H., Richnow, H.H., 2017. Developing empirical monthly groundwater recharge equations based on modeling and remote sensing data – Modeling future groundwater recharge to predict potential climate change impacts. *Journal of Hydrology* 546, 1-13. doi: 10.1016/j.jhydrol.2017.01.005
- Gerrits, A.M.J., Savenije, H.H.G., Veling, E.J.M., Pfister, L., 2009. Analytical derivation of the Budyko curve based on rainfall characteristics and a simple evaporation model. *Water Resour. Res.* 45, W04403. doi:10.1029/2008WR007308.
- Green, T. R., Bates, B.C., Charles S.P., Fleming P.M., 2007. Physically based simulation of potential effects of carbon dioxide-altered climates on groundwater recharge. *Vadose Zone Journal* 6, 597-609.
- Green, T.R., Taniguchi, M., Kooi, H., Gurdak, J.J., Allen, D.M., Hiscock, K.M., Treidel, H., Aureli, A., 2011. Beneath the surface: impacts of climate change on groundwater. *J. Hydrol.* 405, 532–560.
- Haerter, J.O., Hagemann, S., Moseley, C., Piani C., 2011. Climate model bias-correction and the role of timescales, *Hydrol. Earth Syst. Sci.* 15(3), 1065–1079.
- Hartmann, A., Gleeson, T., Rosolem, R., 2015. A large-scale simulation model to assess karstic groundwater recharge over Europe and the Mediterranean. *Geoscientific Model Development* 8, 1729-1746.
- Herrera, S., Fernández, J., Gutiérrez, J.M., 2016. Update of the Spain02 Gridded Observational Dataset for Euro-CORDEX evaluation: Assessing the Effect of the Interpolation Methodology. *International Journal of Climatology* 36, 900–908.
- Herrmann, F., Baghdadi, N., Blaschek, M., 2016. Simulation of future groundwater recharge using a climate model ensemble and SAR-image based soil parameter distributions - A

case study in an intensively-used Mediterranean catchment. *Science of the Total Environment* 543, 889-905.

Huang, L., Zeng, G., Liang, J., Hua, S., Yuan, Y., Li, X. Dong, H., Liu, J., Nie, S., Liu, J., 2017. Combined Impacts of Land Use and Climate Change in the Modeling of Future Groundwater Vulnerability. *Journal of Hydrologic Engineering* 22(7). doi: 10.1061/(ASCE)HE.1943-5584.0001493.

Hurrell, J.W., 1995. Decadal trends in the North Atlantic Oscillation, regional temperatures and precipitation. *Nature* 269, 676-679.

IGME, 1993. Groundwater in Spain: synthetic study, Technical Report. Ministry of Industry and Energy of Spain, Madrid. 591 pp. [in Spanish]. Available at: <http://aguas.igme.es/igme/publica/libro20/lib20.htm>

Islam, S., Singh, R.K., Khan, R.A., 2016. Methods of Estimating Ground water Recharge. *International Journal of Engineering Associates* (ISSN:2320-0804).

Jyrkama, M.I., Sykes, J.F., 2007. The impact of climate change on spatially varying groundwater recharge in the grand river watershed (Ontario). *Journal of Hydrology*, 338, 237-250. doi:10.1016/j.jhydrol.2007.02.036.

Kidd, M., 2017. Groundwater depletion and climate change: future prospects of crop production in the Central High Plains Aquifer. *Water International*, 42(6). doi:10.1080/02508060.2017.1351057

Kirn, L., Mudarra, M., Marín, A., Andreo, B., Hartmann, A., 2017. Improved Assessment of Groundwater Recharge in a Mediterranean Karst Region: Andalusia, Spain. In: Renard P., Bertrand C. (Eds.) EuroKarst 2016, Neuchâtel. *Advances in Karst Science*, 117-125. Springer, Cham. doi:10.1007/978-3-319-45465-8_13.

Kløve, B., Ala-Aho, P., Bertrand, G., Gurdak, J. J., Kupfersberger, H., Kvaerner, J., Muotka, T., Mykrä, H., Preda, E., Rossi, P., et al., 2014. Climate change impacts on groundwater and dependent ecosystems. *Journal of Hydrology* 518, 250:266.

Lerner, D.N., Issar, A.S., Simmers, I., 1990. Groundwater recharge. A guide to understanding and estimating natural recharge. IAH International Contributions to Hydrogeology. 8. Heise, Hannover. 345 pp.

Lopez, A., Fung, F., New, M., Watts, G., Weston, A., Wilby, R.L., 2009. From climate model ensembles to climate change impacts and adaptation: a case study of water resource management in the southwest of England. *Water Resour. Res.* 45. doi:10.1029/2008wr007499.

Martín-Vide, J., López-Bustins, J.A., 2006. The Western Mediterranean Oscillation and Rainfall in the Iberian Peninsula. *International Journal of Climatology* 26, 1455-1475.

Martínez-Valderrama, J., Ibáñez, J., Del Barrio, G., Sanjuán, M.E., Alcalá, F.J., Martínez-

- Vicente, S., Ruiz, A., Puigdefábregas, J., 2016. Present and future of desertification in Spain: implementation of a surveillance system to prevent land degradation. *Science of the Total Environment*, 563-564, 169-178.
- Martínez-Valderrama, J., Ibáñez, J., Del Barrio, G., Alcalá, F.J., Sanjuán, M.E., Ruiz, A., Hirche, A., Puigdefábregas, J., 2018. Doomed to collapse: Why Algerian steppe rangelands are overgrazed and some lessons to help land-use transitions. *Science of the Total Environment* 613-614, 1489-1497. doi:10.1016/j.scitotenv.2017.07.058.
- McIntyre, O., 2017. EU legal protection for ecologically significant groundwater in the context of climate change vulnerability. *Water International*, 42(6). doi:10.1080/02508060.2017.1351060
- McMahon, P.B., Plummer, L.N., Bohlke, J.K., Shapiro, S.D., Hinkle, S.R., 2011. A comparison of recharge rates in aquifers of the United States based on groundwater-based data. *Hydrogeology Journal* 19, 779-800.
- Milly, P.C.D., Betancourt, J., Falkenmark, M., Hirsch, R.M., Kundzewicz, Z.W., Lettenmaier, D.P., Stouffer, D.J., 2008. Stationarity Is Dead: Whither Water Management?. *Science* 319, 573–574.
- Milly, P.C.D., Eagleson, P.S., 1987. Effects of spatial variability on annual average water balance. *Water Resources Research* 23, 2135–2143.
- MIMAM, 2000. White book of water in Spain. Ministry of the Environment, State Secretary of Waters and Coast, General Directorate of Hydraulic Works and Water Quality. Madrid. 637 pp. [in Spanish]. Available at: http://hercules.cedex.es/Informes/Planificacion/2000-Libro_Blanco_del_Agua_en_Espana/
- Minor, T.B., Russell, C.E., Mizell, S.A., 2007. Development of a GIS-based model for extrapolating mesoscale groundwater recharge estimates using integrated geospatial data sets. *Hydrogeology Journal* 15, 183-195.
- Molina, J.L., Pulido-Velázquez, D., García-Aróstegui, J.L., Pulido-Velázquez, M., 2013. Dynamic Bayesian Networks as a Decision Support tool for assessing Climate Change impacts on highly stressed groundwater systems. *Journal of Hydrology* 479, 113–129.
- National Ground Water Association, 2004. Ground Water Sustainability: A White Paper. Available at: <http://www.ngwa.org/Documents/PositionPapers/sustainwhitepaper.pdf>
- Nolan, B.T., Healy, R.W., Taber, P.E., Perkins, K., Hitt, K.J., Wolock, D.M., 2007. Factors influencing ground-water recharge in the eastern United States. *Journal of Hydrology* 332, 187–205.
- Panwar, S., Chakrapani, G.J., 2013. Climate change and its influence on groundwater resources. *Current Science* 105, 37-46.
- Pardo-Iguzquiza, E., Collados-Lara, A.J., Pulido-Velazquez, D., 2017. Estimation of the

- spatiotemporal dynamics of snow covered area by using cellular automata models. *Journal of hydrology* 550, 230-238. doi: 10.1016/j.jhydrol.2017.04.058.
- Parry, M.L., Canziani, O.F., Palutikof, J., Van der Linden, P., Hanson, C.E., 2007. Climate Change 2007: Impacts Adaptation and Vulnerability: Contribution of Working Group II to the Fourth Assessment Report of the Intergovernmental Panel on Climate Change. Cambridge Univ Press, Cambridge, UK, 976 pp.
- Polemio, M., 2016. Monitoring and Management of Karstic Coastal Groundwater in a Changing Environment (Southern Italy): A Review of a Regional Experience. *Water* 8(4), 148.
- Pulido-Velázquez, D., García-Aróstegui, J.L., Molina, J.L., Pulido-Velázquez, M., 2015. Assessment of future groundwater recharge in semi-arid regions under climate change scenarios (Serral-Salinas aquifer, SE Spain). Could increased rainfall variability increase the recharge rate? *Hydrol. Process.* 29, 828–844.
- Pulido-Velazquez, D., Garrote, L., Andreu, J., Martin-Carrasco, F.J., Iglesias, A., 2011. A methodology to diagnose the effect of climate change and to identify adaptive strategies to reduce its impacts in conjunctive-use systems at basin scale. *Journal of Hydrology* 405, 110-122.
- Quintana-Seguí, P., Turco, M., Herrera, S., Miguez-Macho, G., 2017. Validation of a new SAFRAN-based gridded precipitation product for Spain and comparisons to Spain02 and ERA-Interim. *Hydrol. Earth Syst. Sci.* 21, 2187-2201. doi:10.5194/hess-21-2187-2017.
- Räisänen, J., Räty, O., 2012. Projections of daily mean temperature variability in the future: cross-validation tests with ENSEMBLES regional climate simulations. *Climate Dynamics* 41, 1553–1568.
- Scanlon, B.R., Keese, K.E., Flint, A.L., Flint, L.E., Gaye, C.B., Edmunds, W.M., Simmers, I., 2006. Global synthesis of groundwater recharge in semiarid and arid regions. *Hydrological Processes* 20, 3335–3370.
- Scanlon , B.R., Healy, R.W., Cook, P.G., 2002. Choosing appropriate techniques for quantifying groundwater recharge. *Hydrogeology Journal* 10, 18-39.
- Scibek, J., Allen, D.M., 2006. Modeled impacts of predicted climate change on recharge and groundwater levels. *Water Resour Res* 42, W11405.
- Simpson, E.S., Thorud, D.B., Friedman, I., 1972. Distinguishing seasonal recharge to groundwater by deuterium analysis in southern Arizona, in World Water Balance. *Proceedings of the Reading Symposium, July 1970*, 3, 623-633.
- Stigter ,T.Y., Nunes, J.P., Pisani, B., Fakir, Y., Hugman, R., Li, Y., Tomé, S., Ribeiro, L. et al., 2014. Comparative assessment of climate change and its impacts on three coastal aquifers in the Mediterranean. *Reg Environ Chang* 14, 41–56. doi:10.1007/s10113-012-0377-3

- Sun, L., Yang, L., Hao, L., Fang, D., Jin, K., Huang, X., 2017. Hydrological Effects of Vegetation Cover Degradation and Environmental Implications in a Semiarid Temperate Steppe, China. *Sustainability* 9, 281. doi:10.3390/su9020281.
- Taylor, R.G., Scanlon, B., Doell, P., 2013. Ground water and climate change. *Nature Climate Change* 3, 322-329.
- Treidel, H., Martin-Bordes, J.J., Gurdak, J.J., 2012. Climate Change Effects on Groundwater Resources: A Global Synthesis of Findings and Recommendations. International Association of Hydrogeologists (IAH) – International Contributions to Hydrogeology. Taylor & Francis publishing, 414p.
- Trigo, R.M., Pozo-Vazquez, D., Osborn, T.J., Castro-Diez, Y., Gamiz-Fortis, S., Esteban-Parra, M.J., 2004. North Atlantic Oscillation influence on precipitation, river flow and water resources in the Iberian Peninsula. *International Journal of Climatology* 24, 925-944.
- Turc, L., 1954. Water balance of soils: relationship between precipitation, evapotranspiration and runoff (in French). *Annales Agronomiques* 5, 49-595 and 6, 5-131.
- Turc, L., 1961. Estimation of irrigation water requirements, potential evapotranspiration: A simple climatic formula evolved up to date. *Annales Agronomiques* 12(1), 13-49. (in French).
- Vaccaro, J.J., 1992. Sensitivity of groundwater recharge estimates to climate variability and change, Columbia Plateau, Washington. *J. Geo-phys. Res.* 97, 2821-2833.
- Ward, J.K., Tissue, D.T., Thomas, R.B., Strain, B.R., 1999. Comparative responses of model C3 and C4 plants to drought in low and elevated CO₂. *Global Change Biology* 5, 857-867.
- Watanabe, S., Kanae, S., Seto, S., Yeh P.J.-F., Hirabayashi, Y., Oki, T., 2012. Intercomparison of bias-correction methods for monthly temperature and precipitation simulated by multiple climate models. *Journal of Geophysical Research*, 117, D23114. doi:10.1029/2012JD018192.
- Winograd, I.J., Riggs, A.C., Coplen, T.B., 1998. The relative contributions of summer and cool-season precipitation to groundwater recharge, Spring Mountains, Nevada, USA. *Hydrogeology Journal* 6, 77-93.

Tables of the Chapter 8

RCMs \ GCMs	CNRM-CM5	EC-EARTH	MPI-ESM-LR	IPSL-CM5A-MR
CCLM4-8-17	X	X	X	
RCA4	X	X	X	
HIRHAM5		X		
RACMO22E		X		
WRF331F				X

Table 8.1. Regional Climatic Models (RCMs) and General Circulation Models (GCMs) considered for simulations.

Eliminated?	RCM	GCM
No	CCLM4-8-17	CNRM-CM5
No	CCLM4-8-17	EC-EARTH
No	CCLM4-8-17	MPI-ESM-LR
No	HIRHAM5	EC-EARTH
No	RACMO22E	EC-EARTH
No	RCA4	CNRM-CM5
No	RCA4	EC-EARTH
No	RCA4	MPI-ESM-LR
Yes	WRF331F	IPSL-CM5A-MR

Table 8.2. Inferior and non-inferior models in the multicriteria analysis.

Eliminated?	RCM	GCM	Technique
Yes	CCLM4-8-17	CNRM-CM5	First moment
No	CCLM4-8-17	CNRM-CM5	Second moment
Yes	CCLM4-8-17	EC-EARTH	First moment
No	CCLM4-8-17	EC-EARTH	Second moment
Yes	CCLM4-8-17	MPI-ESM-LR	First moment
Yes	CCLM4-8-17	MPI-ESM-LR	Second moment
No	HIRHAM5	EC-EARTH	First moment
No	HIRHAM5	EC-EARTH	Second moment
No	RACMO22E	EC-EARTH	First moment
No	RACMO22E	EC-EARTH	Second moment
No	RCA4	CNRM-CM5	First moment
No	RCA4	CNRM-CM5	Second moment
Yes	RCA4	EC-EARTH	First moment
Yes	RCA4	EC-EARTH	Second moment
No	RCA4	MPI-ESM-LR	First moment
No	RCA4	MPI-ESM-LR	Second moment
Yes	WRF331F	IPSL-CM5A-MR	First moment
Yes	WRF331F	IPSL-CM5A-MR	Second moment

Table 8.3. Inferior and non-inferior combination of models and bias-correction techniques.

Statistic ^a	Historical period				Scenario E1				Scenario E2				Scenario E3				Scenario E4			
	P	T	R ^c	R ^d	P	T	R ^c	R ^d	P	T	R ^c	R ^d	P	T	R ^c	R ^d	P	T	R ^c	R ^d
minimum	190	4.6	14	15	183	5.9	11	11	184	5.9	13	13	191	5.9	12	12	190	5.9	13	13
maximum	2013	21.1	813	823	1989	22.1	726	750	1989	22.1	729	753	2017	22.0	728	753	1997	22.1	728	752
mean	677	14.5	139	144	654	15.6	121	122	654	15.6	126	127	663	15.5	125	126	658	15.6	127	128
median	572	14.5	116	123	550	15.6	99	99	550	15.6	104	105	559	15.5	103	103	555	15.6	106	107
sd	324	2.8	96	96	318	2.9	89	90	318	2.9	89	89	320	2.8	90	91	317	2.8	89	90
cv ^b	0.48	0.19	0.69	0.67	0.49	0.19	0.74	0.74	0.49	0.19	0.71	0.70	0.48	0.18	0.72	0.72	0.48	0.18	0.70	0.70

^a – P, E, and R in mm year⁻¹, and T in °C for minimum, maximum, mean, median, and standard deviation (sd) values.

^b – dimensionless coefficient of variation, cv=sd/mean.

^c – mod_1976-2005

^d – mod_1996-2005

Table 8.4. Basic statistics of governing variables P, T, and R for the historical period, the four considered scenarios, and the two recharge models utilized.

Figures of the Chapter 8

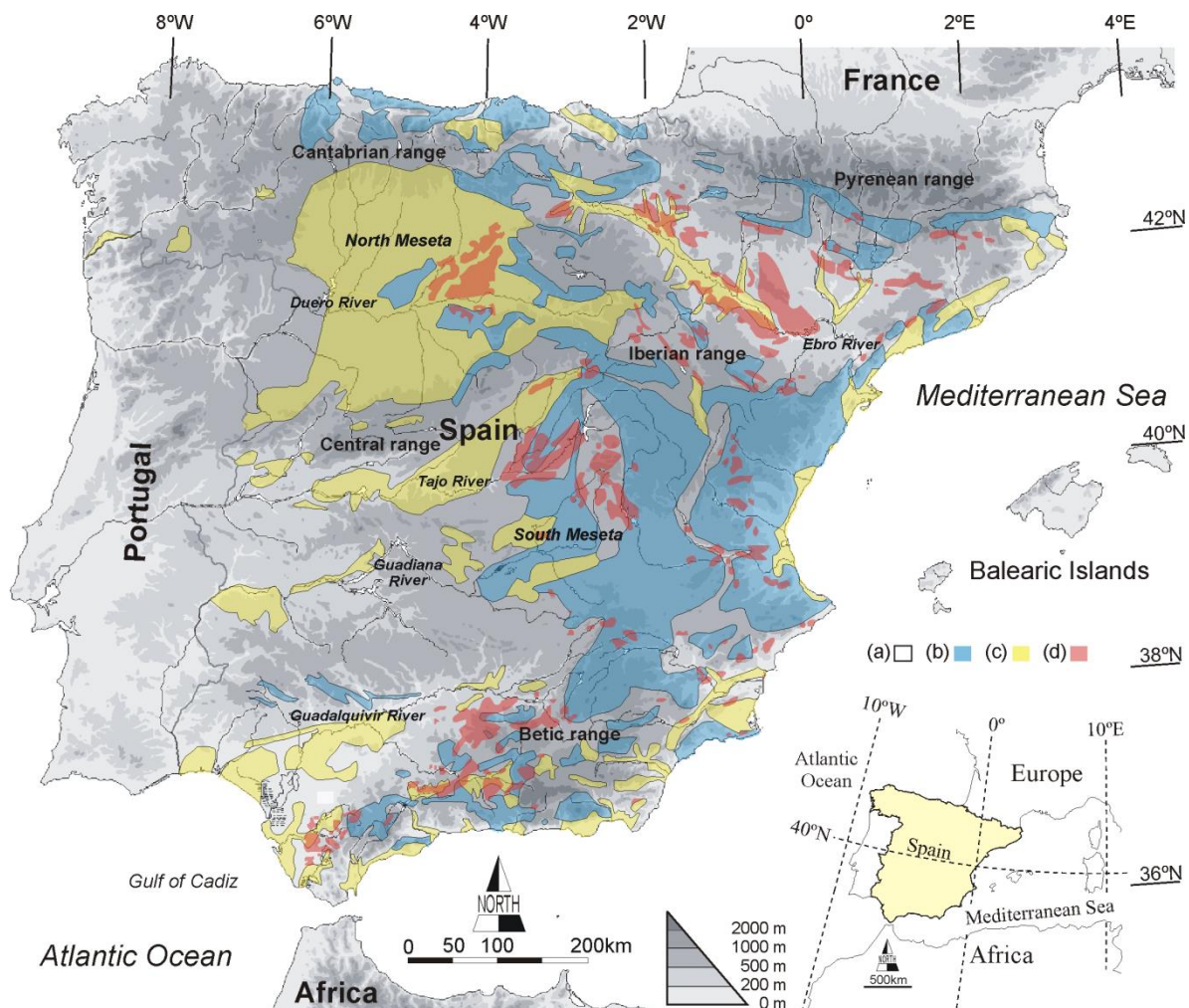


Figure 8.1. Map of continental Spain, showing the main mountain ranges and hydrographic basins, and the hydrogeological behaviour of geological materials according to permeability type (IGME, 1993), modified from Alcalá and Custodio (2014): (a) low to moderate permeability pre-Triassic metamorphic rocks, granitic outcrops, and Triassic to Miocene marly sedimentary formations; (b) moderate to high permeability Palaeozoic to Tertiary carbonates; (c) moderate to high permeability Plio-Quaternary detritic materials; and (d) Triassic to Miocene evaporitic outcrops.

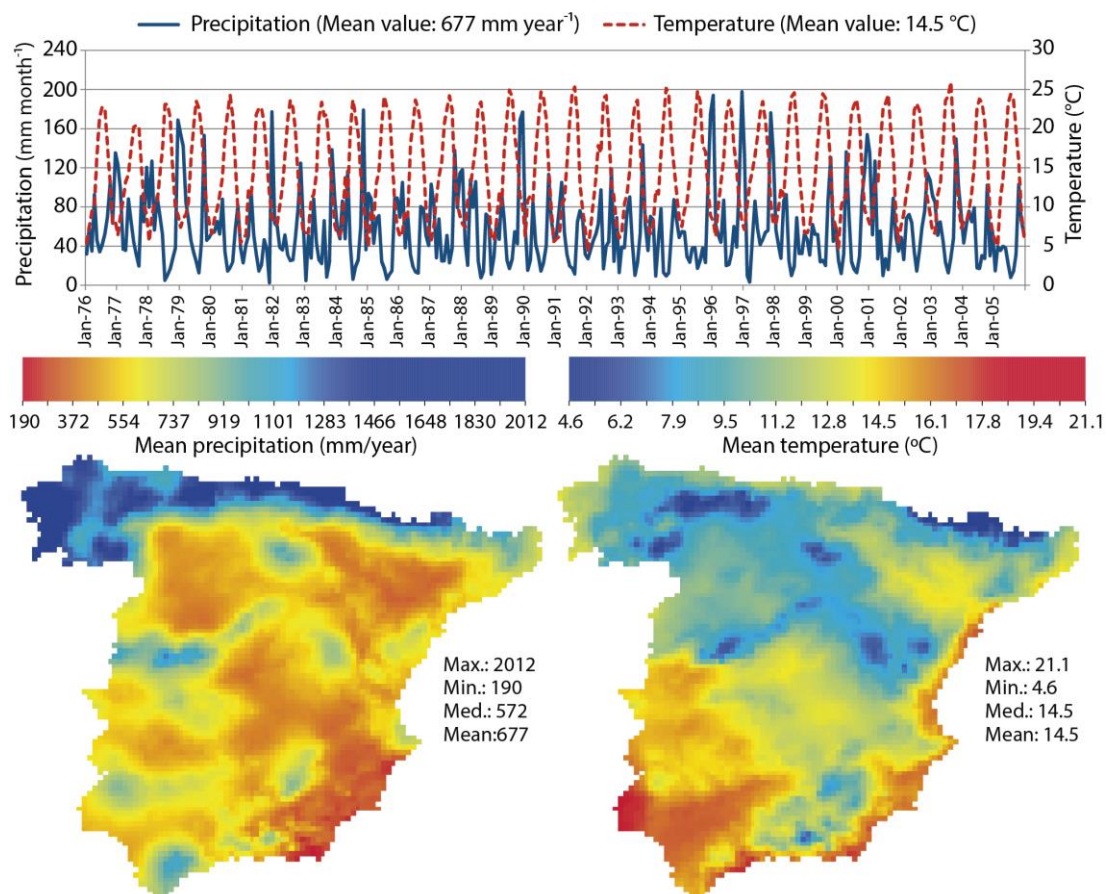


Figure 8.2. Spatio-temporal distribution of historical mean (a) precipitation (mm year⁻¹) and (b) temperature (°C) in continental Spain during the reference period (1976-2005).

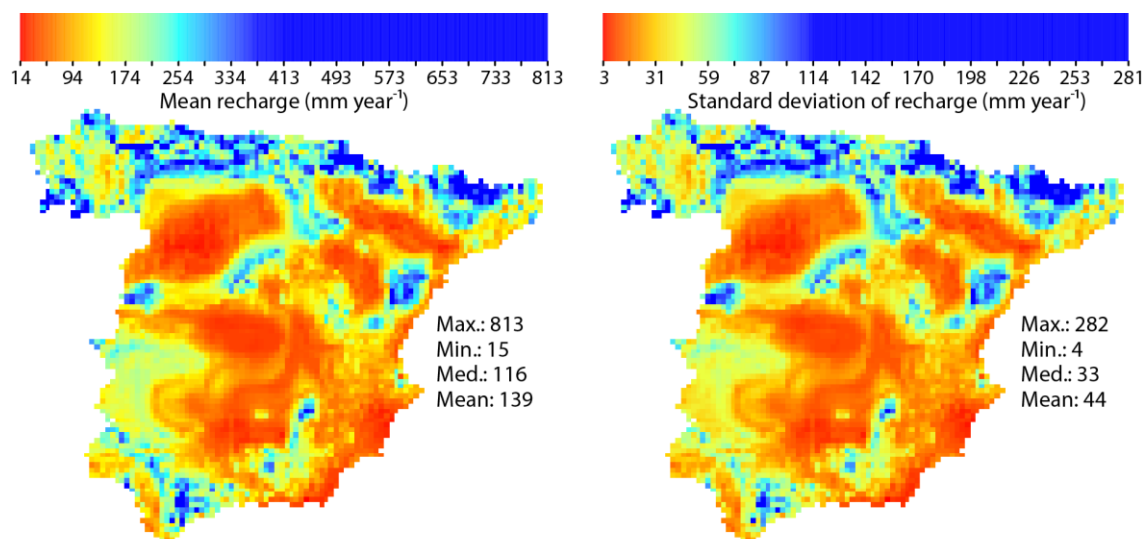


Figure 8.3. Historical net aquifer recharge (NAR) from precipitation over continental Spain from the CMB method application for the period 1996-2005, after Alcalá and Custodio (2014, 2015): (a) annual mean NAR (mm year⁻¹) and (b) standard deviation of annual mean NAR (mm year⁻¹).

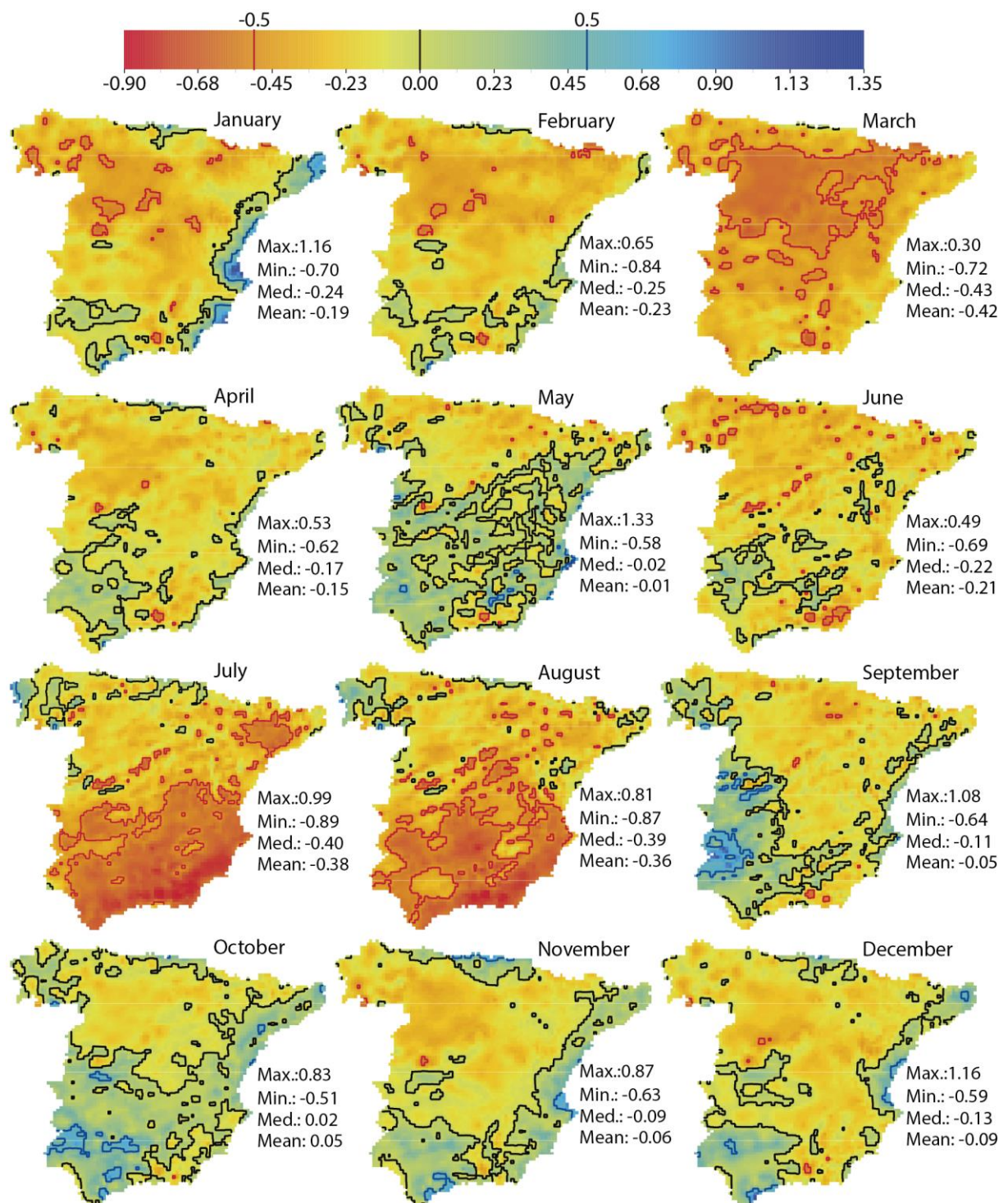


Figure 8.4. Dimensionless spatial monthly mean relative differences between the control simulation and the historical precipitation time series for an average year in the reference period (1976-2005). The ± 0.5 range is indicated.

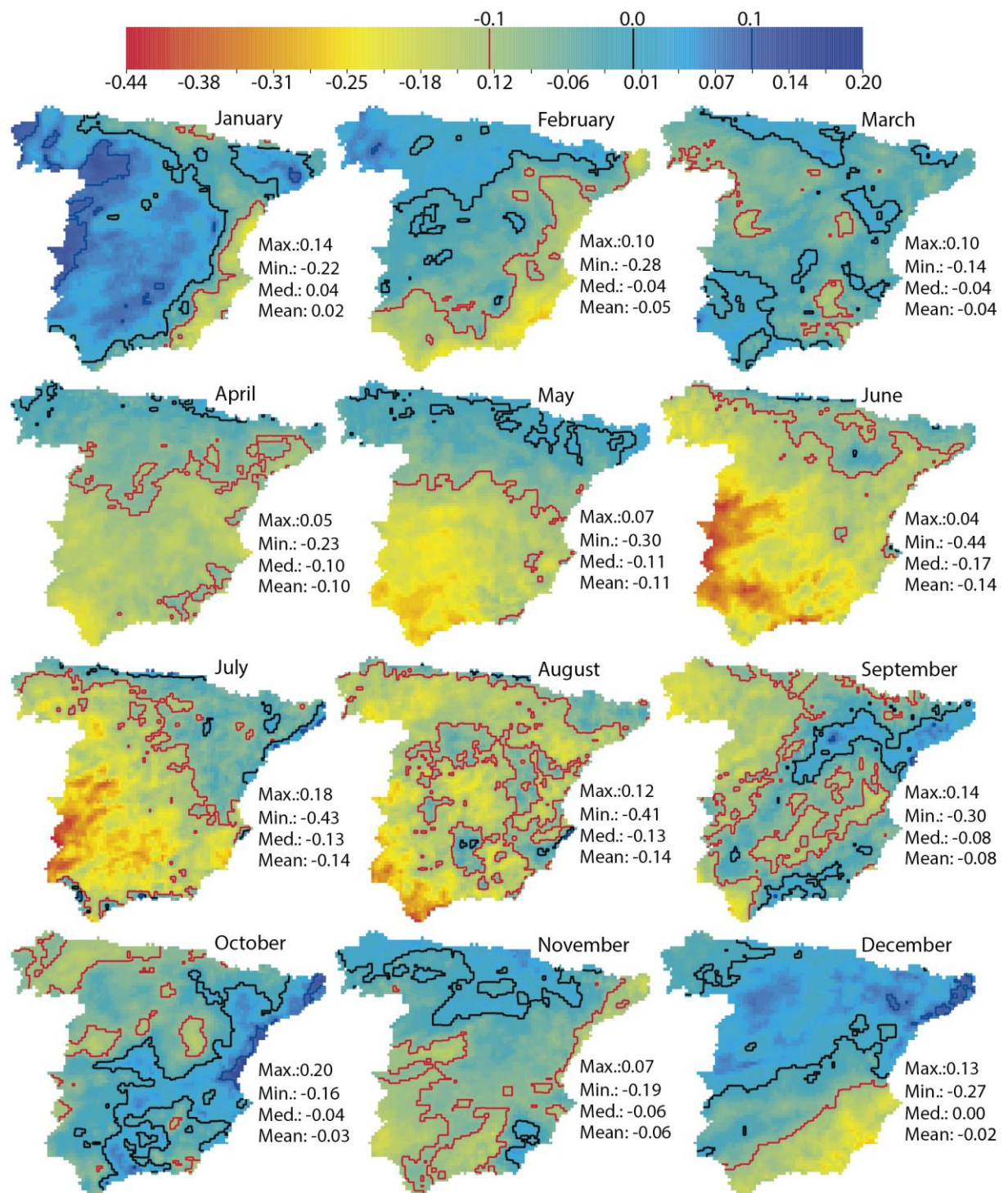


Figure 8.5. Dimensionless spatial monthly mean relative differences between future (2016-2045) and control (1976-2005) precipitation time series. The ± 0.1 range is indicated.

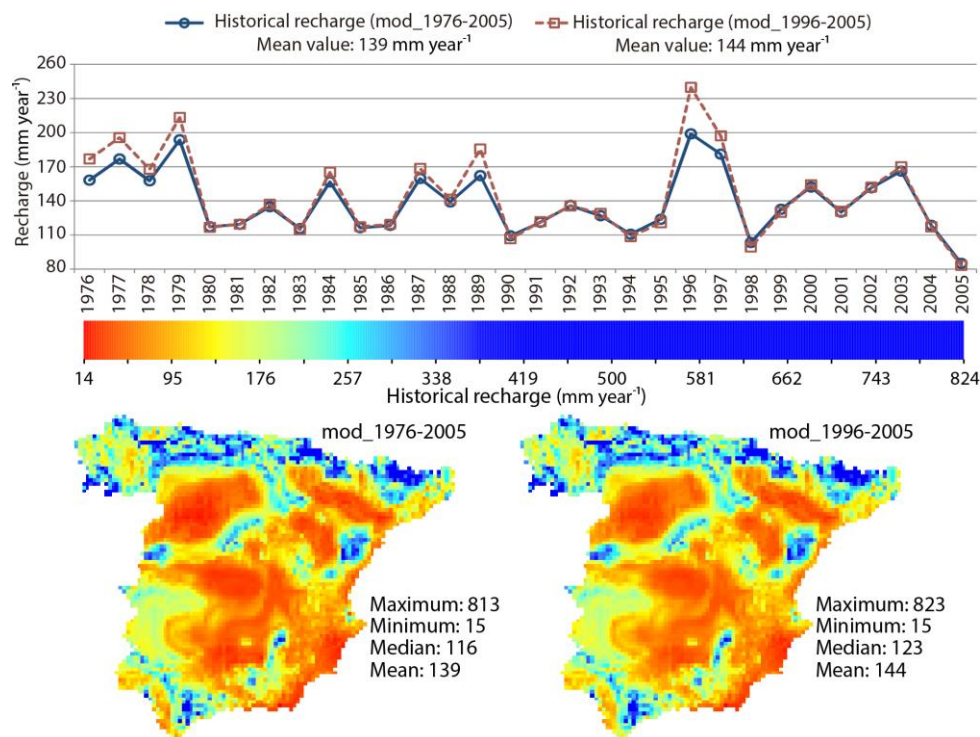


Figure 8.6. Historical mean net aquifer recharge (mm year⁻¹) for the period 1976-2005 obtained when simulating with two different hypotheses regarding the length of the PE recharge time series used to calibrate the precipitation-recharge model: mod_1976-2005 and mod_1996-2005.

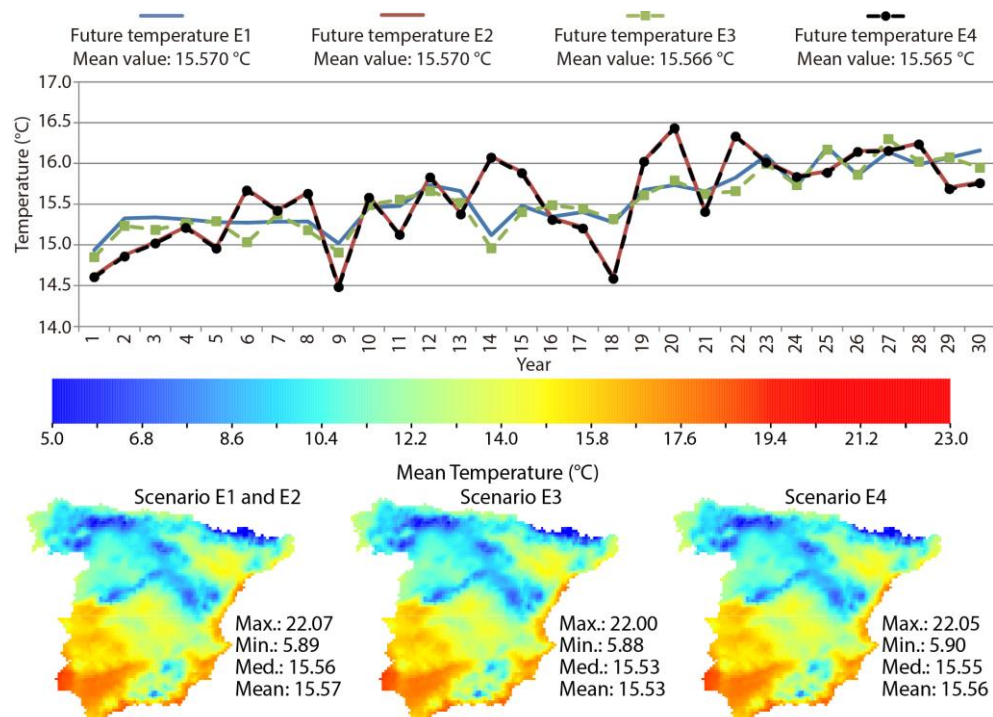


Figure 8.7. Potential future mean temperature (°C) scenarios obtained with the four ensemble options (E1, E2, E3, and E4).

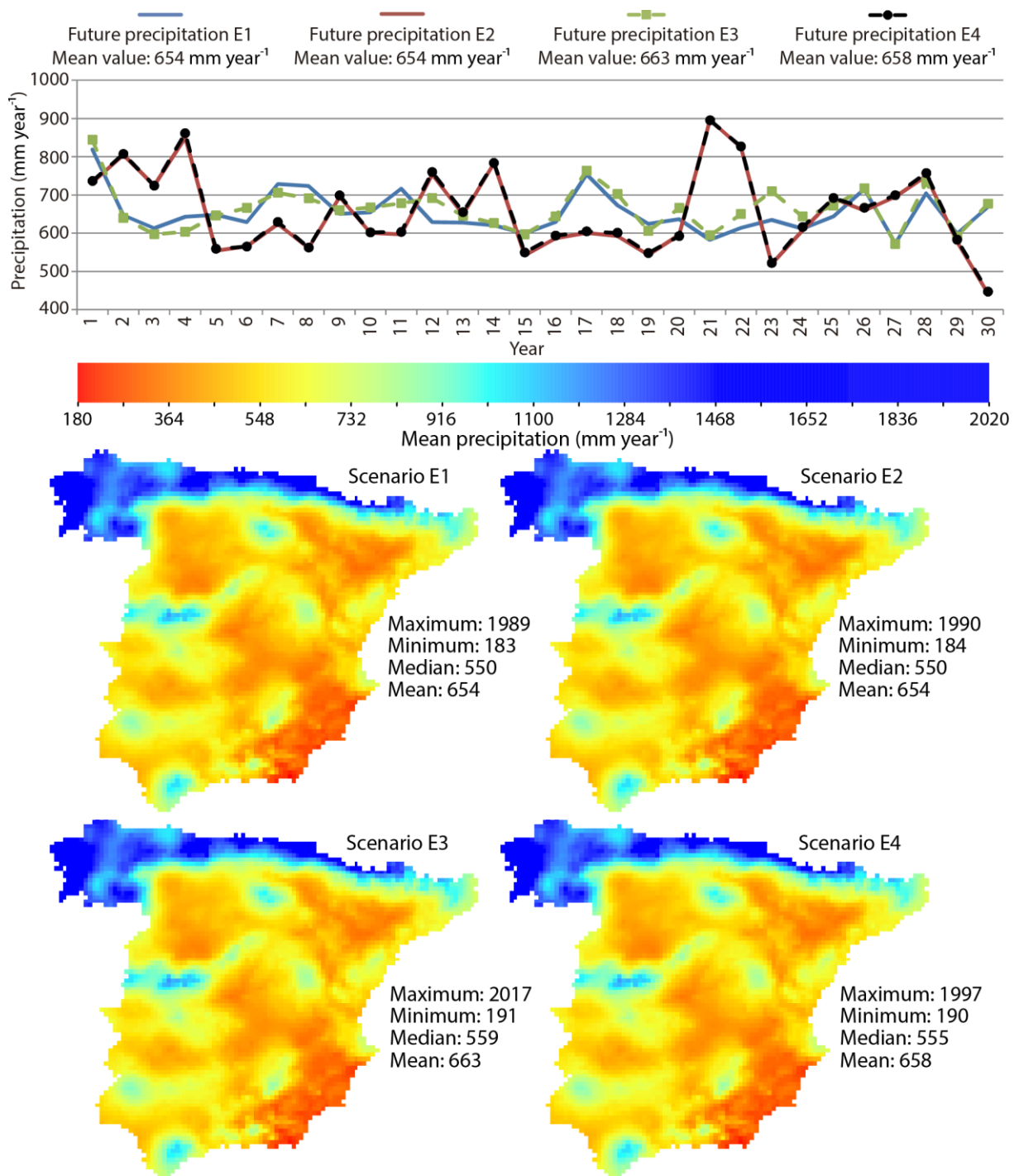


Figure 8.8. Potential future mean precipitation (mm year⁻¹) scenarios obtained with the four ensemble options (E1, E2, E3, and E4).

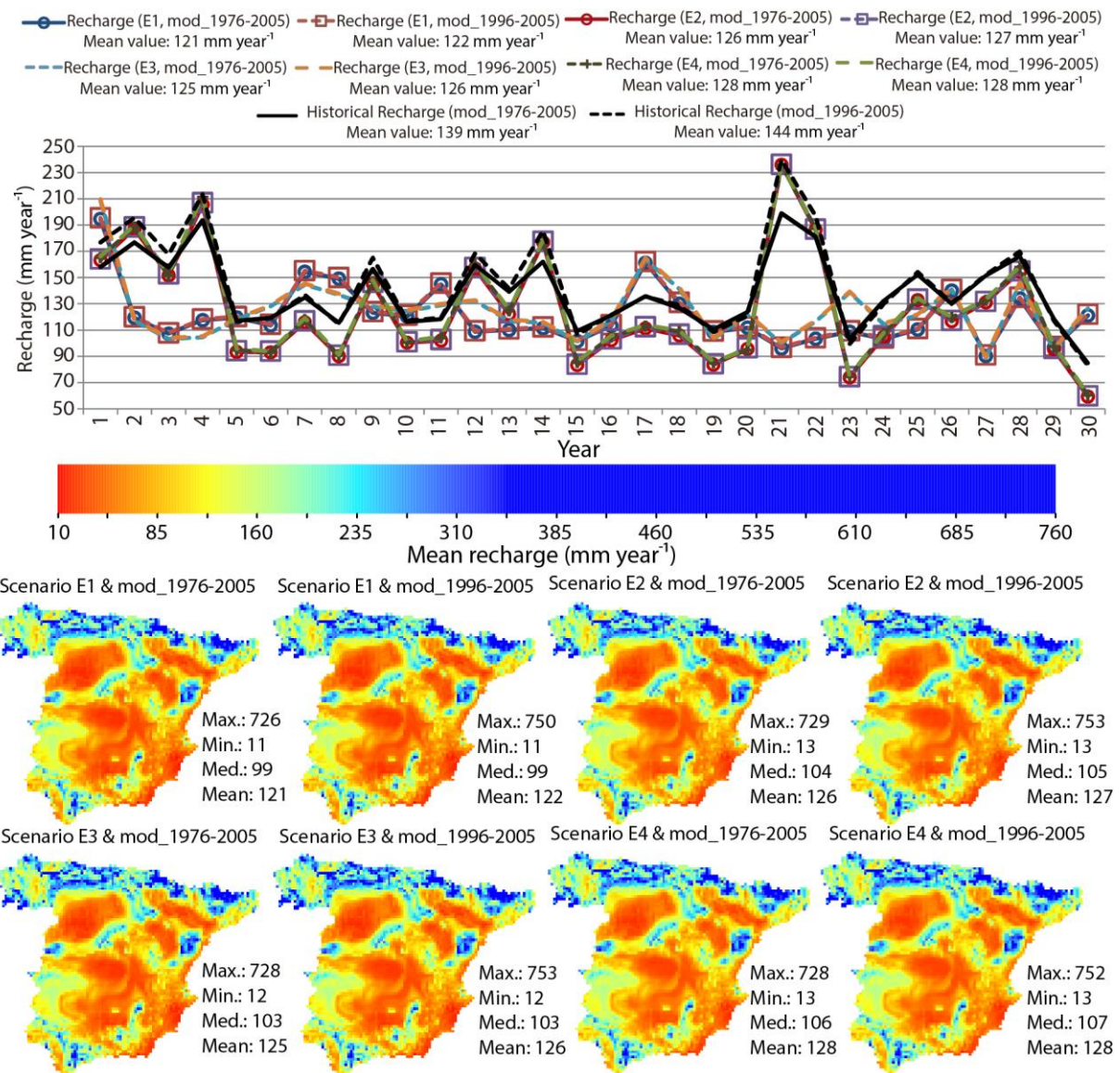


Figure 8.9. Future potential mean net aquifer recharge (mm year⁻¹) scenarios for the period (2011-2045) by combining future potential scenarios defined by the four ensemble options (E1, E2, E3, and E4) and two recharge models (mod_1976-2005 and mod_1996-2005).

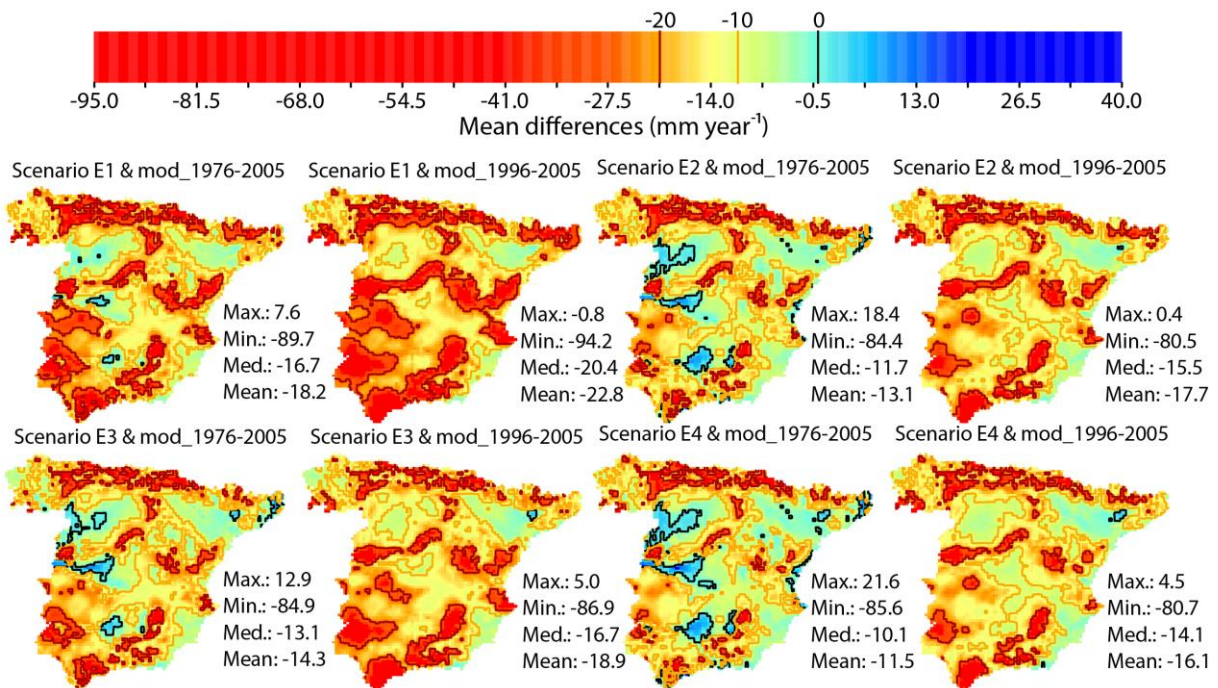


Figure 8.10. Absolute differences in mean net aquifer recharge (mm year^{-1}) for the historical series under four different scenarios (E1, E2, E3, and E4) and recharge models (mod_1976-2005 and mod_1996-2005).

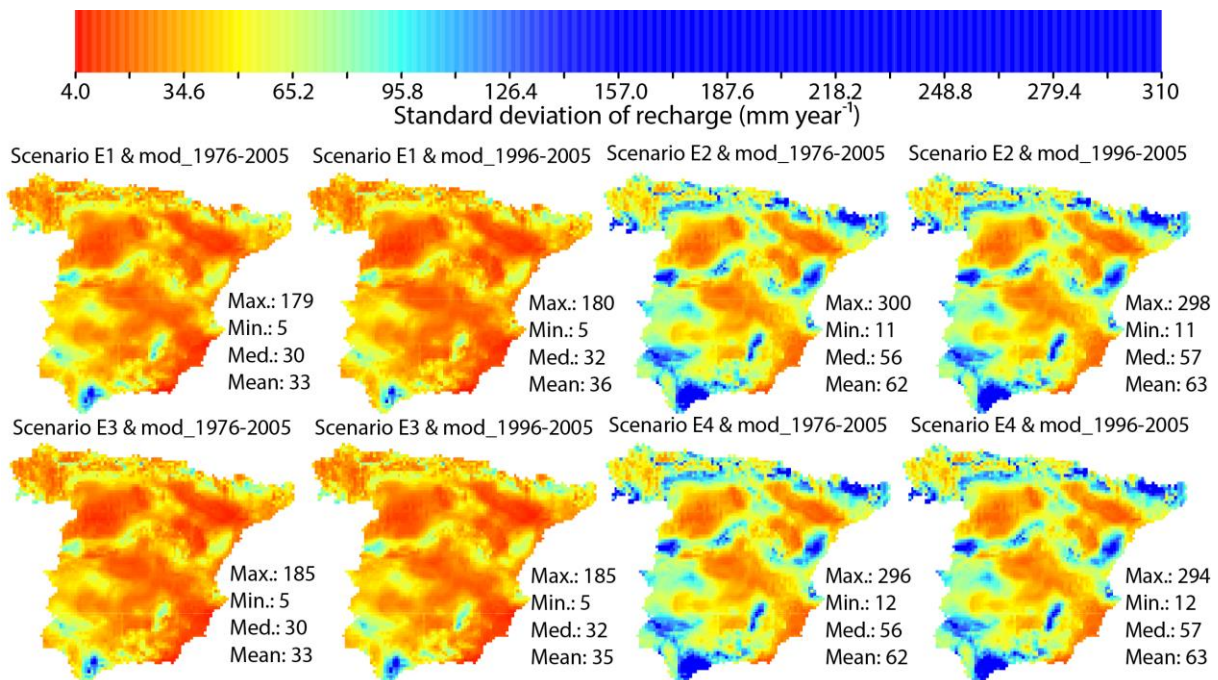


Figure 8.11. Future potential scenarios of standard deviation of mean net aquifer recharge (mm year^{-1}) for the period (2011-2045) from combining future potential scenarios defined by the four ensemble options (E1, E2, E3, and E4) and two recharge models (mod_1976-2005 and mod_1996-2005).

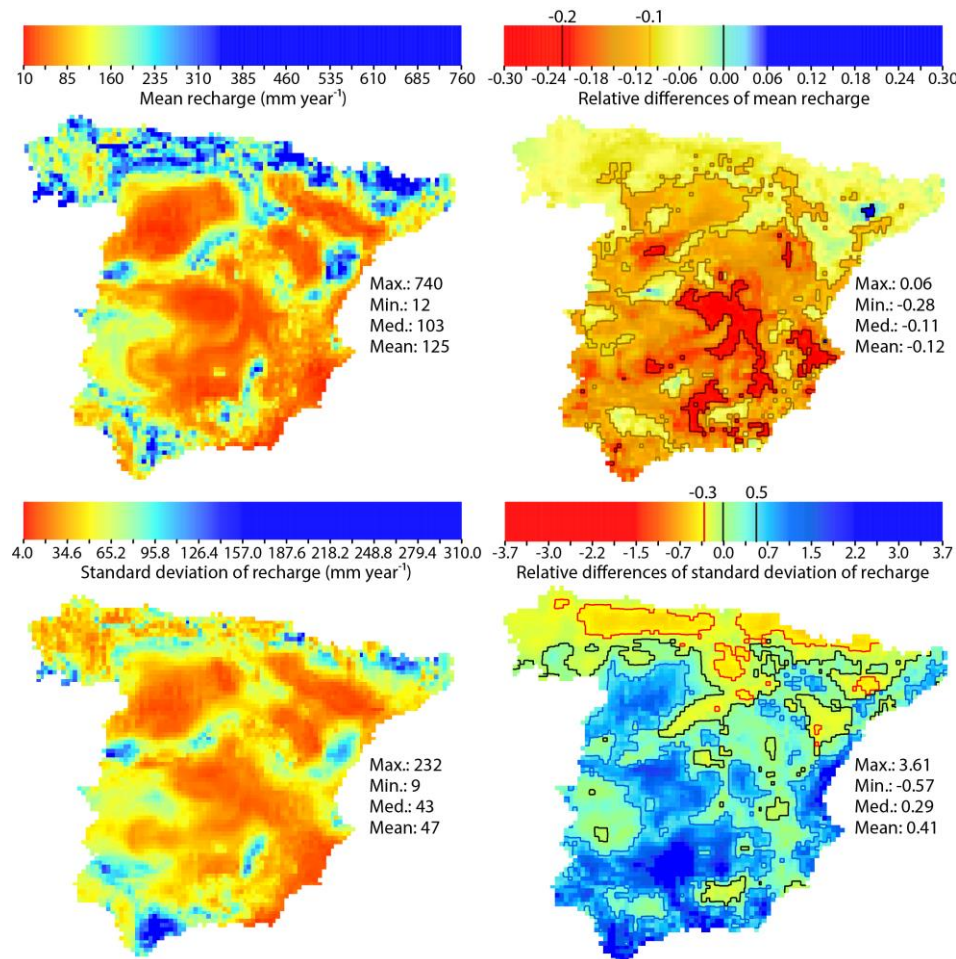


Figure 8.12. Potential future mean net aquifer recharge (NAR) (mm year⁻¹), standard deviation of future mean NAR (mm year⁻¹), and dimensionless relative differences between historical and future scenarios (equi-feasible ensemble of the eight scenarios).

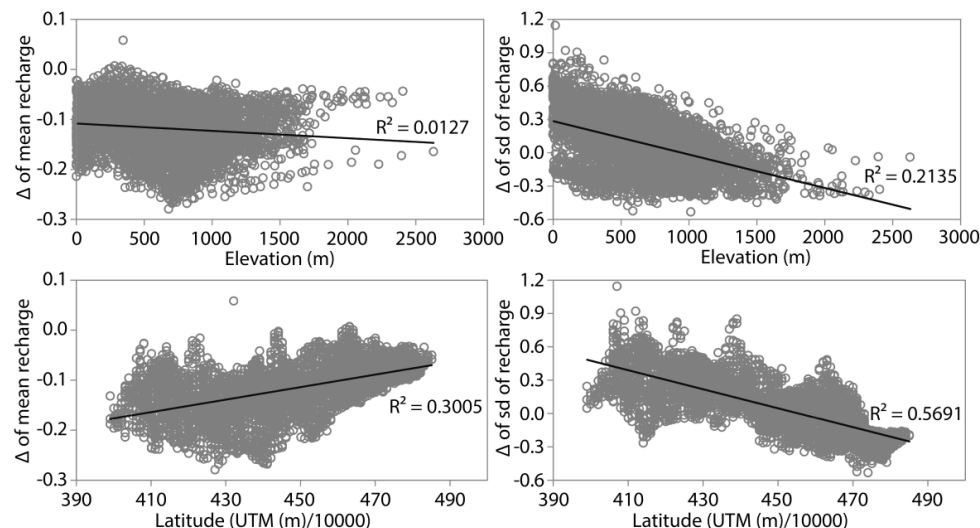


Figure 8.13. Elevation and latitude vs. dimensionless relative differences between future and historical net aquifer recharge (mean and standard deviation).

Chapter 9: General conclusions, limitations and future research

This thesis addresses problems related to the evaluation of the impacts of future potential scenarios of climate change (CC) in resources stored naturally in aquifers and/or snowpacks in systems that cover large areas of land. Groundwater and snowpacks can play a fundamental role in defining CC adaptation strategies that allow a sustainable supply of demands.

The doctoral thesis develops a methodological framework for assessing impacts at different scales (basin, mountain range and country). A methodology has been proposed to generate potential CC scenarios considering droughts, which condition the management of the water resources in arid and semi-arid regions. The objectives achieved in the doctoral thesis represent an important contribution to the field of study; in addition interesting lines of research are identified for the future.

1. Contributions

Each chapter describing the methodology that forms the body of the thesis (chapters 2 to 8) includes specific conclusions for each of the specific objectives addressed. Nonetheless, the principal contributions of this thesis are summarised again in this section.

- Study of the precipitation and temperature gradients with elevation and generation of historical precipitation fields using geostatistical techniques and elevation as secondary information for estimation.

In the Alto Genil basin, an inversion of the precipitation gradient was detected around 1600 m. Although this pattern of precipitation was considered to be due to systematic errors in solid precipitation measurements (a phenomenon known as undercatch), the climate analysis of data in non-snow time led to the conclusion that the inversion of the gradient is real, though its intensity can be amplified by this phenomenon. The temperature shows a linear downward relationship with elevation. Wide differences were observed between the geostatistical techniques used to generate precipitation fields (kriging with linear or quadratic external drift, regression kriging) while the influence of the time scale (annual or monthly) used to define the climate variogram is low. Though the kriging with linear external drift technique shows the best results in the cross validation experiment, the gradient inversion is not reproduced by it. However, the regression kriging technique does show this inversion. Therefore, it is necessary to study different techniques when fields of climatic variables are generated in order to choose the one that contributes to the least uncertainty to the process.

- Development of a methodology applicable at the mountain range scale to calculate snow depth using geostatistical techniques.

A parsimonious methodology is proposed for the estimating snow depth by regression kriging in alpine systems based on (1) explanatory variables (geographic (latitude, longitude, terrain curvature and elevation), orographic (eastness, northness and slope), and “pseudo-climatic” (mean radiation index and maximum upwind slope)) that can be obtained from a digital

elevation model and (2) snow cover area data that can be obtained from satellite information. The methodology has been applied to Sierra Nevada with satisfactory results in the cross validation experiment. The multi-objective analysis of the different regression models detected that the most important explanatory variables in the case study are elevation, northness and slope.

- Optimisation of the snow monitoring network to reduce uncertainty in estimates of snow depth. Application at mountain range scale.

A methodology was developed to optimise the snow depth monitoring network in a mountain range from a regression model that includes various explanatory variables to estimate snow depth. The proposed optimisation methodology minimises the error in the snow depth estimation by regression kriging process, considering two sources of uncertainty: the regression model that takes into account the effect of the explanatory variables, and the kriging that takes into account the location of monitoring points. Distinct optimisation cases are proposed for expanding the network, contracting it, and a combination of both. The methodology was applied to the case study of Sierra Nevada to give a new configuration of the snow depth monitoring network in Sierra Nevada that reduces the overall uncertainty in the estimates by combining the optimal network expansion and reduction cases.

- Development a model to simulate the dynamics of snow cover area by using a cellular automata model. Application to mountain range scale.

A parsimonious cellular automata model was developed to calculate snow cover area from information from climatic indices of precipitation and temperature, digital elevation model, and a series of rules of interaction between the variables. In a first approach, a model has been developed with climatic indices and lumped parameters for the whole mountain range. Subsequently a distributed model with different climatic zones was developed. The parameters of the model were calibrated for each of the climatic zones (defined precipitation and temperature series). Both methodologies were applied to the Sierra Nevada mountain range with satisfactory results in the calibration and validation processes. The distributed version leads to better approximations of the snow cover area dynamics, and allows the study the heterogeneous behaviour of this evolution, reflected in the parameters and historical series.

- Evaluation of the historical net recharge in aquifers by means of an empirical model of net recharge. Application at continental Spain scale.

A parsimonious empirical recharge model has been developed to estimate net recharge to aquifers. It has been applied on a regular mesh of 10 km x 10 km for the case study of continental Spain. It estimates net recharge from precipitation, temperature and actual evapotranspiration. The model uses historical data of average recharge and its standard deviation, which were obtained by using a chloride mass balance method developed in a previous study. The recharge series obtained for each of the cells of the grid considered allowed the spatiotemporal distribution of the recharge to be assessed.

- Proposal of a methodology to generate potential scenarios of CC that takes drought statistics into account.

A methodology was developed to generate potential local or regional CC scenarios exploring different conceptual approaches and correction techniques. A multi-criteria analysis was proposed for the definition of ensembles of non-equifeasible scenarios that takes drought statistics into account. The methodology was applied to the Alto Genil basin, where we obtained variations close to -27% in precipitation and + 32% in temperature for the horizon 2071-2100 using the most pessimistic emissions scenario, RCP8.5.

- Propagation of the potential impacts of CC on snow cover area and net recharge in aquifers. Application at mountain range and country scale respectively.

The described models have been used to propagate the impacts of potential future scenarios of climate change on snow cover area and groundwater recharge. Significant reductions in snow cover area in the Sierra Nevada (around 60% on average) are predicted by the simulation using the cellular automata model and the future climate series generated for the 2071-2100 horizon considering the RCP8.5 emission scenario. In addition, the future series of precipitation and temperature generated show that the potential impacts of climate change will increase with elevation in the case of temperature and decrease with elevation in the case of precipitation. On the other hand, the propagation with the empirical model of net recharge provides reductions in the recharge in 99.8% of Peninsular Spain, which are distributed very heterogeneously. More than 2/3 of the area shows reductions higher than 10% and the average of the reductions obtained in the territory is 12%. In some Mediterranean areas (the region that will suffer most from the effects of CC) we obtained average reductions up to 25%. These results reflect the need to establish the necessary measures to elaborate water policies based on adaptation and mitigation of the effects of CC on water resources systems.

2. Limitations and future lines of research

Although each chapter identifies the limitations of the methodologies proposed, the main limitations of the proposed methodological framework are summarised again in this section. At the same time, these limitations represent potential future lines of research.

The preliminary studies detected an inversion of the precipitation gradient with elevation in the Alto Genil basin. It was concluded that this inversion is real and possibly increased by the undercatch phenomenon. The evaluation of this phenomenon would be an interesting line of future research.

The regression models analysed/proposed to estimate the distribution of snow depth do not include any time-dependent explanatory variable and so they do not allow any approximation of the temporal dynamics in the estimations. On the other hand, snow water equivalent has been preliminarily quantified in the mountain range based on the snow depth estimations obtained with the regression kriging model. Snow water equivalent depends on the depth, cover and density of the snow. Snow depth and cover were studied/modelled as part of this doctoral investigation but, due to lack of data, a value was assumed for snow density.

Normally the density of a snowpack can have important spatiotemporal variations and even in the thickness itself. This constitutes a limitation of the methodology, though at the same time defines a potential line of future research.

The optimisation of the snow depth monitoring network has been carried out to minimise the uncertainty of the estimates. However, the study did not consider the operating costs for the collection of data, which are linked to the accessibility to the monitoring point. This criterion could be included in the definition of the optimal location of monitoring stakes.

In the application of the methodology for the generation of future climate scenarios, the available historical series are too short to perform an explicit calibration and validation of the model. For this reason, the multi-criteria analysis for the ensemble of scenarios was based on the results obtained in the calibration period. It would be interesting to evaluate other case studies where the information series is long enough to perform an explicit validation of the model.

In this thesis, the potential impacts of CC on snow cover area and net recharge have been evaluated. However, the impacts on other variables related to the evolution of resources stored naturally in snowpacks or in aquifer systems have not been investigated. It would be interesting to develop a model that combines, for example, the variables of depth, cover area and density of snow to propagate the potential impacts of the CC on the snow water equivalent.

